Toxicogenomics of synthetic and naturat nanopartictes in the nematode C.etegans

Polak, Natasa

Awarding institution:
King's College London

Toxicogenomics of synthetic and natural nanoparticles in the nematode *C.elegans*

BY NATASA POLAK

Thesis submitted to King's College London for the degree of Doctor of Philosophy

ABSTRACT

Natural and synthetic nanoparticles (NP) are microscopic particles, which are characterized by their small size (< 0.1 µm). It is now well established that exposure to NPs can represent a serious risk to human health and the environment. To establish the modes of action of NP toxicity, this project utilizes the nematode *Caenorhabditis elegans* to conduct baseline studies to screen the toxicological effects (on life-history traits, fitness, and metabolism) of metal oxide based synthetic (30 nm ZnONPs), and naturally occurring (Carbon Black M120 and NIST 1648a) NPs. The results indicate that: 1) The Nanosight NTA technique is a suitable tool to evaluate particle aggregation in biological test media. 2) All tested particles exert a shared toxic response that is manifested by a decrease in reproductive potential. The toxic effects were dose responsive to ZnONPs exposure, but not to NIST and CB. 3) The DCFH-DA assay provided *in vitro* evidence of the oxidative potential of particles, as the intracellular total ROS levels were altered. 4) The whole genome, qPCR analyses, and microscopy provided evidence that the majority of transcripts involved in stress response pathways (e.g. sod family; *cat-2*,*-3*; *hsp-16.1*) did not alter or were only marginally affected by the particles. Nevertheless, the most profound effects were the down regulation of the ribosomal RNA transcript (*rrn-3.1*) with increasing NIST concentrations, and the induction of *cep-1* gene (p53 human orthologous) with ZnONPs. 5) Finally, spectroscopic strategies identified the importance of metallochelators in the protection from ZnONP induced toxicity. Overall, the results of this study suggest that the use of sensitive nematode mutants combined with genomic tools represents a powerful approach to assess the physicochemical toxicity of different types of particles.

Abbreviations and conventions

°C	Degrees in centigrade
µg	Microgram(s)
µL	Microlitre
µM	Micromolar
aa	Amino acids
Ag	Silver
Al	Aluminium
AM	Alveolar macrophages
ANOVA	Analysis of variance
ARE	Antioxidant response element
ASTM	American society for testing and materials
ATP	Adenosine triphosphate
Au	Gold
B[a]P	Benzo(a)pyrene
BC	Before Christ
BC	Black carbon (BC)
Blast(n)	Basic local alignment search tool (nucleotide)
bp	Base pair
BP	Biological processes
Ca^{2+}	Calcium
CAA	Clean air act
CARS	Coherent anti-stokes raman spectroscopy
CAT	Catalase
CB (M120)	Carbon black (MONARCH®120)
CC	Cellular components
Cd	Cadmium
$CdCl_2$	Cadmium chloride
cDNA	Complementary DNA
CeO_2	Cerium (IV) oxide
CGC	*Caenorhabditis* genetics centre
CO	Carbon monoxides
COPD	Chronic obstructive pulmonary disease
cRNA	Biotin-cRNA
Cu	Copper
Cu/Zn SOD	Copper and zinc superoxide dismutase
CYP(s)	Cytochrome P450 protein(s)
DAVID	Database for annotation, visualization and integrated discovery

DCF	Dichlorofluoroscein
DEG	Differently expressed genes
DEP	Diesel exhaust particles
dH_2O	Deionised water
DLS	Dynamic light scattering
DNA	Deoxyribonucleic acid
dNTPs	Deoxyribonucleotide triphophates
E.coli	*Escherichia coli*
EASE score	Expression analysis systematic explorer score
EC50	Effective concentration, 50%
EC number	Enzyme commission number
EDS	Energy dispersive X-ray spectrometer
EDX	Energy dispersive X-ray
EPA	Environmental protection agency
EPS	Extracellular polymer substances
fcRNA	Fragment biotinylated cRNA
Fe	Iron
Fe/Mn SOD	Iron/manganese superoxide dismutase
fps	Frames per second
g	Gravitational force
GCS(h)	Glutamine cysteine synthase (heavy chain)
GFP	Green fluorescent protein
GI	Gastrointestinal
GO	Gene ontology
GPx	Glutathione peroxidase
GSH	Glutathione
H_2DCF-DA	2', 7'- dichlorodihydrofluoroscein diacetate
H_2O	Water
H_2O_2	Hydrogen peroxide
HBE(cells)	Human bronchial epithelial (cells)
HC	Hydrocarbons
Hg	Mercury
HPLC	High purified liquid chromatography
hr(s)	Hour(s)
hsRFP	A mCherry red fluorescent protein, whose coding region is fused to the histone gene *his-57*
IARC	International agency for research on cancer
ICP-MS	Inductively coupled plasma mass spectrometry
ID	Identity

IVT	*In vitro* transcription
KEGG	Kyoto encyclopaedia of genes and genomes
KO	Knockout
L	Litre
LB	Luria broth
LC50	Lethal concentration, 50%
LNA	Locked nucleic acid
LPS	Lipopolysaccharides
M	Molar
MAPK	Mitogen-activated protein kinases
Mb	Mega base pairs
mCherry	A red fluorescent protein
MF	Molecular function
mg	Milligram
min	Minute
miRNA	MicroRNA
mL	Millilitre
mM	Millimolar
MMuLV	Moloney murine leukemia virus reverse transcriptase
Mn	Manganese
Mn/SOD	Manganese superoxide dismutase
MoSCI	Mos1-mediated single copy insertion
MRC	Medical research centre
mETC	Mitochondrial electron transport chain
mRNA	Messenger RNA
MT	Metallothionein
MW	Molecular weight
n	Number
NAAQS	National ambient air quality standards
NADPH (oxidase)	Nicotinamide adenine dinucleotide phosphate-(oxidase)
NCBI	National center for biotechnology information
ncRNA	Noncoding RNA
NF-κB	Nuclear-factor-kappa B
ng(s)	Nanogram(s)
NGM	Nematode growth medium
Ni	Nickel
NIST	National institute of standards and technology
NIST SRM 1648a	National institute of standards and technology standard reference material 1648a for urban particulate matter

NOx	Nitrogen oxides
NP	Nanoparticles
NQO1	NAD(P)H: quinone oxidoreductase
Nrf	Nuclear factor-erythroid-related factor
ns	Non-significant
nt	Nucleotides
NTA	Nanoparticle tracking analysis
O^{2-}	Superoxide radical
O_3	Ozone
OD	Optical density
OE	Overexpressed
OH^-	Hydroxyl anion
OS	Oxidative stress
PAH	Polycyclic aromatic hydrocarbons
Pb	Lead
PBS	Phosphate buffer saline
PC(S)	Phytochelatin (synthase)
PCA	Principle component analysis
PCB	Polychlorinated biphenyls
PCR	Polymerase chain reaction
PM	Particulate matter
P*x*::GFP	Promoter of (selected transcript: x) fused to GFP
qPCR	Quantitative polymerase chain reaction
qRT-PCR	Quantitative real-time polymerase chain reaction
r.p.m.	Rotations per minute
RIN	RNA integrity numbers
RMA	Robust multivariate average algorithm
RNA	Ribonucleic acid
ROS	Reactive oxygen species
rRNA	Ribosomal RNA
RTLF	Respiratory tract lining fluid
sec	Second(s)
SEM	Standard error of mean
Si	Silicon
SO_2	Sulfur dioxide
SRM	Standard reference material
STDEV	Standard deviation
TAE	Tris-acetic acid buffer
TEM	Transmission electron microscope

TEM-EDAX	Transmission electron microscopy energy dispersive X-ray analysis
TGF-beta	Transforming growth factor beta
Ti	Titanium
TiO_2	Titanium dioxide
Tm	Annealing temperature
TNF	Tumour necrosis factor α
tRNA	Transfer RNA
U.S. (A.)	United states of America
uf CB	Ultrafine carbon black
UFP	Ultrafine particle
***unc-47::*GFP**	Invariant GFP-tagged control gene
UPL	Universal probe library
UV	Ultraviolet
V	Vanadium
VOC	Volatile organic compounds
WHO	World health organization
Zn	Zinc
ZnONP(s)	Zinc oxide nanoparticle(s)
ΔΔ CT	Cycle threshold

Summary of nematode strains abbreviations:

WT (N2)	Wild-type (N2)
***mtl-1;mtl-2;pcs-1*(zs2)**	Metallothionein (-1; and -2) and phytochelatin synthase triple knockout (KO) mutant
***sod-1*(tm766)**	Cu/Zn superoxide dismutase-1 knockout (KO) mutant
***sod-2*(gk257)**	Fe/Mn superoxide dismutase-2 knockout (KO) mutant
***sod-3*(tm760)**	Fe/Mn superoxide dismutase-3 knockout (KO) mutant
***skn-1*(zu67)**	Skinhead bZip transcription factor knockout (KO) mutant, orthologous to the mammalian Nrf (Nuclear factor-erythroid-related factor) transcription factor
***pcs-1*(tm1748)**	Phytochelatin synthase knockout (KO) mutant

Summary of gene acronyms:

ACO-1	Aconitase
CCT-1	Chaperonin containing T-complex 1
CEP-1	*C. elegans* P-53-like protein
CNX-1	Calnexin
CRT-1	Calreticulin
CTL (-2; or -3)	Catalase (-2; or -3)
CUC-1	CU copper chaperonin
CYP-35A2	Cytochrome P450 family
DCT-1	DAF-16 (abnormal dauer formation)/FOXO (forkhead box O) controlled, germline tumor affecting
DNJ-1	DNaJ domain (prokaryotic heat shock protein)
F20D6.11	A putative flavin-adenine dinucleotide (FAD)-binding oxidoreductase
FTN-1	Ferritin
GCS-1	Gamma glutamylcysteine synthetase
GSR-1	Glutathione disulfide reductase
GST (-4; -10; or -38)	Glutathione S-transferase (-4; -10; or -38)
HSP (-16.2; -16.41; or -70)	Heat shock protein (-16.2; -16.41; or -70)
M162.5	M162.5 gene
MSRA-1	Methionine sulfoxide-S-reductase
MTL (-1; or -2)	Metallothionein (-1; or -2)
PCS-1	Phytochelatin synthase
PRDX-3	Peroxiredoxin
RRN-3.1	Ribosomal RNA
SKN-1	Skinhead bZip transcription factor
SOD (-1; -2; or -3)	Superoxide dismutase (-1; -2; or-3)
UGT-1	UDP-glycosyltrasferases

TABLE OF CONTENTS

CHAPTER SIX – General discussion

TABLE OF CONTENTS

Figures

CHAPTER ONE – Figures

CHAPTER TWO – Figures

CHAPTER THREE – Figures

CHAPTER FOUR – Figures

CHAPTER FIVE – Figures

CHAPTER SIX – Figures

TABLE OF CONTENTS

Tables

CHAPTER ONE – Table

CHAPTER TWO – Tables

CHAPTER THREE – Tables

CHAPTER FOUR – Tables

CHAPTER FIVE – Tables

CHAPTER SIX – Tables

TABLE OF CONTENTS

Boxes

CHAPTER TWO – Boxes

ACKNOWLEDGEMENTS

The completion of this work owes a great deal of gratitude and appreciation to many people. First of all I would like to take an opportunity to thank my supervisors, Dr Stephen Stürzenbaum and Prof Frank Kelly, for providing guidance throughout my four years of research. With their excellent supervision, support, advice, and help, I managed to identify and resolve obstacles encountered and develop into a strong independent researcher. Secondly, I would also like to express my thanks to Dr David Spurgeon and Dr Daniel Read (Centre for Ecology and Hydrology), for accommodating me at Wallingford and for access and training of the Raman microscope. Special thanks go to several other people and researchers I would like to acknowledge: Dr Ian Mudway and the Lung Biology lab of King's College London for advice, and useful insights that have allowed me to come up with new ideas I could test in my project; Dr David Stokes of Imperial College for his enthusiastic support of my research and training programme; Dr Kerstin Jurkschat of University of Oxford and Dr Berube Kelly of Cardiff University, for their help with electron microscopy imaging and analysis. Finally, special thanks are required for my parents and my sister, who supported and encouraged me throughout my PhD.

My PhD was funded by the MRC-HPA Centre for Environment & Health with extra CASE support from the Centre for Ecology and Hydrology (CEH), Wallingford.

CHAPTER ONE

General introduction

1.1 Nano-sized particles

Nanoscience or nanotechnology is a relatively new field of science. Its conceptual underpinnings were laid out in 1959 during a lecture 'There is plenty of room at the bottom' by Richard Faynman, a physicist who was interested in studying manipulation of molecules at the atom – nano sized level (Feynman, 1959). However, the term "nanotechnology" was not used till 1974, when Norio Taniguchi used it in his paper to describe "the processing of separation, consolidation and deformation of materials by one atom or one molecule" (Taniguchi, 1974). The prefix "nano" origins from the Greek word for dwarf, and is defined as a particle that is of a nanometre scale (nm) or alternatively an ultrafine particle (UFP), and has one or more dimensions of the order of 100 nm or less. Nanoscale materials are characterized by enhanced chemical, physical, and biological properties, which are distinct from their bulk counterparts. Although, nanoparticles (NPs) are a modern science discovery, their unusual properties have been exploited as far back as the 10^{th} century BC in Mesopotamia, where Au (gold) and Ag (silver) NPs were used to generate a glittering effect on ceramic glazes (Sciau, 2012). The Au NPs were even used for medicinal and healing purposes by Egyptians 5000 years ago (Chen et al., 2008). Due to new technological advances, the presence of nanomaterial in commercial products, such as cosmetics, sunscreens, surface coatings, medical applications, water filtrations, and catalytic systems, has increased over the last 20+ years and has raised public concern over the possible dangers of their omni -present use, e.g. research evidence on titanium dioxide and zinc oxide NPs to cause DNA damage (Shilling et al., 2010; Nowack et al., 2012). The direct and indirect exposure to

these materials has ignited a debate over their toxicological and environmental safety, as well as the need for regulations.

In contrast to the modern field of synthetic nanoscience, exposure to air pollution dates back to when humans began to build fires in poorly ventilated caves. Global levels of atmospheric pollution have increased especially since the industrialization of society. Indeed, the ability to absorb and purify the quantities of pollutants present has reached a critical point. The term air pollution encompasses contaminants such as chemicals e.g. polycyclic aromatic hydrocarbons (PAHs), particulate matter (PM), or materials of biological source (e.g. endotoxins), which cause harm to humans and the ecosystems. Epidemiologic studies suggest that each year many people die from pulmonary and cardiovascular diseases directly or indirectly linked to the exposure to ambient air pollution (WHO, 2005). Particulate matter (PM) or natural particles, man-made or natural in origin, are believed to be cause for a large proportion of the observed adverse health effects (Ayres et al., 2008; Valavanidis et al., 2008; Ghio et al., 2012).

1.2 History of nanohazards since the industrial revolution

Scientific interest in air pollution was triggered by a severe London smog episode in 1952 that caused an excess of 4000 deaths (Stegeman and Solow, 2002). During a two week period, the particle concentration was found to be as high as several milligrams per cubic metre of air. As a result, the British government introduced the Clean Air Act legislation (in 1970), which restricted coal burning with the aim to successively reduce pollution levels in the UK cities. At the time it was not known which pollution components (e.g. gasses, acid aerosols, solids) were responsible for the toxic outcomes, and the pioneering work by the Medical Research Centre (MRC) air pollution unit in St.

Bartholomew`s Medical School uncovered that the London smog was highly concentrated with particles, which were less than 100 nm in diameter (Lawther et al., 1968). In the 1990s, a series of epidemiological studies provided evidence that linked deaths (heart and lung diseases) to the exposure to particulate air pollutants (Table 1.1). Human and animal toxicological studies confirmed that smaller, nanosize particles are, unlike larger particles, retained in the lungs or have the ability to translocate through the lymphatic, circulatory, and nervous systems to many organs and tissues, including the brain (Ferin et al., 1992).

The majority of air pollution associated deaths result from cardiac, rather than pulmonary diseases (Hong et al., 2002; Pope et al., 2002). This observation is best explained by the hypothesis that toxicity is not dependent on the total mass of particulates administrated, but rather the level of the particulates that reach the lungs and thus result in a toxic effect, causing the failure of another organ (Brook et al., 2004; Delfino et al., 2005; Godleski, 2006). Therefore it was suggested, that exposure to air pollution (including cigarette smoke) presents a risk factor for development of coronary disease. Small particles have the ability to evade the lungs` primary defence system (macrophage clearance mechanisms) and enter the interstitial space, where they can cause inflammation leading to cytokine release and alteration of blood coagulation (Ferin et al., 1992; Donaldson et al., 2001; Schwarze et al., 2006). This eventually can result in atheroma implications.

Investigations have also focused on the toxicity of other particles, e.g. asbestos fibres, mesoporous silica (SiO_2 NPs or quartz NPs) for potential biomedical applications, metal oxide NPs etc. A study on workers chronically exposed to asbestos (from 1950s to 1960s) suggested that although normally a chemically inert mineral, it can cause an increased risk of fibrosis and lung cancer (Mossman et al., 1990).

Table 1.1: Observed epidemiological associations between particulate matter air pollution and health. (Adapted from *The Royal Society*: Nanoscience and nanotechnologies: opportunities and uncertainties, 2004.)

Death from and exacerbation of heart disease in vulnerable people.
Death from and exacerbation of chronic lung disease in vulnerable people.
Exacerbation of asthma.
Long-term increase in risk of death from heart attack and lung cancer.
A possible precipitation of cot death and stroke in vulnerable individuals.

Studies in rats have shown that lung instillation of metal oxide NPs, such as TiO_2 and ZnO, can generate free radicals and elicit an inflammatory response, which is greater on an equivalent mass basis than the fine or bulk particles of the same material (Baggs et al., 1997; Donaldson et al., 2000; Oberdörster, 2000). This highlights the risk factor associated with the occupational workers' exposure to NPs. In addition, nanomaterials can leak into the environment (e.g. via the dissolution effect of ZnONPs) and cause deleterious effects on the ecosystem (e.g. bactericidal effects) (Li et al., 2011).

Taken together, this emphasizes the importance of investigating the potential of nano-sized particles to affect human and environmental health.

1.3 Pollutants, particulate matter (PM), and nanoparticles (NPs) sources

Depending on the emission source, substances are classified as being either primary pollutants (generated directly from a process) or secondary pollutants (not emitted

directly, but formed via primary pollutants interacting in the air). Some pollutants can be both primary and secondary in their origin. The major sources of carbon monoxide (CO), hydrocarbons (HC), nitrogen oxides (NOx) and ambient particulate matter (PM) originate from vehicle emissions (particularly diesel engines). Sulphur dioxide (SO_2) is a product that arises from fuel combustion in stationary sources (such as for example power plants burning sulphur-containing coal, oil, or gas). The highly reactive ozone (O_3) is a constituent of photochemical smog. Vehicle engines, industry, and commercial cooling and heating are the major sources of volatile organic compounds (VOCs), such as benzene and polycyclic aromatic hydrocarbons (PAHs) (EPA, 2008). The distribution of these compounds can vary in time and space (e.g. during morning rush hours there is a higher number of vehicles on the road, hence increases in outdoor benzene emission levels are detected). Concentrations of many VOCs are found to be up to ten times higher indoors than outdoors, regardless whether homes are located in rural or heavy industrial areas, mainly due to household products such as cosmetics, cleaning products etc. (EPA, 2008).

PM typically consists of a complex mixture of very small solid particles or liquid droplets suspended in the air that can be organic or inorganic in nature (Ghio et al., 2012). They are generated during the transition of a gas into a particulate, a process known as nucleation. Most naturally occurring particulates are generated by volcanic eruptions (e.g. ash particulates), sea spray (salt minerals), bush and forest fires, living vegetation and dust storms. However, anthropogenic particles (linked to human activities, e.g. transport fuels and even food cooking) account for approximately 10 % of the total PM present in the atmosphere, and chemical and physical compositions vary widely (EPA, 2008).

The major source of (outdoor) carbon black (CB) particle pollution arises through the burning of fuels, such as gasoline, oil, diesel or wood. CB is also used as a colour pigment in ink, paints, plastics, and as reinforcing filler in tires and rubber products (IARC, 2010).

Industry has been producing for many decades synthetic particles or nanoparticles (NPs) e.g. printer toners (IARC, 2010). These manufactured nanoparticles exist within raw ingredients either fixed (in solid materials or attached to surfaces) or free (when suspended in fluid). Although their production level is low, when compared to natural or anthropologic nanomaterial, they have attracted considerable amount of attention, as they are found in some cosmetic products, such as sunscreens (e.g. titanium dioxide, zinc oxide), in medicine as an antibacterial agent (e.g. first aid tapes), or used in surface treatments (e.g. lotus leaf effect).

Nanomaterials can enter the environment via spillage during the handling and shipping, wear- and wash-off (e.g. sunscreens), landfills, disposal sites (e.g. electronics) or leaking processes. As nanomaterials are also used in remediation (e.g. nano-iron soil injections), they can potentially cause contamination of the soil, enter the food-chain and affect wildlife (Nriagu and Pacyna, 1998).

1.4 Scale classification, physical properties, and composition

Particles are typically defined by their aerodynamic diameter, and are divided into the following categories: coarse, fine, and ultrafine (Wild et al., 2008) (Fig. 1.1B). The coarse fraction describes particles within a size range between 2.5 µm – 10 µm (PM_{10}), which are formed by abrasion of surfaces, crushing or grinding of larger solid particles.

They are produced by suspension of dust from roads, industry (e.g. coal and oil fly ash), as well as by non-combustible materials, which are released when burning fossil fuels and agricultural processes. PM_{10} is primarily composed of aluminosilicate and other metal oxides of crustal elements (Si, Al, Ti, Fe) (WHO, 2003 and 2004).

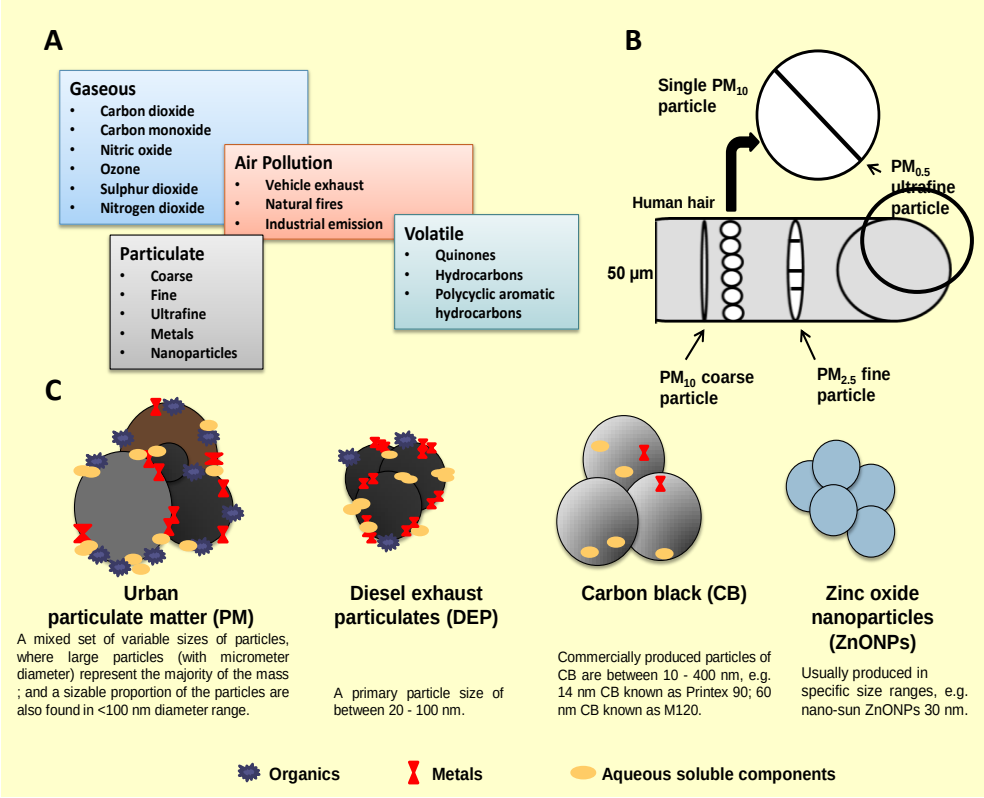

Fig. 1.1: Composition and categorization of air pollution. (A) Pollutants and their sources. Ambient air is composed of a complex mixture comprising irritant gases, particulate matter (PM), toxins and volatile organic compounds (VOCs) e.g. benzene and polycyclic aromatic hydrocarbons (PAHs). **(B)** Size of particulate matter (PM_{10}, $PM_{2.5}$, and $PM_{0.1}$) compared to the diameter of a human hair. **(C)** Different types of environmental and engineered PMs. Air particles carry (on their surface) transition metals, organics, and other soluble components. The chemical composition on particle surface is linked to its source of emission/production. (Adapted from Miller et al., 2012).

In contrast, the fine particulate fraction contains particles that are up to 2.5 µm ($PM_{2.5}$) in size and differ in chemistry and source of origin from PM_{10}. They are generated from the condensation of high-temperature vapours and gases during combustion processes. Fine particles are composed of organic compounds, sulphate compounds, nitrate compounds, carbon compounds, hydrogen ion, ammonium, toxic metals (V, Ni, Pb, Cd, Cu, Zn, Mn, and Fe), and particle bound water (WHO, 2003 and 2004). Important components of ambient PM are also diesel exhaust particles (DEP), which are made of a carbon core with an ability to absorb a mixture of organic chemicals and metals (Fig. 1.1C).

The ultrafine particles (UFP) rise from both natural and anthropogenic sources (Kulmala et al., 2004). In ambient air, the mass of the UFP is very low, approximately 0.5-2 µg/m^3 at background levels. However, their concentration can increase several fold during episodes of high pollution (Oberdörster et al., 2005).

1.5 Physicochemical characteristics of particles as determinants of biological activity

One of the major concerns regarding NPs is their toxicity, which has been assigned to their small size and corresponding large surface area per unit mass. Other factors that drive the toxicity are the morphology, chemical composition, surface reactivity, particle number, solubility of their adducts and many more (Zhao and Nalwa, 2007; SCENIHR /002/05). Above 100 nm in size, material properties are usually affected by 'volume' or 'bulk' effects, which are dependent on atom number, their ratios and bonding characteristics. As particle size decreases, more atoms are located on their surface, thus

increasing the surface-exchange properties and resulting in an increase in reactivity. As catalytic reactions occur at surfaces, the adsorption capacity and reactivity of a nanoparticle will be higher than that of a micro particle of the same mass (Nel et al., 2009).

One key factor that determines the environmental impact of a particle is its solubility. Water - soluble particles can move randomly in aqueous environments, which can be modelled by Brownian motion theory (Nel et al., 2009; Horie et al., 2012). According to Brownian theory, significant levels of particles cause a mathematically calculated collision probability (Brown, 1828).

Nanoparticles also have a tendency to adhere to each other by forces of attraction (via Van der Waals forces) and form aggregates. This phenomenon is known as particle coagulation kinetics and occurs due to instability of small particles. A decrease in the concentration of small particles in the air will generate an overall increase in the aggregate size. In an aggregated state, the behaviour of particles changes and differs from single particles. In addition to density, particle shape and diffusion capacity influence the toxicity at the nanoscale (Renwick et al., 2001; Gratton et al., 2008). Particles can form tubes, sheets and threads, be dumb-belled or rod shaped e.g. as in needle-shaped asbestos fibres.

1.6 Exposure: Dose - response considerations

In toxicological studies, one of the main objectives is to evaluate exposure-dose-response relationships, in order to determine maximum exposure thresholds. Both, dose and dose rate can cause high bolus dose artefacts, therefore complicating the

determination of realistic nanoparticle exposure-dose-effects. For instance, a nanoparticle dose of 100 µg/mL is considered to be low, however this far exceeds the concentration ever to be encountered *in vivo*. Likewise, a dose of several hundred micrograms instilled to rodents, does not represent a realistic *in vivo* inhalation exposure (Oberdörster et al., 2005).

In vitro studies are considered to be models designed to provide background information with the aim to bridge the knowledge gap that still persists in animal studies. However, mechanistic pathways that operate at low doses may also be subject to change once the dose is increased, possibly because the cell`s or animal`s defences are overwhelmed. Therefore, the best way to assess the risk of nanoparticles toxicity would be to use a combination of *in vitro* and *in vivo* studies at nanoparticle concentrations, which most closely resemble realistic exposure levels.

1.7 The paradigms of nanoparticle toxicity and "The UFP hypothesis"

Many studies have proven that although exposure to pollutants is omnipresent, only a small part of the population succumbs to their effects. However, the presence of "nano"-sized particles in air accounts for a partial subset of respiratory and extrapulmonary diseases. Toxicity of ambient particles was defined through controlled clinical studies, which used laboratory generated UFPs to evaluate their deposition rate in healthy subjects (Seaton and Donaldson, 2005), via *in vivo* inhalation/instillation studies in animal models, such as rodents (Alessandrini et al., 2006), and *in vitro* cell-culture studies (Andre et al., 2006). Ambient UFPs were shown to have high respiratory

deposition efficiency in all healthy individuals, mainly due to the small surface area of particles. The deposition was found to be even higher in more susceptible subjects with asthma or chronic obstructive pulmonary disease (COPD) (Pekkanen et al., 1997; Penttinen et al., 2001; WHO, 2004). In addition, exposure to ambient UFPs was also found to result in increased inflammation and the generation of secondary effects, such as blood coagulation and changes in pulmonary diffusion capacity (Anderson et al., 1990; Brown et al., 2002; Oberdörster et al., 2005). Several epidemiological studies describe how manufactured nanomaterials can also induce similar acute effects in exposed workers (Mossman et al., 1990; Gardiner et al., 2001; Song et al., 2009).

In vivo animal studies with a laboratory generated UFP or ambient UFPs suggested that all particle sizes exert a general toxic effect, however, the toxicity depends on the total surface area being inhaled (Holgate, 2010). The effects of UFP toxicity were characterized by means of lung histopathology and lung lavage parameters, blood coagulation cascade effects, and the particle's ability to translocate to extrapulmonary tissues (Faux et al., 2003).

In vitro cell systems provided the first insights into the underlying biochemical mechanisms that are affected, including oxidative-stress pathways (Li et al., 2003) and proinflammatory responses (Brown et al., 2000). This can be attributed to the presence of transition metals and certain organic compounds on the surface of certain nanoparticles types (e.g. combustion generated UFPs) (Stone et al., 2007; Ghio et al., 2012). These have the ability to promote free radical release and alter cell signalling pathways, such as Ca^{2+} and cytokine signalling (Donaldson and Stone, 2003). However, the toxic outcomes also depend on dose, duration of the study, and the chosen toxic end points.

1.8 Entry portals and target tissues

1.8.1 Respiratory tract and epithelial translocation

The main mechanism of inhaled particle deposition is via diffusion into respiratory tract (Oberdörster et al., 2005). Particles smaller than 100 nm in diameter remain suspended and are deposited into alveoli, as those in the 0.1-1 nm size range are not deposited and are typically exhaled (e.g. tobacco smoke). Once the particles reach alveoli, they are usually phagocytosed by scavenger cells. Particles can also be taken up by macrophages and translocated via epithelial cells to interstitial sites, thereby causing a shift from alveolar to interstitial inflammation (Kreyling et al., 2000) (Fig. 1.2 and 1.3).

Particle movement across the epithelium can occur by three different transport mechanisms, which involve direct uptake into epithelial cells (transcellular transport), paracellular transport across tight junctions, or by an alternative bioconjugation pathway. Once particles are inside macrophages, they are either broken down by intracellular enzymes or transported to the mucociliary escalator for subsequent elimination by swallowing. These mechanisms are normally sufficiently effective to cope with air pollution, however, problems can arise when macrophages become saturated and the particle load capacity is reduced (Donaldson et al., 2001). Heavy particle loads and changes in their physiocochemical properties can cause inefficient clearance resulting in tissue inflammation and fibrosis (Ferin et al, 1992; Oberdörster et al, 1994; Oberdörster et al, 2000).

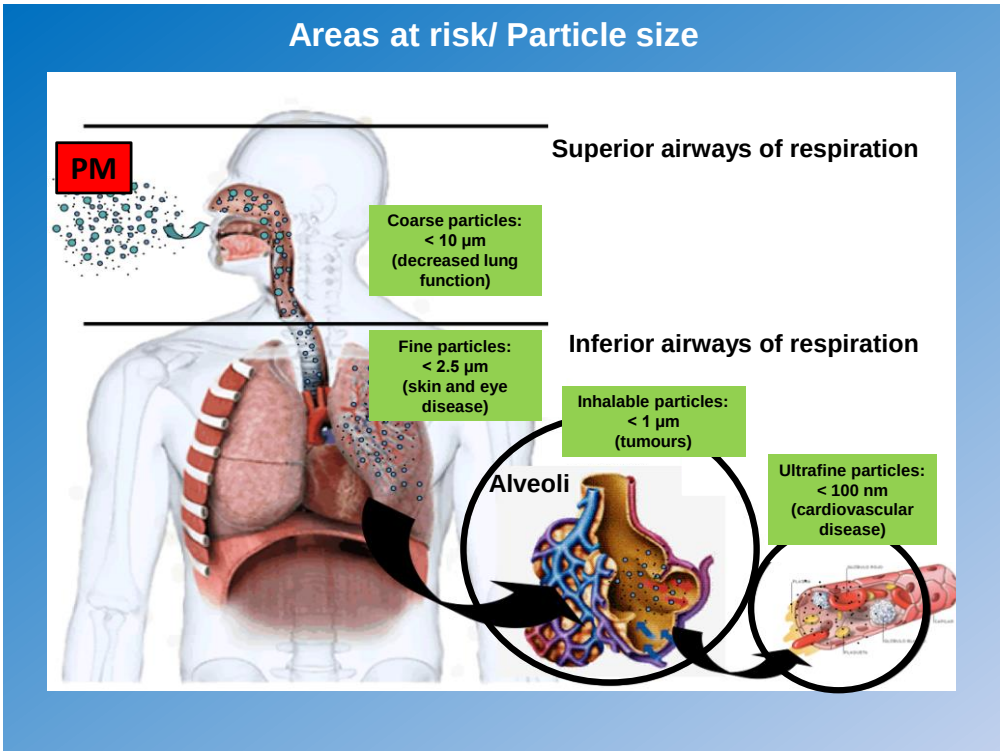

Fig. 1.2: The particulate matter (PM) entry portal and target respiratory tract areas at risk. The inhaled particle size directs the particle deposition. (Adapted from Guarieiro and Guarieiro, 2013).

1.8.2 Dermal exposure and translocation

The penetration of particles through the skin is limited to particles that are smaller than 1 µm, exceptions are areas where the skin has been scratched or injured. To date, a small number of studies have investigated the ability of nanosized material particles (such as titanium dioxide and zinc oxide found in sunscreen formulation) to elicit a systemic effect (Lademann et al., 1999; Nemmar et al., 2003; Schulz et al., 2002). Overall, there are no clear consensus regarding skin absorption rates and the resulting toxic potential, and more research is needed to define and understand the interaction of particles and the skin (Osmond and McCall, 2010; Crosera et al., 2009).

1.8.3 Neuronal translocation

Oberdörster et al., 2005 have reviewed the potential of inhaled solid particles to be translocated to the brain via the olfactory nerve, a notion that was first described more than 60 years ago (Bodian and Howe, 1941). Likewise, epidemiological studies from a heavily polluted area in Mexico City reported that exposure to ambient UFPs caused significant inflammatory and neurodegenerative changes in the olfactory mucosa, bulb, and cortical and subcortical brain structures in dogs (Calderon-Garcidueñas et al., 2002).

1.8.4 Exposure via the gastrointestinal tract

In humans, the gastrointestinal (GI) epithelium utilizes both transcellular and paracellular pathways to transport UFPs (Holgate, 2008). The first pathway involves a clearance mechanism via a respiratory tract mucociliary escalator, which after UFPs have been swallowed, passes them down into the GI tract. Secondly, UFPs can also be transported directly via ingestion into the GI tract (Hillyer and Albrecht, 2001). Direct ingestion usually involves the administration of food or water containing the UFPs. Although not many studies have investigated the uptake and disposition of UFPs by the GI tract in humans, ecotoxicological nanoparticle studies involving fresh water species and species used in a regulatory toxicological context (e.g. *Daphnia magna*, *Oncorhynchus mykiss*, and *Chlorella kessleri*) have provided more insights into the GI mediated uptake of nanoparticles. For example, *D. magna* accumulated fluorescent labelled polystyrene beads in small oil storage droplets, having successfully passed the epithelial gut barrier (The Royal Commission on Environmental Pollution 27th report; Novel Materials in the environment: The case of nanotechnology). It has been suggested

that nanoparticles can be absorbed and transported, via the lymphatic system, to other interstitial organs (Hillyer and Albrecht, 2001), however, others have suggested that once passed through the GI tract, UFPs are rapidly eliminated or excreted (reviewed by Krug and Wick, 2011; Oberdörster et al., 2005).

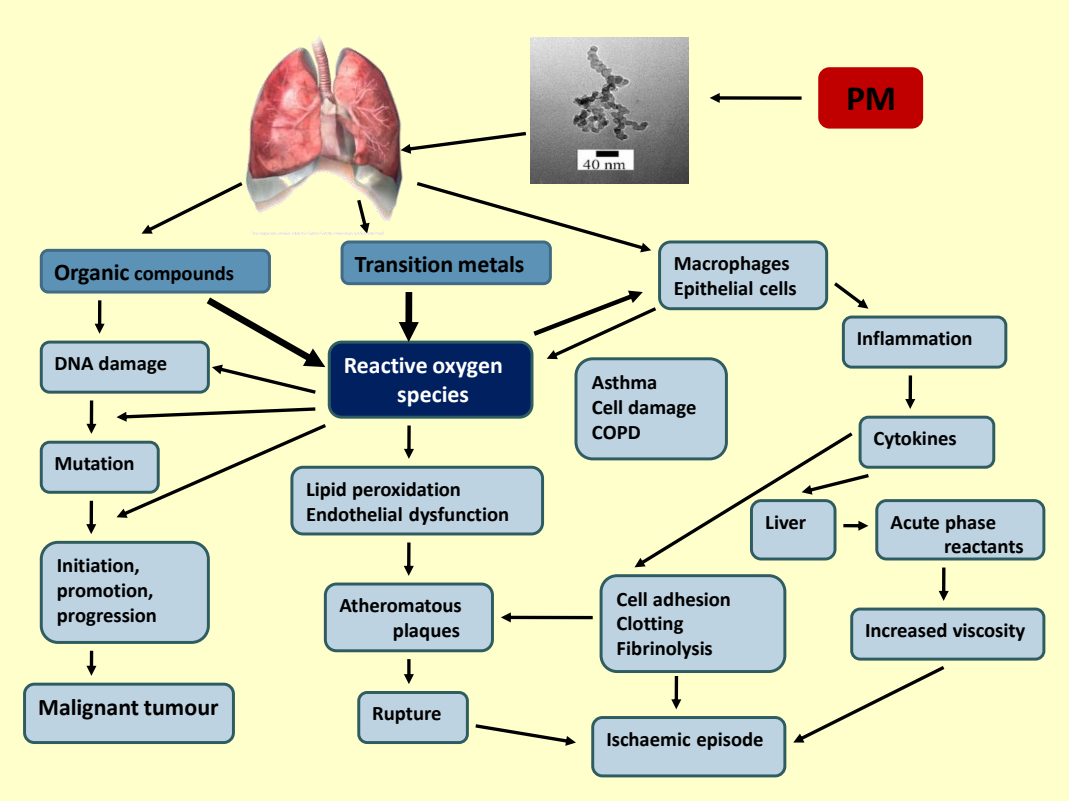

Fig. 1.3: Interactions that may be generated/activated via ultrafine particles (UFP) or nanoparticles (NP) translocation to other organs. (Adapted from Wild et al., 2008).

As mentioned before, particle size and surface chemistry influence particle uptake in the GI tract. As GI fluids are high in ionic strength, this will also encourage particle aggregation (Nel et al., 2009; Horie et al., 2012). Based on the available information derived from *in vitro* and *in vivo* studies, a complex sequence of events involves the interaction and transportation of UFPs, and possible toxic endpoints (Fig. 1.3).

Incidentally, this is also one of the major exposure pathways of UFPs in a nematode model organism (Mohan et al., 2010). Internal aggregation of particles might cause a mechanical obstruction of the intestines and thus increase the possibility of secondary effects to occur e.g. the bag of worm phenotype in *C. elegans* (Pluskota et al., 2009).

1.9 Oxidative stress

According to Sies (1991), oxidative stress is defined as "a disturbance in the prooxidant-antioxidant balance in favour of the former, leading to potential damage". To simplify the definition, oxidative stress is the imbalance between reactive oxygen production and the organismal ability to detoxify the resultant reactive intermediates.

1.9.1 The free radical theory

Reactive oxygen species (ROS) includes an array of chemical molecular species, such as free radicals (e.g. superoxide anions and hydroxyl radicals) and peroxides (e.g. hydrogen peroxide), derived from the metabolism of oxygen. Under normal physiological conditions, electrons circle around atoms in pairs (Kelly, 2003; Rahman and MacNee, 2000; Schafer and Buettner, 2001), however, atoms with unpaired or odd number of electrons markedly increase their reactivity and generate free radicals. Free radicals possess the ability to react indiscriminately with other molecules via oxidation and reduction processes, or "electron stealing" (Gaetke and Chow, 2003), a reaction that can cause extensive cellular damage. The extent of damage depends on the ability of the system to neutralize and eliminate the generated ROS. Overall ROS levels are maintained and regulated via sophisticated enzymatic and non-enzymatic antioxidant

defence systems that include superoxide dismutase (SOD), catalase (CAT), or glutathione (GPx) peroxidase (Bremner, 1998) (Fig. 1.4).

Impairment in maintenance of ROS levels can result in decreased antioxidant protection, an over-abundance of oxidants, and a failure to repair generated oxidative damage. Increased ROS levels can damage and disturb the function of key organic substrates (DNA, proteins, and lipids) and thereby contribute to a variety of disease states, accelerated cell-aging processes or even cell death (Tapiero et al., 2003) (Fig. 1.4 and 1.5).

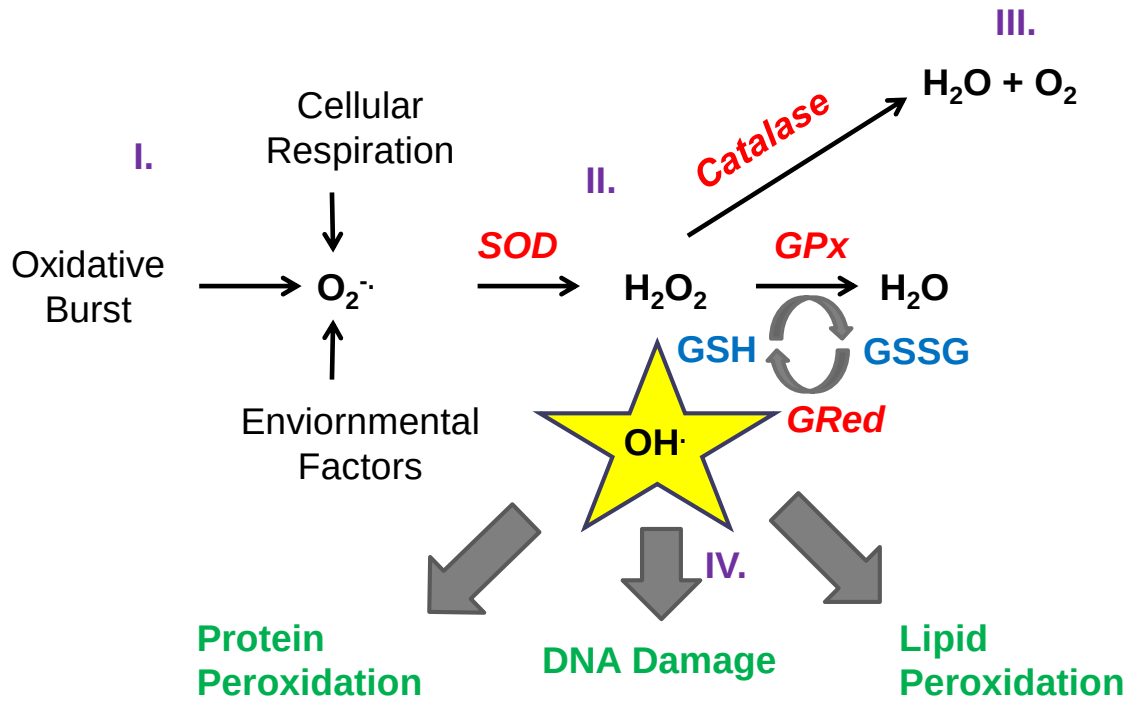

Fig. 1.4: Oxidative stress and cellular enzymatic defence against free radicals. Under normal physiological conditions, the use of oxygen by cells with aerobic metabolism generates potentially deleterious reactive oxygen metabolites. (Adapted from http://www.biozentrum.uni-frankfurt.de/Pharmakologie/EU-Web/index.html).

1.9.2 Air pollution, ultrafine, and nanoparticle generated oxidative stress

Intracellular free radicals are the by-product of normal cellular and metabolic reactions, such as mitochondrial energy production or the cytochrome P450 liver detoxification enzyme system (Cadenas et al., 1977). Other endogenous sources of ROS include peroxisomes, lipoxygenases and the NADPH oxidase enzyme system.

Exogenous sources of ROS production arise from chemotherapeutics, excessive exposure to ultraviolet light, cigarette smoke, consumption of alcohol, medications (e.g. glutathione-depriving drugs), trauma, bacterial or viral infections, and environmental toxins (e.g. transport and industrial emissions).

One of the major exogenous sources of ROS production is air pollution. The exposure to different air pollutants (i.e. large fibres, ambient particles, and engineered nanoparticles) result in the generation of ROS, the development of oxidative stress and inflammation (Brown et al., 2001; Brown et al., 2002; Kelly, 2003; Delfino et al., 2005) (Fig. 1.5). It is still a matter of debate which components of particulate pollutants mitigate adverse health effects. However, evidence from toxicity studies on different synthetic nanoparticles (e.g. asbestos), suggests that it is the small size (less than 100 nm in dimension), the surface reactivity, chemical composition (e.g. organics, transition metals), and dose, that stimulate the production of ROS and cause oxidative stress (Stone et al., 2007; Li et al., 2008). This attractive hypothesis, which has been proposed to be equally relevant to the oxidation potential of ambient particulate matter at the air-lining liquid interface, may explain the heath-associated events observed in exposed populations (Kelly, 2003; Xia et al., 2006; Ghelfi et al., 2008; Ghio et al., 2012).

Fig. 1.5: Mechanisms of particle-induced ROS generation inside and outside the cell.

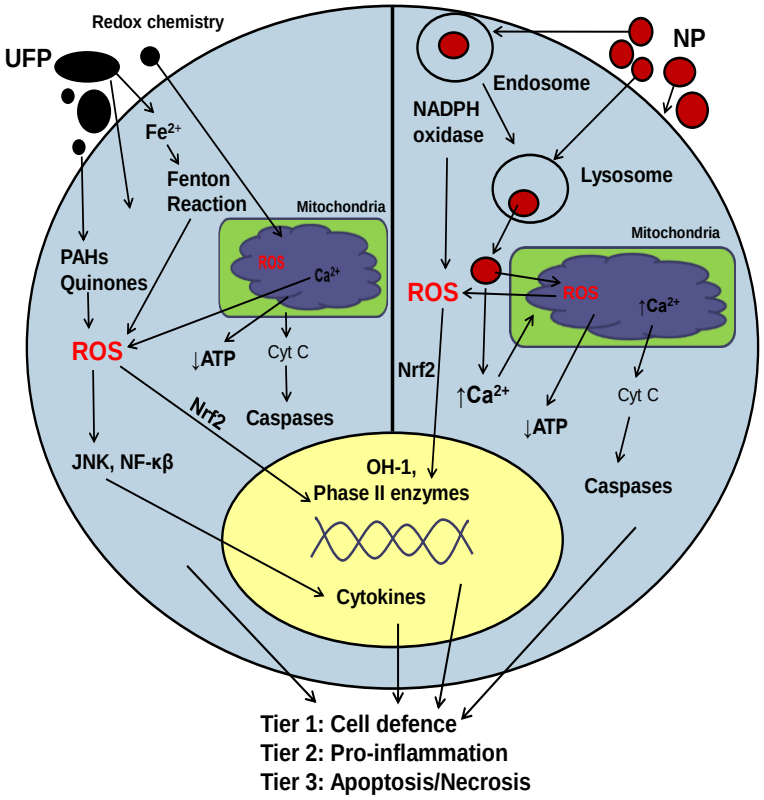

Particle induced oxidative stress will cause cells to undergo different levels of responses, which can be classified as antioxidant defence (Tier 1), pro-inflammatory effects (Tier 2), and cytotoxicity (Tier 3).

Each of these tier responses are activated by different mechanisms in response to specific biological sensors. In the Tier 1 response, the induction of anti-oxidant enzymes (by phase II transcription factors (e.g. Nrf2)) restores the cellular redox equilibrium. If the level of oxidant injury increases, cellular mitogen-activated protein kinases (MAPK-kinases) and the nuclear-factor-kappa B (NF-κB) - cascades induce pro-inflammatory cytokine and chemokine signalling (Tier 2).The highest level of oxidative stress causes activation of cytotoxic cell death/apoptosis via damaging mitochondrial membrane permeability and cause the release of pro-apoptotic factors (Tier 3). The UFPs carry organics and transition metals, which can undergo redox reactions. Nanoparticles enter the cell either by endocytosis, or phagocytsis. Inside the endosome, NPs can generate ROS directly via NADPH oxidase. Endosomes can also fuse with the lysosomes, and once these breaks, NPs can escape and cause ROS damage to cellular organelles (Adapted from Li et al., 2008).

1.10 Toxicity of nanomaterial

1.10.1 Zinc oxide (ZnO) NPs

The expansion of nanotechnologies and the increased synthesis of novel "nano-materials" have raised concern over their safety and impact on human and environmental health. Nanoparticles, such as ZnONPs, are used in some industrial applications, such as sunscreens, cosmetics, food products and medicine (Dafour et al., 2006; Wang et al., 2004; Tayel et al., 2011; Nohynek et al., 2010). Although beneficial to the industry, many *in vitro* and *in vivo* studies have shown that exactly these physicochemical characteristics ("nano") can induce cell injury and generate ROS, giving rise to adverse biological outcomes (Rohrs, 1957; Colvin et al., 2003; Shilling et al., 2010; Nowack et al., 2012).

Zinc oxide (ZnO) NPs belong to a group of metal oxide nanoparticles, which also include $Fe_2O_3^-$, TiO_2^- and CeO^- NPs. The mechanism by which these particles induce oxidative stress in organisms is believed to be similar to ambient UFP, where transition metals on the particle surface can generate $O^{\bullet-}$ via the Fenton reaction (Fig. 1.5). However, in case of ZnONPs, the dissolution and shedding of metal ions ($ZnO \rightarrow Zn^{2+}$) from the particle surface can also catalyse ROS production (George et al., 2010; Li et al., 2011; Polynton et al., 2011; Wang et al., 2009). Finally, some particles have photocatalytic properties and can generate ROS when exposed to light. UV light can generate electron hole pairs in nanoparticles (e.g. TiO_2), which can participate in the generation of $O^{\bullet-}$ and OH^- radicals (Li et al., 2008) (Fig. 1.6).

Due to the rapid expansion of nanomaterial use, the risk has increased that NPs leak into the environment, become airborne, and thereby contribute to adverse health outcomes (such as pulmonary diseases and cancer).

1.10.2 Carbon black (CB) particles

Carbon or carbon black (CB) particles are produced during incomplete combustion processes of biomass, biofuels, and fossil fuels, as well as in industry (e.g. print, tire, rubber) (IARC, 2010). CB, like other ultrafine particles have a high surface-area-to-volume ratio, however chemically it is distinct, as its surface is inert. For this reason, it has been stipulated that CB can be used as a negative control due to the absence of redox activity (Guo, 2009). However, CB particles have a capacity to absorb light, impair the visibility (i.e. formation of haze and fog), reduce agriculture production, and global warming (EPA, 2012), thereby contributing to adverse impacts on human health. To date, there is insufficient scientific evidence associating direct CB effects with adverse respiratory and cardiovascular health outcomes. Nevertheless, ultrafine CB particles play an important role in industrial applications, therefore there is a potential for occupational exposure (Harber et al., 2003; Hailemariam et al., 2012). The health literature from human occupational studies, and from studies on CB exposed rodents, has suggested that CB might be carcinogenic (Nikula et al., 1995; Dasenbrock et al., 1996) and be responsible for adverse cardiovascular effects and inflammation (Harber et al., 2003; Hailemariam et al., 2012; Donaldson et al., 2005; Mills et al., 2006), but probably not by 'direct' oxidant effects.

CB particles are modulated by physical and chemical processes once in the environment, which can attenuate or enhance their properties. An additional chemical coating, such as non-bioavailable PAH (polycyclic aromatic hydrocarbon) or trace metals on their outer otherwise inert carbon surface, can turn these particles into reactive entities that can undergo redox cycling reactions (Fig. 1.6) (Stone et al., 1998; Hussain et al., 2010). However, further research is needed in order to understand in detail the adverse health risks of CB particle exposure.

1.10.3 Urban particulate matter (PM)

In 1997, the U.S. Environmental Protection Agency (EPA) issued new standards for fine, respirable air particulate matter (PM) less than 2.5 µm ($PM_{2.5}$) in size. The National Institute of Standards and Technology (NIST), an agency of the U.S. Commerce Department, have collaborated with the EPA to develop Standard Reference Material (SRM) 1648a for Urban Particulate Matter in order to support the controlled measurement of organic species in the fine PM fraction and to expand the quality assurance capabilities. NIST 1648a is an atmospheric PM that was collected in an urban area. It is a complex mixture consisting of particles that vary in their size, shape, chemical composition, and consists of metals, soot, dust and soil. It is routinely used as a reference material to evaluate and standardize inorganic analyses of atmospheric PM and similar matrix materials (Huggins et al., 2000; Ball et al., 2000; Hatzis et al., 2006). Multiple independent analytical methods have defined the certified concentrations of 24 elements (Huggins et al., 2000; http://ts.nist.gov/MeasurementServices/Reference Materials/PUBLICATIONS.cfm.).

Since NIST is composed of small ultrafine particles and a large surface area, numerous transition metals (e.g. Fe, Cu, Ni, Co and Cr), and high levels of silica and sulphate, it has an ability to produce ROS and generate oxidative stress via the Fenton and Haber Weiss chemistry (Li et al., 2003) (Fig. 1.5 and 1.6). In addition, the redox-cycling organic compounds (e.g. quinones, PAH) give rise to superoxide radical formation ($O^{\bullet -}$) (Fig. 1.5 and 1.6). The toxic potential of NIST can be correlated to its chemical composition, and therefore allows the assessment of complex cellular antioxidant and detoxification pathways. NIST can therefore be utilized to study, both short- and long-term exposure effects of PM, and to develop new hierarchical standardized biological models.

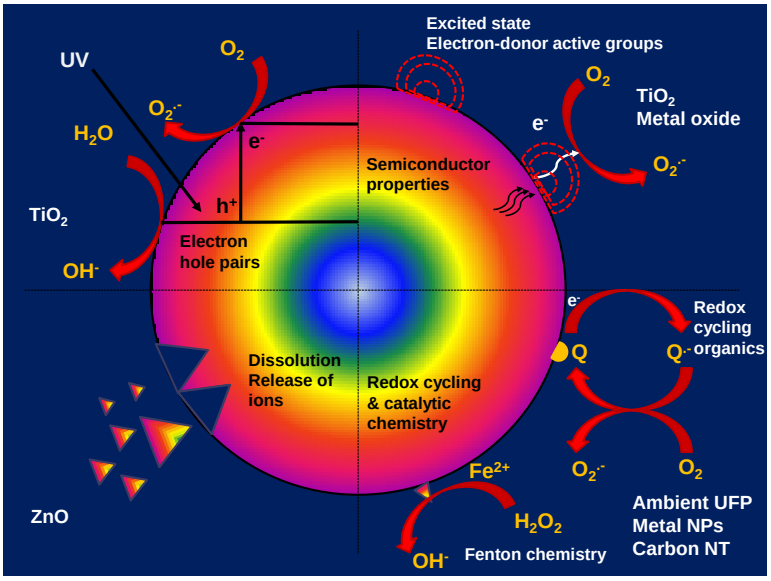

Fig. 1.6: Nanoparticle surface properties mediate the mechanism by which ROS is generated. Dissolution of metal ions from metal oxide nanoparticles (ZnONPs) surfaces can generate ROS and cause particle toxicity. The toxicity of ambient UFPs and CB particles is usually driven by its surface chemical composition, and can undergo either redox cycling (e.g. organics) or catalytic reactions (e.g. transition metals). (Adapted from Li et al., 2008).

1.11 *C. elegans* as experimental model

C. elegans was first described by Maupus (1900) more than 100 years ago. However, not until Sydney Brenner`s seminal paper in 1974 did it emerge as an experimental model organism for molecular and developmental biology (Brenner, 1974). Sequencing the complete 97-Mb genome (Hillier et al., 2005), provided an overview into its genome architecture, which is 20 times the size of the *E. coli* genome but only 1/30 of a human genome.

Caenorhabditis is a small (~ 1 mm in length) non-parasitic member of the *Rhabditidae*, which is a large and diverse group of nematodes (roundworms) usually found in

terrestrial habitats. The Bristol strain was isolated from a mushroom compost near Bristol in England by L.N. Staniland from the National Agricultural Advisory Service, London (Nicholas et al., 1959). The N2 laboratory line was created from the Bristol culture by Sydney Brenner in 1964.

An adult *C. elegans* has a simple unsegmented, vermiform, with a bilaterally symmetrical body shape. The typical nematode body plan consists of basic animal tissues (muscle, nerve, gut and skin), a cuticle integument that is located at the anterior end and an anus at the posterior end (Fig. 1.7A). Primarily, it feeds on bacteria and microbes. Adult species are usually self-fertilising, protandrous hermaphrodites (XX), but in rare cases they can develop into males (XO), which present overall only 0.05-0.1 % of a total wild-type N2 nematode population (Herman et al., 1982). The nuclear genome is organized into six chromosomes (Coulson et al., 1991), five of which are diploid autosome chromosomes and one a sex chromosome. The adult hermaphrodite has 959 somatic cells, of which 81 are muscle cells and 300 are neurons, plus about 2000 germ cells.

The life-cycle of *C. elegans* is very rapid; a worm matures in ~3 days from fertilized egg to an adult when cultured under optimum laboratory conditions i.e. 20°C, grown on Petri dishes, with *E.coli* bacteria as a food source (Fig. 1.7B). *C. elegans* is capable of rudimentary behaviours, including, sensory responses to smell, touch, taste and temperature as well as some more complex behaviour, such as social behaviour, male mating, learning and memory (Rankin et al., 2002; DeBono et al., 2003). Under stressful conditions, such as the absence of food, overcrowding, or increased temperature, the L1 stage hermaphrodite can enter an alternative developmental stage, the non-aging dauer larva stage. In dauer, *C. elegans* is resistant to environmental stresses and can survive for up to three months in absence of food. Once the conditions

become favourable again (e.g. presence of food), worms exit the dauer stage and resume their development (Wood, 1988).

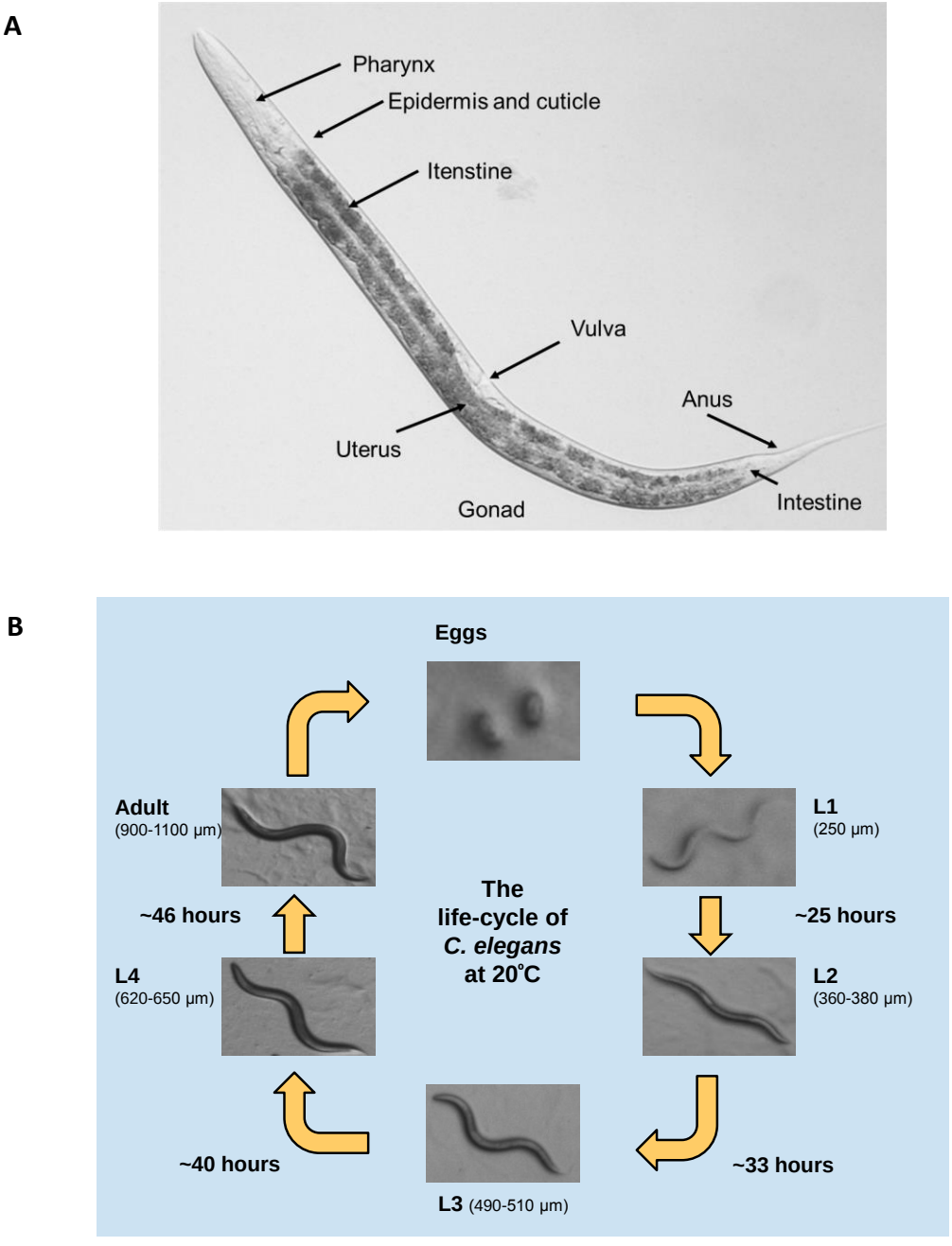

Fig. 1.7: Anatomy of an adult hermaphrodite (A) and life cycle of *C. elegans* at 22°C (B). The whole life-cycle takes about 3 days at 20°C. *C. elegans* develops through four larval (L1 to L4) stages, which are separated by moults. Following the reproduction cycle, *C. elegans* start to age and lose vigor. The average life-span of an adult is approximately of about 2–3 weeks.

Several characteristics and attractive features have contributed to it being one of the premier animal model organisms in biological research, including neurobiology, genetics, developmental biology and more recently environmental toxicology. Some of these features include its ease of handling and inexpensive maintenance, the invariant and fully described developmental program, a short and prolific life-cycle, a well characterized and fully sequenced genome, genetic manipulability, transparent body and small body size. Other characteristics include a rapid generation time, which allows the application of genetic screens.

C. elegans are hermaphrodites that produce 200-300 "self-progeny", thus a large number of worms can be generated. Nevertheless, sexual reproduction can be introduced, which offers the convenience of genetic stocks to be constructed by mating (Wood, 1988). In addition, the transparent body allows the use of reporter gene fusions thus permitting the visualisation of *C. elegans* transcript and protein expression patterns. Based on the ability to observe animal cellular development, a complete cell lineage map was constructed (Sulston and Horvitz, 1977). Their genome has been intensively studied and a large library of knockout (KO) mutants is available. Established genetic methodologies, such as mutagenesis, transgenesis and RNA interference (RNAi) libraries provide exquisite options to study and manipulate *C. elegans* at the molecular level. Bioinformatic analysis has identified that 60-80 % of human genes have homologues in *C. elegans*. Therefore, the nematode model presents a powerful tool to investigate human diseases.

1.11.1 Oxidative stress and *C. elegans*

The nematode *C. elegans* is an emerging toxicity model, as it provides an integrated view of the organismal response to diverse biochemical and environmental stressors. To date, most of the attention has focused on the hypothesis that oxidative stress contributes to the nematode aging process (Honda and Matsuo, 1992; Honda et al., 1993). However, the presence of low concentrations of oxygen increases the life-span of nematodes (Honda et al., 1993). Similar findings were observed when the nematodes food supply was supplemented with antioxidants. The isolation of life-extension mutants, unravelled the gene network that underlies *C. elegans* longevity and provided insights into the resistance mechanisms to oxidative stress (Kenyon et al., 1993). Furthermore, proteomics research has extended our understanding regarding the intricate relationship between oxidative stress and protein deposition that result in age-associated neurodegenerative diseases (Brignull et al., 2007).

1.11.2 *C. elegans* metallothionein and phytochelatins

Phytochelatins (PCs) and metallothioneins (MTs) are cysteine-rich, metal-binding proteins. MTs (MW ranging from 3500 to 14000 Da) are gene-encoded cytosolic polypeptides, which can also accumulate in lysosomes and in the nucleus, whereas PCs are enzymatically synthesized peptides (Cobbett, 2000).

Metallothionein (MT) was first discovered and isolated as a cadmium-binding protein from equine renal cortex in 1957 by Vallee and Margoshe. MT have the ability to bind a wide range of metals including cadmium, zinc, mercury, copper, arsenic, silver, etc. In vertebrates there are four main isoforms (MT-1, MT-2, MT-3 and MT-4). Whilst, MT-1

and MT-2 are expressed in almost all tissues, MT-3 is specific to brain and MT-4 to stratified squamous epithelia (Cobbet and Goldsbrough, 2002). Human MT-1 and MT-2 contain many splice variants, and provide protection against metal toxicity and ROS.

The nematode *C. elegans* genome contains only two MTs, *mtl-1* and *mtl-2*, respectively that are both located on chromosome V. Like their mammalian counterparts, they are known to be involved in heavy metal binding, detoxification (Freedman et al., 1993), radical scavenging and the protection against oxidative stress. Whilst *mtl-1* is continually expressed in the lower pharyngeal bulb, *mtl-1* and *mtl-2* are both induced in the intestine following the exposure to metals, oxidative stress, glucocorticoids or hydric stress. MTs role in oxidative stress has also been confirmed by MT knockout mutants (Zeitoun-Ghandour et al., 2011). Overall, the presence of multiple isoforms, their conservation in expression and structure, strongly indicates that MTs play an important function in cell biology.

Phytochelatins (PCs) were first discovered in fission yeast in 1981 and were initially named cadystins. The name was changed to phytochelatin in 1985, when they were identified in higher plants. In 1989 the enzyme phytochelatin synthase (PCS) was identified (Grill et al., 1989). PCs have since also been found in some algae, including cyanobacteria, earthworms and nematodes.

PCs are small, low molecular weight oligomer proteins (MW of 40.8 kDa in nematodes). They are synthesized from the ubiquitous thiol tripeptide of glutathione and related thiols (GSH, γ-Glu-Cys-Gly) by the transpeptidation reaction catalyzed by PC synthases (γ-glutamyltransferase). Their major function is to act as chelators in heavy-metal detoxification. *C. elegans* contain only one PC synthase *pcs-1*, which is located on chromosome II. *Arabidopsis thalina* (Buchanan et al., 2000) and nematode PC synthase knock-out mutants (Hughes et al., 2009) provide evidence that their sensitivity

to cadmium increases, however their overall life-history traits, when raised in control conditions, reflect those of the respective wild-types. The presence of heavy metal ions induces the reactivity of the phytochelatin synthase, thereby allowing metal ions to bind glutathione (GSH), which contains a blocked thiol group, faster. When the surrounding environment contains high concentrations of metal ions, the cell will produce more PCs in order to survive. This suggests that the PCs primary role in nematodes must be the protection from metal toxicity. The proposed mechanism has been explained in detail by Hughes et al. (2009).

1.11.3 The *C. elegans* superoxide dismutases (SODs)

The antioxidant superoxide dismutase (SOD) is the only eukaryotic enzyme known to be able to catalyse the dismutation of harmful superoxide (O_2^-) into oxygen and hydrogen peroxide. Studies in yeast (Longo et al., 1996), flies (Phillips et al., 1989), and mice (Elchuri et al., 2005) have confirmed that loss of SOD activity results in an increased sensitivity to oxidative stress and shortens the life-span. Therefore, these enzymes provide a major first-line defence against ROS damage in eukaryotic organisms.

SODs were first known as a group of metalloproteins, whose functional activity was first described in 1969 by McCord and Fridovich, while studying an enzymatic function for erythrocuprein (haemocuprein) (McCord and Feridovich, 1969). There are two common forms of the SOD families: a copper and zinc SOD (Cu/Zn SOD), which is located in the cytosol; and a manganese SOD (Mn/SOD), which is located in the mitochondrial matrix. While most of the eukaryotic organisms contain 2 or 3 different superoxide (*sod*) genes, the nematode *C. elegans* genome contains five SOD isoforms

(*sod-1-5*). The *sod-1* and *sod-5* are cytoplasmic Cu/Zn SOD isoforms, *sod-2* and *sod-3* encode for Mn/SOD and are both localized to the mitochondrial matrix, and *sod-4* encodes for extracellular Cu/Zn SOD (Back et al., 2012). *sod-1* contributes 80 % to the total SOD activity, followed by *sod-2* during normal nematode development (Doonan et al., 2008).Two other SOD isoforms, *sod-3* and *sod-5*, functionally play similar role as *sod-1* and *sod-2*, and are found to be up-regulated when nematodes are exposed to oxidative stress, as well as in *daf-2* mutants or when worms enter dauer stage.

In nematodes, SOD-1 (a 180 aa protein) was found to be ubiquitously expressed throughout most tissues, and SOD-2 (221 aa) was primarily expressed in the head and tail of wild-type nematodes. In contrast, SOD-3 (218 aa) is mainly expressed in the pharynx, ventral cord motor neurons, and intestinal cells (Honda et al., 2008). Studies utilizing nematode SOD knock-out mutants have shown that SOD activity is essential for nematode survival of acute stresses, such as the exposure to the herbicide paraquat, however there is no clear evidence that SOD activity is dispensable for normal nematode life-span (Van Raamsdonk and Hekimi, 2012; Doonan et al., 2008). In fact, one study showed that when the SOD gene is increased, the life-span remains unchanged or decreases (Doonan et al., 2008; Van Raamsdonk and Hekimi, 2009). However, in another study an increase in *sod-1* and *sod-2* expression resulted in an extension of the nematode life-span (Honda and Honda, 1999).

Overall, the *C. elegans* SODs genes are transcriptionally activated in the presence of heavy metals e.g. cadmium (Roh et al., 2009); herbicides e.g. paraquat and juglone (Van Raamsdonk and Hekimi, 2009; Yanase et al., 2009), as well as nanoparticles e.g. AgNPs (Roh et al., 2009). This suggests that in nematodes, SODs must provide a functional role in maintaining stress levels.

1.11.4 The *C. elegans* skinhead (SKN-1) bZip transcription factor

In vertebrates, the primary cellular defence against oxidative stress involves expression of phase II detoxification enzymes, which are under transcriptional control of the two Nuclear factor-erythroid-related factor 1 and 2 proteins (NF-E2-related factors Nrf1 and Nrf2 proteins) (Hayes and McMahon, 2001). The Nrf proteins belong to the Cap-N-Collar (CNC) family of basic leucine zipper transcription factors, which recognize the antioxidant response element (ARE) in the promoter of target genes (Osburn and Kensler, 2008) and allow their transcription to take place.

Like Nrf2 in mammals, the nematodes SKN-1 is a single CNC protein, which is required for regulating oxidative stress and mobilizing the conserved phase II detoxification response. A skinhead (SKN-1) is a bZip transcription factor (functionally) orthologous to the mammalian Nrf transcription factors (Bowerman at al., 1992). SKN-1 is distinct from any other bZip proteins, as it lacks a leucine zipper, a DNA-binding domain (Blackwell, 1994). In *C. elegans*, SKN-1 transcription factor is located on chromosome IV. Functionally, it plays an important role in the early stage of nematode embryogenesis. Maternally expressed SKN-1 specifies the fate of a single cell, the EMS blastomere (a mesodermal precursor), giving rise to the development of mesodermal tissues (such as pharyngeal muscle) and intestinal cells (Bowerman et al., 1992). Postembryonic, SKN-1 plays a functional role in the p38 mitogen activated protein kinase (MAPK) pathway in regulating the oxidative stress response (Inoue et al., 2005). In addition, it plays an essential role in regulating adult nematode life-span via a DAF-2-mediated insulin/IGF-1-like signalling cascade (Tullet et al., 2008). Studies have shown that in response to oxidative stress, the AKT-1, AKT-2, and SGK-1 insulin signalling kinases (all downstream of DAF-2) (Tullet et al., 2008), and PMK-1 (involved in p38 MAPK signalling cascade) (Inoue et al, 2005) can phosphorylate SKN-

1, followed by its accumulation in the intestine nuclei and target gene activation. SKN-1 that is constitutively active both in intestinal cells and in ASI neurons can contribute to an increase in *C. elegans* life span, delays aging, and provides protection against oxidative and xenobiotic stress, presumably through endocrine mechanisms. Whole genome transcriptional profiling of *C. elegans* identified that SKN-1 regulates multiple detoxification and antioxidation genes, with functional categories including 20 glutathione-S-transferases (GSTs), 8 short-chain dehydrogenases, 10 glucoronosyltransferase, 2 cytochrome P450 proteins (CYPs) and two ABC superfamily genes (e.g. *ctl-2*; *sod-1*; *gcs-1*; *gst-4*; *gst-38*; *ugt-1*) (Choe et al., 2012). Nematode *skn-1* mutants are also more sensitive to xenobiotic challenges, and have a shortened life-span (Ann and Blackwell, 2003; Inoue et al., 2005). Overall, the *C. elegans* SKN-1 mediated detoxification pathway seems to be part of an ancient, evolutionary conserved defence mechanism against ROS.

1.12 Nanoparticles and ambient particular matter in *C. elegans*

Although, the toxicity of natural particles has, to date, not been studied in *C. elegans* the potential effects of synthetic nanoparticles has. Toxicological research included the screening of synthetic or manufactured NPs, such as zinc oxide (ZnO), aluminium oxide (Al_2O_3), and titanium dioxide (TiO_2) (Wang et al., 2009), silver nanoparticles (Roh et al., 2009; Hunt et al., 2013), platinum NPs (Kim et al., 2008), cerium oxide NPs (Arnold et al., 2013), cadmium (Roh et al., 2009), depleted uranium toxicity (Jiang et al., 2009) and silica-nanoparticles (Pluskota et al., 2009). In summary, most of the studies have provided evidence that NPs induce premature degeneration of reproductive

organs (the bag of worm phenotype, which is characterised by intracorporal hatching of eggs in the parent animal) which might involve their innervation. Some results have also suggested that NPs (e.g. AgNPs) reduce the nematode life-span, probably in response to the particle mediated generation of reactive oxygen species (ROS), and affect nematode development (Hunt et al., 2013). Limited information is known about the NPs biokinetic behaviour, toxicity *in vivo* and their contribution to disease. The use of sensitive nematode mutants combined with functional genomic tools has proven to be a powerful approach to assess the physicochemical toxicity of NPs (qRT-PCR and microarrays e.g. Roh et al., 2009).

Overall, these findings set the stage for this thesis in which the risks of exposure to both synthetic (zinc oxide NPs) and natural (carbon black, and urban particulate matter) nanoparticles was investigated with the ultimate aim to unlock (some of) the complexity of their mechanistic toxicology.

1.13 Aims and objectives

One of the central goals of this study will include complete baseline studies to determine the acute and chronic toxicity of 30nm NanoSun ZnONPs, carbon black (M120), and atmospheric particulate matter (NIST1648a) on wild-type, metal hypersensitive and oxidative stress sensitive nematode mutants. Endpoints measured will encompass life cycle traits (growth, brood and lifespan) and the overall intracellular reactive oxygen species (ROS) production by a fluorescence-based DCFDA probe approach. Transmission electron microscopy (TEM), dynamic light spectroscopy (DLS), and NanoSight NTA techniques will be used as tools to verify particle behaviour within the test solutions. Alteration in the nematode metabolic profile will be

determined by Raman spectroscopy. In addition, whole genome microarray, qPCR, and microscopy will be utilized to define transcriptional responses in order to assess the mechanistic basis of particles toxicity.

The objective of this work will be the utilization of rapid screening processes that measure toxic indices of chemical compounds, and provide fundamental insights into understanding of their toxicity. In addition, baseline studies will be conducted to test whether nematodes can serve as a valuable bioindicator for investigating natural ambient toxicity for future use. Therefore, by combining molecular and organismal / phenotypic assays, it is envisaged to dissect the multi-factorial responses and health risks of PM toxicity. The achievements and results of this challenge are addressed in detail in chapters three, four and five. The final chapter compares and contrasts the findings of the experimental chapters, and addresses the data gaps and future research needs in nanoparticle research.

CHAPTER TWO

Materials and methods

2.1 Materials and chemicals

The sources of suppliers of consumables, materials, and reagents are summarised in Table 2.1 and 2.2. All buffers and solutions routinely used in this study were prepared according to the compositions listed in Table 2.3.

Table 2.1: A list of suppliers of consumables.

Supplier	Consumables
ABGene, UK	0.2 mL PCR tubes; 1.5 mL PCR tubes
Alpha Laboratories, UK	Cryogenic vials, pipette tips
Applied Biosystems, UK	qRT-PCR plates and optical lids
Becton, Dickinson and Company, UK	15 mL Falcon™ conical polystyrene tubes; 50 mL Falcon™ round bottom polystyrene tubes
Fisher Scientific, UK	96-well multiwell plates and lids
Greiner BioOne, Germany	Petri dishes (35 mm, 60 mm, and 90 mm) 12-well multiwell plates and lids
Sigma Chemical Company, UK	Acid washed glass beads
StarLabs, UK	Pipette tips (different sizes)
Sterilin Ltd, UK	Serological pipettes (10 mL, 25 mL)

Table 2.2: List of materials and reagents used in this study and their supplier.

Supplier	Materials and Reagents
ACROS, organics, UK	$MgSO_4$, Na_2HPO_4, K_2HPO_4
BD (Becton, Dickinson and company), UK	Bactoagar, Bactopeptone
BDH, UK	Sodium hydroxide (NaOH)
Bioron, Germany	DNA markers
EMD milliband, US	pH strips, pH paper roll
Invitrogen Ltd, UK	10 × TAE buffer
MP Biochemicals, France	High performance liquid chromatography (HPLC) water, Agarose, Glycerol, Ethidium bromide (EtBr)
OXOLID limited, UK	Phosphate buffered saline (PBS)
Promega Corporations, UK	Reverse Transcription Kit, M-MLV Reverse Transcriptase, GoTaqFlexi Taq Polymerase and buffers, dNTPs
Roche Applied Science, UK	Universal ProbeLibrary qPCR probes
Roche Diagnostics, UK	qPCR ROX master mix
Sigma-Aldrich, UK	Tri-reagent, Oligo dT nucleotides, all customed synthesised primers oligonucleotides, 2`,7`-Dichlorofluorescein diacetate BioReagent, Nystatin, LB broth, Sodium hypochlorite (NaOCl), Cholesterol, Calcium chloride ($CaCl_2$), Cadmium chloride ($CdCl_2$), Potassium phosphate (KH_2PO_4), Magnesium sulphate ($MgSO_4$) Luria-broth (LB) tablets, Sodium phosphate ($Na_2H_2PO_4$), Igepal® CA-630

Table 2.3: The composition of the solutions and buffers used in this study.

Buffer and Solutions	Components
Bleach buffer	5 % NaOH (10 M), 20 % NaOCl (4 %)
Cholesterol (5mg/mL)	5 % (w/v) dissolved in ethanol
Freezing solution (1 litre)	100 mM NaCl, 50 mM KH_2PO_4 (pH 6.0), 30 % glycerol, ddH_2O, bottle and autoclave, finally add 0.3 mM $MgSO_4$.
Luria Broth (LB) media	1 Luria Broth (LB) tablet dissolved in 50 mL ddH_2O
M9 buffer	K_2HPO_4 (3 g), NaCl (5 g), Na_2HPO_4 (6 g), 1 M $MgSO_4$ (1 mL), ddH_2O (up to 1 litre)
NGM agar (1 litre)	NaCl (3 g), Bactoagar (17 g), Bactopeptone (2.3 g), Cholesterol (1 mL),1 M $MgSO_4$ (1 mL), 1 M $CaCl_2$ (1 mL), 1 M K_2HPO_4 (25 mL, pH 6.0), ddH_2O (up to 1 litre)

2.2 Equipment preparation

Microcentrifuge tubes, pipettes, and bottles were sterilized by autoclaving at 121°C at 15 psi for 20 min prior to use. Double sterilizations were performed for items used in RNA extraction, qRT-PCR, and microarray experimentation. The worm platinum picks were sterilized by flame and dipped into 100 % ethanol. Solutions that were heat sensitive were sterilized by filtration through a 0.22 µm Nucleopore™ filter. For agarose gel electrophoresis, casting trays and combs were rinsed thoroughly with deionized water and air dried.

2.3 Preparation of test material

2.3.1 ZnONP preparation

Synthetic surfactant-free P99/30nm NanoSun ZnO nanoparticles (ZnONP, purity 99.5 %) were obtained from Microniser Pty Ltd (Dandenong, Australia). NanoSun P99/30 ZnO, which is manufactured by milling, has no coatings or surface modifications and is close to spherical in shape. Physico-chemically, the average primary particle size is 30 nm with a stated water solubility of 0.0016 g/L at 20ºC and a melting point of 1975°C. NanoSun zinc oxide has been reported to have its point of zero charge in deionised water of pH 6.3. The particles were dispersed by probe sonication for 2 x 30 sec (at amplitude 15) in HPLC –grade water to a final concentration of 500 mg/L.

2.3.2 Carbon Black M120 preparation

MONARCH® 120 (M120) carbon black (CB) particles (furnace black) were obtained from Cabot Corporation (Billerica, US), with a primary particle size of 75 nm. Stock solutions of CB M120 were supplied as 500 µg/mL - dissolved in 5 % methanol (in HPLC water) and stored at -20ºC.

2.3.3 NIST 1648a preparation

Stock solutions of National Institute of Standards and Technology (NIST) Standard Reference Material (SRM) 1648a for urban particulate matter were supplied as 500 µg/mL - dissolved in 5 % methanol (in HPLC water) and stored at -20ºC. Stock solutions were provided by Christina Dunster, in the Kelly laboratory at King`s College London.

2.3.4 Particle preparation for toxicity tests

All particle aliquots were stored at -20°C. Prior to use, all aliquots were rapidly defrosted and vortexed for 10 min to maximize particle separation and ensure equal distribution. The test medium M9 or OP50 bacteria was dosed with the relevant concentration of particles. All OP50 sample mixtures were thoroughly vortexed, then added to the nematode growth medium (NGM) agar plates.

2.4 Maintenance and synchronization of nematode culture

2.4.1. Nematode growth medium

Nematode growth medium (NGM) agar plates were prepared following the protocol listed in Table 2.3. The molten agar was cooled to 60°C in a water bath, and then added to Petri dishes in a laminar flow cabinet using sterile strippettes (Sterilin, UK). 20 mL of agar solution was poured into large 90 mm cell culture dishes, 10mL into medium 60 mm dishes, and 5 mL into small 35 mm culture dishes (Greiner Bio One, Germany). The 12-well sterile tissue culture plates (Greiner Bio One, Germany) contained 2.5 mL of agar per well.

2.4.2. Fungicide preparation

The fungicide nystatin was prepared in filtered HPLC water, followed by filter sterilization through a 0.22 µm Nucleopore^{TM} filter, and stored at -20°C. Nystatin was added to solutions at temperatures below 60°C.

2.4.3. OP50 *Escherichia coli* strain preparation

Stock cultures of OP50 were stored at -80°C and the bacterial cultures were grown in autoclaved LB medium (10 g peptone, 10 g yeast extract, 5 g NaCl/ L water) for 16 hrs at 37°C and shaking at 150 r.p.m.

2.4.4. Strains of *C. elegans* – test organism

Bristol strain N2 (obtained from the *Caenorhabditis* Genetic Center (CGC) stock collection University of Minnesota, St. Paul, MN, USA) was used as wild-type (WT) in all experiments. In addition to the wild-type strain, the triple knockout *mtl-1;mtl-2;pcs-1*(zs2), previously generated in the Stürzenbaum lab at King's College London, was used.

Table 2.4: Nematode strains utilized in the study.

Strain name	Genotype	Allele	Received/Made up
wild-type (N2)	WT		CGC
***mtl-1;mtl-2;pcs-1*(zs2)**	Δ*mtl-1, Δmtl-2,Δpcs-1*	zs2/ tm1770;gk125;tm1748	generated by S. Hughes
***sod-1*(tm766)**	Δ*sod-1*	tm766	kindly donated by Prof D. Gems
***sod-2*(gk257)**	Δ*sod-2*	gk257	CGC
***sod-3*(tm760)**	Δ*sod-3*	tm760	CGC
***skn-1*(zu67)**	Δ*skn-1*	zu67	CGC
***pcs-1*(tm1748)**	Δ*pcs-1*	tm1748	CGC
P*mtl-2*::GFP	*mtl-2* promoter::GFP fusion		kindly donated by Dr S. Stürzenbaum
P*pcs-1*::GFP	*pcs-1* promoter::GFP fusion		kindly donated by Dr I. Hope

To examine oxidative stress potential of the material, additional experiments were performed with the following single knock-out strains: *sod-1*(tm766) (kindly donated by Prof David Gems lab), *sod-2*(gk257), *sod-3*(tm760), and *skn-1*(zu67) (obtained from the CGC stock collection University of Minnesota, St. Paul, MN, USA). All nematode strains utilized in this study are listed in Table 2.4.

2.4.5. *C. elegans* maintenance

All nematodes were reared according to standard procedures (Brenner, 1974) on nematode growth medium (NGM) in Petri dishes at 20ºC in a constant temperature incubator. The bacterial food source was OP50 strain *Escherichia coli* (a uracil-requiring *E. coli* strain to prevent overgrowth of the bacterial culture). Worms were typically exposed to test particles from age-synchronized L1 larval stage culture to L4 stage.

2.4.6. Freezing stock of *C. elegans*

To maintain *C. elegans* stocks, aliquots of strains were frozen in liquid nitrogen and stored at -80°C (Brenner, 1974). All nematode strains were synchronized by egg preparation method (section 2.4.7) to L1 stage in a 15 mL conical centrifuge tube. The nematodes were centrifuged for 2 min at 2600g, followed by removal of the supernatant to reduce the volume to 1.5 mL. An equal volume of freezing solution (Table 2.3) was added to the sample. After mixing, 500 µL of the nematode samples were aliquoted to 1.8 mL cryogenic tubes (Alpha Laboratories, UK). To ensure slow freezing (approximately 1ºC/min), the tubes were placed into a styrofoam rack at -80°C. The following day, one vial was allowed to defrost at room temperature and the viability of

nematodes was checked by pouring the liquid on a NGM plate containing a lawn of *E.coli* OP50.

2.4.7. Egg preparation

To produce age-synchronized nematode cultures (L1 stage), eggs from mature adults were isolated using a 10 % alkaline hypochlorite solution (bleach solution). Bleach solution (Table 2.3) dissolves worm tissues, except bleach-resistant eggs and also destroys any fungal or bacterial contaminants. Gravid adults were rinsed off the NGM agar plates with M9 buffer (Table 2.3) (Hitchcock et al., 1998) into a 15 mL centrifuge tube. The nematodes were pelleted for 2 min at 2600 g and the supernatant was carefully removed by pippeting and replaced by 10 mL of bleaching solution. The sample was vigorously shaken for 2-3 minutes and centrifuged for 1 min at 2600 g. The supernatant was again removed and 10 mL of M9 buffer was added, and then centrifuged for 1 min at 2600 g. The washing step was repeated at least 4 times or until the bleach odour was no longer detected. After removing the supernatant in the final step, 10 mL of M9 buffer was added to the pellet and the centrifuge tube was rotated at room temperature overnight. This allowed egg hatching into arrested L1 stage nematodes.

2.5 *C. elegans* life cycle analysis

2.5.1 Experimental design

For all acute toxicity tests, nematodes were age synchronized to L1 stage, followed by rotation at 20°C in the presence of fresh M9 and particles (Carbon Back M120/or NIST

1648a) (Fig. 2.1). After 12 hrs, the particles were removed by washing in M9 and nematodes were plated on fresh OP50 inoculated NGM plates. Chronic toxicity tests were performed on synchronized L1 staged nematodes, which were placed onto NGM plates, freshly inoculated with particle (ZnONPs/Carbon Black M120/or NIST 1648a) dosed OP50 bacteria (Fig. 2.2). The nematodes were cultured at 20°C, and daily transferred to plates inoculated with freshly dosed OP50 and subjected to the toxicity tests.

2.5.2 Nematode exposure

2.5.2.1 Acute exposure: Toxicity test in M9 saline solution

The nematode population was staged as previously described. The following day, the number of hatched progeny was determined by means of a titer. The L1 nematodes were distributed equally into 6 mL centrifuge tubes containing CB M120/or NIST 1648a concentrations (0, 5, 10, 25, 50 or 75 µg/mL) and made up to an equal volume (2 mL) with M9 buffer. Samples were rotated in the absence of food at room temperature for 24 hrs. Following treatment, samples were centrifuged for 1 min at 2600 g. The supernatant was removed and replaced with 10 mL of M9 buffer. The tubes were centrifuged again for 1 min at 2600 g. This step was repeated at least three times or until particles were removed. Following washing, 20-30 worms were transferred onto tissue culture plates (5.5 cm in diameter), which contained 10 mL of NGM agar seeded with 100 µL of *E. coli* OP50. Each condition was replicated in triplicates. To avoid starvation or competition, nematodes were transferred daily to freshly inoculated 60 mm medium-sized plates. All plates were incubated at 20°C for 120 hrs (t_0 = L1-L2s transferred to plates).

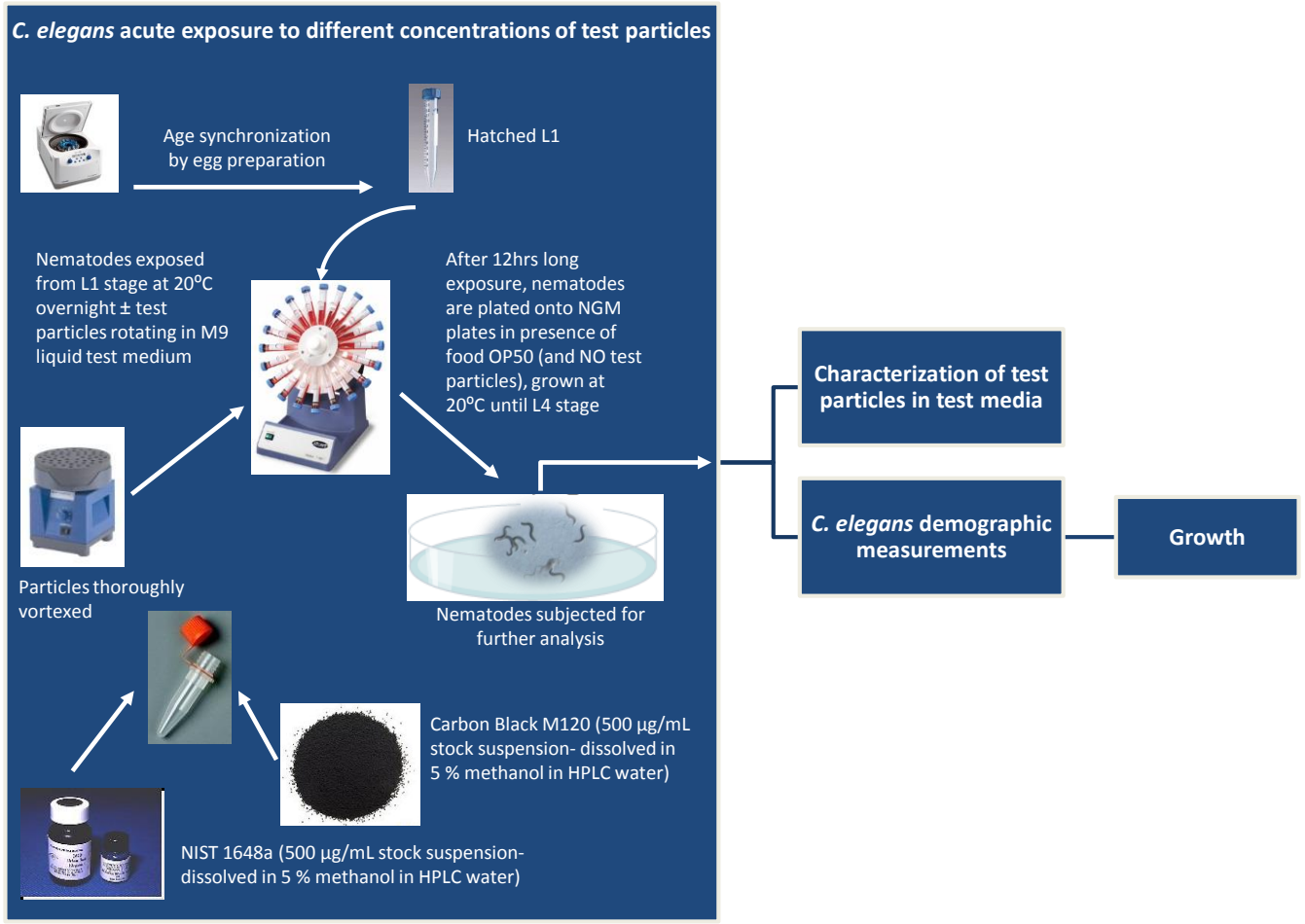

Fig. 2.1: A schematic representation of experimental design of *C. elegans* acute toxicity test.

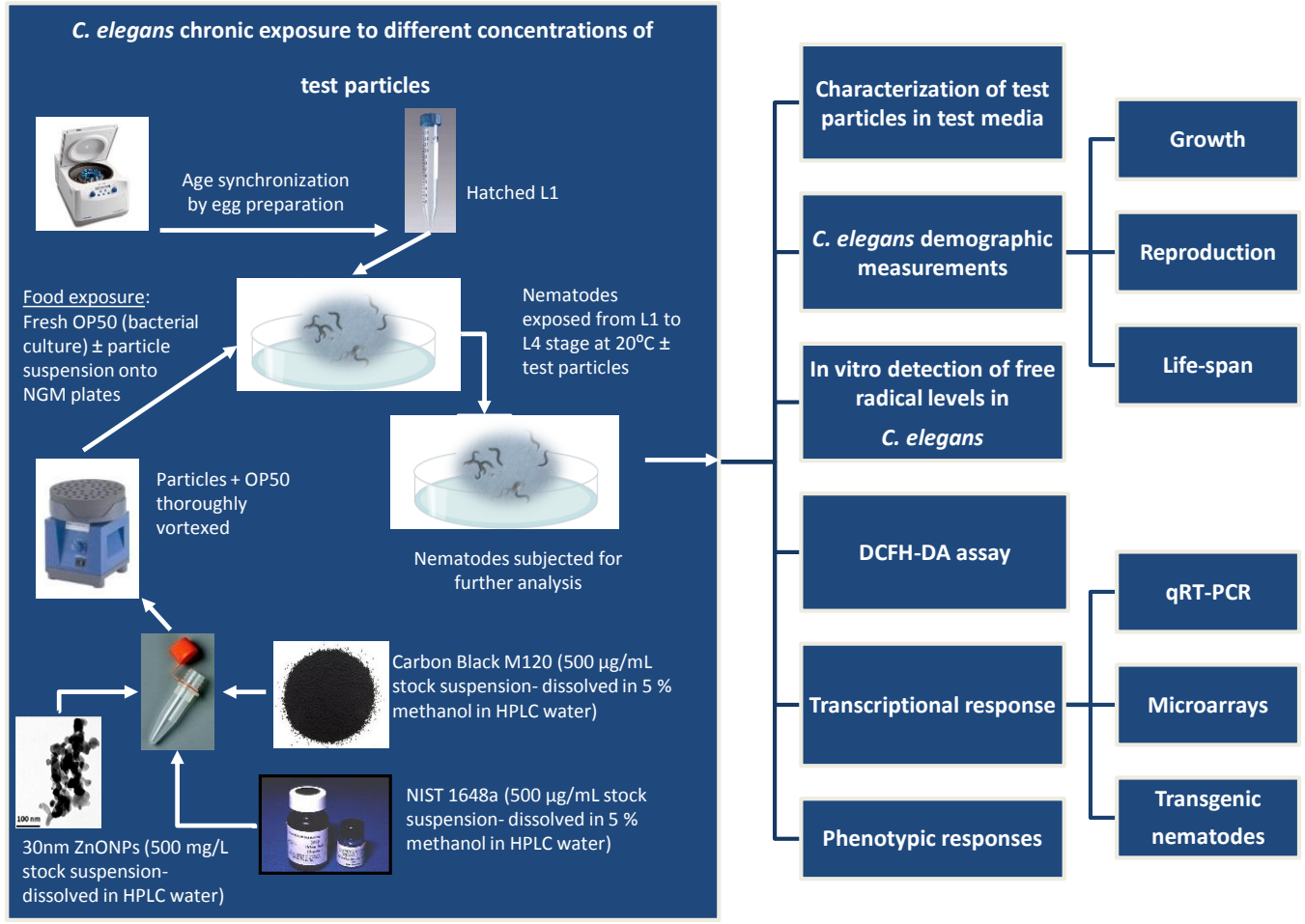

Fig. 2.2: A schematic representation of experimental design of *C. elegans* chronic toxicity tests.

2.5.2.2 Chronic exposure: Agar – Toxicity test in OP50 bacterial culture

Newly hatched (L1) worms were maintained on large (90 mm) tissue culture plates (Greiner Bio-One Ltd., UK), which contained 20 mL of NGM agar and were inoculated with 200 µL of OP50 supplemented with/or without particles. To avoid starvation, a maximum of 500 worms were maintained on each plate. All plates were incubated at 20°C for up to 5 days.

2.5.3 Flat volumetric surface area assessment-Image analysis

Growth experiments were performed on wild-type and mutant worms. In both cases synchronized, newly hatched (L1) individuals were maintained on large tissue culture plates (Greiner Bio-One Ltd., UK). All plates contained 20 mL of NGM agar and were inoculated with 200 µL of OP50 supplemented with/or without particles. To avoid starvation, a maximum of 30 worms were kept per well and transferred daily to freshly prepared NGM plates. All plates were incubated at 20°C.

Digital images were taken of 20 individuals per treatment with a Nikon microscope and camera (Nikon UK Ltd., Kingston upon Thames, UK). The images were taken at 24 hrs intervals and were analysed using Image ProExpress v5.1 (Image ProExpress, Media Cybernetics, Wokingham, UK). The software allows the outline of each nematode to be traced and thus the flat volumetric area within the perimeter of the nematode to be calculated. Each growth assay was repeated two times per test condition.

2.5.4 Nematode reproduction-brood size assay

Synchronized wild-type and mutant nematodes were transferred as late L4s onto individual 12-well tissue culture plates. Each well contained 2.5 mL of NGM agar with 20 µL of bacterial lawn supplemented with a corresponding concentration of particles, and a single nematode (12 nematode individuals per plate). The parental nematodes were transferred daily to new 12-well plates, until the completion of the egg laying period. Hatched progeny was allowed to grow to L1/2 stage and then counted. The progeny number produced by a single parental nematode was added up from the various plates to give the final brood size. Reproduction was recorded for 36 individuals at each concentration for statistical purposes. All plates were incubated at 20°C.

2.5.5 Nematode life-span

To determine the lifespan, approximately 400 nematodes per condition (particles/or no particles) were monitored from the L1 stage until death. Each day worms were transferred to a newly prepared large NGM plate with 200 µL of bacterial lawn supplemented with a corresponding concentration of particles. To avoid starvation a maximum of 200 worms were maintained on each plate. Their survival was scored daily by gently stroking nematode with a platinum wire. Worms were scored as dead when they failed to respond completely to light prodding. All dead and censored worms were accounted when submitted to data analysis.

The Kaplan-Meier method was used for survival data plotting and processing. It is a method used to measure the fraction of subjects (e.g. worms) living for a certain amount of time after toxicant exposure (Kaplan and Meier, 1958; Rich et al., 2010). The graph generated by GraphPad Prism (GraphPad Software Inc., San Diego, USA) software

presents the percentage of nematodes surviving at each examination point plotted against time (e.g. days). The survival curve begins at 100 %, where subjects survival is considered to be stable, regardless of the total number (N) of starting individuals in the experiment. The N values of subjects living at the start of life-span analysis may be different within the study group, e.g. there might be a higher starting number of individuals present in the control group than in exposed. Another advantage of using this type of analysis is that the method takes into account censored data, for example if a worm is lost. The survival curves are drawn as a step function, where each step indicates losses/deaths. To compare different Kaplan–Meier curves, a statistical analysis was performed using the Log-rank (Mantel-Cox) Test, where a control was compared to each particle exposed nematodes, indicated by $p < 0.0001$. The key parameters used to interpret and compare the survival data were the median and maximum lifespan values. The median survival is the time at which fractional survival equals 50 % of the total number of worms alive. Maximum lifespan of the nematode is defined by the longest living individual within the population.

2.6 Dietary effects – OP50

The toxic effect of particles on *E. coli* OP50 was examined, mainly to exclude the presence of possible dietary restriction effects. Stock cultures of *E. coli* (OP50) were grown for 16 hrs in LB medium at 37°C and shaking at 200 r.p.m. The following day, 1 mL of bacterial suspension was pippeted into a cuvette to measure OD (absorbance) at 600 nm. The OP50 stock was diluted to OD 0.1, to which a corresponding particle concentration was added. The particle-containing samples were incubated at 37°C and shaking at 200 r.p.m. Change in bacterial OD was observed over a period of 24 hrs.

2.7 pH of exposure media

The pH of the test solution was determined using a pH indicator strip (colorpHast® pH Test Strips (non-bleeding), EMD Millipore, US) and pH-indicator paper (Neutralit® (EMD Millipore, US) with a colour scale of pH 5.5 - 6.0 - 6.5 - 7.0 - 7.5 - 8.0 - 8.5 - 9.0. The pH paper/or strips were immersed into the sample solution until no further colour change was observed (1 - 10 min), and read while still moist.

2.8 Characterization of ZnONPs, Carbon Black M120, and NIST 1648a

2.8.1 Transmission electron microscopy (TEM) imaging of ZnONPs and Energy dispersive X-ray spectrometer (EDS)

Samples of ZnO particles in HPLC water, LB broth with bacteria, and mixtures of particles and feeding media were prepared. A drop of the dispersion was deposited on a holey carbon coated copper TEM grid and dried at room temperature for several hours before examination by TEM. Experiments were carried out on a JEOL 2010 analytical TEM, with a LaB6 electron gun and operated between 80 and 200 kV (Department of Materials, University of Oxford, Kidlington, UK). This instrument has a resolution of 0.19 nm, an electron probe size down to 0.5 nm and a maximum specimen tilt of ± 10 degrees along both axes. The instrument is equipped with an Oxford Instruments LZ5 windowless energy dispersive X-ray spectrometer (EDS) controlled by INCA. It has facilities for point analysis as well as mapping and line scanning through the SemiStem controller.

2.8.2 Transmission electron microscopy (TEM) imaging of Carbon Black M120 and NIST 1648a

Stock suspensions of CB M120 and NIST 1648a particle samples were used for characterization. Particles were prepared in freshly prepared M9 saline solution and OP50 bacterial culture. The particles shape and size were both visualized by transmission electron microscopy (TEM) JEOL-JEM-1210 (Cardiff School of Biosciences, Cardiff, UK). For sample preparation, 50 µL of stock particle suspensions were dried onto nickel-coated grids and imaged by TEM at 80 kV. Approximately 10-20 individual pictures of particles were taken at 0.6-0.8 sec exposure meter.

2.8.3 Dynamic light scattering (DLS)

Particle size distribution of the ZnONPs in test media and in the presence of bacteria was evaluated using the Malvern instruments Zetasizer Nano ZS (Department of Materials, University of Oxford, Kidlington, UK). The dynamic light scattering (DLS) is a non-invasive technique for measuring the size of molecules and particles typically in the submicron region down to the nanometer range.

2.8.4 Nanoparticle tracking analysis (NTA) by NanoSight

Carbon Black M120 and NIST 1648a particles were characterized in the test media (M9 saline solution and *E.coli* OP50) using NanoSight LM10 (NanoSight Ltd., UK). NanoSight allows the characterization of the particles size distribution and their aggregates.

Particles were prepared at a stock concentration of 150 µg/mL in 5% methanol. For the particle dispersion in the test media analysis, M9 and OP50 were prepared one day before the analysis was conducted. M9 saline solution was prepared according to a standard protocol (Hitchcock et al., 1998) and autoclaved. OP50 bacterial culture was grown overnight in LB broth. The OP50 bacterial sample was too concentrated to carry out NTA (nanoparticle tracking and analysis), therefore a dilution 1:2 with LB-broth was made. Particles (stored at -20°C) were defrosted, warmed up to room temperature and added to the test media just prior to the NTA was carried out.

NTA tracks particles movements under Brownian motion and estimates their hydro-dynamic radius, using the Stokes-Einstein equation. NanoSight provides information about particle size in a range between 10 nm – 6000 nm, dependent on the nanoparticle material (NanoSight, Ltd). All sample preparation and measurements were carried out at Cardiff School of Biosciences, Cardiff University, UK. The data analysis was performed with NanoSight using a version build 0112 of NTA 2.0 software. For each analysis, 500 µL of sample was added to a scattering cell with a disposable syringe through which a focused laser beam was passed (nominally 40mW at absorbance 635 nm). The optical microscope-based system allowed particles within the path of the beam to be observed within a field view of 100 × 100 µm. Brightness and gain were adjusted accordingly to obtain a clear image with black background and clear visibility of particle centres. NTA automatically located the centre of every individual particle, followed it and measured the average distance it moved per frame. For each test solution, multiple 30 sec videos (900 sequential images at 30 fps (frame per second)) were recorded applying automatic threshold detection. Finally, NTA tracked the particles and their sizes, and determined the average distance travelled (Montes-Burgoes

et al., 2010). An estimated concentration and particle mean, median and mode size was calculated.

2.9 DCFH-DA assay

The level of total ROS generation in nematodes was estimated using the 2', 7'-dichlorodihydrofluoroscein diacetate (H_2DCFDA; Molecular Probes) dye (Fig. 2.3).

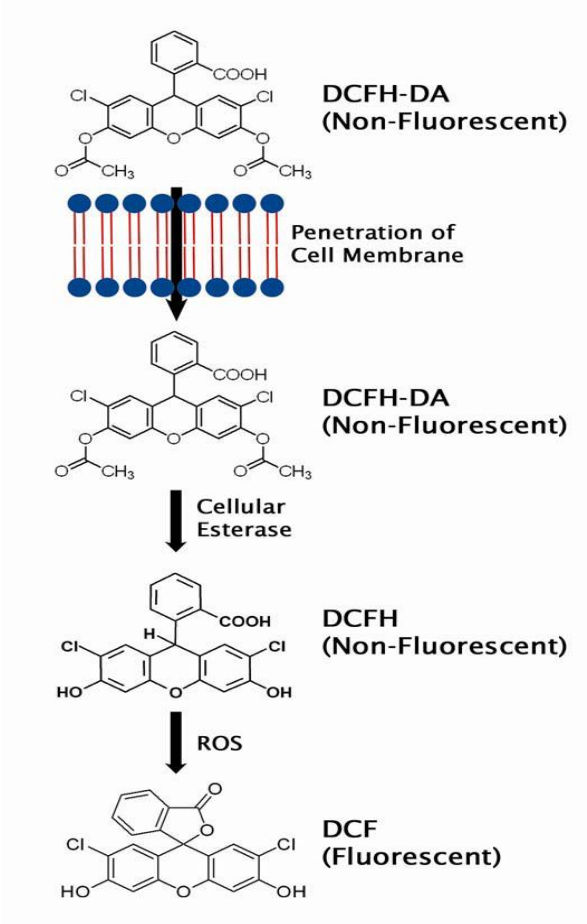

Fig. 2.3: Mechanism of the DCFH-DA assay. DCFH-DA penetrates the cell membrane, where it is initially de-esterified to form non-fluorescent DCFH. In presence of ROS, DCFH oxidizes and yields a fluorescent moiety (DCF adapted from Cell Biolabs, Inc., 2009).

2.9.1 Sample preparation: *C. elegans* treatment

A minimum of 1000 age-synchronized (L1) nematodes per condition were grown to L4 stage at 20°C. The worms were washed 4 times in M9 buffer and twice in PBS

(phosphate buffered saline). Finally, the supernatant was removed to a final volume of 500 µL. Worms were counted in 3 µL titres, taking 10 titres per sample. The pelleted worms were frozen at -80°C overnight for at least 8 hrs, but less than 24 hrs due to the unstable, transient nature of ROS. The following day, worms were defrosted on ice and homogenized by sonication (3 × 20 sec pulses, amplitude 15). To avoid exposure to excessive heat, samples were always maintained on ice.

2.9.2 DCFH-DA assay of ROS levels

The DCFH-DA (50 µL of 100 µM in PBS) was added to 50 µL of worm homogenate in the absence of exposure to direct light. The plates were incubated (protected from light) at 37°C and analysed for ROS production using a microplate reader at excitation 485 nm and emission 528 nm. Fluorescence readings were normalized to worm numbers.

2.10 Raman spectroscopy

2.10.1 Raman spectroscopy: Sample preparation

To investigate phenotypic changes in nematodes exposed to ZnONPs, Raman microspectroscopy was used to determine the biomolecular composition of nematodes. Both wild-type and mutant *C. elegans* were exposed to 0 and 50 mg/L ZnONP for 48 hrs (from L1 stage to L4 stage). The L4 stage worms were picked from the plates and air dried in a droplet of ultrapure water (Sigma, UK) onto a microscope slide overlaid with a CaF_2 disc.

Raman spectroscopy was carried out at the Centre for Ecology and Hydrology, Wallingford, UK, on a Horiba LabRAM HR800 Raman microspectrometer (Horiba

Scientific, UK) equipped with an Olympus BX-41 microscope and an Andor electronically cooled CCD detector. The spectrometer has a 600 grooves/mm grating and a slit width of 100 µm. Raman spectra were collected from two areas, namely 1) the region immediately posterior to the pharynx, and 2) the tail muscle. Nematodes were observed using a 100x/0.9 numerical-aperture air objective (Olympus; Mplan) and a CCD camera. Laser illumination was achieved by means of a 532-nm Nd:YAG laser, with the incident laser power set to 5-8 mW. Spectra were collected from 25 worms per treatment, with an acquisition time of 30 sec and two averaged accumulations at each point. From each individual worm, five spectra were taken within a 20 x 20 µm region from the head and tail regions as described earlier.

2.10.2 Raman spectroscopy: Data analysis

Cosmic spikes present in the spectra were automatically removed using the LabSpec v5 software (Horiba Scientific, UK). Raw spectra were concatenated to between 400 cm^{-1} and 1800 cm^{-1} wavenumbers, and the resultant data normalized using LabSpec v5. To visually explore the differences between the spectra collected from the NP exposed and control nematodes, the Raman spectra were analysed using Principal Component Analysis (PCA) in the Vegan package in R (Oksanen et al., 2012; RCore Team, 2012). The Adonis function in Vegan was used, to test for differences between control and treatment groups when considering the spectra collected from the head and tail regions separately. This partitioned dissimilarities of variation using Euclidian distances, and allowed a permutation test to be conducted with 1000 iterations to inspect the significance of those partitions.

2.11 Photomicroscopy of transgenic nematodes

The transgenic strains carrying either the P*mtl-2*::GFP or P*pcs-1*::GFP reporter construct were maintained at 20ºC from L1 larval stage to L4 stage on seeded plates dosed with 0 and 50 mg/L ZnONPs. For imaging, L4 worms were picked onto a glass slide carrying a droplet of M9 solution. Sodium azide (2 %) (Sigma, UK) was added to immobilize nematodes and finally covered with a coverslip. Nematode images were captured on an inverted fluorescence microscope, using blue laser scanning fluorescence (λ_{ex} = 450-490nm) and DIC (Nomarski) imaging. All images were captured with a Nikon camera (Nikon UK Ltd., Kingston upon Thames, UK) at 20 × magnification and were analysed using the Image J software (Image J 1.45s, National Institute of Health, US).

2.12 Transcription-activated fluorescent reporters in Knudra transgenes

Transgenic nematodes were used to detect oxidative or metal stress responses induced by particles. The use of these nematodes represents a new toxicogenomic approach for detecting toxin-induced pathways.

2.12.1 Knudra transgenes: Nematode preparation

Transgenic nematodes, which were generated by Knudra Tansgenics, US (http://www.knudra.com/product/custom-transgenics), were utilized for this diagnostic toxicology platform. These transgenic nematodes were generated using a MosSCI transgenesis procedure (Frokjaer-Jensen et al., 2008), which creates a transcription-

dependent fluorescence of a transgene at a defined locus upon exposure to a toxicant. In these dual-integrated strains, a red fluorescent protein (mCherry) is driven by the promoter of the gene of interest, and the constitutive green fluorescent protein (GFP) is fused to an invariant control gene.

In detail, fluorescent reporters are constructed from the promoters of toxin-sensitive genes linked, in frame, to the coding region of a red fluorescent protein hsRFP (or mCherry), fused to the histone gene *his-57*. The gene is cloned into a pNU142 (Amp^r) vector, which carries left (2094 bp) and right (1825 bp) homologous Mos1 recombination arms, and a *unc-119* gene which is used as a positive selection marker. A single copy insertion is made into the Mos1 ttTi5605 site by injection into the gonad of a nematode expressing GFP, which is homozygous for oxIs12 (*unc-47::*GFP) and ttTi5605 alleles. The transformed MosSCI nematode integrants are harvested and validated by PCR for a single copy insertion at Mos1 locus. A 325 bp product is specific to homozygous strains for insertion at Mos1 loci (Gunaratna, et al. Manuscript draft for BioTechniques, Knudra Transgenesis, US; Frokjaer-Jensen et al., 2008). As a result, two coloured fluorescent nematodes are generated.

The biosensor panel utilized included the following reporters: *mtl-2*::mCherry, *hsp-16.41*::mCherry, *hsp-16.2*::mCherry, *cyp-35A2*::mCherry, *gcs-1*::mCherry, *gst-4*::mCherry, *gst-38*::mCherry, *ugt-1*::mCherry, and *dnj-13*::mCherry (Table 2.5). These transgenic nematodes have a reproducible and robust response to a specific type of toxicant insult, such as exposure to a heat-shock primarily activates the *hsp* genes, *hsp-16.2::*mCherry; and exposure to metals, e.g. cadmium, activates metallothionein *mtl-2*::mCherry expression. For heat shock, plates with L4 staged transgenic nematodes (at density of 200 worms per plate) were exposed at 30°C for 4 hrs, and then allowed to recover for 1.5 hrs at 20°C prior to imaging. For cadmium exposure, L1 staged

transgenic nematodes were grown on fresh NGM plates, seeded with OP50 supplemented with 20 µM $CdCl_2$ for 48 hrs (to L4 stage) at 20°C.

To assess the particle mediated activation of fluorescence, all transgenic nematodes were staged, and grown on NGM agar plates seeded with fresh OP50 supplemented with 0 and 50 µg/mL of the corresponding concentration of particles (from L1 larval stage to L4 stage). Worms were incubated at 20°C and maintained at densities of less than 200 adult animals per plate. For imaging, L4 worms were picked onto a glass slide carrying a droplet of M9 solution. Sodium azide (2 %) (Sigma, UK) was added to immobilize worms and covered using a standard coverslip.

2.12.2 Knudra transgenes: Nematode imaging

Nematode images were captured on an inverted fluorescence Nikon microscope at 20 × magnification, using a blue laser scanning fluorescence (λ_{ex} = 450-490nm), Texas Red green laser scanning fluorescence (λ_{ex} = 575-620nm) and DIC (Nomarski) imaging. All images were recorded using a Nikon camera (Nikon UK Ltd., Kingston upon Thames, UK) and analysed by means of the Image J software (Image J 1.45s, National Institute of Health, US).

2.12.3 Knudra transgenes: Data analysis

The fluorescent intensity readings were normalized by calculating the ratio of toxicant-particle induced mCherry/GFP signal divided by the control mCherry/GFP signal.

Table 2.5: The list of KNUDRA transgenic nematode strains that were utilized for screening (Knudra Transgenics, US).

Strain name (isolation number)	Genotype	Allele
mtl-2 COP 42 (13.8.47)	oxIs268[P*unc-47*:GFP] I ; knuSi28[P*mtl-2*: :hRFP: :H2B: :*tbb-2*utr] II ; *unc-119*(ed3) III	Two colour: plasmid 156 promoter for *mtl-2* driving hRFP::H2B reporter in P*unc-47* : GFP bkgrd
hsp-16.2 COP 50 (4.8.47)	oxIs268[P*unc-47*:GFP] I ; knuSi17[P*hsp-16.2*: :hRFP: :H2B: :*tbb-2*utr] II ; *unc-119*(ed3) III	Two colour: plasmid 157 promoter for *hsp-16.2* driving hRFP::H2B reporter in P*unc-47*:: GFP bkgrd
hsp-16.41 COP 52 (12.5.47)	oxIs268[P*unc-47*:GFP] I ; knuSi11[P*hsp-16.41*: :hRFP: :H2B: :*tbb-2*utr] II ; *unc-119*(ed3) III	Two colour: plasmid 157 promoter for *mtl-2* driving hRFP::H2B reporter in P*unc-47*:: GFP bkgrd
cyp-35A2 COP 58 (25.3.47)	oxIs268[P*unc-47*:GFP] I ; knuSi34[P*cyp-35A2*: :hRFP: :H2B: :*tbb-2*utr] II ; *unc-119*(ed3) III	Two colour: plasmid 155 promoter for *hsp-16.41* driving hRFP::H2B reporter in P*unc-47*:: GFP bkgrd
gcs-1 COP 23 (5.23.47)	oxIs268[P*unc-47*:GFP] I ; knuSi3[P*gcs-1*: :hRFP: :H2B: :*tbb-2*utr] II ; *unc-119*(ed3) III	Two colour: plasmid pch149 promoter for *gcs-1* driving hRFP::H2B reporter in P*unc-47*:: GFP bkgrd
gst-4 COP 57 (15.15.47)	oxIs268[P*unc-47*:GFP] I ; knuSi21[P*gst-4*: :hRFP: :H2B: :*tbb-2*utr] II ; *unc-119*(ed3) III	Two colour: plasmid 158 promoter for *gst-4* driving hRFP::H2B reporter in P*unc-47*:: GFP bkgrd
gst-38 COP 54 (7.7.47)	oxIs268[P*unc-47*:GFP] I ; knuSi23[P*gst-38*: :hRFP: :H2B: :*tbb-2*utr] II ; *unc-119*(ed3) III	Two colour: plasmid 152 promoter for *gst-38* driving hRFP::H2B reporter in P*unc-47*:: GFP bkgrd
ugt-1 COP 59 (8.13.47)	oxIs268[P*unc-47*:GFP] I ; knuSi27[P*ugt-1*: :hRFP: :H2B: :*tbb-2*utr] II ; *unc-119*(ed3) III	Two colour: plasmid 150 promoter for *ugt-1* driving hRFP::H2B reporter in P*unc-47*:: GFP bkgrd
dnj-13 COP 71 (30.18.47)	oxIs268[P*unc-47*:GFP] I ; knuSi39[P*dnj-13*: :hRFP: :H2B: :*tbb-2*utr] II ; *unc-119*(ed3) III	Two colour: plasmid 165 promoter for *dnj-13* driving hRFP::H2B reporter in P*unc-47*:: GFP bkgrd. Injected into strain GFP background. No outcrossing done.

2.13 Total RNA extraction

The total RNA was extracted from 3000 nematodes per sample/condition with Tri-reagent (Sigma-Aldrich, Poole, Dorset, UK). Samples were vortexed for 3 min with an equal amount of acid-washed glass beads (Sigma-Aldrich, Poole, Dorset, UK) and the supernatant was transferred to a microcentrifuge tube and incubated at room temperature for 5 min. Chloroform (200 µL) was added to the mixture before vigorously shaking (by hand) for 10 sec. This mixture was incubated at room temperature for 12 min and centrifuged at 4°C for 15 min at 12000 × g. Isopropanol (500 µL) was added to the supernatant after transferring to a clean microcentrifuge tube. The mixture was inverted by hand 6 times and incubated at room temperature for 12 min followed by a further centrifugation at 4°C for 10 min at 12000 × g. The supernatant was removed and 1 mL 75 % ethanol was added to the pellet. The mixture was centrifuged at 4°C for 5 min at 12000 × g. The pellet was allowed to dry by removing the supernatant and placing under sterile airflow before being resuspended in RNA-ase free water. The quality of the RNA was analysed by 1 % agarose gel electrophoresis and the RNA suspension was stored at -80°C.

2.13.1 Agarose gel electrophoresis– assessment of RNA quality

To visualize RNA, agarose gel electrophoresis was applied. Gels typically contained a 1 % (w/v) agarose in 1 × TAE buffer and 0.5 µg/mL ethidium bromide. To every sample (5 µL), 1 µL of loading dye was added prior to loading into gel wells. Furthermore, appropriate marker ladders (Bioron, Germany) were loaded into adjacent wells to allow the size of the fragments to be determined. The gel was run at an electric current of 138

volts for 15-20 min in 1 × TAE buffer. The bands were visualized under UV-light, and the photo of the gels was taken with a UV trans-illuminator camera.

2.13.2 Nanodrop – assessment of quality and purity of RNA

The concentration and quality of RNA was quantified using a Nanodrop ND1000 spectrometer (ND-1000 Spectrophotometer, Nanodrop Technologies Inc, US). A reading ratio A260/A280 provided information on phenol or protein contamination, and the A260/A230 ratio indicated sample ethanol or salt contamination.

2.14 Polymerase chain reaction

2.14.1 cDNA synthesis

cDNA was synthesized from 500 ng of RNA by means of an oligo-dT primer. Components used to synthesize cDNA were as follows: 4 µL M-MLV (Moloney Murine Leukemia Virus) 5 x Reaction Buffer, 2 µL Deoxyribonucleotide triphosphate (dNTP) (equal amounts of dATP, dCTP, dGTP and dTTP) (100 mM) of each base), 1 µL Oligo dT primer (100 pM/µL), 500 ng RNA, 50U M-MLV Reverse Transcriptase (Promega, UK) and HPLC water to make up to a final volume of 20 µL. The tubes were incubated for 60 min at 42°C, followed by 10 min at 72°C. The cDNA was stored at -20°C.

2.14.2 Polymerase chain reaction (PCR) amplification

For PCR, reaction a standard mix was used: 10 % (v/v) 10 × GoTaq Flexi buffer (Promega,UK), 2.5 mM $MgCl_2$, 0.2 mM dNTPs, forward and reverse primer (each at 1pM), DNA template at 1 µg, and filtered HPLC water to make a final volume of 10 µL.

95°C for 5 min
95°C for 30 sec
X°C for 30 sec } **30 cycles**
72°C for Y time
72°C for 5 min
hold at 4°C

Box 2.1: The basic PCR cycling conditions: initial denaturation at 95ºC × 5 min, then 30 cycles of denaturation at 95ºC × 30 sec → annealing at XºC × 30 sec → extension at 72ºC × Y sec, and then final extension at 72ºC for 5 min and hold at 4ºC. Where X ºC is the specific annealing temperature calculated on the basis of the primers set used and Y is the extension time (usually for 1kb DNA amplification, 1 min extension time is required).

The PCR amplification was executed in a ThermoCycler (PTC 225 Peltier ThermoCycler, MJ Research, US) and the cycling conditions (temperatures, and length of time applied in each cycle) were optimized based on the set of primers used (Box 2.1).

2.14.3 Quantitative polymerase chain reaction (qRT-PCR)

Quantitative PCR of selected transcripts was carried out using the ABI Prism7000a platform (Applied BioSystems, Warrington, UK) and normalized with the *rla-1* house keeping gene. All primers and probe sequences were obtained from the Universal ProbeLibrary (Roche Applied Science, UK), guided by Assay Design feature

(https://www.roche-applied-science.com/sis/rtpcr/upl/index.jsp?id=UP030000).

All primer and probe sequences for each gene investigated are provided in Appendix: Materials and methods. For each qPCR reaction a mastermix was prepared containing 12.5 µL ROX master Mix (Roche, UK), 3 µL diluted cDNA (approximately 150 ng/µL), 0.25 µL of probe (10 µM), 1 µL of each primer (10 pM) and made up to final volume 25 µL. qRT-PCR was performed using standard ABI Prism cycling conditions (2 min at 50°C, followed by 10 min at 95°C, than 40 cycles of 15 sec at 95°C and 1 min at 60°C), and data analysed using the ABI 7000 system software, and the ΔΔ CT (cycle threshold) method to calculate the fold change in gene expression. All genes expressions were normalized to *rla*-1, an invariant acidic ribosomal subunit protein P1 housekeeping gene. All qRT-PCR experiments were performed in triplicate. The quantification was performed using at least samples from two independent experiments.

2.14.4 Primers and Probe designs

To design primers and probes, a Universal ProbeLibrary (Roche Applied Science, UK), with the guidance of the Assay Design feature (https://www.roche-applied-science.com/sis/rtpcr/upl/index.jsp?id=UP030000) was used. The Assay Design Center allows the design of intron-spanning qPCR assays,

including primer and probe sequences, amplicon size, location, and a variety of ranking options for assays. For each assay, the software predicts an optimal set of primers and corresponding probe (for criteria see Box 2.2).

The amplicon size: between 70-150 bases.	
The primer design based on standard guidelines: • Length of primers: approximately 20 bases. • Primer GC content ~ 50 % (less G, and with more C bases). • The melting temperature (T_m): between 59-61°C. • The two primers should not differ in their T_m by more than 2°C. • For increased primer specificity, at last 5 bases should have no more than two G /or two C bases at the 3' end.	The probe design based on standard guidelines: • Length of probe: approximately 8- to 9 - mer. • Probes should be, if possible, intron/exon spanning to prevent genomic DNA amplification, and located 3-10 bases away from both primers. • The melting temperature (T_m): 8-10°C higher than the correspondent primers. • Probe GC content ~50 %; there should be more Cs than Gs, and not a G at the 5' end.

Box 2.2: Guidelines for primers and probes design for qRT-PCR assay reactions.

Primers (oligonucleotides) were synthesized by Sigma, UK, and the UPL probes were obtained from the Genomics Centre, King's College London. The UPLs are a modified set of 165 short oligonucluotides (8 – to 9 – mer) fluorescently-labelled hydrolysis probes that are specifically designed by Roche, UK for organism-specific qRT-PCR analysis of any gene in the genome. The UPL probe contains a covalently attached 5' fluorescin (FAM) dye, and a dark quencher dye at the 3' end. A Locked Nucleic Acid

(LNA) is incorporated into the probe sequence, to maintain the required specificity and melting temperature (T_m).

2.15 Whole genome Microarrays

2.15.1 Experimental design: Nematode exposures for microarrays

Age-synchronized wild-type nematodes were exposed to five concentrations of NIST 1648a (solvent control, 1, 5, 10, 20, and 50 µg/mL) for 48 hrs (from L1 stage to L4 stage). All exposures were performed on NGM plates with OP50 bacteria as food source supplemented with/or without NIST. RNA was extracted from about 3000 nematodes per condition using Trizol (Invitrogen), according to the protocol described in Materials and methods section 2.13. All RNA samples were stored at -80°C prior to being subjected to microarray analysis (Fig. 2.4). All RNA samples were diluted to 500 ng with the RNase-free H_2O. The concentration and quality was confirmed by means of a Nanodrop ND-1000 spectrophotometer.

2.15.2 RNA integrity analysis

To validate the quality of the RNA samples, the samples were run on bioanalyzer (Agilent Small RNA kit, 2100 Bioanalyser, Agilent, UK). The Agilent Bioanalyzer is a microfluidics-based platform (a capillary electrophoresis machine), which utilises lab-on-a-chip technology to size, quantify, and check the quality of DNA, RNA, proteins and cells.

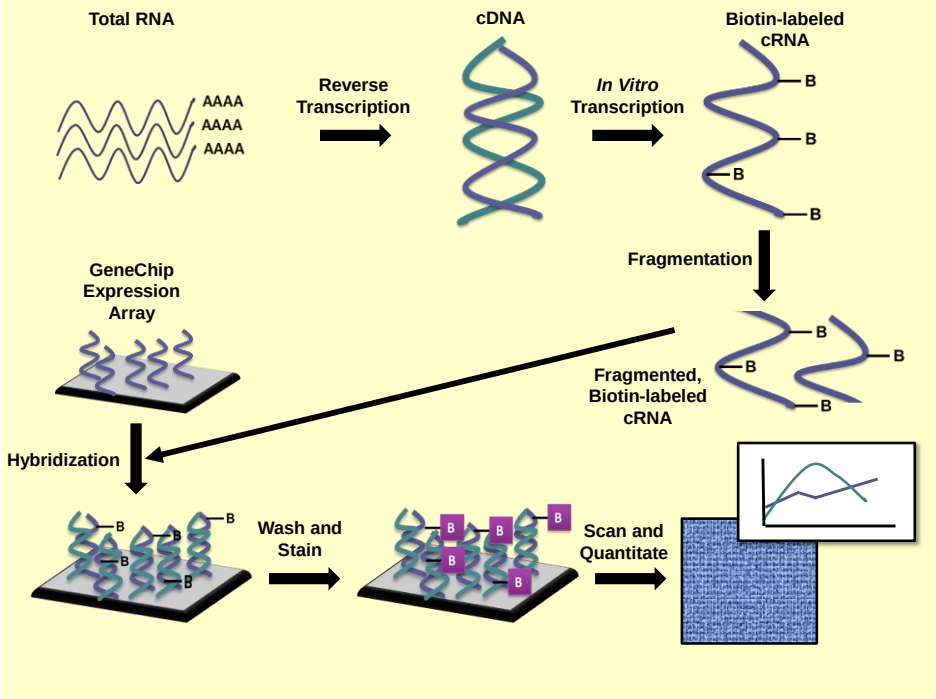

Fig. 2.4: The basic process of carrying out microarrays. Taken from affymetrix.com, this diagram represents the protocol how expression of an organism can be analysed using DNA microarrays.

High quality results are delivered in a digital format within 30 min. It returns highly reproducible data, and consumes minimal sample volumes (50 pg of total RNA per analysis). The RNA LabChip® Kit was used to evaluate the integrity of RNA samples. This kit allows quantitation of small RNA samples of 6 and 150 nt in size and 50 to 2000 pg/µL in concentration. The analysis was performed following the protocol provided with the kit (Agilent Small RNA kit guide, Agilent, UK). First the samples were deposited into an RNA Nano LabChip, followed by running the analysis on the Agilent Bioananlyzer to generate a digital electropherogram. The RNA integrity numbers (RIN) algorithm was applied to electrophoretic RNA measurements to calculate and rank the RNA integrity from 1 to 10 RIN score, where level 10 score is completely intact RNA.

2.15.3 RNA amplification, biotin labelling, and DNA microarray analysis

The RNA samples were processed with the MessageAMP™ Premier RNA Amplification Kit (Ambion, Austin, TX, USA), which relies on the T7 *in vitro* transcription (IVT) amplification technology method (Van Gelder et al., 1990) (Fig. 2.5). Synthesis of first- and second- strand cDNA, and biotin-labelled cRNA was performed following the protocol provided by the manufacturer (Ambion, Austin, TX, US). Control RNA samples (supplied by Ambion) were used as a positive control. The cRNA concentration was assessed by Nanodrop spectrophotometry (for results see Appendix: NIST 1648a). The cRNA size was assessed with the Agilent Bioanalyzer (Appendix: NIST 1648a). A successful IVT reaction yields at least 30-50 µg of biotin-cRNA per 20 µL sample.

2.15.4 Fragmentation of biotinylated cRNA (fcRNA)

To fragment biotinylated cRNA, 15 µg of cRNA and 8 µL of 5 × Array Fragmentation Buffer was used to make up to 31 µL total reaction mixture volume, following the GeneChip® 3' IVT Express Kit User Manual guidelines. The reaction was incubated at 94°C for 35 min, and then kept on ice. Prior to hybridization, the fragmentation products (1 µL) were analysed on an Agilent Bionalayzer (for results see Appendix: NIST 1648a.). A successful fragmentation results in 35- to 200- nt cRNA fragments with an RNA peak at around 100-120 nucleotides.

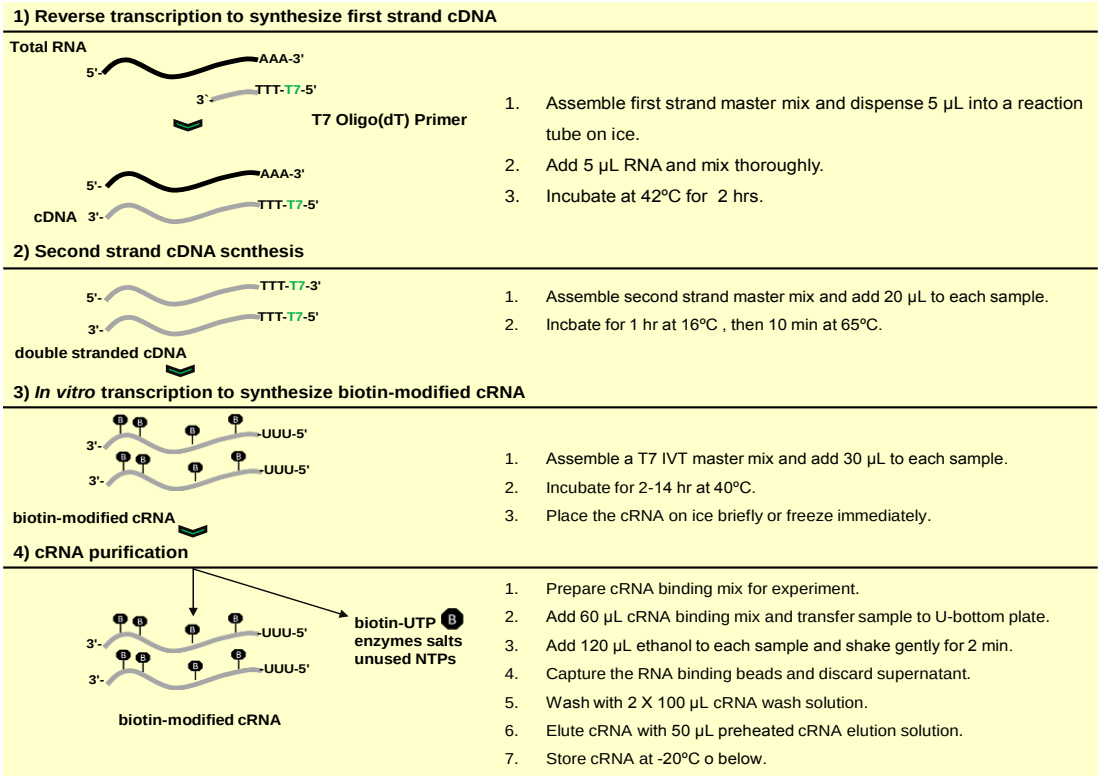

Fig. 2.5: MessageAMP™ Premier RNA Amplification procedure (Ambion, Austin, TX, USA). Step 1: A cDNA with a T7 promoter sequence was synthesized. **Step 2:** The single-stranded cDNA was converted into a double-stranded DNA (dsDNA) template for transcription. In order to degrade the RNA and synthesize second-strand cDNA, DNA polymerase and RNaseH was used. **Step 3:** The biotin-labelled cRNA was generated from the double-stranded cDNA templates with the T7 Biotin IVT Mix. **Step 4:** Any inorganic phosphates, salts, unincorporated nucleotides, and enzymes were removed to generate pure and stable cRNA. (Adapted from the MessageAMP™ Premier RNA Amplification Kit.)

2.15.5 Hybridization of fragmented cRNA (fcRNA) to the GeneChip

A Hybridization Cocktail Mastermix was prepared following the instructions (Box 2.3) and stored at -20°C. To ensure that the cRNA is fully resuspended, the B2 Oligo tubes and 20 × GeneChip Eukaryotic control were heated to 65°C for 5 min. Prior to the hybridization, the probe arrays were allowed to warm up to room temperature (to avoid

septa from cracking, and leaking). The cRNA (30 µL) was transferred to 1.5 mL RNAase- free screw-cap tubes, to which 270 µL of the hybridization cocktail mastermix was added and mixed by pipetting. The completed hybridization cocktail was first heat denatured at 99°C for 5 min, and then placed for 5 min into the 45°C prewarmed hybridization oven. All tubes were centrifuged at maximum speed for 5 min, to remove the insoluble fraction from the hybridization cocktail.

- 30 µL fragmented and labelled cRNA
- 5 µL of control oligonucleotides B2 (3 nM)
- 15 µL of 20× Eukaryotic Hybridization controls (bioB, bioC, bioD, cre)
- 3 µL of Herring sperm DNA (10 mg/mL)
- 3 µL of acetylated BSA (50 mg/mL)
- 150 µL of 2 × Hybridization buffer
- 30 µL of DMSO
- 64 µL of RNAase-free H_2O

Total Volume: 270 µL

Box 2.3: Hybridization cocktail mastermix for the GeneChip hybridization (note: 300 µL of hybridization cocktail is sufficient for three chip hybridizations). The protocol is based on the standard labelling protocol (Genomic centre, King's College London, UK).

The microarray chips were first allowed to warm up to room temperature to equilibrate, then filled with 250 µL 1 × Hybridization buffer (GenChip® 3' IVT Express Kit Manual, Affymetrix, US) and placed into a rotisserie oven set to 45°C for 10 min, 60 r.p.m. rotating for prehybridisation. Thereafter, the prehybridization solution was replaced with 200 µL of clarified hybridisation cocktail. Arrays were returned to the hybridization oven for ≥ 16 hrs, rotating at 60 r.p.m. to allow hybridization to take place at 45ºC.

2.15.6 Washing, staining and scanning

After the overnight microarray hybridization was completed, the hybridization cocktail was removed from the chip and replaced with 250 µL of the Wash Buffer A (The GeneChip® Expression Wash, Stain and Scan User Manual, P/N 702731, Affymetrix, US), to remove nonspecific binding. The chips were placed into the fluidics station and the hybridization cocktail was aliquoted back into the tubes and stored at -20°C.

For chip staining, 600 µL of the Stain solution and 600 µL of Antibody solution were prepared in separate 1.5 mL microcentrifuge tubes, following the instructions (Box 2.4). Each chip was washed, to remove any unhybridized cRNA, and subsequently stained following the standard protocol (The GeneChip® Expression Wash, Stain and Scan User Manual, P/N 702731, Affymetrix, US). Finally, the arrays were scanned on an Affymetrix GeneChip® Scanner 3000 (Affymetrix, US), which is controlled by Affymetrix ® Microarray Suite or GCOS.

Stain solution mastermix:	**Antibody solution mastermix:**
• 600 µL of the 2 × Stain Buffer • 48 µL of acetylated BSA (50 mg/mL) • 540 µL of DI H_2O • 12 µL of Streptavidin Phycoerythrin (SAPE) (1 mg/mL) Total volume of 1200 µL.	• 300 µL of 2 × Stain Buffer • 266.4 µL of DI H_2O • 24 µL of acetylated BSA (50 mg/mL) • 6 µL of normal Goat IgG (10 mg/mL) • 3.6 µL of biotinylated antibody (0.5 mg/mL) Total volume of 600 µL.

Box 2.4: Stain solution and Antibody solution mastermix. The protocol is based on the standard labelling protocol (Genomic centre, King's College London, UK).

2.15.7 Raw data analysis and quality control checks

The pre-processing of raw microarray data was done in Affymetrix ® Microarray Suite or GCOS. First, a probe-specific background correction was applied, followed by quality GeneChip® Probe Arrays controls: 1) Hybridization controls: bioB, bioC, bioD from *E. coli* and cre from P1 bacteriophage; 2) Poly-A controls: dap, lys, phe, thr, trp from *B. subtilis*; and 3) *C. elegans* maintenance genes: actin, catalase, GAPDH, *gly14*, ubiquitin. The data intensities were log transformed by use of the robust multivariate average (RMA) algorithm (Irizarry et al., 2003), and normalized within and between arrays with a quantile method. If the hybridization signal for a specific probe was significant above background level ($p < 0.005$), and it was deemed to be present across all arrays, the gene was considered for analysis.

2.15.8 Statistical analysis, DAVID Bioinformatics Resources 6.7, Qlucore

The list of all differentially expressed genes and annotations (Wormbase, http://www.wormbase.org) was outputted as an Excel file. The list was first sorted according to the STDEV and $p < 0.05$, followed by fold-changes (on a binary logarithmic scale). The fold-cut off values deemed to be "biologically significant" were defined as > 1.5 and less than < 0.8 – fold (compared to control gene expression for data comparisons between different conditions). The differences between treatments were visualized by principal component analysis (PCA) performed in Qlucore Omics Explorer Version 2.3 (Qlucore AB, Lund, Sweden), which uses ANOVA statistics to generate lists of significantly changing genes. The software system also takes into account batch effects.

Differential expressed genes (DEGs) showing a "biologically significant" fold change with NIST exposure, regardless to the dose applied, were sorted in Excel. For probe annotation and gene ontology (GO) analysis, all transcripts that fell into the specified selection criteria were first visualized using Venn diagrams searching for common overlapping targets across the data set, which were then entered into the Database for Annotation, Visualization and Integrated Discovery (DAVID) for functional annotation. Functional clusters were identified using DAVID Bioinformatics Resources 6.7, DAVID's Functional Annotational Clustering tool (Dennis, et al. 2003) using the highest classification stringency. The Enrichment Score on each term was used to predict whether representation of a gene group among selected genes was biologically significant. The p-values correspond to the probability that the members are clustered together by chance (Fisher Exact P-Value = 0, represents the perfect enrichment).

2.15.9 Microarray validation

For the microarray validation, a qRT-PCR was performed on 24 genes, and expression profiles were compared using both independently derived RNA samples and RNA samples that were utilized for microarray processing. The expression profiles of successfully analysed transcripts were compared with their expression profile from microarray platform.

The genes chosen for microarray validation were selected on the following criteria: transcripts, which are functionally involved in stress response pathways (e.g. sod family; *cat-2*, *cat-3*, *gsr-1*, GSTs, and *hsp-16.1*); genes that are involved in transition metal binding (e.g. *mtl-1*, *mtl-2*, *ftn-1*, and *cuc-1*), and calcium channel activity (e.g. *unc-68*); and finally transcripts whose expression is linked to development (e.g. *cnx-1*,

and *clec-13*), metabolic processes (e.g. *gei-7*, and *aco-1*), apoptosis (*cep-1*), and transcriptional regulation (e.g. *rrn-3.1*, *skn-1*, and *sdz-24*).

The cDNA was synthesized following the protocol described in Materials and methods section 2.14.2 and the qRT-PCR was performed using the ABI Prism7000a platform (Applied BioSystemy, Warrington, UK). All primers and probe sequences were obtained from the Universal probe Library (Roche Applied Science, UK) (list is available in Appendix: Materials and methods), and the 25 µL reactions were performed in triplicate (protocol 2.14.3). The expression data was normalized to the *rla-1* reference gene (encoding an acidic ribosomal subunit protein P1), an invariant control gene that was not affected by NIST 1648a treatment either within the microarray data/or following qRT-PCR. The ΔΔ CT (cycle threshold) method was used to calculate the fold change in gene expression (Pfaffl et al., 2002).

2.16 Data analysis

Statistical analysis was performed using the Graphpad Prism software package (Graphpad Software Inc. USA). Significance was calculated by means of a one-way ANOVA followed by Tukey post-hoc test. Where indicated, the 2-way ANOVA was utilized to determine the interaction based on two experimental factors, nematode strain and particle treatment matched group sets of measurements, followed by Bonferroni multiple comparison test.

Statistical significance is indicated by ns (non-significant), * is $p<0.05$, **$p<0.01$, ***$p<0.001$ and ****$p<0.0001$.

CHAPTER THREE

ZnONP induced toxicity in

Caenorhabditis elegans

3.1 Introduction

Over the past two decades the field of nanotechnology has expanded significantly, primarily due to the growing use of nano-sized particles in industry and research. NPs are characterized by a large surface area per unit mass, a quantum physical trait which has facilitated the manipulation of nanomaterials to exert new or enhanced optical, electronic and/or mechanical properties (Oberdörster et al., 2005). More specifically, metal oxide nanomaterials, such as zinc oxide nanoparticles (ZnONPs), are antimicrobial and therefore widely used by the cosmetics and painting industries, in bio-medicine to enhance cell imaging and drug delivery, and even in agriculture to control food borne pathogens (Dafour et al., 2006; Stoimenov et al., 2002; Wang et al., 2004; Tayel et al., 2011; Nohynek et al., 2010).

Despite their potential commercial advantages, it has been recognised that exposure to ZnONPs may pose a risk to human health (Rohrs, 1957; Shilling et al., 2010) and to the environment (Colvin et al., 2003; Nowack et al., 2012). The harmful effects of ZnONPs are driven by their physicochemical properties (dissolution and formation rate, their morphology and chemical composition, surface reactivity, particle numbers, etc.) and the resulting physical damage caused by the aggregation and agglomeration of nanoparticles (Bai et al., 2010; Jiang et al., 2009; Zhang et al., 2010). Furthermore, ZnONPs mediated toxicity may result from the release of free ionic zinc (George et al.,

2010; Li et al., 2011; Poynton et al., 2011; Wang et al., 2009) which induces cellular damage via the generation of free ROS, which in turn can promote pro-inflammatory effects (Kao et al., 2012; Mocchegiani et al., 2011).

The bio-kinetic behaviour and *in vivo* toxicity of ZnONPs exposure has, to date, been investigated in several non-mammalian systems including *in vitro* cell-based assays (Sharma et al., 2012a; Sharma et al., 2012b; Ahamed et al., 2011; Wu et al., 2010), bacteria (Li et al., 2011b; Reddy et al., 2007), algae (Franklin et al., 2007), plants (Lin et al., 2007), crustaceans (Poynton et al., 2011), fish (Bai et al., 2010), earthworms (Hooper et al., 2011) and nematodes (Ma et al., 2009; Wang et al., 2009). Indeed, the nematode *Caenorhabditis elegans*, a powerful model organism due to the availability of a completely sequenced genome (Hillier et al., 2005) and the many available molecular genetic tools has been used in ecotoxicological research to study the molecular to organismal level responses to ROS and heavy metal challenges (Roh et al., 2006; Hughes et al., 2007; Swain et al., 2004; Swain et al., 2010; Zeitoun-Ghandour et al., 2010; Zeitoun-Ghandour et al., 2011). The roles of the metallochelators metallothionein (MT) and phytochelatin (PC) are assumed to be multi-functional, including metal sequestration, transportation, detoxification as well as antioxidant protection (Margoshes et al., 1957; Sato et al., 1993; Cobbett, 2000; Vatamaniuk et al., 2005; Vatamaniuk et al., 2001; Swain et al., 2004; Freedman et al., 1993). When nematodes are exposed to excess metal ions, such as Cd^{2+} or Zn^{2+}, the expression of MTs and PCs is attenuated and thereby prevents metal accumulation and cytosolic damage (Hughes et al., 2007; Ma et al., 2009). In contrast, organisms with impaired metallochelator function suffer from metal-induced cellular stress, as well as an impaired developmental and reproductive capacity (Hughes et al., 2009; Zeitoun-Ghandour et al., 2011). Given

this extensive knowledgebase, *C.elegans* is an ideal model organism to study the toxicogenomics of ZnONPs exposure.

3.2 Aims

The aim of the work described in this chapter was to study the particle-specific effects of manufactured metal oxide nanoparticles by examining the toxicogenomic responses in the small free living nematode *Caenorhabditis elegans*. Wild-type nematodes and a metal sensitive triple knockout mutant (*mtl-1;mtl-2;pcs-1*(zs2)) were exposed to ZnONPs (0 - 50 mg/L) and strain specific effects on transcription, reactive oxygen species (ROS) generation, the biomolecular phenotype (measured by Raman microspectroscopy) and key endpoints of the nematode life cycle were investigated. The interplay between ZnONPs exposure, metal ion release and/or ROS activity were defined, with the aim to establish whether toxic effects are amplified in nematodes lacking key metal chelators.

3.3 Results

3.3.1 Characterization of ZnONPs

3.3.1.1 Transmission electron microscope (TEM) imaging

The shape and size of ZnONPs suspended in stock solution was examined by transmission electron microscopy (TEM). The majority of ZnO nanoparticles were acicular in shape and clustered typically in the 30 nm to several 100 nm range (Fig. 3.1A), which may be attributed to the reduced surface charge (the initial zeta potential of NPs in DI water was 20.7 ± 2.0 mV (Heggelund et al., 2014)), and thus weaker electrostatic repulsive forces.

Time-dependant changes in agglomerate levels were assessed by measuring particle size distribution in LB broth in the absence of bacteria at 0 hours and 24 hours (Fig. 3.1B-C), and in the presence of OP50 bacteria at 0 hours and 24 hours (Fig. 3.1D-E). Although the formation of particle clusters was observed as soon as the nanoparticles were added to the LB broth (the 0 hour time point), the level of agglomeration did not increase over time. Based on the TEM images, ZnONP agglomerates did not seem to enter the bacteria nor damage their morphology. However, continuous contact with the ZnONPs caused the bacteria to secrete extracellular polymeric substances (EPS) which coated the nanoparticles within the 24 hour timeframe (Fig. 3.1E).

In addition, energy dispersive X-ray (EDX) analyses and chemical mapping was utilized to define the zinc gradient, namely the relationship between Zn concentration and distance to a nanoparticle (Fig. 3.1F-G). The Zn content, as measured by TEM-EDX, was approximately 50 % at the ZnO particles. Moving 1 µm and 3 µm from the ZnO agglomerates reduced the Zn content to 6 % and < 3 %, respectively. Given that

background levels were 1-2 % Zn indicates that Zn dissolves from the ZnO agglomerates and diffuses into the medium within 24 hours.

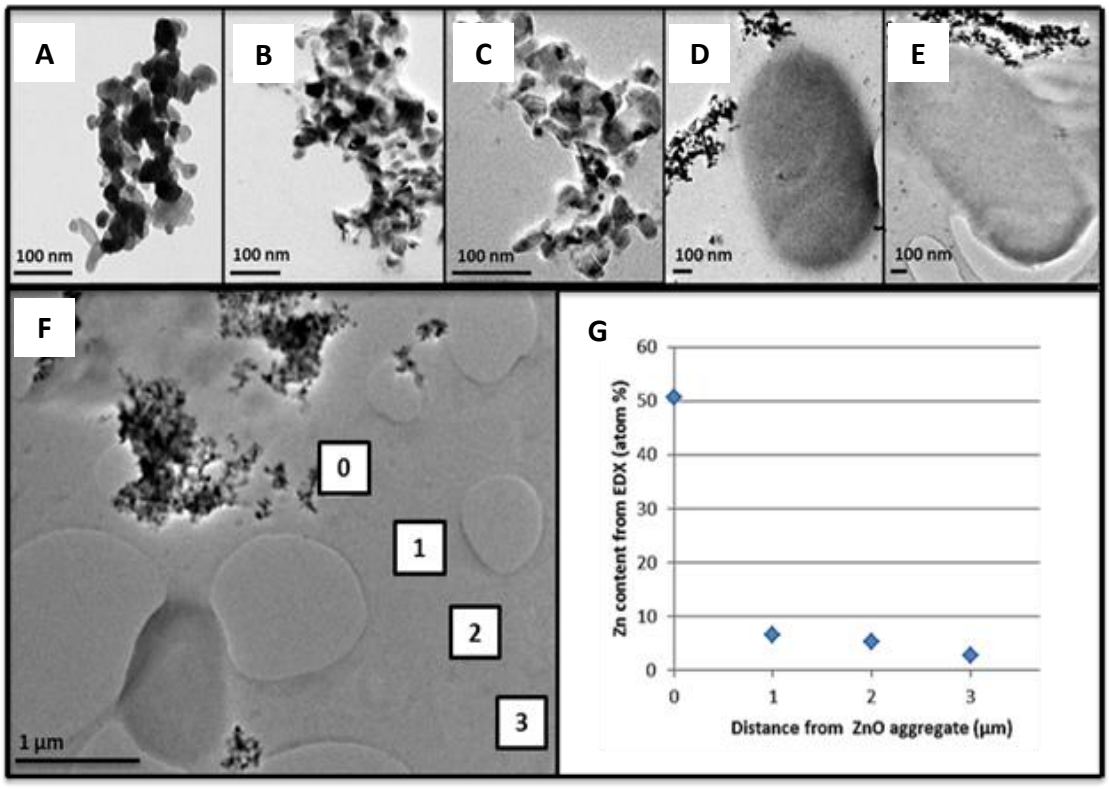

Fig. 3.1: **TEM images of the nanoparticles.** Images of ZnONPs in HPLC water (A), in LB-broth (no bacteria) at 0 hrs (B), at 24 hrs (C), in LB-broth with bacteria (OP50) at 0 hrs (D), and after 24 hrs (E). Energy Dispersive X-ray (EDX) analyses and chemical mapping on four micron-sized windows (F) was performed to determine the percentage of Zn content (G). Representative images from n=12 in total. Note: adjacent to the ZnONP agglomerate, elemental Zn levels were 50 % (spectrum 0) and decreased with distance from the ZnONPs (spectrum 1, 2 and 3).

3.3.1.2 Dynamic Light Scattering (DLS)

Dynamic Light Scattering (DLS), a technique that measures particle dimensions in the biological test medium, was performed on ZnONP suspensions in LB broth (with and

without OP50 bacteria). In LB broth, ZnONPs assembled into clusters of 1 micron diameter (Fig. 3.2A). However, as the bacteria are of a similar size and appear as a broad peak when measured with DLS (Fig. 3.2B) it was not possible to distinguish peaks from the ZnO particles and the bacteria (Fig. 3.2C). These results suggest that ZnONPs exist mainly as stable agglomerate complexes in the test medium and this is independent of bacteria status.

3.3.2 Effects on dietary restriction

An investigation was carried out in order to explore whether nanosized ZnO suspensions exert antimicrobial effects on bacteria. Whilst chronic exposures up to 50 mg/L ZnONP did not affect the sigmoidal growth characteristics of OP50 *E.coli*, strong antibacterial effects were observed at 100 mg/L ZnONPs, a finding that was statistically significant ($p<0.05$) (Fig. 3.3). These effects were not due to a time or concentration dependant change in pH, as pH of the bacterial solution remained at ~pH7 over a period of 72 hours (see Appendix: ZnONPs). For this reason, an upper limit of 50 mg/L ZnONPs was chosen for all experiments, mainly to avoid possible effects induced by dietary restriction.

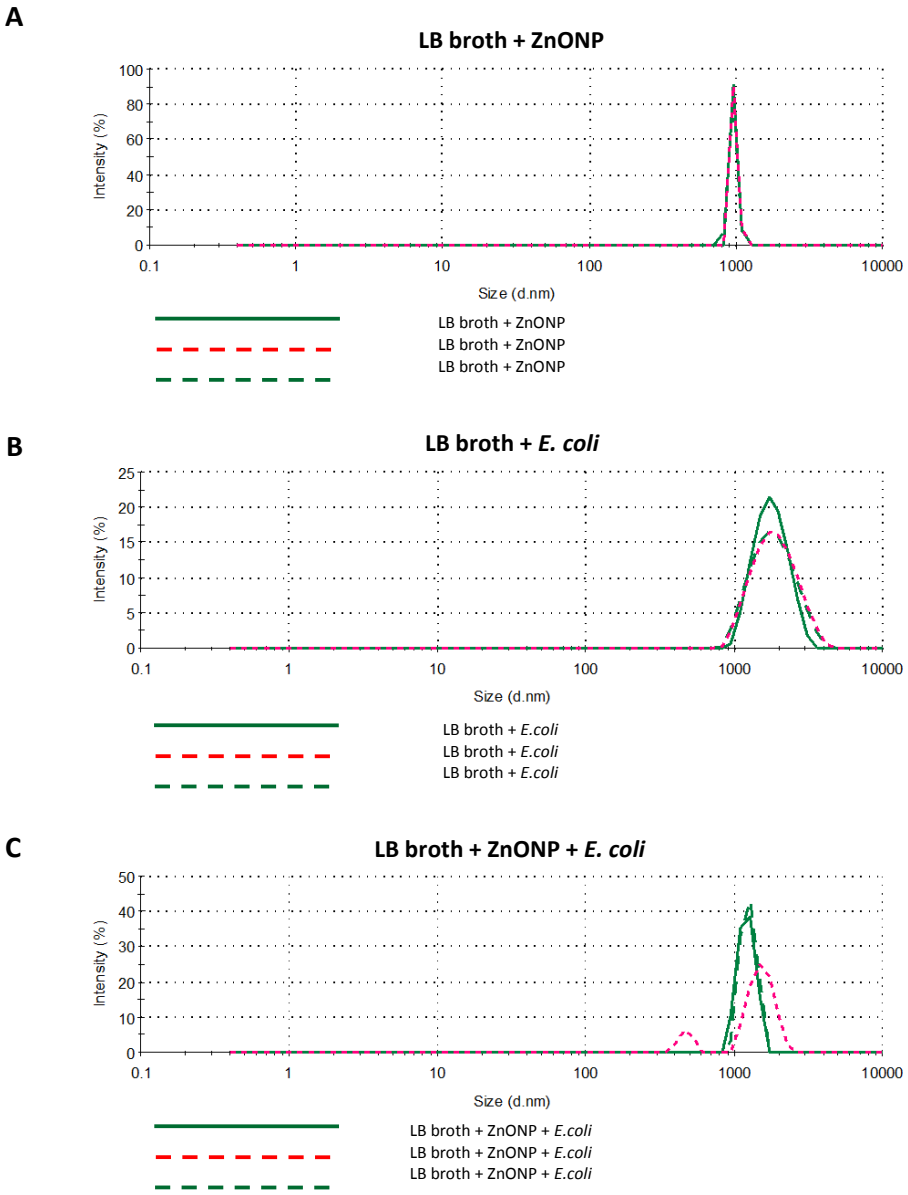

Figure legend:

- **Size (d. nm)** – particle size distribution in the range of 0.1 nanometers up to 10 microns
- **Intensity (%)** – The percentage intensity of the amount of light scattered, which is dependent on the molecular weight, size, and shape of a particle (agglomerates), and the refractive indices of the particle and solvent.

Fig. 3.2: Measuring the size of ZnONPs agglomerates by Dynamic Light Scattering (DLS) spectrometry. The characterization was performed at ZnONPs in HPLC water (A), ZnO particles in LB broth without OP50 bacteria (B) and in LB broth with OP50 bacteria (C). Three replicates were tested per condition.

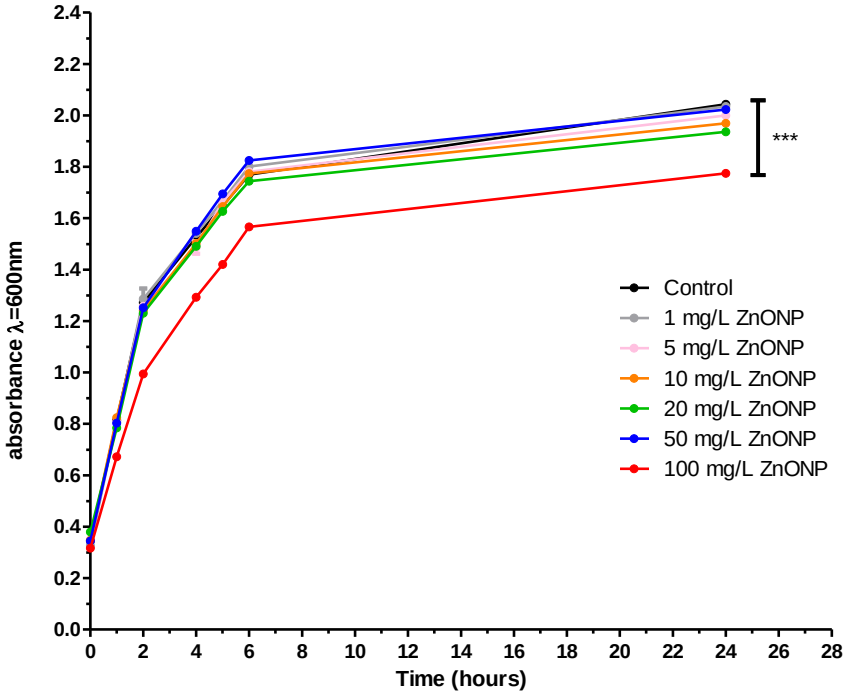

Fig. 3.3: ZnONPs induced effects on bacterial growth. OP50 *E. coli* was incubated at 37°C for 24 hours in the absence and presence of ZnONPs. Error bars denote ± SEM (n=4). Statistical analysis was performed using the one-way ANOVA comparing untreated and ZnONPs treated group sets of measurements with significance, *** denotes $p<0.001$.

3.3.3 Exposure to ZnONPs induces the expression of P*mtl-2*::GFP and P*pcs-1*::GFP

The two *C. elegans* metallothioneins (MTs), *mtl-1* and *mtl-2* (encoding CeMT-1 and CeMT-2, respectively), are key players in the protection against metal and ROS toxicosis (Swain et al, 2004; Zeitoun-Ghandour et al., 2011). In addition, phytochelatin synthase, *pcs-1*, encodes a metal-dependant antioxidant enzyme (Schwartz et al., 2010; Vatamaniuk et al., 2001; Vatamaniuk et al., 2005), which with GSH synthesizes phytochelatins (PCs). In nematodes, *pcs-1* is expressed in the pharynx and rectal valves

where it is believed to be regulated by changes in oxidant status rather than changes in gene expression (Vatamaniuk et al., 2005).

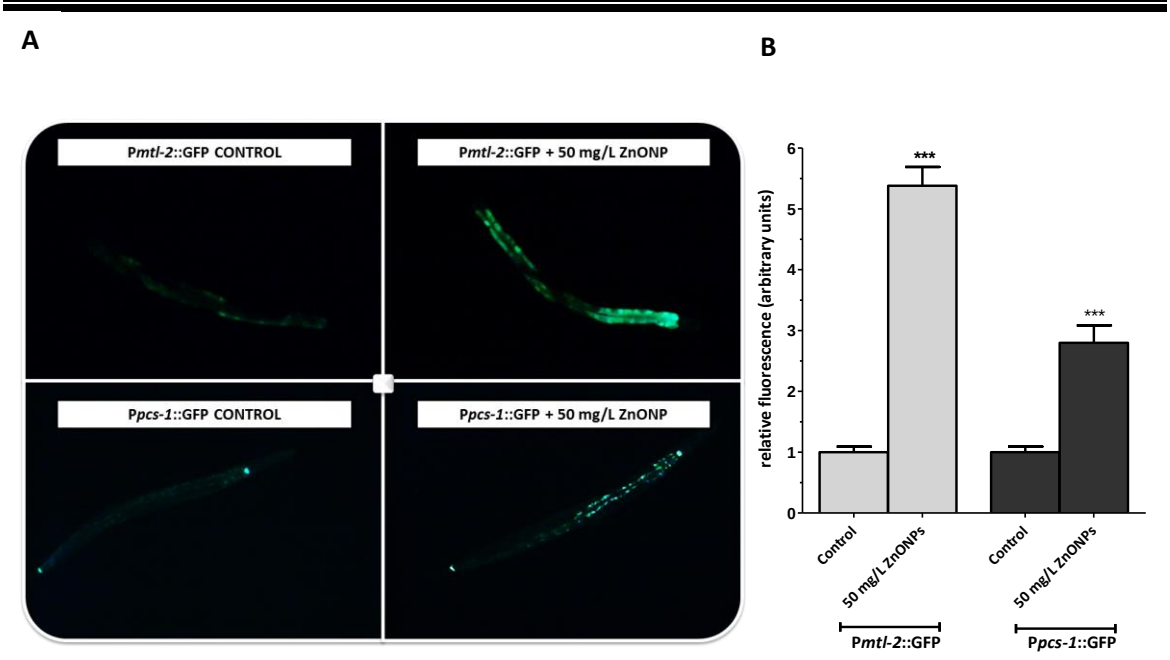

Fig. 3.4: Induction of green fluorescence protein (GFP) (measured as relative fluorescence units) in transgenic P*mtl-2*::GFP and P*pcs-1*::GFP worms in response to ZnONPs. Exposure to ZnONPs induces intestinal *mtl-2*; and pharyngeal and rectal valve *pcs-1* expression in the transgenic nematodes. The fluorescence images are representative control and ZnONPs exposed nematodes, illustrating the induction potential of P*mtl-2*::GFP and P*pcs-1*::GFP following a ZnONPs challenge (50 mg/L) **(A)**. A quantitative analysis of GFP induction (measured as relative fluorescence units) confirmed that a significant transcriptional of response *mtl-2* and *pcs-1* is mediated by ZnONPs **(B)**. Error bars represent the standard error (n=10) and statistical analysis was performed using the Wilcoxon signed rank test, where ***denotes $p<0.001$.

In order to determine whether these metallochelators are transcriptionally activated by ZnONPs, transgenic worms bearing extra-chromosomal copies of the promoter fusion construct P*mtl-2*::GFP or P*pcs-1*::GFP were exposed to 50 mg/L ZnONPs. The

induction of P*mtl-2*::GFP was most profound in the intestinal region and was marked by a 5.3 - fold increase in relative fluorescence (Fig. 3.4). Whilst expression of P*mtl-2*::GFP under control conditions (in the absence of ZnONPs) was overall negligible, P*pcs-1*::GFP was shown to be constitutively expressed in the posterior pharyngeal cells and the anal valve. Following the ZnONPs challenge, P*pcs-1*::GFP fluorescence increased by 2.8 - fold, again mainly in the intestinal cells (Fig. 3.4).

3.3.4 Defining ZnONP-mediated changes in fluorescent reporters using a transgenic *C. elegans* system

Changes in the transcription-activated fluorescence (upon ZnONPs exposure) were quantified using transgenic worms generated and provided by Knudra Transgenics, USA. These MosSCI transgenic nematodes were created as a biosensor platform for toxicological diagnosis/profiling of toxic compounds. The stable (integrated) transgenes are generated based on the technology of MosSCI transgenesis (Frokjaer-Jensen et al., 2008). The transgenic strains are dual-labelled with the promoter of a constitutively expressed housekeeping gene tagged to green fluorescent protein (GFP), and a promoter of a toxin-sensitive gene tagged to mCherry red fluorescent protein (RFP). The two-coloured transgenic worm is created by injecting a vector carrying a hsRFP reporter (an mCherry protein fused to the *his-57* histone gene) into a nematode expressing GFP (*unc-47*::GFP). The GFP functions as an internal control in the analysis, as it allows the normalisation of background signal or population/nematode size differences, and the fluorescence of mCherry is activated by the respective xenobiotic.

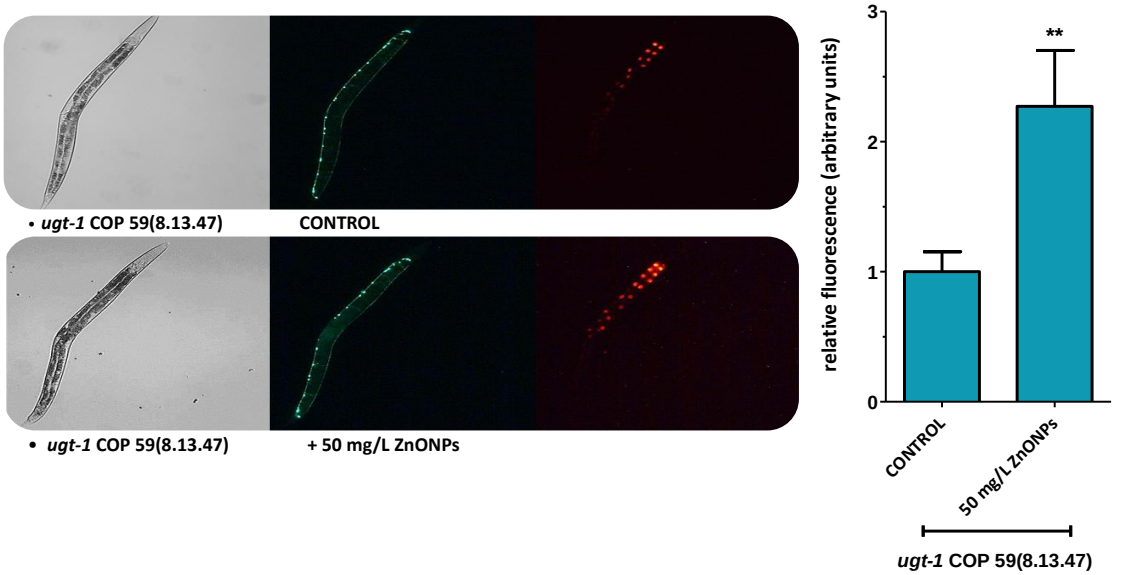

Fig. 3.5: Fluorescence images and a quantitative analysis of a significant induction of *ugt-1::*mCherry expressed as relative fluorescence units following normalization to the invariant *unc-47::*GFP. 10 worms were observed in each experimental condition (0 and 50 mg/L ZnONPs) and error bars represent ± SEM. Statistical analysis was performed using the Wilcoxon signed rank test, where **denotes $p<0.01$.

The following transgenic strains bearing intra-chromosomal promoter fusions were selected: two heat shock proteins (*hsp-16.2*, and *hsp-16.41*), a cytochrome P450 (*cyp-35A2*), an ortholog of gamma-glutamine cysteine synthase heavy chain (GCS(h)) (*gcs-1*), a glutathione-S-transferase (*gst-4*, and *gst-38*), a uridine diphosphate-glucuronosyl/glucosyl transferase gene (*ugt-1*), and a gene encoding a protein containing a DnaJ ('J') domain (*dnj-13*). All strains were exposed to 0, and 50 mg/L ZnONP. A 48 hour exposure to ZnONPs results in the most profound, statistically significant increase in *ugt-1* expression (measured as relative fluorescence units) in the anterior intestinal region (Fig. 3.5). An analysis of fluorescence from 10 nematodes, quantified this as a 2.3 – fold increase ($p=0.0052$) (Fig. 3.5). No other significant differences were found in any of the other transgenic nematode strains following the

ZnONPs challenge (Fig. 3.6). All transcripts expression remained at the basal-control level.

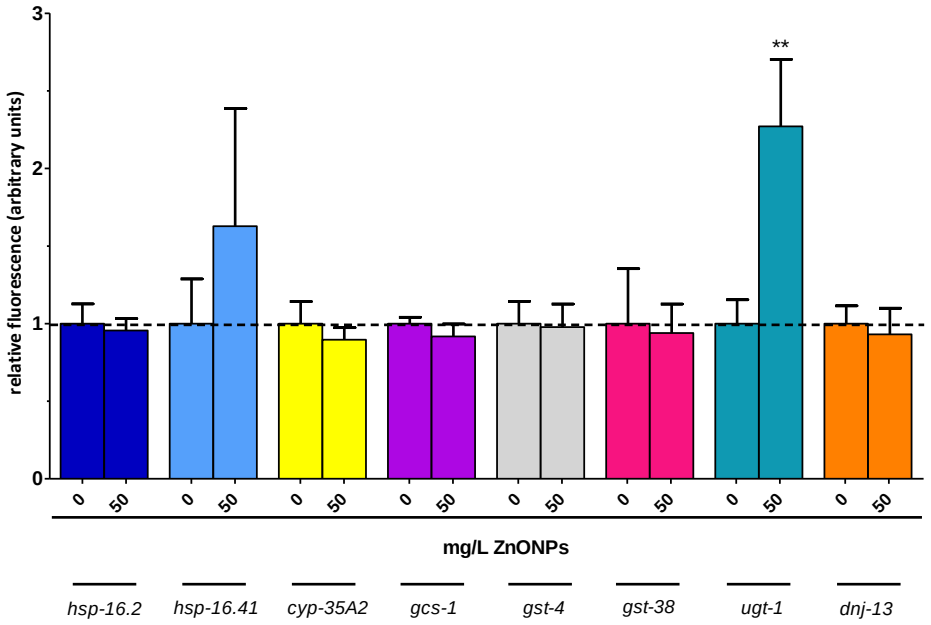

Fig. 3.6: Quantitative analysis of the transcription-activated promoter of the genes of interest::mCherry expressed as relative fluorescence units following normalization to the invariant *unc-47*::GFP in response to ZnONPs. 10 worms were observed in each experimental condition (0 and 50 mg/L ZnONPs) and error bars represent ± SEM. Statistical analysis was performed using the Wilcoxon signed rank test, where **denotes $p<0.01$. Note: whilst *hsp-16.41* was induced by ZnONPs exposure, only *ugt-1* was deemed to be statistically significant.

3.3.5 Quantitative assessment of ZnONPs- responsive gene expression

A quantitative real-time polymerase chain reaction (qRT-PCR) was performed on a number of genes, which were previously identified as possible biomarkers of NPs toxicity (Akhtar et al., 2012) or due to their established involvement in oxidative stress response pathways and anti-apoptotic activity (Van Raamsdonk et al., 2010; Huang et al., 2010). The following transcripts were examined: metallothionein (*mtl-1*), superoxide dismutases (*sod-1*, and *sod-3*), catalases (*ctl-2*, and *ctl-3*), peroxidase (*prdx-*

3), and a heat shock protein (*hsp-16.1*). In addition, the expression level of two further transcripts was determined, namely *cep-1* (an ortholog of the human tumour suppressor p53) and *dct-1* (which resembles the mammalian BCL2/adenovirus E1B 19kDa protein-interacting protein 3, BNIP3).

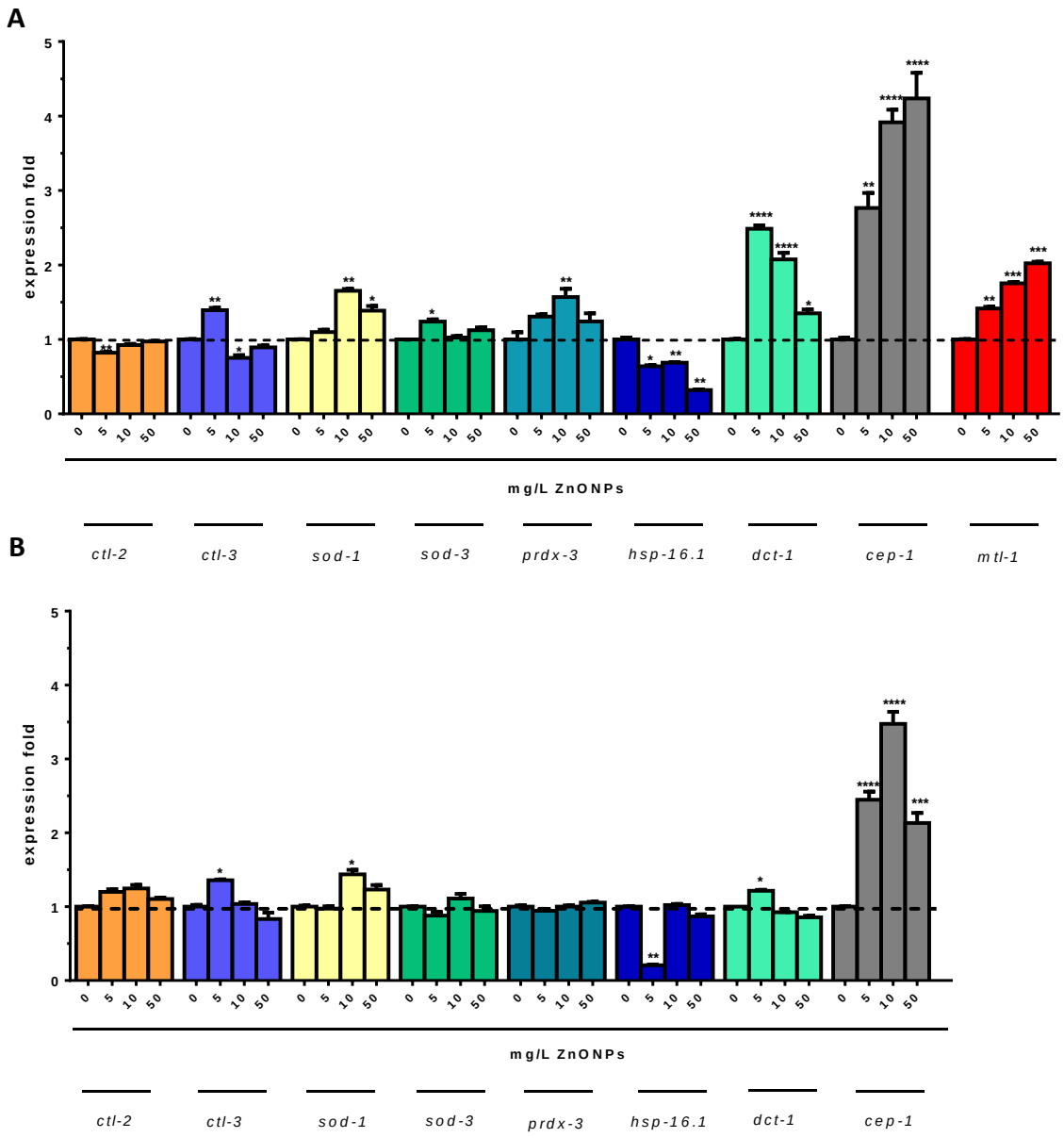

Fig. 3.7: Quantitative assessment of ZnONPs- responsive gene expression of wild-type (A) and *mtl-1;mtl-2;pcs-1*(zs2) mutant nematodes (B). Technical repeats n=3, biological repeats n=2. Error bars represent mean ± SEM. Statistical analysis utilized the one-way ANOVA comparing untreated and ZnONPs treated matched group sets of measurements, where * $p<0.05$, ** $p<0.01$, *** $p<0.001$, and ****$p<0.0001$.

Four transcripts (*mtl-1*, *sod-1*, *cep-1*, and *dct-1*) were significantly induced and the *hsp-16.1* transcript was found to be significantly down-regulated by ZnONP exposure (Fig. 3.7A). The analysis facilitated transcript-based assessment of the physiological status of the nematode following a 48 hour exposure to ZnONPs (0 – 50 mg/L).

The mRNA expression levels were also quantified in the triple knockout mutant *mtl-1;mtl-2;pcs-1*(zs2) nematode (bar the *mtl-1*, which cannot be measured in the null background). As in wild-type, *cep-1* was significantly upregulated upon ZnONP exposure, but *dct-1* was not. The *hsp-16.1* transcript was significantly down-regulated by 5 mg/L ZnONPs concentration, however the transcript expression remained at the basal level at all other tested doses (Fig. 3.7B). The remaining transcripts tested (*ctl-2*, *ctl-3*, *sod-1*, *prdx-3*) did not change upon ZnONPs exposure (Fig. 3.7B) (for a replicated experiment see Appendix: ZnONPs).

3.3.6 Detection of free radical levels in *C. elegans* exposed to ZnONPs

Given that the ZnONPs are capable of generating ROS in nematodes, a cell permeable DCFH-DA dye was utilized to facilitate the direct quantitative intracellular ROS measurements and thereby explore the stress response level of the nematodes to ZnONPs. Intracellular ROS production was measured in wild-type, and *mtl-1;mtl-2;pcs-1*(zs2) mutant *C. elegans* in the presence or absence of 20 and 50 mg/L ZnONPs for 48 hours (Fig. 3.8).

This assay provided evidence that the relative base-line level of the ROS generated in cells in both the wild-type control and the mutant control nematodes is similar. An exposure to ZnONPs resulted in a significant ($p<0.05$) decrease in the total intracellular

ROS levels in the wild-type strain (the total fluorescence intensity of the DCF moiety decreased by 13.23 %, and 11.69 % compared to the control levels). In contrast, the ROS levels in the *mtl-1;mtl-2;pcs-1*(zs2) strain significantly ($p<0.05$) increased by 100.7% and 12.6 %, when exposed to ZnONPs (Fig. 3.8).

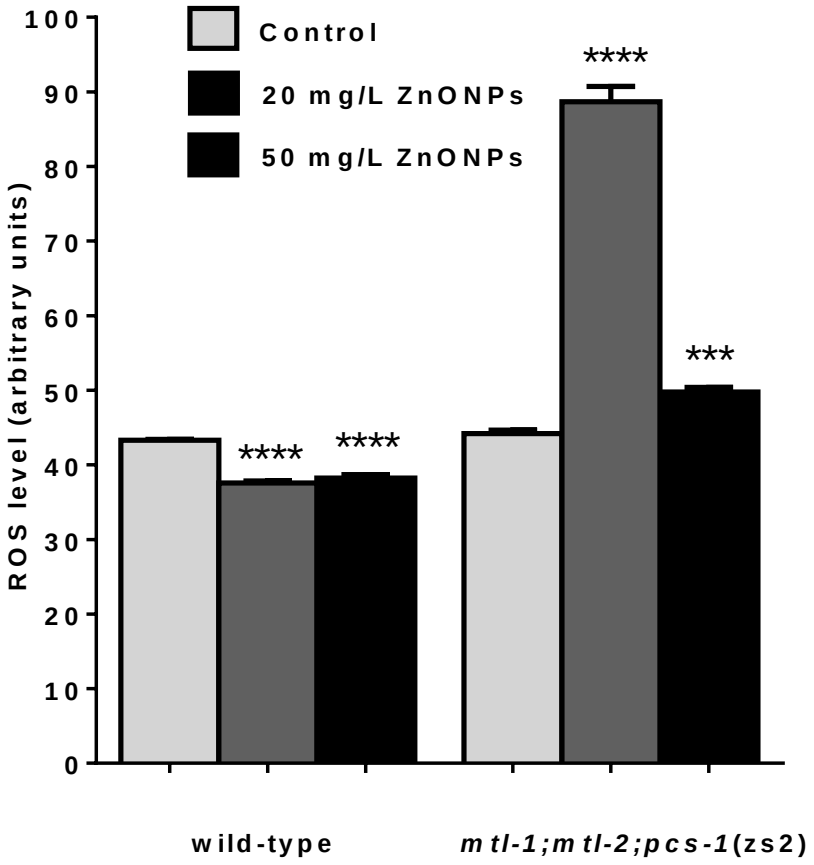

Fig. 3.8: Detection of free radical H_2O_2 levels in *C. elegans* exposed to ZnONPs. Wild-type worms and *mtl-1;mtl-2;pcs-1*(zs2) worms were exposed to 20 and 50 mg/L ZnONP. DCFH-DA was used to determine the production of ROS by meausring fluorescence at excitation 485 nm and emission 528 nm. Error bars represent mean ± SEM from n=4 technical repeats, and n=2 biological repeats). Statistical analysis was performed using the 2-way ANOVA Test to determine the interaction based on two experimental factors, nematode strain and ZnONPs treatment matched group sets of measurements, followed by Bonferroni multiple comparison test, where * is $p<0.05$, and ***$p<0.001$.

3.3.7 Raman spectroscopy

Raman spectroscopy can provide a phenotypic fingerprint of constituent biomolecules without the need of labelling or staining. The fine spatial scale mapping ability of Raman, particularly Coherent Anti-Stokes Raman Spectroscopy (CARS), has successfully been used to localise metal oxide nanoparticles in tissues (Moger et al., 2008; Galloway et al., 2010; Johnston et al., 2010). Here Raman spectroscopy was utilised to generate fingerprints from biological tissues to identify changes in the biomolecular phenotype in control and ZnONPs exposed wild-type and *mtl-1;mtl-2;pcs-1*(zs2) nematodes. An example of nematode tissue Raman spectra is represented in Fig. 3.9, with tentative peak assignments in Table 3.1.

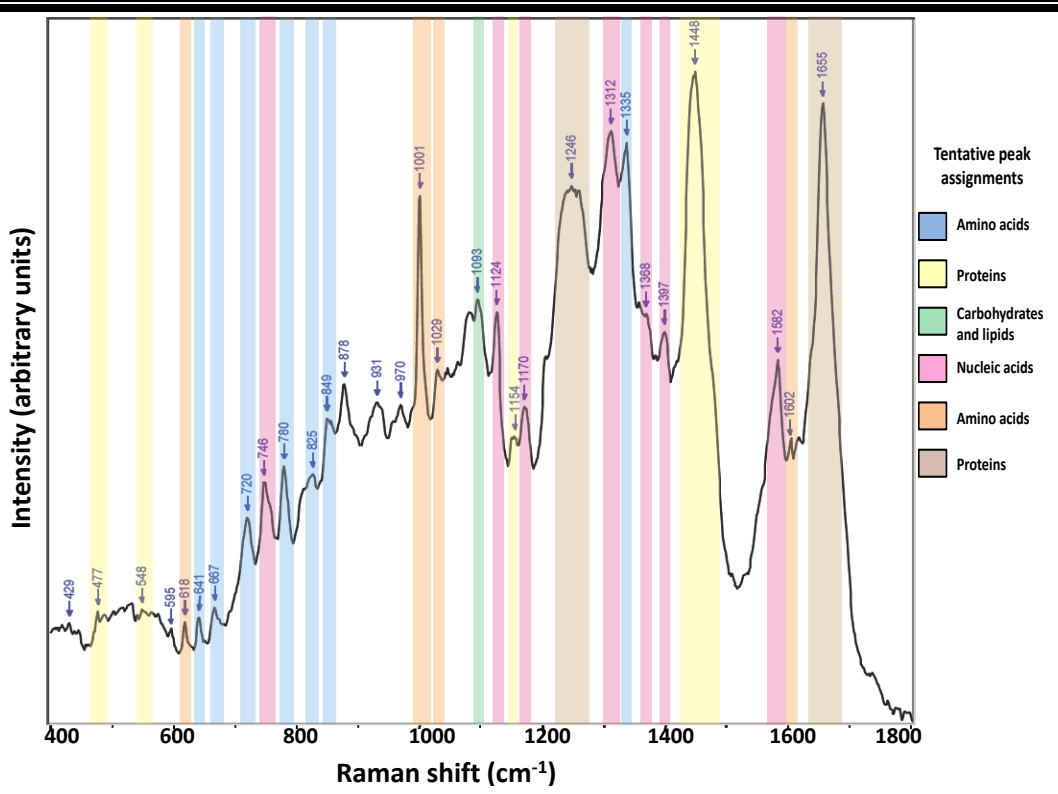

Fig. 3.9: A representative Raman spectrum and tentative peak assignments of nematode tissue. Each peak can be assigned to different classes of organismal biomolecules, such as amino acids, nucleic acids, proteins, carbohydrates and lipids.

Table 3.1: Assignment of Raman shift peaks.

1. Maquelin, K. *et al.* Identification of medically relevant microorganisms by vibrational spectroscopy. *Journal of Microbiological Methods.* **2002**, *51*:255-271.

2. Schuster, K.C.; Reese, I.; Urlaub, E.; Gapes, J.R.; Lendl, B. Multidimensional information on the chemical composition of single bacterial cells by confocal Raman microspectroscopy. *Analytical Chemistry.* **2000**, *72*:5529-5534.

3. Johannessen, C.; White, P.C.; Abdali, S. Resonance Raman optical activity and surface enhanced resonance Raman optical activity analysis of cytochrome c. *The journal of physical chemistry. A.* **2007**, *111*:7771-6.

4. Uzunbajakava, N. *et al.* Nonresonant Raman imaging of protein distribution in single human cells. *Biopolymers.* **2003**, *72*:1-9.

5. Harz, A.; Rosch, P.; Popp, J. Vibrational Spectroscopy-A Powerful Tool for the Rapid Identification of Microbial Cells at the Single-Cell Level. *Cytometry Part A.* **2009**, *75A:*104-113.

Frequency (cm^{-1})	Assignment	References
477	Skeletal modes of carbohydrates (starch)	1
549	COC glycosidic ring def	2
618	Phenylalanine (skeletal)	1
641	Tyrosine (skeletal)	1
667	Guanine	1
720	Adenine	1
746	Cytochrome c	3
780	Cytosine, uracil (ring, str)	1,4
825	Nucleic acids (C–O–P– O–C in RNA backbone)	2
849	Buried tyrosine	1
1001	Phenylalanine, substituted benzene derivatives	1
1029	Carbohydrates, mainly – C–C– (skeletal), C–O, def (C–O–H)	2
1093	Phosphate, CC skeletal, and COC str from glycosidic link	1
1124	Cytochrome c	3
1154	n(CC, CN), r(CH3)	1
1170	Tyrosine, phenylalanine	4
1246	Amide III random, lipids	2
1312	Cytochrome c	3
1335	Adenine, guanine, tyrosine, tryptophan	4,5
1386	Cytochrome c	3
1397	Cytochrome c	3
1448	C–H2 def	1
1582	Cytochrome c	3
1602	Phenylalanine	1
1655	Amide I	1

The Principal Component Analysis (PCA) on the spectra obtained from the head and tail regions of wild-type and *mtl-1;mtl-2;pcs-1*(zs2) nematodes raised in the absence of ZnONP yielded only minor, statistically non-significant, differences in the global phenotypic fingerprint (Fig. 3.10). Likewise, no statistically significant differences were identified between the respective head and tail regions of control and ZnONPs exposed wild-type nematodes (Fig. 3.11). In contrast, a statistically significant separation of the spectra was observed in the head and tail region of the *mtl-1;mtl-2;pcs-1*(zs2) mutant upon exposure to ZnONPs (head: R^2 = 0.102, p = 0.001; and tail: R^2 = 0.0438, p = 0.009) (Fig. 3.12). The fact that a statistically distinct phenotypic effect of ZnONPs exposure was only observed in *mtl-1;mtl-2;pcs-1*(zs2), confirms that the phenotype of the metallochaperone mutant is more affected by ZnONP exposure than wild-type nematodes. Examination of the average spectra derived from control and ZnONPs exposed nematodes gave some indication of the phenotypic changes (Fig. 3.13). Exposure to ZnONPs in *mtl-1;mtl-2;pcs-1*(zs2) nematodes caused reductions in peak intensities of proteins, amino acids (cytochrome c, amide I, phenylalanine) and nucleic acids, highlighting a broad effect on the nematode phenotype. Whether this physiological response to ZnONPs is directly dependant on metallothioneins and/or phytochelatins remains to be established.

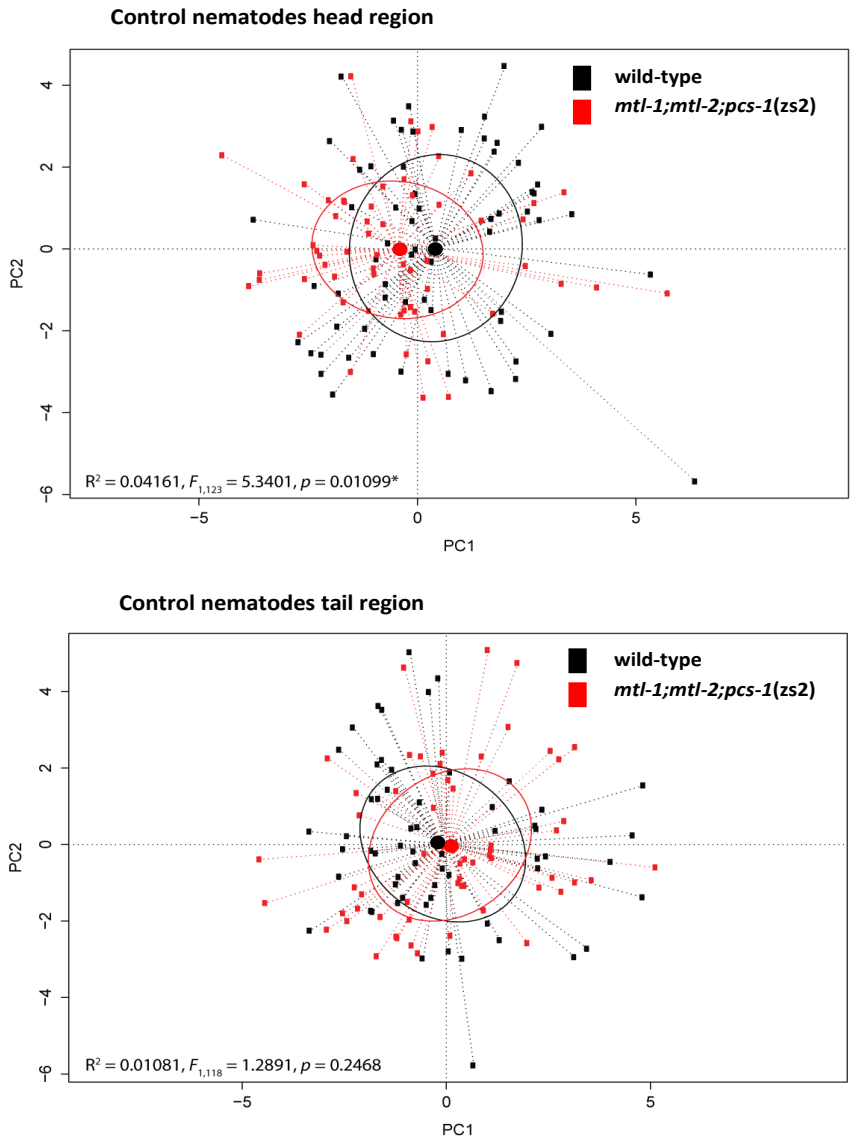

Fig. 3.10: Raman spectroscopy. Principal Component Analysis (PCA) in wild-type and *mtl-1;mtl-2;pcs-1*(zs2) nematode. PCA showing the relationship between the Raman phenotype of control wild-type and *mtl-1;mtl-2;pcs-1*(zs2) mutant nematodes in the head and tail regions. Points represent replicates within (n=5 per nematode) as well as between nematodes (n=25 per treatment). Black points represent spectra from control wild-type nematodes, red points represent spectra from *mtl-1;mtl-2;pcs-1*(zs2) mutant nematodes. Black and red ellipses represent standard deviations of point scores for the wild-type and *mtl-1;mtl-2;pcs-1*(zs2) mutant groups, respectively.

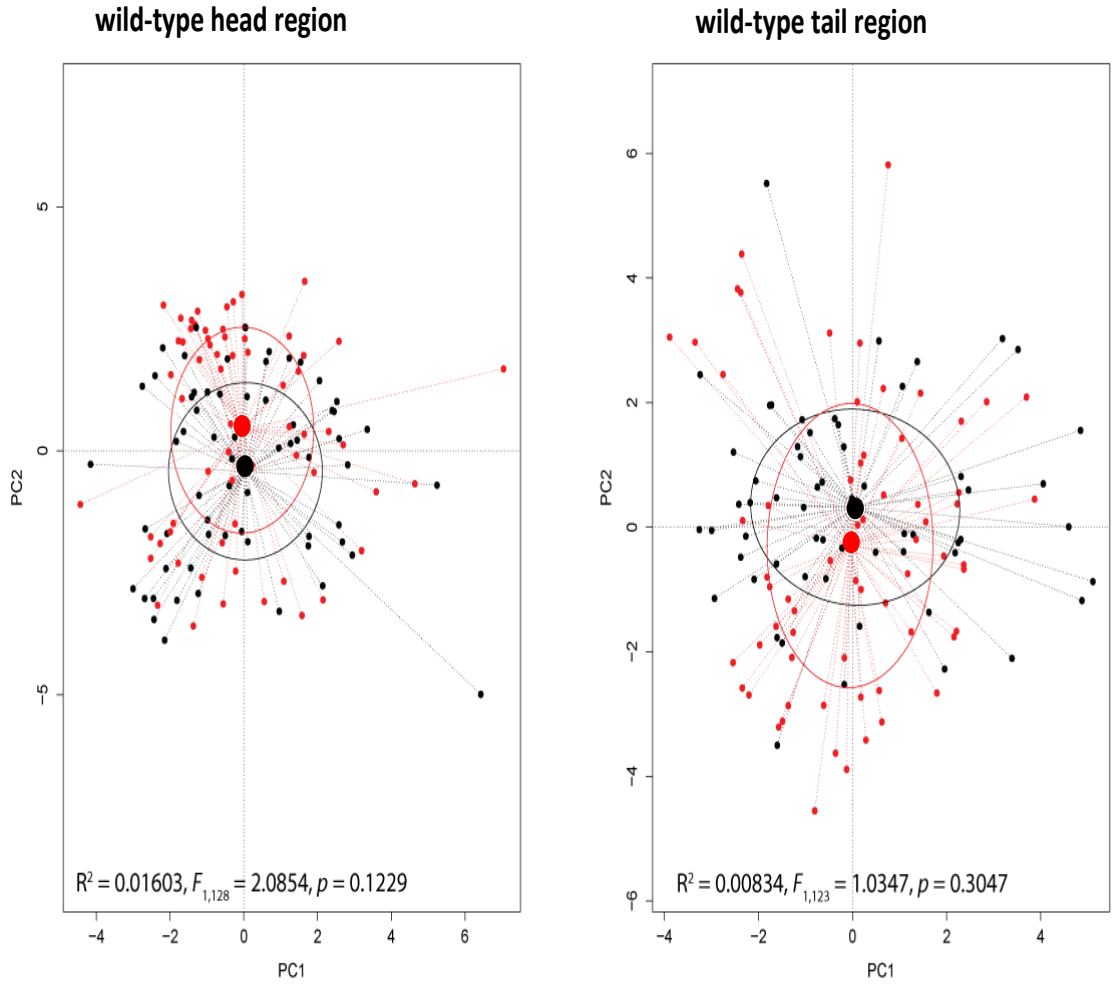

Fig. 3.11: Raman spectroscopy. Principal Component Analysis (PCA) in wild-type nematode. PCA showing the relationship between the Raman phenotype of ZnONPs exposed and control treatments in wild-type nematode in the head and tail regions. Points represent replicates within (n=5 per nematode) as well as between nematodes (n=25 per treatment). Black points represent spectra from control nematodes, red points represent spectra from ZnONPs exposed nematodes. Black and red ellipses represent standard deviations of point scores for the control and treatment groups, respectively.

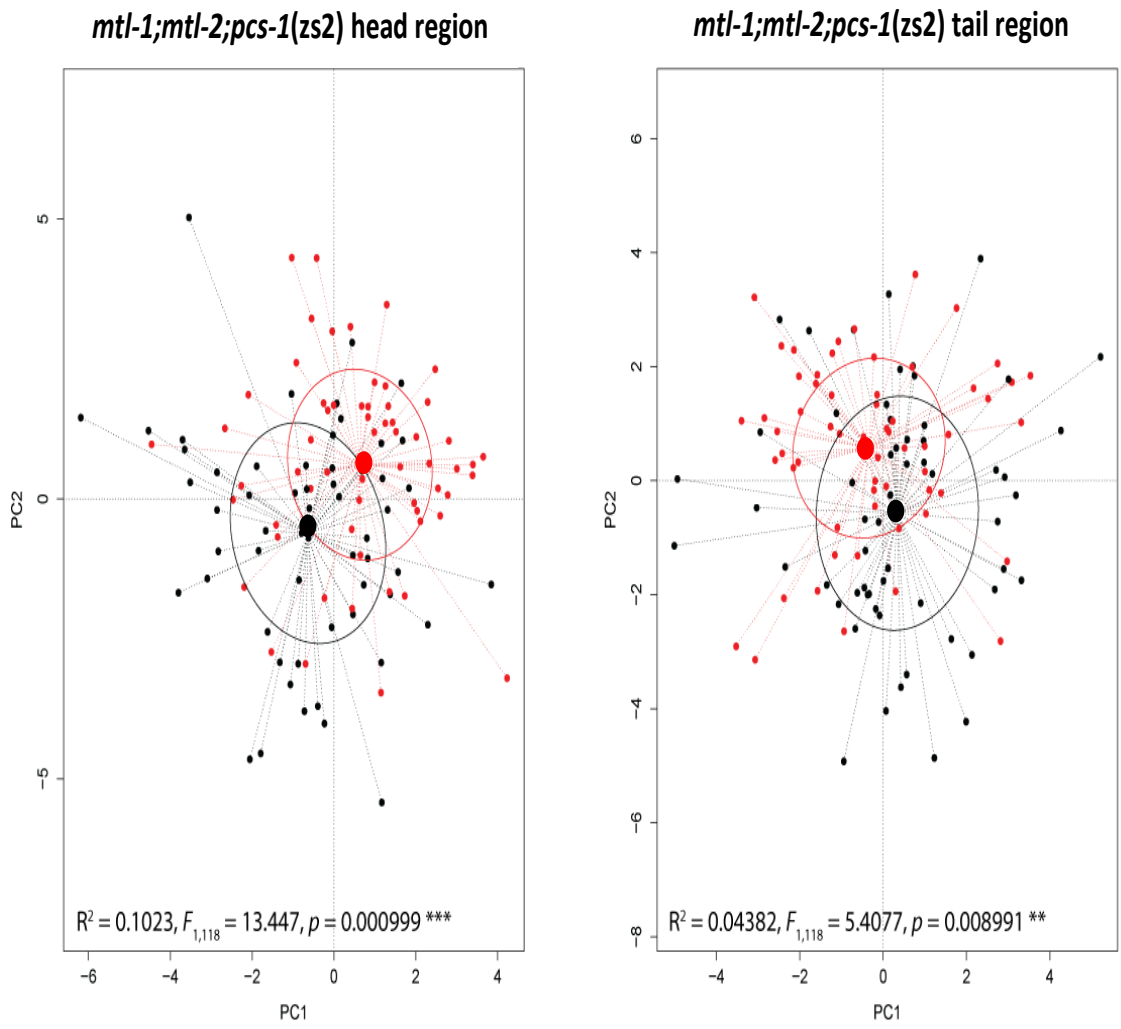

Fig. 3.12: Raman spectroscopy. Principal Component Analysis (PCA) in *mtl-1;mtl-2;pcs-1*(zs2) nematode. PCA showing the relationship between the Raman phenotype of ZnONPs exposed and control treatments in *mtl-1;mtl-2;pcs-1*(zs2) mutant nematode in the head and tail regions. Points represent replicates within (n=5 per nematode) as well as between nematodes (n=25 per treatment). Black points represent spectra from control nematodes, red points represent spectra from ZnONPs exposed nematodes. Black and red ellipses represent standard deviations of point scores for the control and treatment groups, respectively.

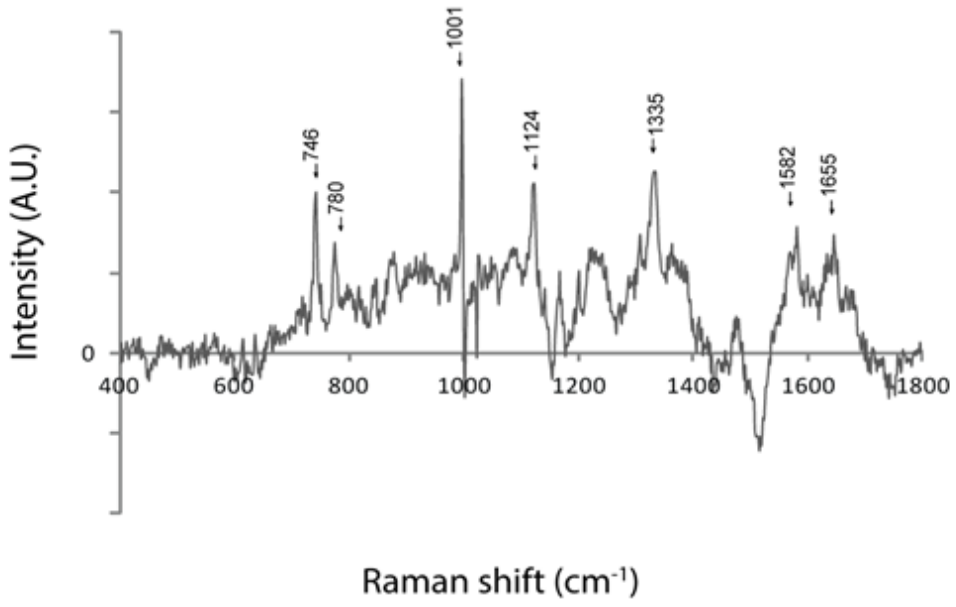

Fig. 3.13: A representative mutant nematode Raman subtracted plot. A subtracted dataset represents the identification of the major differential wavelengths peaks that changed in *mtl-1;mtl-2;pcs-1*(zs2) nematodes, following ZnONPs exposure. The following biomolecules were found to be affected by ZnONPs: cytochrome c (assigned Raman peaks: 746, 1124, and 1582), nucleic acids (assigned Raman peaks: 780, and 1335), phenylalanine (assigned Raman peak: 1001), and amide I (assigned Raman peak: 1655).

3.3.8 The effects of ZnONPs on life-history traits of *C. elegans*

Long-term exposure experiments provide a better overview of the physiological status of an animal when exposed to a toxicant. Therefore, sensitivity of physiological level responses (growth, reproductive capacity, and survival) of *C. elegans* to ZnONPs exposure were compared with those at the molecular level (gene expression). In general, NPs were shown to reduce nematode lifespan, possibly in response to the particle mediated generation of reactive oxygen species (ROS), and induce a premature

degeneration of reproductive organs (manifested by a bag of worms phenotype which is characterized by intracorporal hatching of eggs in the parent animal).

Furthermore, the effects on growth, reproductive capacity and lifespan were examined following the chronic exposures to ZnONPs in wild-type and *mtl-1;mtl-2;pcs-1*(zs2).

3.3.8.1 ZnONPs affect the growth of wild-type and *mtl-1;mtl-2;pcs-1*(zs2) nematodes

The initial growth rate was similar in both strains and seemingly not affected by ZnONPs exposure and all nematodes, irrespective of the strain or exposure condition, reached adulthood within 4 days post-hatching (data not shown). However, a significant reduction in final adult body size (measured at day 6 post hatch) was observed in ZnONPs exposed nematodes (Fig. 3.14), a phenotypic effect that was found to be concentration dependant and more pronounced in *mtl-1;mtl-2;pcs-1*(zs2) (Table 3.2). In wild-type nematodes, the difference in final body size was statistically significant only at higher concentrations (20 and 50 mg/L ZnONPs), but the *mtl-1;mtl-2;pcs-1*(zs2) mutant was more sensitive to ZnONPs exposure (a statistical difference was observed at all concentrations tested, namely 5 - 50 mg/L ZnONPs).

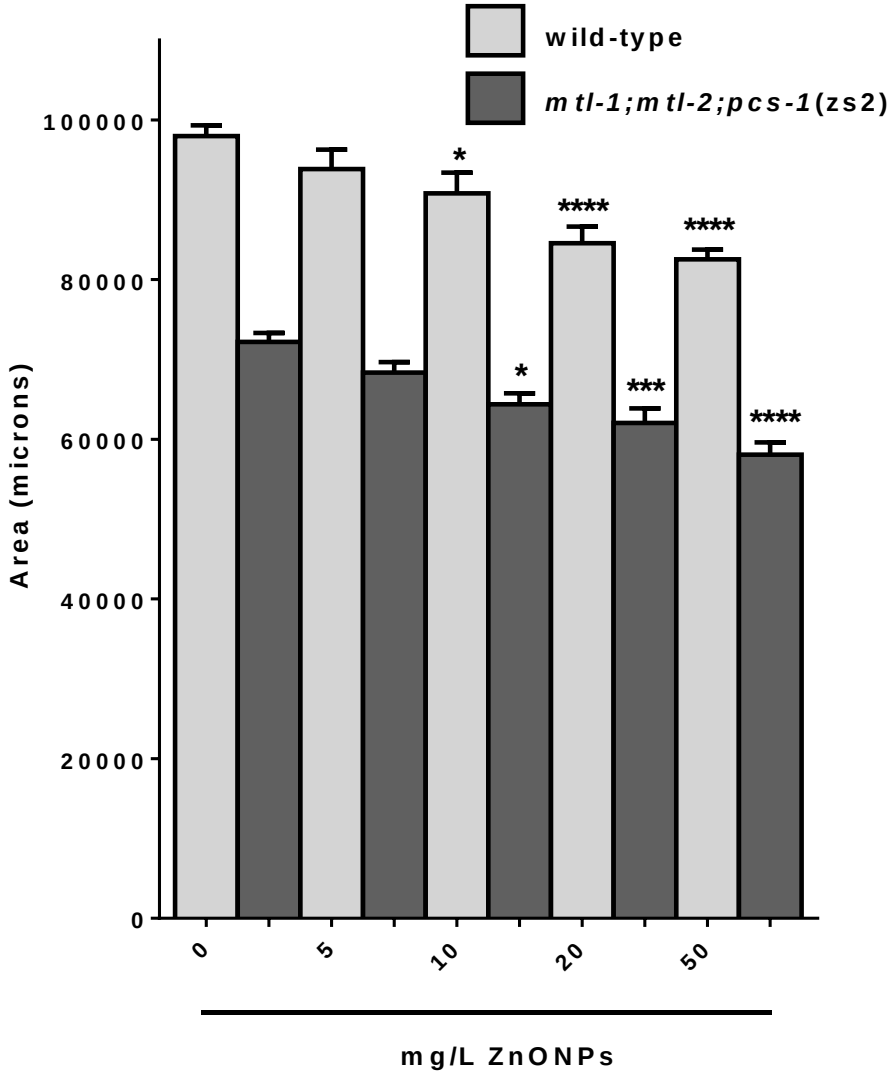

Fig. 3.14: Flat volumetric surface area of wild-type and *mtl-1;mtl-2;pcs-1*(zs2) nematodes chronically exposed to ZnONPs. The data (mean ± SEM (n=20)) present the end point result of change in surface area of the nematode at 144 hours post L1 stage, expressed in microns. Statistical analysis was performed using the two-way ANOVA to determine the interaction based on two experimental factors, nematode strain and ZnONPs treatment matched group sets of measurements, followed by Bonferroni multiple comparison test, where * 0<0.05, *** p<0.001, and ****p<0.0001.

Table 3.2: Growth and reproduction traits investigated in ZnONPs exposed wild-type and *mtl-1;mtl-2;pcs-1*(zs2) mutant strain. Growth was examined by analysing the total surface area of the worm; and the reproduction was assessed by counting the number of viable offspring per individual. (ns (non-significant), *p<0.05, **p<0.01, and ***p<0.001).

			ZnONPs (mg/L)				
Exposure parameters	**Strain**		**0**	**5**	**10**	**20**	**50**
Growth	**wild-type**	**N**	20	20	20	20	20
		Surface area (microns)	97961 ± 1360	93839 ± 2425	90817 ± 2575	84543 ± 2098	82551 ± 1201
		Surface area (% of control)	100	95.53	92.46	86.07	84.04
		Statistical significance		ns	ns	***	***
	***mtl-1;mtl-2; pcs-1*(zs2)**	**N**	20	20	20	20	20
		Surface area (microns)	72192 ± 1117	68368 ± 1303	64396 ± 1357	62037 ± 1839	58086 ± 1529
		Surface area (% of control)	100	94.7	89.2	85.93	80.46
		Statistical significance		***	***	***	***
Reproduction	**wild-type**	**N**	35	34	34	33	36
		Total brood size ± SEM	233.2 ± 2.4	222.5 ± 2.9	210.3 ± 2.05	201 ±2.5	191.8 ± 2.3
		Brood size (% of control)	100	95.42	90.19	86.21	82.25
		Statistical significance		*	***	***	***
	***mtl-1;mtl-2; pcs-1*(zs2)**	**N**	34	33	34	35	36
		Total brood size ± SEM	160.4 ± 1.1	138.4 ± 0.9	128.6 ± 1.1	119.9 ± 1.1	109.7 ± 1
		Brood size (% of control)	100	86.31	80.23	74.76	68.41
		Statistical significance		***	***	***	***

3.3.8.2 ZnONPs affect the reproduction of wild-type and *mtl-1;mtl-2;pcs-1*(zs2) nematodes

Others have reported that nanomaterials can cause a reduction in nematode reproduction (Roh et al., 2009; Wang et al., 2009; Pluskota et al., 2009; Kim et al., 2008).

Therefore the reproductive capacity of wild-type and the triple-knockout mutant following exposure to ZnONPs was examined. In control conditions (i.e. in the absence of ZnONPs), wild-type and *mtl-1;mtl-2;pcs-1*(zs2) produced 233.2 ± 2.4 and 160.4 ± 1.1 viable eggs, respectively (Table 3.2). Analysis of the full data-set using two-way ANOVA indicated a significant effect of both strain ($p<0.001$) and exposure concentration ($p<0.001$) on brood size.

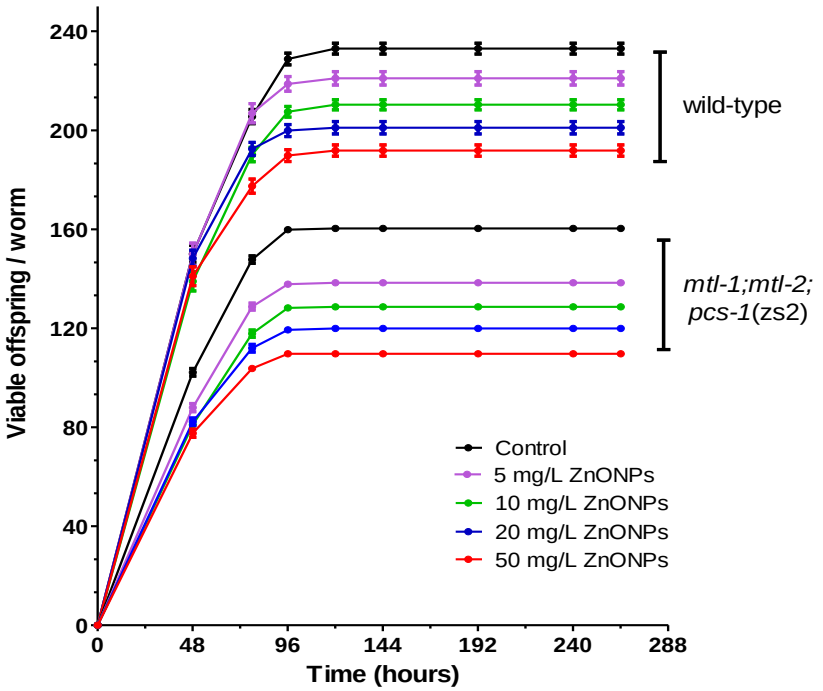

Fig. 3.15: Total cumulative brood size of wild-type and *mtl-1;mtl-2;pcs-1*(zs2) nematode strains chronically exposed to ZnONPs. To compare statistical significance of data between groups, Tukey's Multiple Comparison Test was used at each ZnONPs concentration. Error bars shown are standard error of the mean (n=36). Statistical analysis utilized the one-way ANOVA comparing untreated and ZnONPs treated unmatched group sets of measurements ($p<0.05$).

A significant interaction term was also found supporting the dependence of sensitivity to ZnONPs exposure on the tested strain. This was evident by the fact that exposure to ZnONPs resulted in a significant concentration-dependent reduction in reproductive output. In wild-type worms this was moderately significant ($p<0.05$) at 5 mg/L ZnONPs, and highly significant ($p<0.001$) at higher concentrations, but notably already highly significantly different ($p<0.001$) in the mutant strain at 5 mg/L ZnONPs exposure (Fig. 3.15; Table 3.2).

3.3.8.3 ZnONPs affect wild-type and *mtl-1;mtl-2;pcs-1*(zs2) nematode life-span

On control plates, median survival of wild-type nematodes was 13 days, but only 11 days for *mtl-1;mtl-2;pcs-1*(zs2) (Table 3.3). As with development and brood-size, exposure to ZnONPs induced a significant concentration-dependent effect on the median life-span of the wild-type worms.

Table 3.3: Life-span in ZnONPs exposed wild-type and *mtl-1;mtl-2;pcs-1*(zs2). Life-span was investigated by counting the number of surviving nematodes at 24 hour time intervals (Kaplan-Meier survival method), where ns (non-significant), and ****denotes $p< 0.0001$.

			ZnONPs (mg/L)				
Exposure parameters	**Strain**		**0**	**5**	**10**	**20**	**50**
Life-span	**wild-type**	**N**	370	370	370	370	370
		Median survival (days)	13	12	11	11	11
		Statistical significance		****	****	****	****
	***mtl-1;mtl-2; pcs-1*(zs2)**	**N**	400	400	400	400	400
		Median survival (days)	11	10	9	9	8
		Statistical significance		****	****	****	****

Wild-type life-span was decreased by a day at 5 mg/L ZnONPs, and a further day at higher ZnONPs concentrations. Analogous effects were observed with mutant nematodes, however at the highest concentration the death rate was accelerated and nematodes died 3 days earlier compared to their respective controls (Fig. 3.16). All exposure effects were found to be highly significant ($p<0.0001$) (Table 3.3).

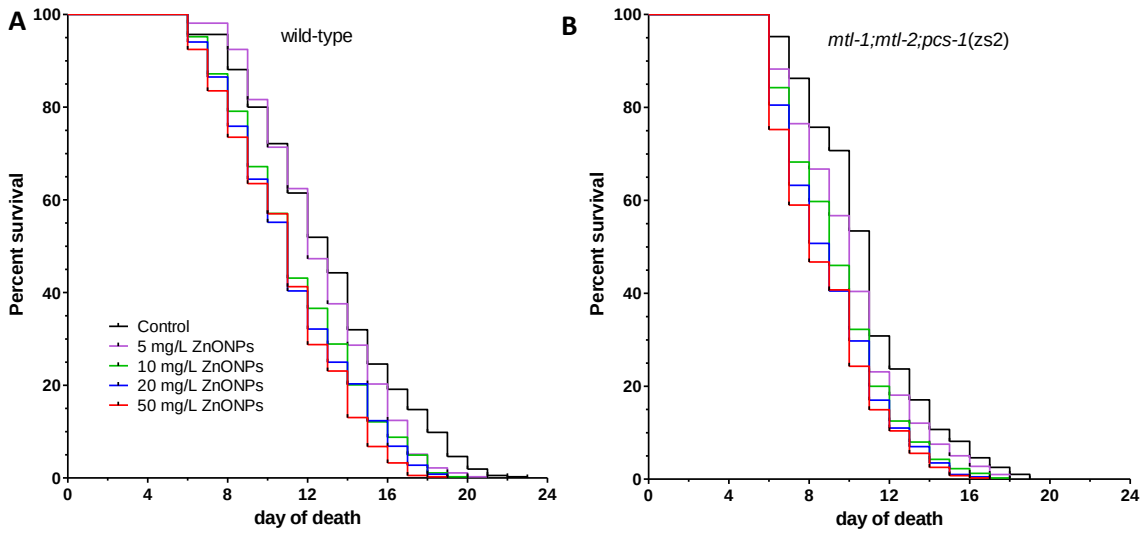

Fig. 3.16: Lifespan of wild-type (A) and *mtl-1;mtl-2;pcs-1*(zs2) (B) exposed to ZnONPs. Synchronised nematodes were chronically exposed from L1 stage to L4 stage to ZnONPs and transferred to standard NGM plates. The wild-type medium life-span was of 13 days, as the *mtl-1;mtl-2;pcs-1*(zs2) mutant medium life-span was of 11 days. Lifespan was significantly affected following ZnONPs exposures in both wild-type and *mtl-1;mtl-2;pcs-1*(zs2) nematodes. Statistical analysis was performed using the Log-rank (Mantel-Cox) Test for comparison of survival curves comparing to control at each ZnONPs concentrations ($p<0.0001$). The median survival is the time at which fractional survival equals 50 %.

3.4 Discussion

3.4.1 Particle characterization and effect of test medium on physicochemical properties of ZnONPs

As previously suggested (Nel et al., 2009), it is essential to study the biophysicochemical interactions at the nano–bio interface, as the level of agglomeration can influence the uptake rate of ZnONPs by animals (Bai et al., 2010; Mohan et al., 2010; Hanley et al., 2009; Mudunkotuwa et al., 2012). Although, the physicochemical properties of ZnONPs have been previously defined when in dry powder (by Microniser Pty Ltd, Dandenong, Australia), it was deemed important to characterize the ZnONPs stock solutions and their degree of agglomeration in the different exposure media, prior to any *C. elegans* toxicity studies.

Transmission electron imaging (TEM) provided information about the shape and size of ZnONPs once suspended in stock solutions. In ultrapure water, the particles existed in single or in agglomerated state. The agglomeration of ZnONPs is possibly due to lower surface charge and thus weaker electrostatic repulsive forces of particles (Nel et al., 2009; Li et al., 2011). In LB medium, ZnONPs were mainly found to be present as agglomerates. In addition, Dynamic Light Scattering (DLS) provided information about the predominant particle dimension state in media. Results supported the TEM observations, namely that in the test medium, ZnONPs assemble into 1 micron stable agglomerate complexes, which notably are independent of bacteria status.

Oxidisible metals, such as is ZnO, can have an antibacterial effect and disrupt the cell membrane when presented to the bacteria (Xie et al., 2011). To investigate whether ZnONPs can inflict damage on OP50 bacteria, the ultrastructural characteristics of untreated and ZnONPs dosed bacteria were examined by TEM. The results show that

the continuous contact with ZnONPs did not induce any morphological changes to *E. coli*, however there was evidence that bacteria secreted extracellular polymeric substances (EPS), which coated the ZnONPs agglomerates. As the secretion of bacteria EPS occurred in response to the prolonged contact with ZnONPs, it is possible to conclude that the release of ionic Zn^{2+} (within 24 hrs time frame) must have contributed to the observed effects. Nevertheless, it is likely that high concentrations of ZnONPs are able to inflict changes to the metabolic system of *E. coli*, and damage to their membrane permeability. Unfortunately, TEM imaging does not give sufficient evidence to support this notion (Roselli et al., 2003; Liu et al., 2009).

The stability of metal oxide nanoparticle agglomerates can also be affected by the chemical composition of the test media (Li et al., 2011; Mudunkotuwa et al., 2011; Kao et al., 2012). Hence, EDX analyses and chemical mapping on a few micron-sized windows was employed to provide information upon the solubility of ZnONPs. TEM-EDX results showed that stable zinc complexes were the major source of dissolved zinc in the OP50 medium, as a dose- and time- dependent dissolution effect of the ZnONPs resulted in an increased concentration of both labile organic complexes and free Zn^{2+} ions. The LB medium is a nutritionally rich medium that comprises mainly of amino acids and polypeptides, such as e.g. tryptone and yeast extract. Amino acids and peptides can form complexes with free Zn^{2+}, as the nucleic acids containing phosphates can form zinc precipitates (Li et al., 2011). However, there was no evidence that the ZnONPs were fully dissolved at the given concentrations, and therefore, the stability of ZnONP aggregates, and their role in toxicity would need to be further investigated.

3.4.2 Effects on dietary restriction

To investigate whether exposure to ZnONPs can induce an indirect effect via caloric restriction, bacterial growth was monitored in the presence and absence of ZnO particles. Whilst lower doses (<50 mg/L) of ZnONPs did not affect bacterial growth, it was significantly inhibited at higher doses (>50 mg/L ZnONPs). In consequence, a maximum dose of 50 mg/L ZnONPs was selected.

It is conceivable that ZnONPs inhibit the growth of bacteria (Li et al., 2011; Zhang et al., 2010; Tayel et al., 2011; Reddy et al., 2007; Liu et al., 2009). In this study, OP50 bacteria were able to reach stationary growth phase possibly because of the nutrient supplement present in the LB broth. In addition, *E. coli* bacteria may have resisted ZnONPs toxicity by excreting large amounts of extracellular polymer substances (EPS) during their growth phase (Liu et al., 2009), which was observed by TEM.

Several other factors can modulate the tolerance towards ZnONPs, such as pH of test medium. However, the pH of the OP50 was shown to remain constant pH7 (see Appendix: ZnONPs).

3.4.3 ZnONPs induce an oxidative stress response

In *C. elegans* two metallothioneins (MTs), CeMT-1 and CeMT-2 are believed to be key players in the protection against metal toxicity and providing protection against ROS and environmental toxins. The *mtl-1* is constitutively expressed in the second pharyngeal bulb, and when under stress conditions (e.g. exposure to cadmium) it is induced in the intestine of the nematode. The expression of *mtl-2* is confined to the intestines, but is equally stress inducible, and plays an important role in providing

protection against heavy metals (Swain et al., 2004; Zeitoun-Ghandour et al., 2011). Apart from *mtl-1* and *mtl-2*, PCS encodes for an antioxidant enzyme, whose activity depends on heavy metal ions (Schwartz et al., 2010; Vatamaniuk et al., 2005). The PCS uses glutathione (GSH), whose thiol group has been blocked in order to synthesize phytochelatin (PC). The expression of *pcs-1* is in the pharyngeal and rectal valves, where it is regulated by changes in its activity rather than changes in PCS gene expression itself (Vatamaniuk et al., 2005). Under normal (control) conditions, PCS is localized in the cytoplasm, where it maintains daily nematode metabolic homeostasis, however, under stress conditions, the antioxidant activity increases significantly in order to prevent damage to the cells (Hughes et al., 2007).

In order to determine whether metallochelators are involved in providing protection against ZnONPs induced toxicity, the gene expression of *mtl-2* and *pcs-1* were investigated at the molecular level utilizing transgenic worms bearing either the P*mtl-2*::GFP or P*pcs-1*::GFP construct. In these transgenic nematodes, the green fluorescent protein (GFP) is fused to the promoter of either *mtl-2* or *pcs-1*, where it serves as a stress response reporter. The expression of, *mtl-2* and *pcs-1*, were increased in nematodes exposed to ZnONPs, which indicates that the nanoparticles are bioavailable to the organism and inflict changes on a molecular level.

In addition, two-coloured fluorescent reporter transgenes (generated by Knudra Transgenics, USA) were chosen to quantitatively assess and explore selected pathways of toxin activation. The use of transgenic nematodes allowed a rapid screen of well-established biomarkers upon ZnONP exposure. In detail, the oxidative stress reporter panel consisted of 8 toxin-activated transcripts (*ugt-1*, *gcs-1*, *cyp-35A2*, *gst-4*, *gst-38*, *hsp-16.2*, *hsp-16.41*, and *dnj-13*), however their expression was not significantly affected by ZnONPs. In fact, only one transcript was found to be significantly

stimulated by ZnONPs, namely a uridine 5'-diphospho-glucuronosyltransferase (UDP-glycosyltrasferase or *ugt-1*). The *ugt-1* belongs to a family group of enzymes, generally known as glycosyltrasferases (UGTs) (King et al., 2000), which catalyse the transfer of glucuronic acid component of UDP-glucuronic acid to a small hydrophobic molecule. This process in known as glucuronidation, and plays an important role in the cell phase II metabolism of xenobiotic substances, such as are removal of endogenous and dietary substances, toxins, and drugs (Runge-Morris and Kocarek, 2009). UGTs work closely together with other phase II metabolic enzymes in these elimination processes. To date, around 66 UGT-encoding genes have been identified in the *C. elegans* genome, but very little is known about their involvement in detoxification and biotrasformation (WormBase, Version: WS236, 2012). A microarray examination of the polychlorinated biphenyls (PCBs) congomer 52 - toxin treated nematodes suggested that these enzymes may play an important part in PCB metabolism, as their expression was found to be increased (Menzel et al., 2005). It is therefore possible that UGT-1 contributes to the metabolic detoxification of the ZnONPs, however, this notion should be re-validated by means of additional experimental methods, e.g. qRT-PCR.

Compared to the usage of conventional toxicological endpoints (e.g. reproduction and lethality), transgenic nematodes were able to provide insight as to how key transcripts, such as metallochelators, are involved in nematode response to ZnONP exposure. The results are well aligned to findings by Ma et al. (2009), where the *mtl-2* gene was also found to be induced in nematodes exposed to ZnONPs.

ZnONPs may hypothetically inflict stress, as nanoparticle agglomerates and as ionic Zn^{2+}, which can potentially be absorbed or taken up by the nematode intestinal epithelial cells. To study the mechanistic and functional role of metallochelators, the

study also investigated the biological responses in wild-type nematodes, and in *mtl-1;mtl-2;pcs-1*(zs2) mutant worms.

3.4.4 Free radical levels in *C. elegans* exposed to ZnONPs

The generation and accumulation of free radicals affects organismal development, brood size and longevity in *C. elegans* (Honda and Honda, 2002; Hughes and Stürzenbaum, 2007; Zeitoun-Ghandour et al., 2010). Given that ZnONPs transcriptionally activate metallochelators, which in turn are thought to be involved in ROS generation in nematodes (Ma et al., 2009a/b), a cell permeable DCFH-DA dye was used to conduct quantitative intracellular ROS measurements to explore differences in ROS levels in wild-type and the triple mutant raised in the presence or absence of ZnONPs for 48 hours. The DCFH-DA assay has previously been applied to detect the formation of metal-induced free radical compounds (Halliwell and Whiteman, 2004) but has also been criticized for its low specificity (Cohn et al., 2008; Karlsson et al., 2010). In untreated conditions, both wild-type and the mutant nematodes exhibited a similar base-line level of endogenous ROS. Nevertheless, exposure to ZnONPs increased the total ROS levels in *mtl-1;mtl-2;pcs-1*(zs2) worms, a response that was in contrast to the decreased ROS levels observed in wild-type nematodes. It is therefore tempting to hypothesize that the observed differential response is due to the presence or absence of functional metallochelators. In wild-type, the presence of metallochelators provides antioxidant protection to the organism; this protection is significantly impaired in the triple knockout mutant, findings that mirror observations reported by others (Sharma et al., 2012a/b; Ahamed et al., 2011; Sharma et al., 2009; Hanley et al., 2009; Huang et al., 2010).

3.4.5 Quantitative assessment of ZnONP-responsive transcripts

A quantitative approach was chosen to assess the transcriptional responsiveness of target genes previously identified as possible biomarkers of NP toxicity (Akhtar et al., 2012) or due to their established involvement in the key stress response pathways (van Raamsdonk and Hekimi, 2010; Huang et al., 2010). The qRT-PCR results revealed that there was a dose-responsive induction of *sod-1*, *prdx-3*, *cep-1*, *dct-1*, and *mtl-1* genes in the wild-type nematodes, while the expression of other genes remained at the control level. In contrast, in the *mtl-1;mtl-2;pcs-1*(zs2) background, only *cep-1* was significantly induced.

Exposure to ZnONPs generates free radical species, which once in contact with the cellular environment, can oxidize and reduce macromolecules (proteins, lipids, DNA), thus damaging the cell (Sharma et al., 2012; Sharma et al., 2009). Hence, due to their small size, ZnONPs might be able to reach the nucleus and interact with DNA molecules (Sharma et al., 2012; Martinez et al., 2003). This study uncovered evidence that ZnONPs may induce DNA damage. In *C. elegans cep-1* plays a synergistic role as mammalian tumour-suppressor protein p53 (Derry et al., 2001), and *dct-1* encodes for a protein with similarity to the mammalian BNIP3 (BCL2/adenovirus E1B 19kDa) (Yasuda et al., 1999, Pinkston-Gosse et al., 2007). The observed increase in transcript levels of *cep-1* and *dct-1* at lower ZnONP doses, suggests the presence of apoptotic and cytotoxic effects. Interestingly, the expression of the *cep-1* remained elevated at higher ZnONP doses, but decreased in the case of the *dct-1* transcript. A similar observation was also reported by Akhtar et al. (2012).

Overall, all findings correlated well with studies performed with primary human bronchial epithelial cells (Wu et al., 2010), human lung epidermal cells (Sharma et al.,

2009), human alveolar adenocarcinoma cells (Ahamed et al., 2011), mouse liver (Sharma et al., 2012), and human liver cells (Sharma et al., 2012), in all cases the carcinogenicity of ZnONPs was highlighted.

3.4.6 Raman spectroscopy

Raman spectroscopy provides a snapshot of the physiology of the cell in a non-invasive manner without the need to label, or stain the samples. It is ideal for examining small, functional changes that are specific to cellular processes. Raman measurements can be observed directly from biofluids, as well as *in vivo* from organisms, such as the nematode. The types of biological molecules that can be identified have been highlighted (assigned) according to the Raman shift they present (Fig. 3.9; Table 3.1).

The Principal Component Analysis (PCA) on the spectra obtained from the head and tail region from wild-type and a *mtl-1;mtl-2;pcs-1*(zs2) nematodes showed minor phenotypic differences in the global biomolecular fingerprint when in control conditions. However, upon ZnONP exposure, strong statistically significant phenotypic changes were observed in the head and tail regions of *mtl-1;mtl-2;pcs-1*(zs2). Conversely, only minor metabolic effects were detected in ZnONP exposed wild-type nematodes. Taken together, this suggests that the mutant nematode is more susceptible to the ZnONPs toxicity than the wild-type.

Raman can also be used to detect and localize metal oxide nanoparticle aggregates within tissues (Moger, 2008; Galloway et al., 2010; Johnston et al., 2010). In this study, an attempt was made to localise the ZnONP aggregates within the nematode (see Appendix: ZnONPs). However, this proved to be particularly difficult, as the nematode spectrum was higher in intensity than that of ZnONP aggregates. In addition, the beam

of the laser covers only a small portion of scanning area compared to the large total surface area of a nematode, therefore the probability of finding a nano-sized particle in a cell would be expected to be very low. At higher ZnONP exposures, the fluorescence was greatly increased in certain areas of the worm (head, middle, and tail regions) (see Appendix: ZnONPs). This observation confirms that the Raman approach can be a useful tool for examining nanoparticle induced effects in *in vivo* settings.

3.4.7 Life-cycle consequences of ZnONP exposure

Molecular biomarkers are informative only when they can be used to predict the effects on survival, growth or reproduction. Indeed, conventional life-history traits are still widely accepted as essential toxicological endpoints when monitoring and assessing ecological risk to human health. To date, nanotoxicological research utilizing *C. elegans* as a model organism has included the screening of synthetic NPs, such as ZnO, Al_2O_3 and titanium dioxide (TiO_2) (Wang et al., 2009), silver nanoparticles (Roh et al., 2009), platinum nanoparticle (Kim et al., 2008), cadmium (Roh et al., 2009), depleted uranium toxicity (George-Jiang et al., 2009) and silica nanoparticles (Pluskota et al., 2009). In summary, most of the results suggested that NPs reduce the nematode life-span, probably in response to the particle mediated generation of reactive oxygen species (ROS). There is also evidence that NPs induce premature degeneration of reproductive organs (the bag of worms phenotype which is characterized by intracorporal hatching of eggs in the parent animal), which might involve their innervation.

In this study organismal level endpoints were quantified, which showed that in wild-type and *mtl-1;mtl-2;pcs-1*(zs2) worms the growth (Fig.3.14), brood size (Fig. 3.15), and life-span (Fig. 3.16) were significantly affected when challenged chronically with

ZnONPs. Given that the effects were found to be nematode strain specific and amplified in the mutant strain, provides strong evidence that metallochelators may play an important role in the detoxification process of ZnONPs. Previous studies have shown that nematodes lacking metallothioneins are characterized by an increased sensitivity to Cd, which is reflected in a severe reduction of reproduction (Hughes et al., 2009). Here, lower toxic effect observed in the wild-type nematodes is presumably because the metallothioneins and phytochelatins are able to sequester excess Zn. Due to the time-dependent dissolution of the ZnONPs to release deleterious levels of ionic Zn, it takes time to accumulate a toxic load (Franklin et al., 2007; Polynton et al., 2011).

3.5 Conclusion

Zinc oxide nanoparticles (ZnONPs) are used in large quantities by the cosmetic, food and textile industries. However, surprisingly little is known about the toxicogenomic effects of ZnONP exposure. Here, *C. elegans* wild-type and metal sensitive triple knockout mutant (*mtl-1;mtl-2;pcs-1*(zs2)) nematodes, were exposed to the ZnONP (0 - 50 mg/L) to study strain and exposure specific effects on transcription, radical oxidative species generation, the biomolecular phenotype (measured by Raman microspectroscopy) and key endpoints of the nematode life cycle. The analyses pinpointed that metallochelator transcripts (*mtl-1*, *mtl-2* and *pcs-1*) and an apoptotic marker (*cep-1*) are transcriptionally upregulated. In addition, the DCFH-DA assay provided *in vitro* evidence of the oxidative potential of ZnONPs in the metal exposure sensitive triple mutant. Raman spectroscopy highlighted that the biomolecular phenotype changes significantly in the metal sensitive knockout worm upon ZnONPs exposure, suggesting that these metallochelators are instrumental in the protection against cytotoxic damage. Finally, ZnONPs exposure was shown to decrease growth

and development, reproductive capacity, and life-span, effects which were amplified in the triple knockout. Overall, the toxicogenomic and spectroscopic strategies identified the importance of metallochelators in the protection from ZnONP induced toxicity. Individuals (genotypes) housing mutations in key metallochelators, are more susceptible to ZnONP toxicosis.

CHAPTER FOUR

Carbon Black M120 induced toxicity in *Caenorhabditis elegans*

4.1 Introduction

Carbon black (CB) is a generic term for particulate elemental carbon, manufactured by vapour-phase pyrolysis of hydrocarbon mixtures, such as coal tar, fluid catalytic and ethylene cracking tar, and vegetable oil. It is one of the most commonly used nanomaterials in the tyre industry and printing (IARC, 2010). The size range of commercially produced particles of CB is between 10 nm and 400 nm (e.g. 14 nm CB known as Printex 90; 75 nm CB is known as M120) and their aggregates range from 100 nm to 800 nm. It also contains a high surface-area-to-volume ratio, but low levels of non-bioavailable PAH (polycyclic aromatic hydrocarbon).

Exposures to CB vary markedly between and within the production industry itself (Harber et al., 2003; Hailemariam et al., 2012). There has been an increased awareness on the environmental level of CB emissions and exposure (Ma and Ma, 2002). The International Agency for Research on Cancer (IARC) stated that "Carbon black might be carcinogenic in humans" (Baan et al., 2006) and that the acute exposure to high concentrations of CB dust may cause irritation in the upper respiratory tract (Van Tongeren et al., 2002; Gardiner et al., 2001). Health effects associated with CB nanoparticles (NPs) exposure are lung cancer (Valberg and Watson, 1996), chronic obstructive pulmonary disease (COPD) (Anderson et al., 1990; van Beurden et al., 2003) and cardiovascular diseases (Donaldson et al., 2005; Mills et al., 2006). However,

due to the lack of direct evidence it is still difficult to characterize and quantify the exposure risk to humans (Sorahan et al., 2001). Consequently, CB has been classified as *Group 2B agent (mixture): a possible carcinogen to humans* (IARC, 2010). In contrast, *in vivo* inhalation studies in rats have demonstrated the carcinogenicity of CB (Dasenbrock et al., 1996; Nikula et al., 1995). Whilst it has also been stipulated that CB can be used as a negative control due to the absence of redox activity (Guo et al., 2009), many experimental studies oppose this notion. Li et al., (1999) demonstrated that both particle size and surface area are linked to the reactivity of CB, findings that were also confirmed by Koike and Kobayashi, (2006). In addition, CB has been shown to have *in vivo* and *in vitro* effects on lung inflammation (Brown et al., 2000; Wilson et al., 2002). There is clear evidence from *in vitro* studies that CB particles can generate reactive oxygen species (ROS) when they come in contact with biological surfaces (Hussain et al., 2010; Stone et al., 1998), as well as activate serum factors (e.g. C5a complement) (Renwick et al., 2004), and increase the production of the tumour necrosis factor α (TNFα) (Shukla et al., 2000).

To date, the research base of complex nanomaterials, including particulate matter (PM), diesel exhaust particles (DEP) and CB, is very scant and has at large, failed to define the true relationship between systemic uptake and subsequent toxic effects. Thus, in order to increase our understanding regarding their possible toxic profiles, there is a need for new standardized and systematized experimental models. Therefore, utilizing new animal models, such as the nematode *C. elegans*, may prove valuable for studying the acute and chronic toxic effects of complex nanomaterials. Thanks to their small size, ease of handling, genetic amenability, low cost and culture conditions, this organism is compatible with whole-animal large scale screenings (Giacomotto and Segalat, 2010),

to identify new pathways and cell targets, and thereby provide the means to link toxicant chemical composition and biological activity.

4.2 Aims

The aim of work described in this chapter was to investigate the toxicogenomic effects of Carbon Black M120 exposure upon the nematode organism *C. elegans*. Wild-type, metal sensitive triple knockout mutant (*mtl-1;mtl-2;pcs-1*(zs2)), and oxidative stress sensitive mutants (*sod-1*(tm760), *sod-2*(gk257), and *sod-3*(tm760)) nematode strains were raised in the presence or absence of CB. These nematode strains were chosen in order to investigate whether certain susceptible subgroups (i.e. the mutants) elicit an enhanced susceptibility to CB exposure (Pope et al., 1999; Gilmour et al., 2004). Two major life-cycle indices (growth and reproduction) were examined; the oxidative stress was quantified by measuring ROS production, and transcriptional changes of target genes were evaluated via a MosSCI transgenic nematodes system characterized by transcriptional-activated fluorescent reporters. In short, functional genomics tools were used to explore and quantify how the nematode organism responds to CB intervention.

4.3 Results

4.3.1 Characterization of Carbon Black M120

4.3.1.1 Transmission electron microscopy (TEM) imaging

Particle size, its surface area and degree of the agglomeration of MONARCH® 120 (M120) carbon black (CB) particles (furnace black) have previously been defined, however only as dry powders (Cabot Corporation, Billerica, US). For the *C. elegans* toxicity studies, it was deemed important to characterize CB particles when suspended in 5 % methanol and M9 medium by transmission electron microscopy (TEM), because they will be presented to the *C. elegans* in this form. Particle sizes were found to range from 60 nm up to several hundred nm in size (Fig. 4.1A-B). Particle shape was typically spherical to ellipsoidal. CB material consisted of monotonous particle types, which were mainly present in clusters (either aggregates or agglomerates). TEM imaging indicated that in M9 medium, salts attach and form a crystal coat around the CB particle surfaces. The crystal coating contributes to the increased size of CB agglomerate clusters (Fig. 4.1C-D).

4.3.1.2 Nanoparticle tracking analysis (NTA) by NanoSight

Time-dependent changes in the level of CB agglomerates were characterized by measuring particle size distribution in the M9 test medium at 0 hrs and 24 hrs (Fig. 4.2A-B), and in the presence of OP50 bacteria at 0 hrs (Fig. 4.3) by the NanoSight nanoparticle tracking analysis (NTA) method. Given that smaller particles of a similar refractive index scatter less light, than the larger ones, NTA was able to distinguish between different CB sized populations.

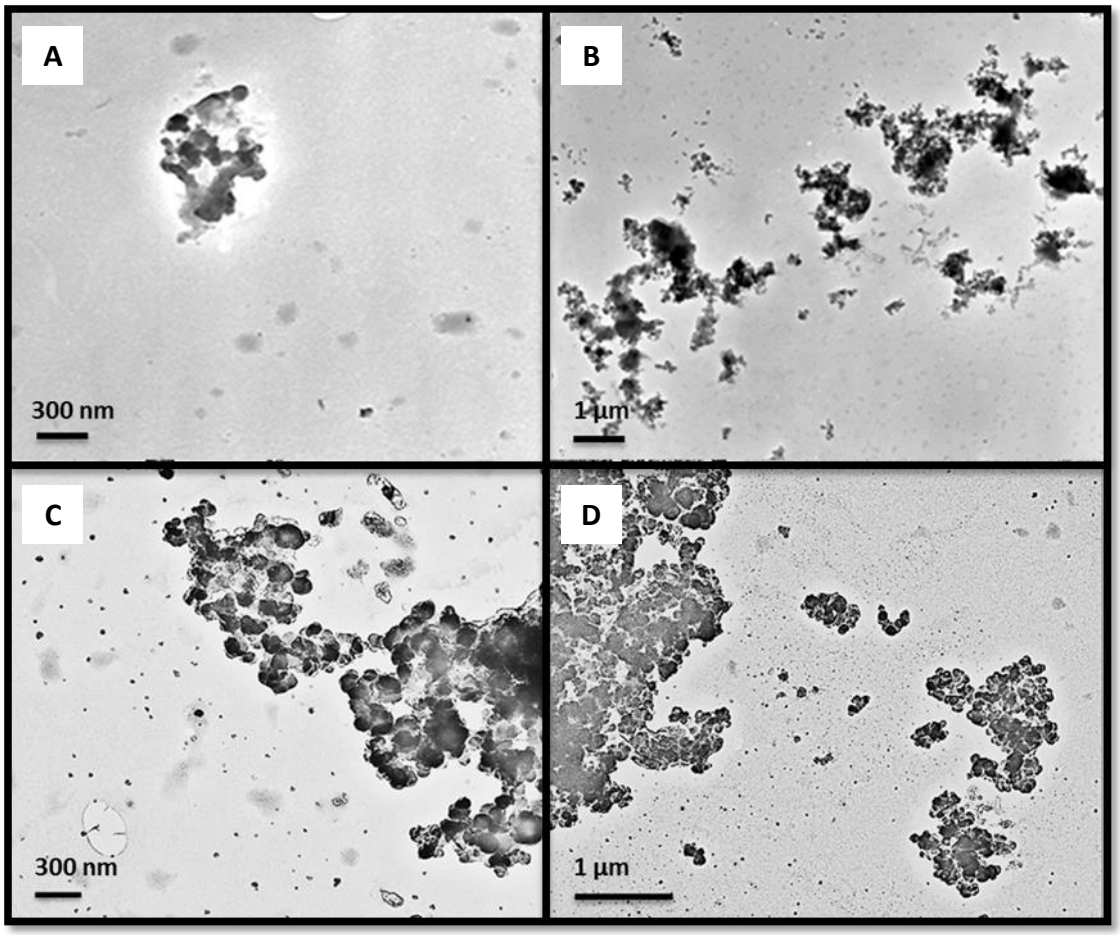

Fig. 4.1: **TEM images of the nanoparticles.** Characterization of Carbon Black M120 in the test solution: in 5 % methanol (in HPLC water) at 16.0 k × magnification **(A)** and 5.0 k × magnification **(B)**; and M9 saline solution at 16.0 k × magnification **(C)** and 8.0 k × magnification **(D)**. Representative images from n=9 in total.

A broad particle size-to-size distribution was observed, which ranged from approximately 50 nm to 400 nm in diameter. In the OP50 bacteria, the size measurement of CB agglomerate was affected by the protein aggregation and viscosity of the medium, which was later rectified by diluting the samples. The software analysis suggested that CB particles, once added to the biological solvent tend to cluster and form stable particle liaisons in a size range of 50- to 200- nm (Fig. 4.2A and 4.3; Table 4.1).

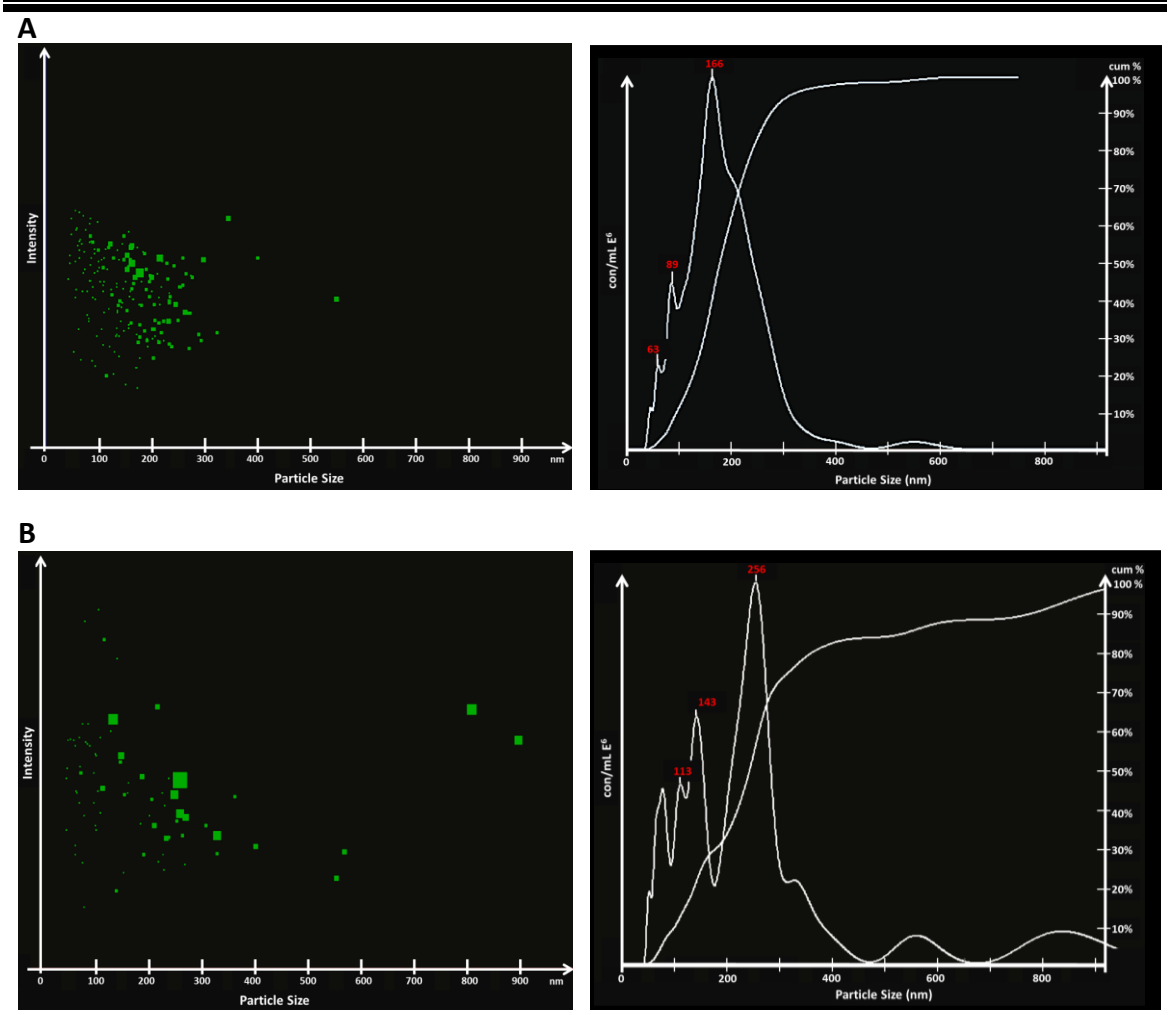

Fig. 4.2: NanoSight characterization and size distribution of CB M120 in the M9 test media. Videos of CB particles in the M9 at 0 hrs (A), and after 24 hrs (B) were recorded at a frequency of 30 fps (frames per second), tracked, and subjected to the analysis (for detailed methodology see Chapter 2: Materials and methods).

In addition, the agglomerate clusters were found to be more uniform in their size in M9 medium than in OP50 bacteria. The particle number concentrations as identified by the NTA were the following: in the M9 test media at 0 hrs 9.2×10^7 particles/ mL, and at 24 hrs 5×10^7 particles / mL. The particle number concentration in OP50 test media was recorded to be 8.8×10^7 particles /mL. Once particles were added to the test media, the level of agglomeration was less prominent in M9 than in OP50. The dominant particle sizes at 0 hrs were 166 nm in the M9 media (Fig. 4.2A) and 207 nm in OP50 (Fig. 4.3;

Table 4.1). However, over time a number of aggregates significantly increased in M9 in their size range to 550- up to 800- nm, with dominant particle sizes of 143 nm and 256 nm (Fig. 4.2B; Table 4.1).

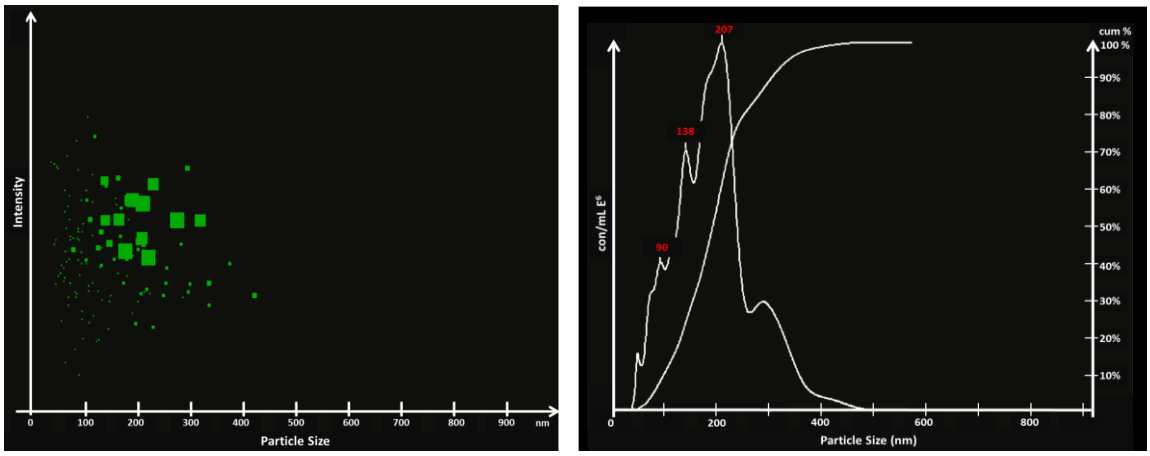

Fig. 4.3: NanoSight characterization and size distribution of the CB M120 and their aggregates in freshly added (0 hrs) OP50 biological test medium. Videos of CB particles in OP50 were recorded at a frequency of 30 fps (frames per second), tracked, and subjected to the analysis (for detailed methodology see Chapter 2: Materials and methods).

Table 4.1: NanoSight mediated assessment of CB M120 particle size distribution immediately after addition to the test solution (0 hrs), or after 24 hrs incubation at room temperature (24 hrs).

Sample	Particle size range (nm)	Mean	SD
Carbon Black M120 in M9 test medium (0 hrs)	50 – 350	185	78
Carbon Black M120 in M9 test medium (24 hrs)	50 – 900	282	209
Carbon Black M120 in OP50 bacteria of optical density of ~1.0 (0 hrs)	50 – 400	188	74

4.3.2 Effects of Carbon Black M120 supplementation on OP50 bacterial food source

An investigation was carried out in order to examine potential pro/antibacterial effects of CB M120 suspensions on OP50 bacteria. Bacterial growth was found not to be affected by CB concentrations up to 25 µg/mL dose. However, their growth was significantly promoted at the higher CB concentrations of 50 and 100 µg/mL ($p<0.05$) (Fig. 4.4). This response was dose-dependent. Supplementation of 25 µg/mL CB did not affect the pH of the bacterial solution, as pH remained at ~pH7.4 over a period of 24 hours (Appendix: Carbon Black M120).

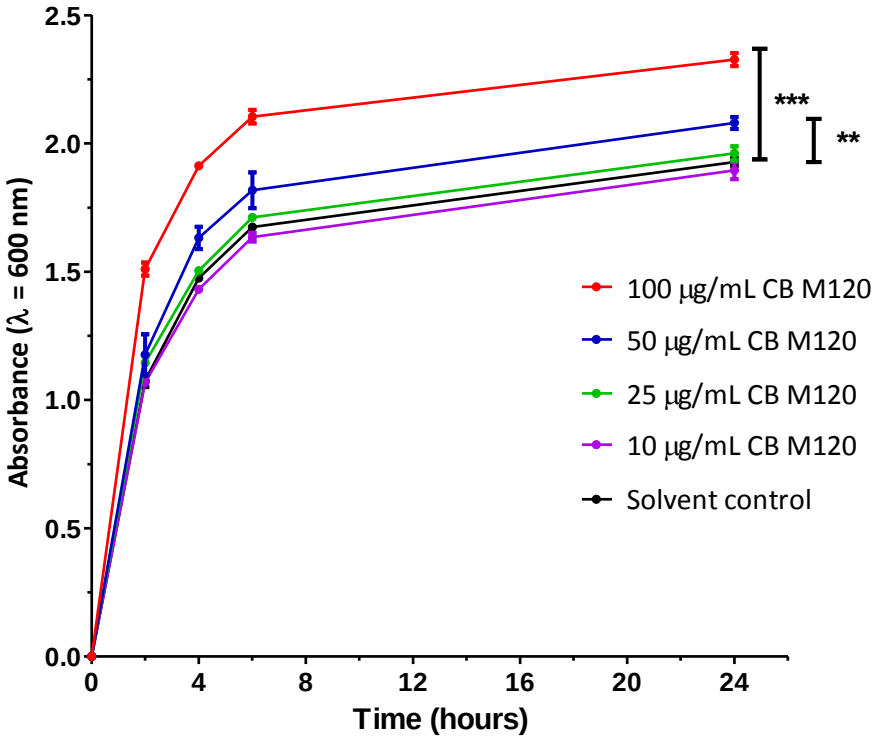

Fig. 4.4: Effects on dietary restriction. OP50 *E. coli* was incubated at 37°C for 24 hours in the absence and presence of CB M120. Error bars denote ± SEM (n=4). Statistical analysis was performed using the one-way ANOVA comparing untreated and CB M120 treated group sets of measurements with significance, where **is $p<0.01$, and ***$p<0.001$.

4.3.3 Changes in transcription-activated fluorescent reporters in Carbon Black M120 exposure using a transgenic *C. elegans* system

To quantitatively examine transcriptional responses of specific target genes following the exposure to CB M120, MosSCI transgenic nematodes were utilized (generated and provided by Knudra Transgenics, US).

The following panel of transgenic biosensor reporters, known to be involved in oxidative stress response pathways and inflammatory activity were selected: *mtl-2*, *hsp-16.2*, *hsp-16.41*, *cyp-35A2*, *gcs-1*, *gst-4*, *gst-38*, *ugt-1*, and *dnj-13*.

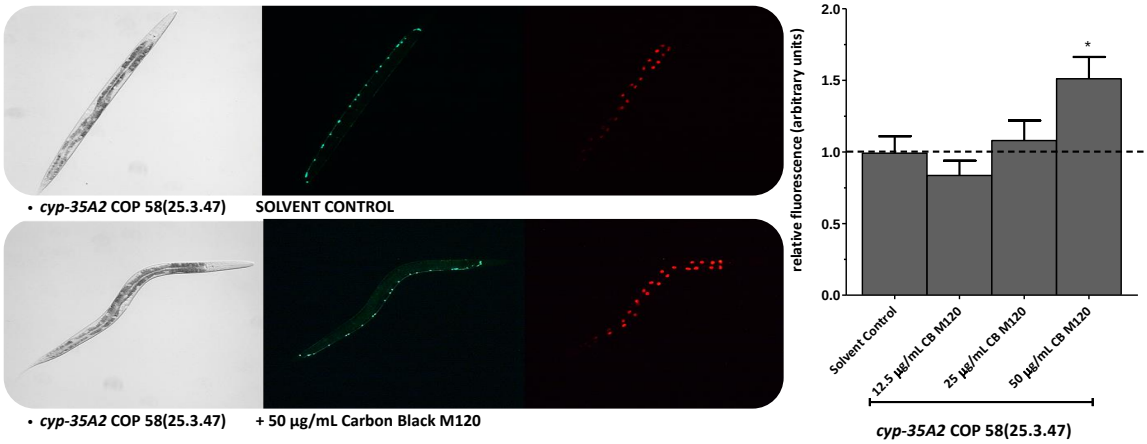

Fig. 4.5: Fluorescence images and a quantitative analysis of induction of *cyp-35A2::*mCherry expressed as relative fluorescence units following normalization to the invariant *unc-47::*GFP, provided evidence of a significant induction of *cyp-35A2* upon CB M120 treatment. 10 worms were observed in each experimental condition and error bars represent ± SEM. Statistical analysis was performed using the one-way ANOVA, where * denotes $p<0.05$.

In order to determine the threshold dose at which transgenic nematodes are likely to be transcriptionally activated by CB, transgenic worms bearing intra-chromosomal copies of the promoter fusion construct *cyp-35A2* were exposed to 0, 12.5, 25, and 50 µg/mL

CB. A 48 hour exposure to CB induced a statistically significant increase in *cyp-35A2* expression (measured as relative fluorescence units) at the highest (50 µg/mL) CB concentration (Fig. 4.5). A quantitative analysis using 10 worms, defined this as a 1.5 - fold increase (p = 0.002). All other transgenic strains were therefore also exposed to 50 µg/mL CB (Fig. 4.6), but none of the tested transcripts was found to significantly change following treatment at this concentration.

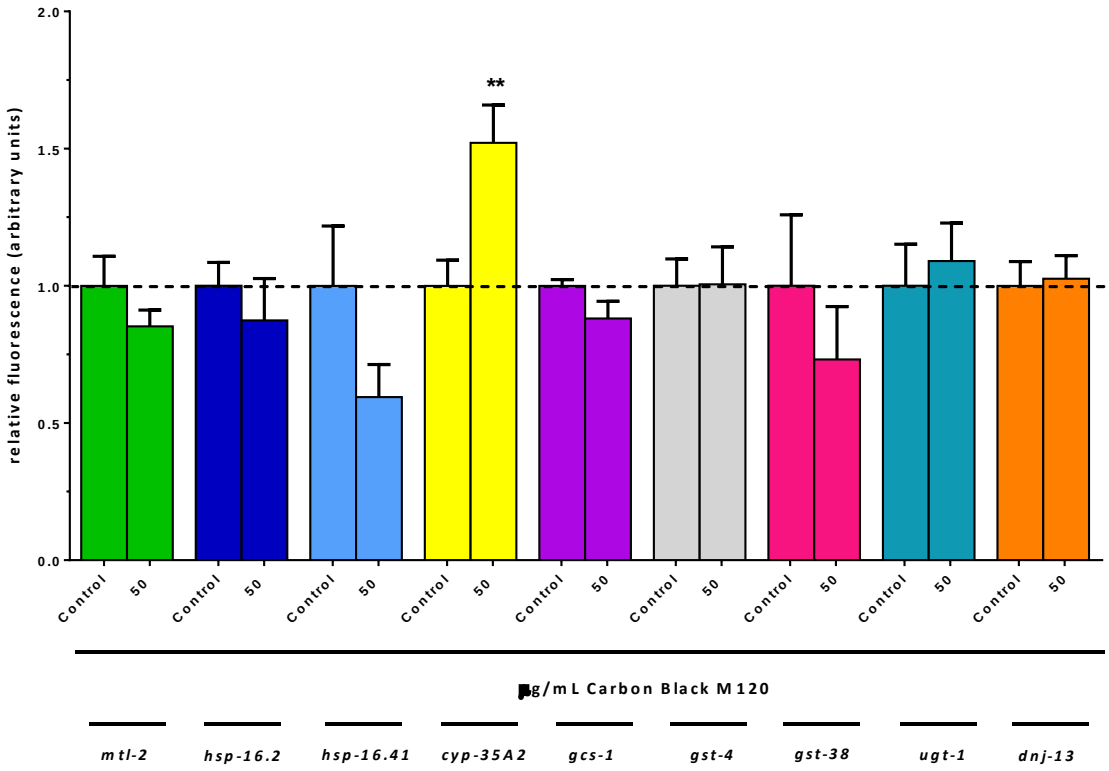

Fig. 4.6: Quantitative analysis of the transcriptional-activated promoter of the genes of interest::mCherry expressed as relative fluorescence units following normalization to the invariant *unc-47*::GFP in response to Carbon Black M120 treatment. 10 worms were observed in each experimental condition (0 and 50 µg/mL CB M120) and error bars represent ± SEM. Statistical analysis was performed using the Wilcoxon signed rank test, where **p<0.01.

The analysis also indicated a non-significant decrease of two other transcripts upon CB exposure, namely *hsp-16.41* and *gst-38,* which may be of significance if the

experimental size was increased. There were no other significant differences in any of the other transgenic nematode strains examined.

4.3.4 Detection of free radical species (ROS) in *C. elegans* exposed to Carbon Black M120

The measurement of intracellular ROS production in wild-type, metal hypersensitive (*mtl-1;mtl-2;pcs-1*(zs2)) mutant, and oxidative stress sensitive SOD nematode mutants exposed to CB M120 for 48 hours is represented in Fig. 4.7. The intracellular ROS production was assessed in the wild-type and the *mtl-1;mtl-2;pcs-1*(zs2) mutant following the exposure to 25 and 50 µg/mL CB, and SOD mutants were exposed to 25 µg/mL CB.

This assay provided quantitative evidence that the base-line level of the ROS generated in cells in the wild-type and the metal hypersensitive (*mtl-1;mtl-2;pcs-1*(zs2)) nematodes is comparable (Fig. 4.7). In contrast, the SOD nematode mutants exhibit higher base-line level of the intracellular ROS compared to wild-type or/and the metal hypersensitive mutant (Fig. 4.7). The magnitude of the intracellular ROS levels in *sod-1*(tm776) mutants were shown to be approximately 6 - fold higher than in wild-type and 2.5 - fold greater than the background ROS level in the other two MnSOD mutants tested. Both MnSOD nematodes exhibit a similar intracellular ROS background, which is approximately twice as high as in the wild-type strain.

An exposure to CB resulted in a significant increase in the total intracellular ROS levels in the wild-type and *mtl-1;mtl-2;pcs-1*(zs2) mutant strain ($p<0.0001$). The total fluorescence intensity of the DCF moiety increased by 46 %, and 54.7 % in the wild-

type strain, and for 110.9 %, and 143.3 % in the CB treated *mtl-1;mtl-2;pcs-1*(zs2) mutant strain compared to the control levels.

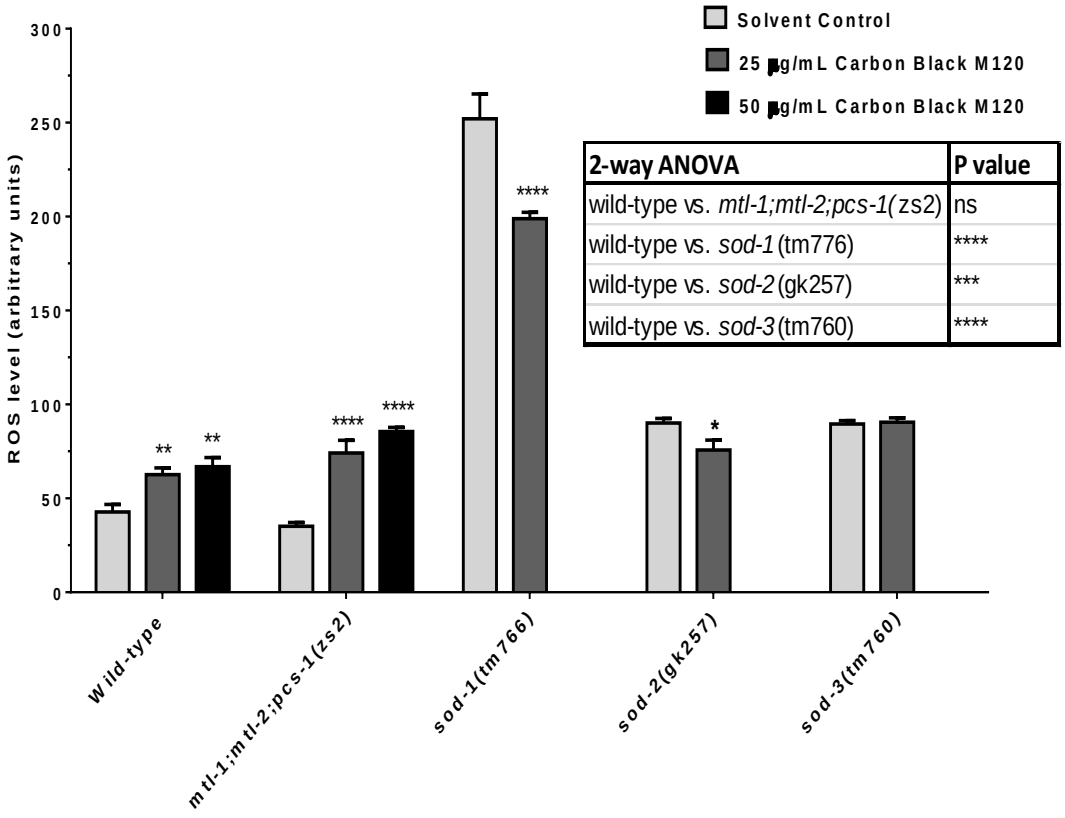

Fig. 4.7: Detection of free radical levels in *C. elegans* exposed to Carbon Black M120. Wild-type worms, *mtl-1;mtl-2;pcs-1*(zs2), *sod-1*(tm776), *sod-2*(gk257) and *sod-3*(tm760) worms were exposed to different CB concentrations. DCF-DA was used to determine the production of ROS. Fluorescence was measured at excitation 485 nm and emission 528 nm. N=3 (technical repeats n=3, biological repeats n=2). Error bars represent mean ±SEM. Statistical analysis was performed using both the Wilcoxon signed rank test, and the two-way ANOVA to determine the interaction based on two experimental factors, nematode strain and CB treatment matched group sets of measurements, followed by Bonferroni multiple comparison test, where ns is (non-significant), *p<0.05, **p<0.01, ***p<0.001, and ****p< 0.0001.

In contrast, exposure to 25 µg/mL CB resulted in a significant 21.1 % decrease in the *sod-1*(tm776) strain, and 15.9 % decrease in the total ROS levels in the *sod-2*(gk257) strain compared to control (Fig. 4.7). There was no change in the intracellular pool of ROS in *sod-3*(tm760) nematodes upon CB exposure. All effects were found to be nematode strain and exposure significant ($p<0.0001$), bar for *mtl-1;mtl-2;pcs-1*(zs2) mutant strain ($p>0.05$).

4.3.5 The effects of Carbon Black M120 exposure on the life-history traits of *C. elegans*

4.3.5.1 Acute exposure of wild-type strain to Carbon Black

As particle mediated toxicity can vary significantly between different exposure assay`s parameters (Sochova et al., 2007; Wang et al., 2009), the toxic effects of CB M120 particles were initially investigated using aqueous M9 saline solution (in the absence of bacterial food). However, this type of exposure can only be conducted in short-term toxicant exposure studies (max. 24 hours). Growth of *C. elegans* under optimal conditions is exponential during the four molt stages until it reaches a final plateau phase (Jager et al., 2005). However, this trait can be negatively or positively affected by some toxicants composed of e.g. metals (Hughes and Stürzenbaum, 2007).

Volumetric growth in *C. elegans* was examined in the presence and absence of CB. Wild-type nematodes were first exposed at L1 stage in M9 to 0, 5, 10, 25, 50, or 75 µg/mL CB for 24 hours. Following this acute exposure, nematodes were placed onto fresh NGM agar plates with OP50 bacteria food without CB. A representative data plot of result change in nematode surface area taken post 120 hrs of exposure is represented

in Fig. 4.8. There were no statistical significant changes in the surface area of the nematode observed following exposure to CB particles at any time point examined (data not shown).

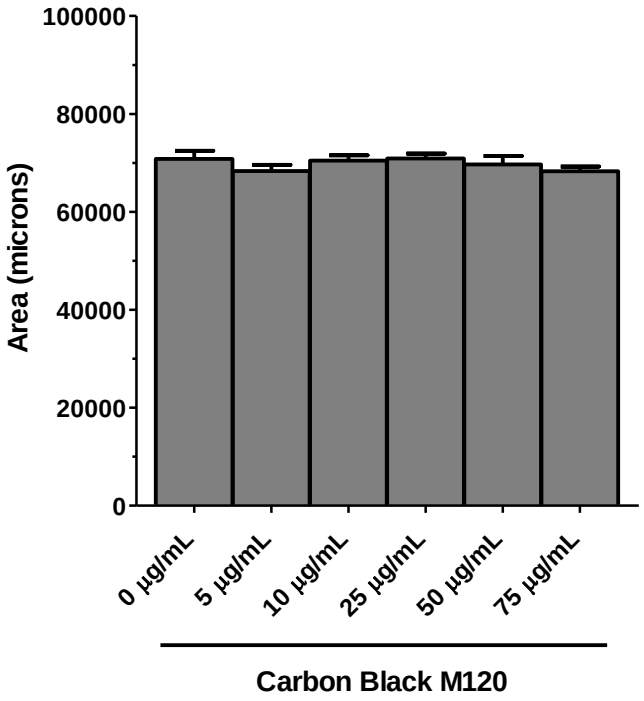

Fig. 4.8: Flat volumetric surface area of wild-type nematodes subjected to an acute exposure in M9 test medium to different Carbon Black M120 concentrations. The data plotted present the end point result of change in surface area of the nematode post 120 hours of omitted particle exposure, expressed in microns. Data are represented as mean ± SEM (n=20). Statistical analysis was performed using a one-way ANOVA comparing untreated and CB treated matched group sets of measurements, ($p<0.05$).

4.3.5.2 Chronic exposure of wild-type and metal sensitive triple knockout mutant (*mtl-1;mtl-2;pcs-1*(zs2)) strain to Carbon Black M120

Long-term exposure experiments provide a better snapshot of the physiological status of an animal when exposed to a toxicant. Therefore, organismal and population-relevant toxic endpoints (growth and fertility) were examined after chronic exposures to CB

M120 in the wild type and metal hypersensitive *mtl-1;mtl-2;pcs-1*(zs2) nematode strains.

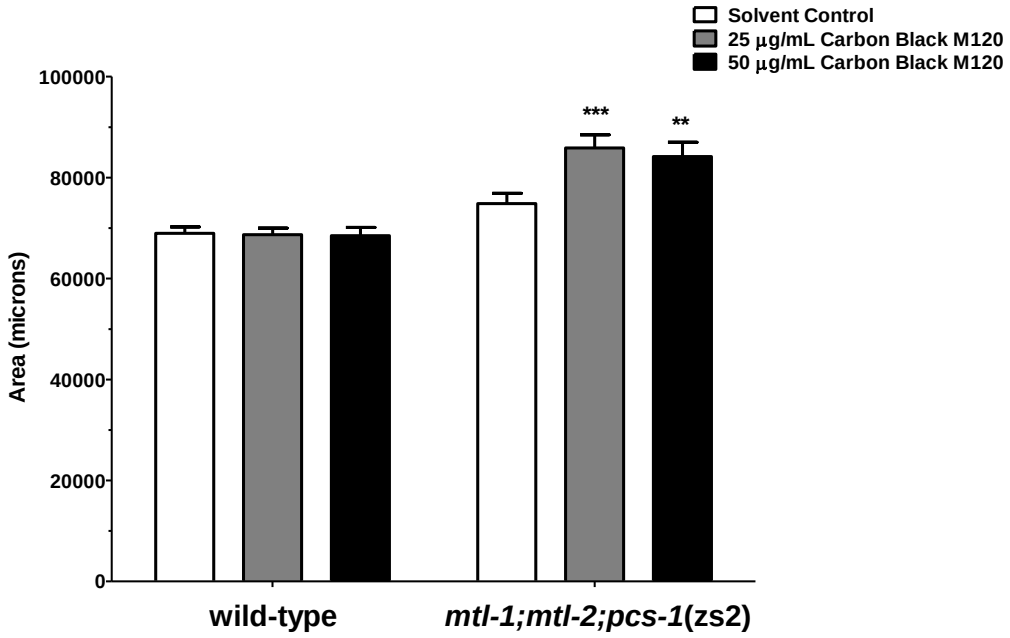

Fig. 4.9: Flat volumetric area of wild-type and *mtl-1;mtl-2;pcs-1*(zs2) nematode strains chronic exposure to different Carbon Black M120 concentrations. The data plotted present the end point result of change in surface area of the nematode at 120 hours post L1 stage, expressed in microns. Data are represented as mean ± SEM (n=20). Statistical analysis was performed using the one-way ANOVA comparing untreated and CB treated unmatched group sets of measurements, where ***is $p<0.01$, and ***$p<0.001$.

On CB exposure, the initial growth rate of nematodes (both wild-type and mutants) was similar to untreated controls, irrespective of strain or exposure condition. All nematodes reached adulthood within 4 days post-hatching and in absence of signs in nematode growth delay or shift in the rate (data not shown). In the control conditions the wild-type reached, over the period of 120 hours, flat volumetric surface area of 68974 ± 1263 microns. The chronic exposure to 25 and 50 µg/mL CB did not induce any significant physiological detectable changes in the wild-type body size (Fig. 4.9, Table 4.2) ($p<0.05$). The shape and rate of the exponential growth curves were indistinguishable

from each other. In contrast, the exposure to CB resulted in a phenotypic effect on the *mtl-1;mtl-2;pcs-1*(zs2) mutant strain, namely a statistically significant increase in mutant body size at all tested CB concentrations (Fig. 4.9, Table 4.2) ($p<0.05$).

Exposure to CB M120 had a significant effect on the reproductive capacity of wild-type and the triple-knockout mutant following exposure to CB particles (Fig. 4.10). In (solvent) control conditions, the wild-type nematodes produced on average 226 ± 1.5 viable eggs, a number within the expected norm. In contrast, the number of viable offspring in the *mtl-1;mtl-2;pcs-1*(zs2) was only 94.1 ± 3.2 (Table 4.2). Under non-solvent control conditions, this strain produces 160.4 ± 1.1 viable eggs. Analysis of the full data-set using two-way ANOVA indicated a significant effect of both strain ($p<0.0001$) and exposure concentration ($p<0.0001$) on brood size. Exposure to CB significantly reduced the average total number of viable eggs produced by wild-type worms only at the 25 µg/mL CB dose (Fig. 4.10). At this dose the reproductive output was significantly decreased to 203.1 ± 3.3 ($p<0.05$) (Table 4.2). There was no significant effect observed in wild-type nematodes dosed with 50 µg/mL CB (Table 4.2). A similar trend was observed in the *mtl-1;mtl-2;pcs-1*(zs2) mutant, where exposure to CB resulted in a non-dose dependent, however significant reduction in the number of viable eggs to 69.6 ± 3 when exposed to 25 µg/mL of CB, and to 70.3 ± 2.6 at 50 µg/mL CB doses ($p<0.05$) (Table 4.2).

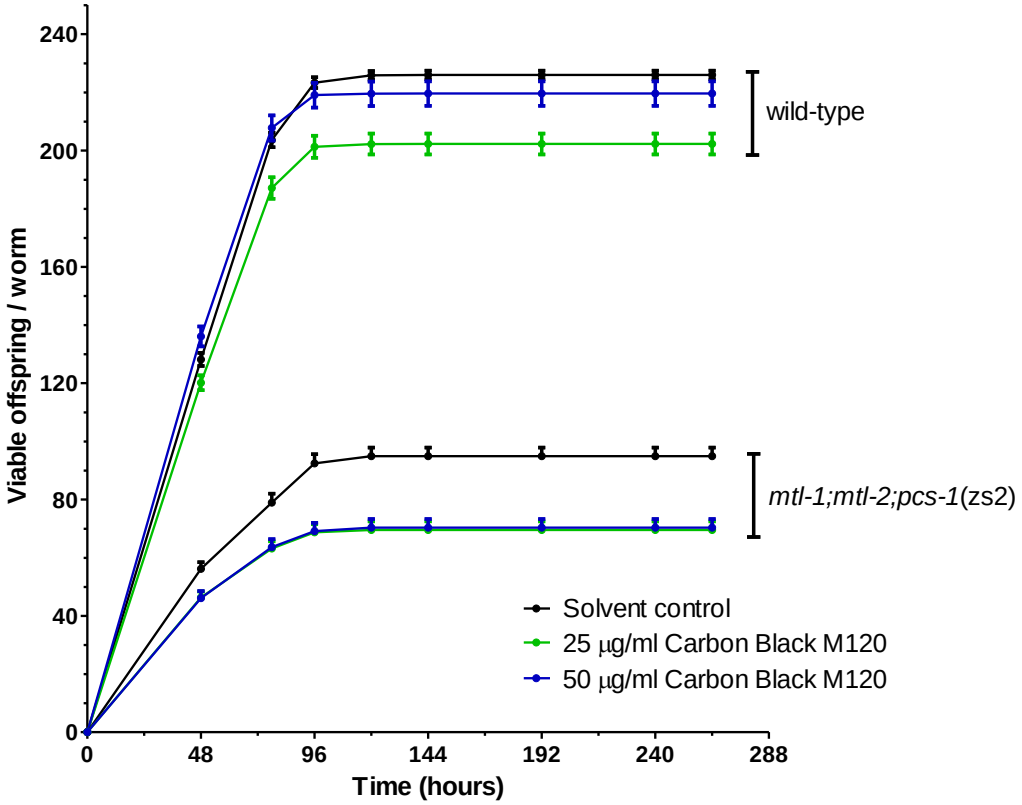

Fig. 4.10: Total cumulative brood size of wild-type and *mtl-1;mtl-2;pcs-1*(zs2) nematode strains exposed to different Carbon black M120 concentrations. To compare statistical significance of data between groups, Tukey's Multiple Comparison Test was used at each CB concentration. Error bars shown are standard error of the mean (n=36 for the wild-type; and n = 24 for the *mtl-1;mtl-2;pcs-1*(zs2) nematode strain). Statistical analysis was performed using the two-way ANOVA comparing untreated and CB treated unmatched group sets of measurements ($p<0.05$).

Table 4.2: Life-history traits of wild-type and *mtl-1;mtl-2;pcs-1*(zs2) mutants raised in the presence or absence of Carbon Black M120. Growth was examined by analysing the total surface area of the worm; and the reproduction was assessed by counting the number of viable offspring per individual. (ns (non-significant), *p<0.05, **p<0.01, and ***p<0.001).

			Carbon Black M120 (µg/mL)		
Strain			**0**	**25**	**50**
Growth	**wild-type**	**N**	20	20	20
		Surface area (microns)	68974 ± 1360	68704 ± 1301	68495 ± 1656
		Surface area (% of control)	100	99.6	99.3
		Statistical significance		ns	ns
	***mtl-1;mtl-2;pcs-1*(zs2)**	**N**	20	20	20
		Surface area (microns)	74834 ± 2067	85879 ± 2599	84180 ± 2823
		Surface area (% of control)	100	115	113
		Statistical significance		***	**
Reproduction	**wild-type**	**N**	33	32	34
		Total brood size ± SEM	226 ± 1.45	203.1 ± 3.34	219.6 ± 4.21
		Brood size (% of control)	100	89.9	97
		Statistical significance		*	***
	***mtl-1;mtl-2;pcs-1*(zs2)**	**N**	21	22	23
		Total brood size ± SEM	94.10 ± 3.15	69.55 ± 2.95	70.32 ± 2.97
		Brood size (% of control)	100	74	74.7
		Statistical significance		***	***

4.3.5.3 Chronic exposure of SOD (superoxide dismutase) mutant strains to Carbon Black M120

There is growing scientific evidence that particle specific characteristics, such as their composition, surface area, and size can generate an oxidative stress potential in biological systems and cause damage to the target molecules, such as proteins and DNA (Kelly, 2003; Love et al., 2012; Nell et al., 2009). Therefore measuring the generation

of intracellular free radicals e.g. superoxide radical (O^{2-}), may potentially serve as a suitable biological marker of CB toxicity in order to address the antioxidative theory of aging process in nematodes (Doonan et al, 2008; Landis and Tower, 2005). Pools of cytoplasmic, extracellular and mitochondrial superoxide radicals are detoxified in nematodes by the assigned SOD isoforms. In order to address the role of antioxidant enzymes in the protection against the oxidative potential of particles, the organismal effects of *sod-1*, *sod-2*, and *sod-3* deletion were examined.

The *sod-1*(tm776) nematode strain is a copper/zinc superoxide dismutase (Cu/Zn SOD) 612 bp deletion mutant. The SOD-1 enzyme is known to play an important role in protecting cells against oxidative damage and aging (Yanase et al., 2009). Therefore, the loss of this allele may impose a greater sensitivity to the free radicals, believed to be generated upon exposure to particles. Raised in control conditions, the *sod-1*(tm776) nematode mutants were approximately 10 % smaller in size compared to the wild-type strain (Fig. 4.11). The initial growth rates of CB treated and untreated *sod-1*(tm776) nematodes were similar to each other (data not shown), but changes in volumetric area became apparent at 120 hours, when the surface area of nematodes exposed to 25 µg/mL CB concentration significantly increased by 14 % ($p<0.05$) (Table 4.3). Additionally, the body size of *sod-1*(tm776) strain was also examined at lower CB concentrations. The outcome results showed that exposure to CB exhibits a dose-independent increase in the nematode body size (Appendix: Carbon Black M120).

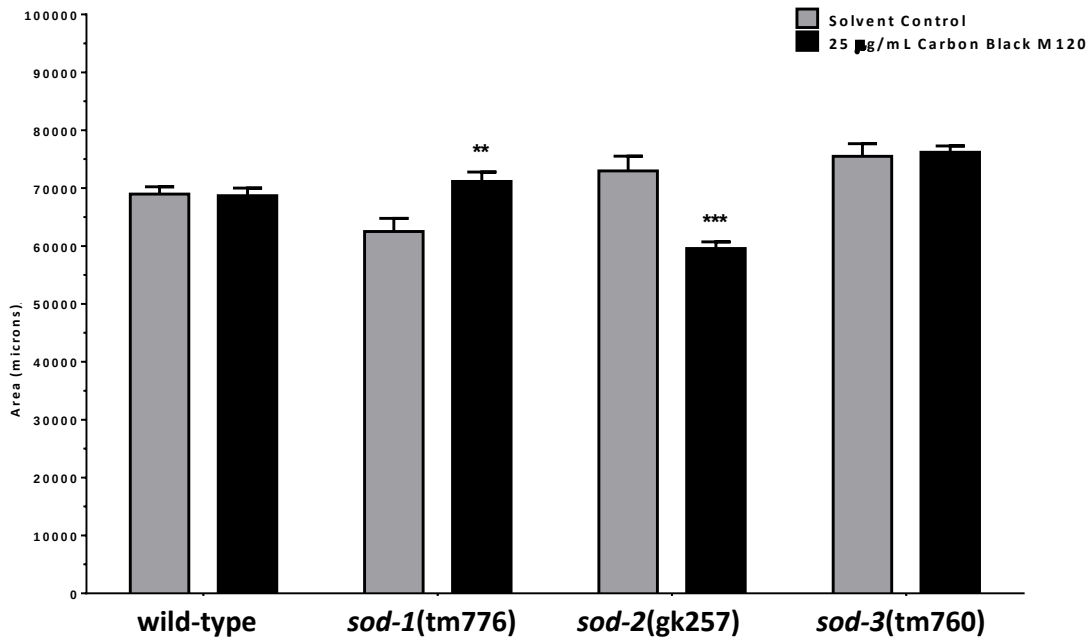

Fig. 4.11: Flat volumetric surface area of wild-type and SOD mutant strains chronically exposed to different Carbon Black M120 concentrations. The graphs present the end point result of change in surface area at 120 hours post L1 stage, expressed as a change in surface area of the nematode in microns. Data are represented as mean ± SEM (n=20). Statistical analysis was performed using the one-way ANOVA comparing untreated and CB treated unmatched group sets of measurements, where ** is $p<0.01$, and ***$p<0.001$.

The *sod-2*(gk257) nematode strain is an iron/manganese superoxide dismutase (Fe/Mn SOD) enzyme mutant, characterized by an insertion (TTATATTTGACTATTTGA) and a 159 bp deletion. It is predicted to be mitochondrial and to provide protection against oxidative stress (Van Raamsdonk and Hekimi, 2009). In control conditions, the *sod-2*(gk275) mutant strains were similar in size compared to the wild-type strain (Fig. 4.11). There was no significant delay or shift in body size during CB treatment compared to the untreated nematode (data not shown). At 120 hrs, an exposure to 25 µg/mL CB concentrations significantly reduced the body size of the treated nematode ($p<0.05$) (Table 4.3). Additionally, the changes in volumetric growth of *sod-2*(gk257)

strain as a response to CB exposure were also examined at lower concentrations (Appendix: Carbon Black M120). Notably, the reduction in mutant body size was CB dose responsive. The *sod-3*(tm760) nematode strain is an iron/manganese superoxide dismutase (Fe/Mn SOD) enzyme deletion mutant allele. The loss of 715 bp may impose a greater sensitivity to free radicals, believed to be generated upon exposure to particles. No significant changes in either growth rate or body size of chronically exposed (120 hours) CB *sod-3*(tm760) mutants were found, compared to untreated ($p>0.05$) (Fig. 4.11, Table 4.3). In addition, no significant changes in either growth or development were observed in *sod-3*(tm760) mutants when examined at lower CB concentrations (Appendix: Carbon Black M120).

Table 4.3: Volumetric area of SOD mutants raised in the presence or absence of Carbon Black M120. Growth was examined by analysing the total surface area of the worm. (ns (non-significant), **p<0.01, and ***p<0.001).

			Carbon Black M120 (µg/mL)		
Strain			**0**	**25**	**50**
Growth	***sod-1*(tm776)**	**N**	20	20	N/A
		Surface area (microns)	62502 ± 2283	71163 ± 1617	N/A
		Surface area (% of control)	100	114	N/A
		Statistical significance		**	
	***sod-2*(gk257)**	**N**	20	20	N/A
		Surface area (microns)	72979 ± 2550	59577 ± 1141	N/A
		Surface area (% of control)	100	82	N/A
		Statistical significance		***	
	***sod-3*(tm760)**	**N**	20	20	N/A
		Surface area (microns)	75510 ± 2166	76201 ± 1074	N/A
		Surface area (% of control)	100	101	N/A
		Statistical significance		ns	

4.4 Discussion

4.4.1 Particle characterization and effect of test medium on physicochemical properties of Carbon Black

One of the major challenges when working with nano-sized particles is their tendency to change their aggregation status when transferred from the solvent stock solution to the exposure matrix (food or saline solution), which often contains a high percentage of organic matter (Wani et al., 2011). This physicochemical particle property can play an important role in influencing their toxicity. In order to ensure that the screening system resembles a realistic and relevant environmental condition, only physical methods were used to create homogenous CB M120 dispersion. Physical characterization performed on CB suggested that carbon particles exist in the test media in both individual and aggregated states. The introduction of CB particles into the biological test medium changes their physicochemical characteristics and bioavailability according to the Brownian theory (i.e. via random particle movements in a fluid) (Montes–Burgos et al., 2010). Therefore, particle dimension and morphology should be taken into consideration as they might play an important role when evaluating particle - induced toxicity.

Transmission electron imaging (TEM) provided information about CB shape and size in the stock solution; however it could not provide detailed information on the particle state once in a biological test medium. The results from TEM imaging suggested that in the M9 test medium particle surface is modified by salt crystals, which coat the particle agglomerate clusters. These crystals contribute to the increase in the overall size of the aggregates. TEM imaging of CB particles in the OP50 bacteria could not be performed, as both the contents of biological solutions (live bacteria) and rapid aggregation of

particles damaged the observation grid, prevented imaging. For this reason, the NanoSight NTA (NanoSight Ltd, UK) technique that uses light dispersion was used to characterize particles in the biological solutions. NTA (NanoSight LM-10 and LM-20) instruments define not only the predominant particle dimension, but also all other particles present in the solution (Carr and Warren, 2012). This technique has been evaluated previously for the measurement of nanoparticles in the size range of 30 to 1000 nm (Boyd et al., 2011), protein aggregates (Filipe et al., 2010), as well as in nanomedicines (Gercel-Taylor et al., 2012). In addition, the American Society for Testing and Materials (ASTM) published guidelines on the Measurement of Particle Size Distribution of nanomaterials in Suspensions using NTA (ASTM E2834 – 12).

NanoSight characterisation suggested that particles are more mobile in M9 solution, thereby increasing the chances to collide into each other. Coagulation kinetics causes formation of aggregates, which are maintained via Van der Waals forces (Nel et al., 2009). Smaller particles tend to become less stable, which leads to an overall increase in their size and associated aggregates. As the M9 solution is primarily composed of sodium and potassium salts (Hitchcock et al., 1998), addition of CB particles causes the formation of crystal aggregates via salt-particle interactions (as observed with TEM imaging). An event, that occurs over time. The particle-crystal formation theory could in future, be further exploited by employing X-rad and TEM-EDAX methodologies.

The dimension of the aggregates formed can influence the deposition rate of the particles. In addition, larger aggregates can maintain higher surface reactivities, which may render them less stable and more prone to break up. How stable the newly formed particle clusters are over time, would need further investigation in order to understand their contribution in generating toxicosis. It is also important to note that there is a question of reproducibility of each analysis performed. As particle samples were of low

concentration (less than 10^7 particles/mL) and consisted of particles of different diameters, thorough and reproducible analysis could include an extended timeframe. Nevertheless, it is possible to conclude that the NanoSight can be used as the initial screening index when studying the characteristics of the nanoparticles.

To date, the NTA technique has been favoured by a number of scientists over the DLS, because of the low cost, ease of use, high sample throughput, rapid results, and the requirement of only small sample volumes. The disadvantage of the NTA is that some samples need to be diluted in order to be analysed (Domingos et al., 2009). Compared to the DLS method, NTA can generate more detailed and accurate data on particle behaviour, their dispersion, intensity, and size distribution of aggregates in biological suspensions (Filipe et al., 2010). Nevertheless, from a toxicological perspective, where particle growth and aggregation behaviour in the biological media needs to be defined, NTA is better suited for conducting this type of analysis.

4.4.2 Carbon Black M120 effect on OP50 bacteria food source

To investigate if the exposure to CB M120 induces an indirect effect on *C. elegans* via caloric restriction, bacterial growth was monitored in the presence and absence of particles. At the lower CB concentrations (< than 25 µg/mL), no significant change on bacterial growth was observed. Whilst, at higher doses (> than 25 µg/mL), CB seemed to stimulate bacterial growth significantly. CB most likely presents an additional carbonatious source of food to the OP50, therefore hypothetically increasing their growth rate. This notion would need further investigation. Nevertheless, all bacteria reached the stationary growth phase, regardless of the CB dose applied.

The *E. coli* bacterium is an organotroph organism that obtains hydrogen or electrons from organic substrates. Hence, it is conceivable that the source of carbon represents a nutritious energy food source to the bacteria, thereby allowing superior bacterial growth (Saier, 1998; Muñoz-Elías and Mckinney, 2006). This suggests that CB particles may alter the organismal metabolism exposed to artificial culture conditions in the laboratory. A similar observation was made by Lundborg et al. (2007) who showed that there was a dose dependent increase in *Streptococcus pneumoniae* bacterial survival with carbon-loaded macrophages.

In the human lung, alveolar macrophages (AM) mediate antimicrobial functions against invading pathogens, providing protection by phagocytosing particles deposited in the peripheral lung (Bowden, 1984; Gordon and Reid, 2002; Lundborg et al., 2001). Enhanced bacterial growth by carbon particles may contribute to the susceptibility to infection by microorganisms leading to increased impairment of AM function (Lundborg et al., 2001; Gordon and Reid, 2002). In addition, long term exposures to environmental particles can markedly impair AM phagocytic capacity, thereby additionally increase the risk for infections (Lundborg et al., 2001; Zelikoff et al., 2003). These events may play an important role in the adverse health effects seen in epidemiological studies of patients with asthma, and COPD when exposed to ultrafine particles (Pope and Dockery, 1999; Donaldson et al., 2001).

4.4.3 The transcriptional response of *C. elegans* exposed to Carbon Black M120

In this study, KNUDRA transgenic nematodes were chosen to quantitatively assess the transcriptional response of selected target genes to CB M120 toxicity. These

bioengineered, two-colour transgenic nematodes are designed to act as biosensor reporters of toxicant responsive pathways (Boulin and Bessereau, 2007; Frøkjaer-Jensen et al., 2008). They offer rapid, inexpensive, and accurate diagnostic profiling of transcriptional responses of toxic (potential hazardous) material. A panel of established genes known to be involved in oxidative stress response pathways and inflammatory activity were examined: *mtl-2* and *ugt-1* to detect oxidative metal toxicity; *gcs-1;* xenobiotic metabolism enzymes (*cyp-35A2*, *gst-4*, *gst-38*), and heat-shock proteins (*hsp-16.2*, *hsp-16.41*) to screen for xenobiotic environmental stresses responses, and a chaperone DnaJ protein/also known as Hsp40 (*dnj-13*).

The transcriptional responses were examined at the maximum concentration 50 µg/mL of CB. This dose was selected based on the results obtained from the transgenic *cyp-35A2*::mCherry worm. In addition, it is important to note that a 48 hour exposure time provided only a snapshot of the transcriptional status. Overall, the expression pattern of most of the tested genes did not deviate significantly from basal (control) level (Fig. 4.6). Analogous transcriptional response of *cyp365A2* was previously reported in *C. elegans* exposed to CeO_2 and TiO_2 nanoparticles (Roh et al., 2010), as well as in response to treatment with xenobiotics (PCBs and PAHs) (Menzel et al. 2001, 2005). However, the *C. elegans* genome harbours over 80 cytochrome P450 (CYP) encoding genes, but very little is known about their exact biological function. The *cyp-35A2* is generally expressed in the nematode intestines, where it functions as an NADPH-dependent monooxygenase that metabolizes endogenous and exogenous compounds. It was also reported to be involved in the fat storage pathway (Menzel et al., 2005). The increase in the relative fluorescence level of this transcript in the present study suggests that *cyp35A2* may be interlinked with the metabolic bioactivation of CBs. This is not an unprecedented finding, as the induction of CYP1A1 mRNA (Takano et al., 2002), and

other P450 family 1 isoenzymes, including CYP1A2 and CYP1B1 (Hatanaka et al., 2001) was observed in rats exposed to DEPs. However, in contrast, exposure to CB failed to induce CYP protein or activity in human monocytes (Eder et al., 2009) and in a rat study (Rengasamy et al., 2003).

The quantitative assessment of the relative change in MosSCI nematode fluorescence revealed that the expression of small HSP transcripts (*hsp-16.2* and *hsp-16.41*) was downregulated on CB exposure, however this was not statistically significant. HSPs are usually among the most highly inducible cytoprotective molecular chaperone proteins that confer a protective role during physical (e.g. heat) or chemical stresses (Lindquist, 1986; Strayer et al., 2003). Their expression correlates specifically with the presence of stressors that induce protein damage. Nevertheless, in this study CB failed to induce the stress reporter enzyme hsp16, which is in contradiction with previous reports stating that CB stimulates the secretion of hsp70 in epithelial cells (Ramage et al., 2004). Andre et al. (2006) reported that after a 4 hrs of inhalation of ufCB the mouse lung induces mainly HSPs, whereas after a 24 hrs exposure, a range of immunomodulatory proteins are activated. Note that the dosing and exposure conditions cannot be directly compared between experimental settings. Whether the *hsp-16* downregulation found in this study is specific to a nematode response to CB exposure remains to be established.

Entering the cellular environment, CB particles can physically damage and oxidize macromolecules (proteins, lipids, DNA) and thereby cause oxidative damage that leads to inflammation (Levy et al., 2012; Donaldson et al., 2001; Brown et al., 2000; Garza et al., 2008; Koike and Kobayashi, 2006). These toxic effects were highlighted in studies examining the ability of DEPs (Ma and Ma, 2002; Nikula et al., 1995; Heinrich et al., 1995) and carbon nanotubes (Jia et al., 2005) and thought to be inflammogenic and carcinogenic. Finally, the use of new transgenesis technologies allows us to successfully

apply *C. elegans* as a useful genetic model organism, in order to understand and explore toxicant influences from genes to function (Boulin and Hobert, 2012).

4.4.4 Reactive oxidative species (ROS) generation upon Carbon Black exposure

The smaller the particle is, the greater its surface area to volume ratio is, hence the greater its ability to generate ROS and, cause oxidative stress. This is a widely discussed paradigm describing the toxicity of NPs. In cell-free systems the ROS production of CB was examined using the diesterified probe DCFH (Catheart et al., 1983), which demonstrated that ufCB are more potent than larger particles at generating ROS (Wilson et al., 2002). Wilson et al. (2002) also showed that in MM6 cells, the exposure to ufCB generates more intracellular ROS, than larger fine carbon particles. Stone et al. (1998) and Sayes et al. (2005) also confirmed that ufCB induce cytotoxicity and oxidative stress more than fine carbon. In *in vivo* settings, rats that have been instilled with CB have also been shown to induce a greater oxidative stress and proinflammatory response to the ultrafine particulate size than their fine particle counterparts (Renwick et al., 2004; Li et al., 1999).

In *C. elegans*, the generation of free radicals and their accumulation affects organismal development, brood size, and longevity (Zeitoun-Ghandour et al., 2011; Honda et al., 2002; Hughes and Stürzenbaum, 2007). Following incubation with CB, a significant dose specific increase in ROS was observed in wild-type and metal hypersensitive nematode strains (Fig. 4.7). This suggested that CB exposure increased the oxidant stress in both nematode strains. In contrast, CB was a poor inducer of ROS levels in the SOD mutants. The intracellular level of ROS was reduced in the *sod-1*(tm776) and *sod-*

2(gk257) nematodes, or remained unchanged as in the *sod-3*(tm760) mutants (Fig. 4.7). These observations might be best explained by the difference in baseline levels of total endogenous superoxide in each nematode strain, therefore also differing in their respective threshold sensitivities to stress conditions. Furthermore, many antioxidant systems are present in the *C. elegans* (e.g. MTs, PCSs etc.), which might be differentially activated in different nematode mutants. For example, *C. elegans* carry five SOD genes, *sod-1* and *sod-5* are primarily cytoplasmic CuZnSODs, *sod-2* and *sod-3* are mitochondrial MnSODs, and *sod-4* functions as an extracellular CuZnSOD (Landis and Tower, 2005). SOD-1 and SOD-2 are known to be the major contributors of total SOD activity in *C. elegans*, however the absence of any one of them, results in other isoenzymes to functionally compensate the lost of activity (Back et al., 2012). These contradicting results demonstrate the complexity of the *C. elegans* antioxidant responses to environmental stresses.

The main pathway involved in the conversion of DCFH to the fluorescent product DCF is through ROS challenge, via for example hydrogen peroxide and hydroxyl radicals (Halliwell et al., 2004; Cohn et al., 2008). Superoxide radicals are very unstable and highly reactive molecules that have been viewed as a major contributor to aging (Back et al., 2012). Once generated, they are, within seconds, converted to H_2O_2 by SODs. H_2O_2 is in turn converted to H_2O and O_2 by catalase, glutathione peroxidase and other antioxidant enzymes. According to the oxidative damage theory, SOD should protect the organism against oxidative damage and aging process (Hekimi et al., 2011), however many studies have shown that in nematodes the SOD protection role is not simple (Doonan et al., 2008; Van Raamsdonk and Hekime, 2011; Back et al., 2012). Abrogation of *sod-1* in nematodes causes a minor decrease in normal life-span, and general increase in both cytosolic and mitochondrial superoxide level (Yanase et al.,

2009). The strain is viable, with a normal development and fertility rates, but sensitized to certain environment stressors, such as paraquat (Yanase et al., 2009). The inactivation of *sod-1* was found to cause intracellular imbalance in ROS, mitochondrial dysfunction and accumulation of oxidative damage in some studies (Yang et al., 2007; Gems and Doonan, 2009), but not in others (Doonan et al., 2008). In studies where *sod-1* was overexpressed (OE) the life span of a nematode was increased (Cabreiro et al., 2011). Surprisingly, the *sod-1* OE strain was also found to be hypersensitive to oxidative stress, and not resistant as was initially hypothesized. The loss of MnSODs, *sod-2* and *sod-3*, causes a reduction in oxidative stress resistance (Back et al., 2012; Van Raamsdonk and Hekime, 2009), and no change in the life-span of the nematode under control conditions (Doonan et al., 2008; Yang et al., 2007; Honda et al., 2008). In one study *sod-2* deletion resulted even in the *C. elegans* life-span extension (Van Raamsdonk and Hekime, 2009). It was hypothesized that MnSODs are required for diminishing intracellular ROS, however they are not essential for the nematode survival. All these studies indicate that *C. elegans* have developed a very fine-tuned antioxidant system that allows them to cope and survive when exposed to oxidant stressors. It is likely that the increase in ROS levels observed in this study can be attributed to the particle/and aggregate load/and size in *C. elegans* intestinal epithelial cells (Koike and Kobayashi, 2006; Hussain et al., 2009; Garza et al., 2008). The toxic outcome is also dependent on the concentration and length of exposure to CB. In addition, CB agglomerates have been linked to the generation of cellular stress by damaging the epithelial cell layer (Weissenberg et al., 2010), as well as proteins, e.g. by impairing phagocytosis due to overloading (Ferin et al., 1992; Donaldson et al., 2001; Levy et al., 2012). These would damage the cellular components and increase the release of ROS e.g. phagocytotic burst of H_2O_2 and their functional impairment (Xia et al., 2006; Renwick et al., 2001). General increase of the cellular ROS pool causes mitochondrial membrane

depolarization, increase in Ca^{2+} and cytochrome c leakage (Hussain et al., 2010; Brown et al., 2000). These events lead to cell inflammation and cytokine activation, as it has been shown by *in vitro* (cell lines) (Hussain et al., 2009; Koike and Kobayashi, 2006) and *in vivo* (rat, murine) studies (Gilmour et al., 2004; Renwick et al., 2004; Brown et al., 2000; Li et al., 1999; Bourdon et al., 2012).

4.4.5 The key endpoints of the nematode life cycle following Carbon Black M120 exposure

Population based epidemiology studies have linked the Carbon Black (CB) toxicity (such as mortality), with either environmental (e.g. exposure to particulate components of DEP) (Ma and Ma, 2002)) or occupational (for example, carbon black workers (Van Tongeren et al., 2002; Hailemariam et al., 2012)) exposures. Most of the clinical data reporting on the health effects (including respiratory outcomes, cardiovascular diseases, cancers, and hospital admissions) are collected, reviewed, and linked post-mortem. Nevertheless, studies carried out in animals did show that there is an increased risk that carbon particles can contribute to respiratory inflammation (Brown et al., 2000; Li et al., 1999; Glimour et al., 2004), and even cancer (Valberg and Watson, 1996). In 2012, the World Health Organization stated that "black carbon (BC) may operate as a universal carrier of a wide variety combustion-derived chemical constituents of varying toxicity to sensitive targets in the human body such as the lungs, the body's major defense cells and possibly the systemic blood circulation." As pointed out by Öberdoster and colleagues in 2006, there is an increased need for providing more toxicological information on both short- and chronic- effects of CB on organismal systemic responses that are environmentally relevant.

In this study, the nematode growth was used as one of a life-cycle trait to assess the toxic effect elicited on CB exposure. An acute, 24 hrs liquid exposure of wild-type L1 larvae to CB did not induce any significantly toxic effects on final nematode body size. The lack of CB induced response may have been due to the physicochemical characteristics of CB in the exposure media (e.g. increase in particle aggregate size over time). Most likely, the presence of potassium and sodium salts within the M9 solution increases the carbon particle agglomerate size, thereby preventing L1 larvae from taking them up. Therefore, by increasing the exposure duration rather than concentration, and changing the delivery method, more toxicant is taken up and thus the adverse outcome is more profound (Fig. 4.9). Indeed, adverse health (systemic) effects have also been documented in rats following long-term "chronic" exposure to relatively low concentrations of CB (Nikula et al., 1995) and DEP (Mauderly et al., 1987) Particles.

Switching to a bacterial vehicle for particle delivery to the nematodes allowed the assessment of chronic exposures to CB on the nematode life-cycle endpoints (growth and reproduction). Life-history studies conducted with wild-type and the *mtl-1;mtl-2;pcs-1*(zs2) strain provided evidence that CB influences the reproductive output of both nematode strains. It is interesting to note that although brood size was reduced in both strains exposed to CB, the body size was significantly affected only in the *mtl-1;mtl-2;pcs-1*(zs2) mutant. The negative effects of the nanoparticles on the nematode reproduction have been reported previously (Roh et al., 2009; Wang et al., 2009; Pluskota et al., 2009; Kim et al., 2008). It is suggested that single particles and agglomerates both accumulate in the nematode intestines and impose an internal pressure (Appendix: Carbon Black M120). Particle accumulation/load may have resulted in the decrease in number of viable eggs accompanied by a significant increase in bag of worm phenotype. This phenotype generally occurs in aged nematodes with

vulva abnormalities, such as defects in vulva development, or can be the result of a complete absence of the egg laying organ (Pluskota et al., 2009). It is possible that CB particles mediated the generation of reactive oxygen species (ROS), as suggested by the observed increase in DCF product both in wild-type and *mtl-1;mtl-2;pcs-1*(zs2). ROS can lead to a premature degeneration of reproductive organs and cause intracorporal hatching of eggs in the parent animal.

Alternatively, prior to entering the nematode intestinal lumen, the surface of CB particles may get coated/modified with bacterial protein secretions, such as LPS, which could potentially contribute to cellular inflammation and toxic outcome. An inflammatory response accompanied by an increase in intracellular oxidative damage can result in an age-dependent functional decline in an organism (Honda et al., 2002). Further research needs to be conducted to decipher which factor(s) contribute most towards possible toxic effects observed in this study.

Interestingly, the chronic exposure of SOD mutants to CB elicited only small effects on body size. The deletion of the nematode allele *sod-1*(tm776) was expected to be most sensitive to ROS, however no development delays were observed. The mitochondrial SOD mutant isoforms, *sod-2* and *sod-3*, were differentially affected by the CB exposure in terms of their body size, significantly decreased in *sod-2* and with no change observed in the *sod-3*. The precise contribution of each SOD isoenzyme in scavenging ROS upon CB induced toxicosis still remains elusive. In order to maintain endogenous ROS levels, the expression, localization, and half-life of each SOD isoenzyme in the cell has to be balanced. In addition, nematodes are thought to benefit from additional antioxidant systems that can be switched on or off when under stress (Back et al., 2012).

Surprisingly, it has also been recently found that in the absence of all five SOD isoforms the nematode life-span is not affected in control conditions (Van Raamsdonk and Hekime, 2012), however the strain is sensitive to a number of stressors (heat, osmotic stress and oxidative stress). The lack of evidence in life-span reduction in a SOD mutant might be due to the *C. elegans* being able to counterbalance between toxicity level of superoxides produced and its own adaptation to reduced superoxide detoxification (Back et al., 2012; Van Raamsdonk and Hekime, 2012). Therefore, when wild-type nematodes are introduced to a stress environment, low levels of an oxidant inducer may increase the nematode life-span and intracellular ROS until optimum superoxide concentration is reached (e.g. low concentrations of paraquat induce a pro-survival signal) (Van Raamsdonk and Hekime, 2012). However, once the maximum level of endogenous superoxide is engaged, any further increase will cause the nematode life-span to decline (a toxic side effect of superoxide increase). In control conditions, the *sod-2* mutant is closer to its optimum superoxide concentrations than the wild-type or *sod-1* mutant, as shown by Van Raamsdonk and Hekime, 2012. SODs do play an important protective role in scavenging free radicals, but they are not essential for life in a nematode (Back et al., 2012). How the deletion of a major antioxidant, will shift the whole mechanism of superoxide pool is still unknown and unpredictable. Overall, it can be hypothesised that MTs and PCS, as well as SODs, all contribute to carbon black detoxification but via mechanistically distinct pathways.

4.5 Conclusion

During this study it has become apparent that neither wild-type, nor any of the mutant (a metal hypersensitive *mtl-1;mtl-2;pcs-1*(zs2), or the oxidative stress sensitive *sod-*

1(tm766), *sod-2*(gk257), and *sod-3*(tm760)) nematode strains were strongly affected by the CB M120 exposure. From preliminary work it was also possible to extrapolate that acute exposure to CB does not affect wild-type nematode development. The low level of toxicity observed can be explained by the time-dependent agglomeration of CB particles in the M9 medium, thereby reducing the nematode particle accumulation rate and toxicity. However, the fact that toxic effects on the nematode life-cycle indices (growth and reproduction) where observed, when the exposures were performed via the OP50 bacteria and the exposure period extended, highlights the importance of defining meaningful exposure settings.

This study also proposed that CB M120 particles induce an oxidative response in the nematode, as ROS production was found to be increased in both wild-type and a metal hypersensitive mutant. In addition, stimulation of cytochrome P450`s, specifically the *cyp35A2* transcript, in response to CB induced (possible) toxicity highlighted that changes at the transcriptional level occurred. Overall, the use of toxicogenomics in combination with imaging techniques is a valuable approach to examine the contributions from carbon black material to systemic nematode responses.

CHAPTER FIVE

NIST 1648a induced toxicity in *Caenorhabditis elegans*

5.1 Introduction

Exposure to natural and man-made combustion derived PM (e.g. metals, PAHs, organic components and certain toxins) presents an adverse risk factor to both the environment and human health (Miller et al., 1993; Dockery et al., 1993; Schwartz, 1994). Historically, human beings have always been exposed to airborne nanosized or ultrafine particles (diameter less than 100 nm), for example generated from burning biomass for the purpose of heating and cooking. However, following the industrial revolution and development of automotive transportation, the particle pollution exposures have increased dramatically and have in recent years become a matter of concern (WHO, 2004; Valavanidis et al., 2008; EPA, 2009).

Exposure to ambient pollutants, such as PM, can elicit oxidative stress (Li et al., 1996; Kelly, 2003). However, the mechanism by which PM exerts its adverse health effects is still not fully understood. There is growing evidence that certain constituents on the PM surface, such as combustion derived volatile organic compounds (VOCs), inorganic materials of different solubility (e.g. metals, nitrates, sulphates), endotoxins and pollen, might be the major drivers of the proinflammatory effects observed in both acellular and living systems (Brown et al., 2001; Kelly, 2003; Beck-Speier et al., 2005). In addition, it has also been stipulated that particle size, as well as its surface area, contribute to UFP redox activity, formation of free ROS and the generation of oxidative stress (Kelly, 2003; Li et al., 2003; Lodovici et al., 2011; Ghio et al., 2012).

Epidemiological studies have demonstrated a positive association between elevated ambient PM concentrations and human morbidity and mortality rates in susceptible cohorts of the population, such as asthmatics, children, and elderly (Dockery et al., 1993; Schwartz 1994; Pekkanen et al., 1997; Samet et al., 2000). Human and animal controlled exposure studies identified a further relationship between the PM exposure and adverse respiratory (Lebowitz, 1996; Curtis et al., 2006; Magas et al., 2007), cardiovascular (Bhatnagar, 2006), neurological (Calderon-Garciduenas et al., 2002), reproductive (Wang and Pinkerton, 2007), as well as developmental (Maisonet et al., 2004) effects. However, some studies failed to find any association links (Pekkanen et al., 1997; Tiittanen et al., 1999). Inhalation and/or instillation of model UFP studies in rodents have shown that particles induce a consistent mild inflammation in their respiratory tract, and those effects were found to be exuberated in susceptible animal models (Ferin et al., 1992; Kadiinska et al., 1997; Elder et al., 2000). In addition, lung histopathology, and blood coagulation studies also reported evidence that UFPs cause inflammatory damage (Ferin et al., 1990; Ferin and Oberdörster, 1992, Oberdörster et al., 2000; Elder et al., 2004).

In general, the production of oxidants appears to be a fundamental driver of the biological effects seen after PM exposure (Ghio et al., 2012). Different methodologies have been used to define the underlying mechanisms and cellular pathways. For example, the PM capacity to induce proinflammatory and oxidative stress responses has been examined in *in vitro* settings, by measuring changes in cell signalling pathways and expression of oxidative- and inflammatory- related genes (Brown et al., 2000; Brown et al., 2001; Li et al., 2003). The oxidative potential of ambient particles was also confirmed in cellular-free systems by measuring antioxidant enzyme depletion

from a synthetic respiratory tract lining fluid (RTLF) (Zielinski et al., 1999; Mudway et al., 2004).

Often uncertainties and disagreement persist over the interpretation of the results collected from UFP studies, questioning which physical and chemical properties of the particle are responsible for driving adverse health effects, or the particle dose and duration needed to observe pathophyisiological changes to take place, as well as the different routes of exposures and end points investigated (Costa et al., 1997; Ayres et al., 2008). In order to deal with health risks and the observed discrepancy in data collected, quality regulations need to be adopted. Therefore, the Clean Air Act (CAA) required the U.S. Environmental Protection Agency (EPA) in 1997 to set national ambient air quality standards (NAAQS) for PM less than 2.5 µm ($PM_{2.5}$) in size. The National Institute of Standards and Technology (NIST), an agency of the U.S. Commerce Department, has collaborated with the EPA to develop a Standard Reference Material (SRM), 1648a Urban Particulate Matter (NIST 1648a), which was collected in an urban area, to expand quality assurance capabilities and source species considered to be harmful to the public health and the environment. It is now routinely used as a reference material to evaluate and standardize inorganic analyses of atmospheric PM and similar matrix materials (Huggins et al., 2000; Ball et al., 2000; Hatzis et al., 2006).

Nevertheless, the exploration of new methodologies is still hampered by many uncertainties which limit us from fully understanding the intricate details that define the mechanisms of toxicology and their contribution to disease. Emergence of new model organisms, such as the invertebrate nematode *Caenorhabditis elegans*, can offer power tools to unlock the complexity of mechanistic toxicology and toxicogenomics (Lee et al., 2004). Indeed, *C. elegans* is an ideal model to study complex biological processes (e.g. oxidative damage induced by a polymorphic, metal oxide based PM), and therefore

well suited to establish the link(s) between molecular genetics and effects on life-history parameters. To date, the *C. elegans* has not been exploited extensively as an experimental model to investigate bio-interactions with ambient PM. Therefore, the overall objective of this research was to conduct baseline studies to test whether nematodes can serve as a bioindicator for investigating natural ambient PM toxicity.

5.2 Aims

The aim of this study was to utilize a National Institute of Standards and Technology (NIST) standard reference material (SRM) for atmospheric particulate matter (NIST 1648a) to determine acute and/or chronic toxic effects on *Caenorhabditis elegans* exposed wild-type, metal hypersensitive, and oxidative stress sensitive mutant strains. Endpoints measured included life cycle traits (growth, brood, and life-span) and the overall intracellular reactive oxygen species (ROS) production by the DCFH-DA assay. Transmission electron microscopy (TEM) and NanoSight NTA techniques were used as tools to verify particle behaviour within the test solutions. In addition, whole genome microarrays and qRT-PCR approaches were utilized to define and characterize unique genes and signalling pathways associated with exposure to NIST toxicity. Overall, by combining molecular and organismal phenotypic assays it is aimed to dissect the multi-factorial responses and health risks of PM toxicity.

5.3 Results

5.3.1 Characterization of NIST 1648a

5.3.1.1 Transmission electron microscopy (TEM) imaging

Particle size, surface area and degree of the agglomeration of NIST 1648a powder and when dissolved in solvent was previously defined (Mackey et al, 1998; Huggins et al., 2000; NIST SRM 1648a, U.S. Department of Commerce 2011). As the NIST particles will be presented to *C. elegans* via suspension in 5 % methanol and M9 buffer, it was deemed important to characterize NIST particles by TEM. NIST material was primarily polymorphic in its composition. The particle sizes were found to range from less than 50 nm up to several hundred nm (Fig. 5.1). Particle shape was spherical to ellipsoidal, and they were primarily present as agglomerates or aggregates. TEM imaging indicated that in M9 medium, salts attach and form a crystal coat around some (Fig. 5.1C), but not all NIST particles (Fig. 5.1D). The crystal coating contributes to the increased size of the NIST aggregate clusters.

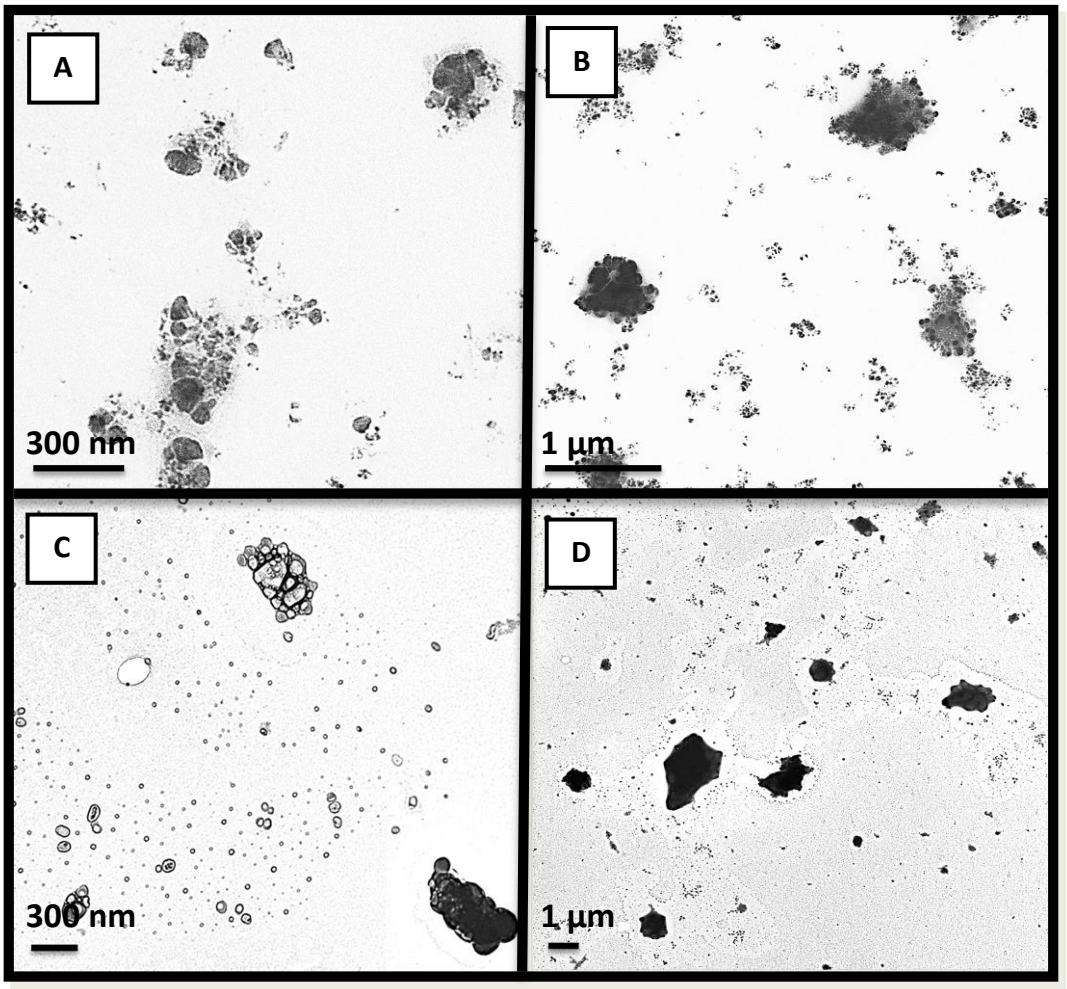

Fig. 5.1: **TEM images of NIST nanoparticles.** Characterization of the NIST 1648a in the test solution: in 5 % methanol (in HPLC water) at 16.0 k × magnification **(A)** and 10.0 k × magnification **(B)**; and M9 saline solution at 20.0 k × magnification **(C)** and 4.0 k × magnification **(D)**. Representative images from n=17 in total.

5.3.1.2 Nanoparticle tracking analysis (NTA) by NanoSight

The size distribution of NIST 1648a particle agglomerates in the M9 test solution (Fig. 5.2A-B) and OP50 bacteria (Fig. 5.2C) was characterized using the NanoSight NTA method. The NTA distinguished the nature of different NIST sized populations based on the altered scattering intensities, whereupon particles of smaller sizes but of a similar refractive index scatter less light, than the larger ones.

A wide particle size-to-size distribution was observed, which ranged from smaller single particles of roughly 50 nm to 100 nm in diameter. In the OP50 bacteria, NIST particle movement and size measurements of agglomerates were affected by the medium viscosity and protein aggregation. This was rectified by diluting the OP50 bacteria with LB broth prior to dispersing/adding NIST to the media samples. The NTA analysis suggested that NIST tends to aggregate once added to the biological solvent, with particle liaisons being slightly more intense in the OP50 bacteria than in the M9 solution. Particle movement in OP50 solution was also reduced, thus resulting in a more uniform aggregate size distribution than in M9 (Fig. 5.2 and 5.3).

Once introduced to the biological medium (0 hours), a greater percentage of the NIST particle agglomerate clusters were within the 50- to 400- nm range in the M9 (Fig. 5.2A; Table 5.1) than in the OP50 medium (Fig. 5.3, Table 5.1), where a proportion of the clusters ranged from 50 nm to 600 nm. The particle concentrations were as follows: in the M9 test media at 0 hour 2.4×10^7 particles/ mL and at 24 hours 1.4×10^7 particles / mL. The particle concentration in OP50 test media was recorded to be 4.3×10^7 particles /mL. The dominant peaks of the NIST particle at 0 hours were 76, 115, and 399 nm in the M9 media (Fig. 5.2A), whereas in OP50 they were 96, and 138 nm (Fig. 5.3).

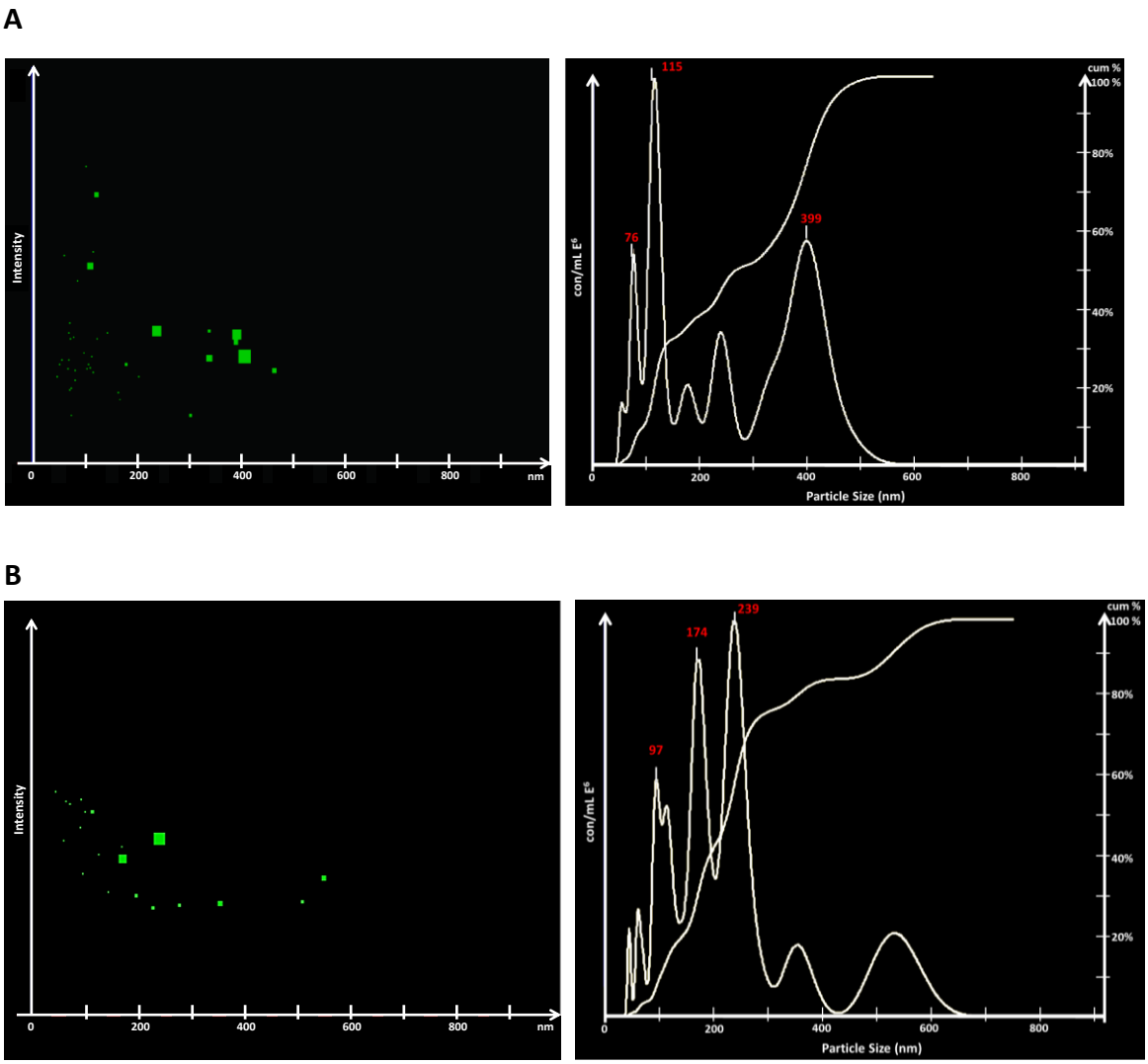

Fig. 5.2: NanoSight characterization and size distribution of NIST 1648a in the M9 solution. Videos of NIST particles in the M9 at 0 hour **(A),** and at 24 hour **(B)** were recorded at a frequency of 30 fps (frames per second), tracked, and subjected to the analysis (for detailed methodology see Chapter 2: Materials and methods).

The analysis also revealed that after 24 hours in M9 test medium, the dominant particles were 97, 174, and 239 nm in size (Fig. 5.2B); and the number of agglomerate clusters did not increase over time (Fig. 5.2B). NanoSight real-time video feature allows time dependent phenomena such as aggregation or dissolution to be followed both qualitatively and quantitatively. However, NIST particle size distribution changes could

only be analysed in the saline M9 solution and could not be investigated in OP50, as the bacteria would either reach a maximum optical density (OD) concentration if fully aerated, or die if maintained in a sealed chamber (without oxygen). Therefore, NTA cannot be used to study the time-dependent morphological changes in particle size and concentration when suspended in OP50 bacteria.

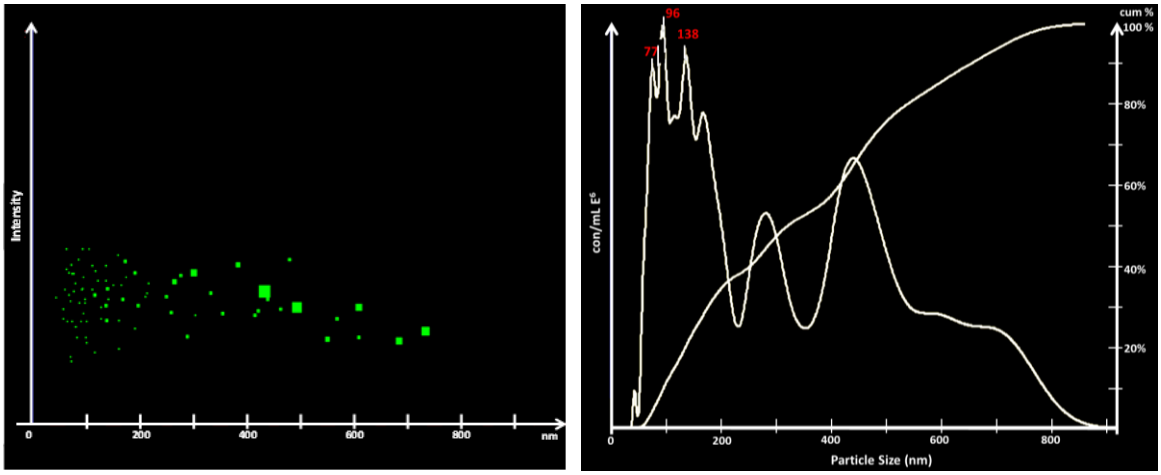

Fig. 5.3: NanoSight characterization and size distribution of NIST 1648a in the OP50 bacteria test media at 0 hour. Videos of were recorded at a frequency of 30 fps (frames per second), tracked, and subjected to the analysis (for detailed methodology see Chapter 2: Materials and methods).

Table 5.1: NanoSight mediated assessment of NIST 1648a particle size distribution immediately after addition to the test solution (0 hrs), or after 24 hrs incubation at room temperature (24 hrs).

Sample	Particle size range (nm)	Mean	SD
NIST 1648a in M9 test medium (0 hrs)	50 – 432	257	134
NIST 1648a in M9 test medium (24 hrs)	50 – 550	245	137
NIST 1648a in OP50 bacteria of optical density of ~1.0 (0 hrs)	50 – 652	335	202

5.3.2 Effect of NIST 1648a supplementation on OP50 bacterial food source

Previous studies have suggested that quality and quantity of bacterial food source can affect nematodes, including their growth, survival, and reproduction (Walker et al., 2005). In order to address this, bacterial growth was examined in the presence of NIST 1648a suspensions. No significant pro/antibacterial effects on the OP50 bacteria growth were observed at any of the tested NIST concentrations (Fig. 5.4). The pH was measured in fresh and 24 hours old bacterial solution in the presence and absence of NIST. Results showed that the pH of the OP50 was ~ pH7.4 (Appendix: NIST 1648a), and was not affected by NIST supplementation over a period of 24 hours. Based on these results, it was concluded that NIST concentrations of up to 100 µg/mL could be used without impairing the nutritional volume of the *E. coli* OP50 feeding strain.

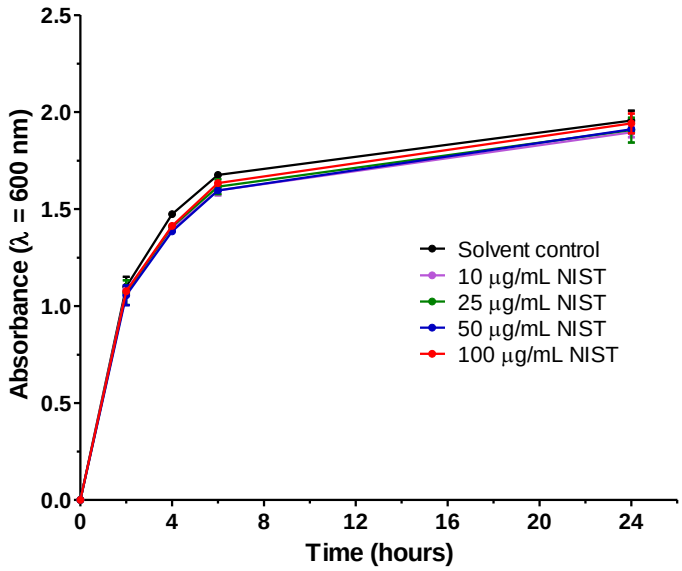

Fig. 5.4: Effects on dietary restriction. OP50 *E. coli* was incubated at 37^{0}C for 24 hours in the absence and presence of NIST 1648a. Error bars denote ± SEM (n=4). Statistical analysis was performed using the one-way ANOVA comparing untreated and NIST treated group sets of measurements. No statistical significant differences were observed.

5.3.3 Changes in transcription-activated fluorescent reporters upon NIST 1648a exposure using a transgenic *C. elegans* system

To quantitatively and qualitatively assess nematode transcriptional responses of specific target genes following an exposure to NIST 1648a, the MosSCI transgenic nematodes were utilized (generated by Knudra Transgenics, USA). In these integrated dual coloured nematodes, the mCherry fluorescence protein is under control of the promoter of the target gene of interest, and a green fluorescence protein GFP (*unc-47*::GFP) is constitutively expressed as an internal control (for detailed description of the transgenic strains see Chapter 2: Materials and methods).

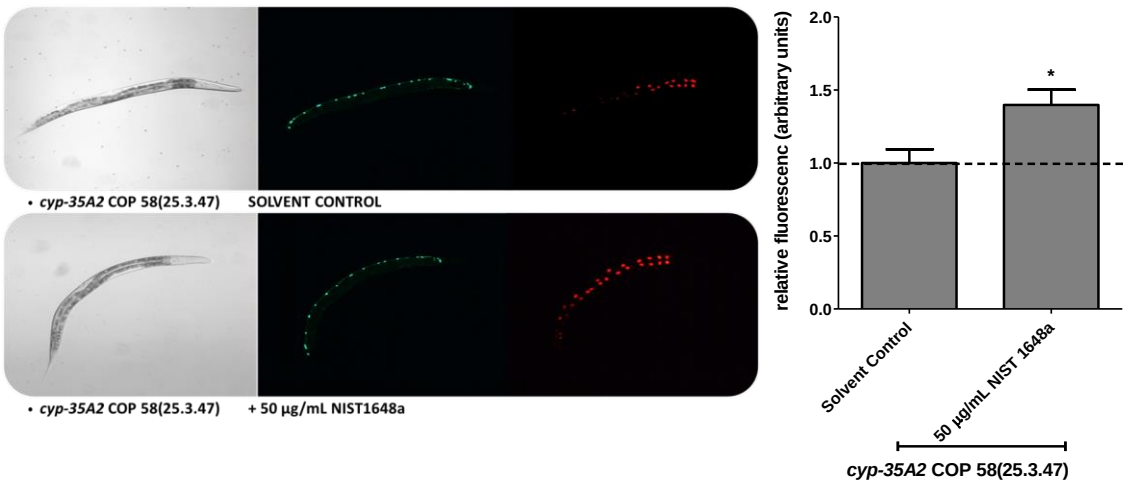

Fig. 5.5: Fluorescence images and a quantitative analysis of a significant induction of *cyp-35A2::*mCherry expressed as relative fluorescence units following normalization to the invariant *unc-47::*GFP. 10 worms were observed in each experimental condition (0 and 50 µg/mL NIST 1648a) and error bars represent ± SEM. Statistical analysis was performed using the Wilcoxon signed rank test, where *denotes $p<0.05$.

In order to determine which target genes are transcriptionally activated by NIST, a 48 hour exposure to 50 µg/mL dose was carried out. The following panel of transgenic biosensor reporters were tested: *mtl-2*, *hsp-16.2*, *hsp-16.41*, *cyp-35A2*, *gcs-1*, *gst-4*, *gst-38*, *ugt-1*, and *dnj-13*.

Transgenic worms bearing the promoter fusion construct of *cyp35-A2* and *gcs-1* were found to be significantly induced in nematodes exposed to NIST. A quantitative analysis of 10 worms, showed that *cyp-35A2* was induced by a significant 1.4 - fold ($p<0.01$) (Fig. 5.5).

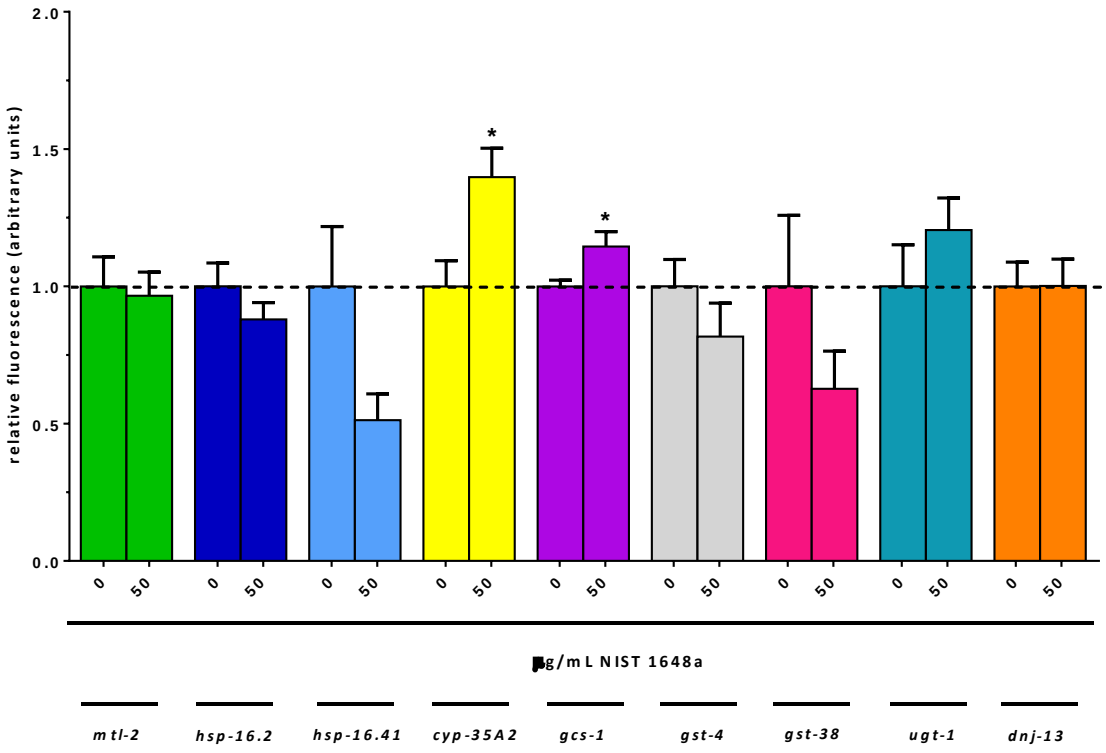

Fig. 5.6: Quantitative analysis of the transcription-activated promoter of the genes of interest::mCherry expressed as relative fluorescence units following normalization to the invariant *unc-47*::GFP in response to NIST 1648a treatment. 10 worms were observed in each experimental condition (0 and 50 µg/mL NIST) and error bars represent ± SEM. Statistical analysis was performed using the Wilcoxon signed rank test, where *is $p<0.05$.

In addition, the *gcs-1* transcript was also statistically significantly induced, albeit by a modest 1.1 - fold ($p<0.005$) (Fig. 5.6). The *ugt-1* transcript was also found to increase upon NIST exposure, despite being statistically non-significant. The analysis uncovered that two other transcripts, namely *hsp-16.4* and *gst-38*, decreased by 0.5 - and 0.6 - fold, respectively (Fig. 5.6). Although statistically non-significant, this may be biologically meaningful. No other significant differences were observed in any other transgenic nematode strains examined.

5.3.4 Detection of free radical H_2O_2 levels in *C. elegans* exposed to NIST 1648a

Intracellular ROS production was measured in wild-type, a metal hypersensitive mutant, and several oxidative stress sensitive mutants maintained in the presence or absence of 25 µg/mL NIST 1648a for 48 hours (Fig. 5.7).

In the absence of NIST, the relative base-line levels of ROS in wild-type and the metal hypersensitive (*mtl-1;mtl-2;pcs-1*(zs2)) are comparable (Fig. 5.7). The SOD nematode mutants exhibit higher base-line levels of intracellular ROS when compared to wild-type or/and metal hypersensitive mutant, as well as to the SKN mutant. The SKN mutant is characterized by a very low base-line level of intracellular ROS (Fig. 5.7).

An exposure to 25 µg/mL NIST resulted in a statistically significant increase in the total intracellular ROS levels in wild-type and the *skn-1*(zu67) mutant (Fig. 5.7). Consequently, the total fluorescence intensity of the DCF moiety increased by 66.2 % in the wild-type strain ($p<0.001$), and by 29 % in the *skn-1*(zu67) mutant ($p<0.05$), in response to the NIST exposure.

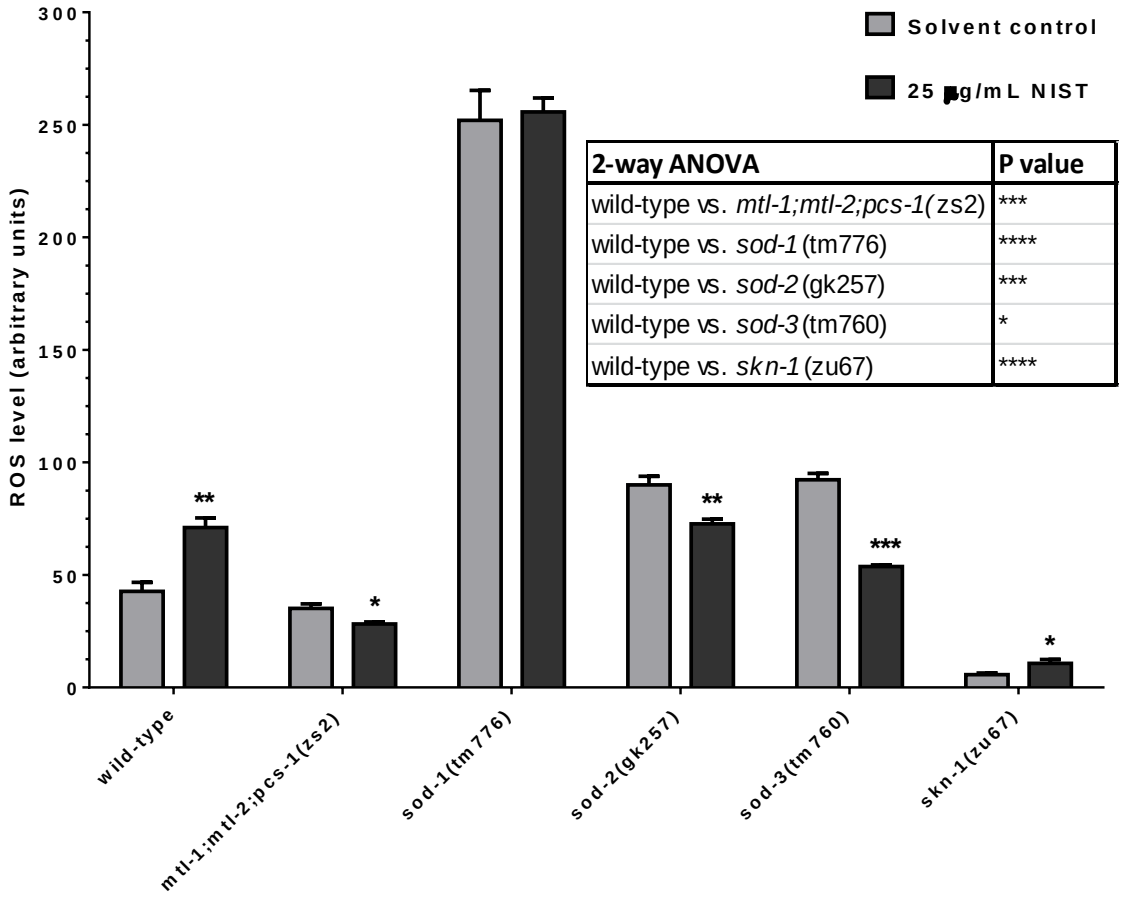

Fig. 5.7: Detection of free radical levels in *C. elegans* exposed to NIST 1648a. Wild-type worms, *mtl-1;mtl-2;pcs-1*(zs2), *sod-1*(tm776), *sod-2*(gk257), *sod-3*(tm760), and *skn-1*(zu67) mutants were exposed to 25 µg/mL NIST. The DCFH-DA assay was used to determine the production of ROS. Fluorescence was measured at excitation 485 nm and emission 528 nm. Technical repeats n=3, biological repeats n=2. Error bars represent mean ± SEM. Statistical analysis was performed using both the Wilcoxon signed rank test and the two-way ANOVA to determine the interaction based on two experimental factors, nematode strain and NIST treatment matched group sets of measurements, followed by Bonferroni multiple comparison test, where *is $p<0.05$, **$p<0.01$, ***$p<0.001$, and ****$p<0.0001$.

Perhaps surprisingly, exposure to 25 µg/mL NIST resulted in a significant 19.9 % decrease of total ROS levels in the metal hypersensitive *mtl-1;mtl-2;pcs-1*(zs2) strain compared to control levels ($p<0.0001$). The total fluorescence intensity of the DCF

moiety was also found to be significantly decreased in *sod-2*(gk257) and *sod-3*(tm760) mutants, by 19.2 % and 43.1 % respectively ($p<0.0001$) (Fig. 5.7). The effects were found to be both nematode strain and exposure significant ($p<0.0001$). No changes in the intracellular pool of ROS were observed in the *sod-1*(tm776) mutants exposed to NIST.

5.3.5 Quantitative assessment (qRT-PCR) of NIST 1648a-responsive gene expression

5.3.5.1 Changes in gene expression in wild-type *C. elegans* exposed to NIST 1648a for 15 hours

A careful evaluation of the relationship between exposure and time response is essential to any toxicological assessment. In order to examine how the exposure time affects the transcriptional activity in a nematode, the wild-type nematodes were subjected to NIST 1648a for 15 hours and their transcript expression levels were quantified and compared to the 48 hours exposure regime. Newly hatched (L1) worms were maintained on large NGM agar tissue culture plates inoculated with 200 µL of OP50 without NIST particles. To avoid starvation, a maximum of 500 worms were maintained on each plate. 15 hours prior to reaching L4 stage, nematodes were washed off the plates and exposed to freshly prepared NGM agar tissue culture plates inoculated with 200 µL of OP50 supplemented with NIST particles. All plates were incubated at 20°C. In parallel, nematode samples exposed to NIST for 48 hours from (L1 stage to L4 stage) were prepared according to a standard exposure protocol (see Chapter: Materials and methods).

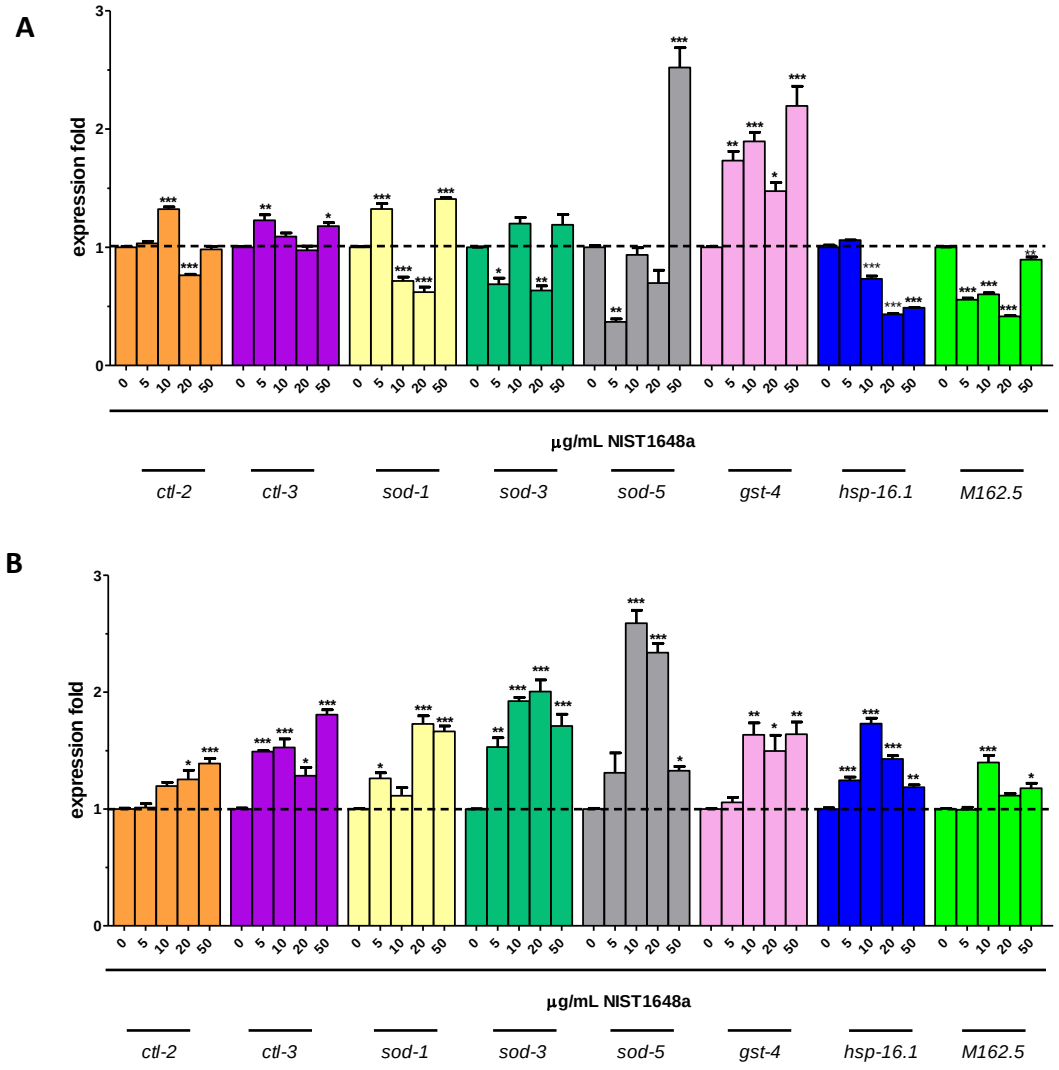

Fig. 5.8: Quantitative assessment of NIST 1648a-responsive gene expression in wild-type strain exposed to NIST for 15 hours (A) vs 48 hours (B). Technical repeats n=3, biological repeats n=1. Error bars represent mean ± SEM. Statistical analysis was performed using the two-tailed Student's t-test comparing untreated and NIST treated group sets of measurements with significance, where *is $p<0.05$, **$p<0.01$, and ***$p<0.001$.

All worms were collected at L4 stage and RNA extracted for subsequent cDNA synthesis. This ensured that all worms were equal age, irrespective of exposure time. The qRT-PCR results revealed that a 15 hours NIST exposure affected to some extent the transcripts tested (Fig. 5.8A). Whilst, *gst-4* was found to be significantly up-regulated by all doses of NIST ($p<0.0001$), *sod-5* was significantly elevated only at 50

µg/mL NIST ($p<0.0001$). In addition, four transcripts (*sod-1*, *sod-3*, *hsp-6.1*, and M162.5) were found to be significantly down-regulated. In contrast, when nematodes were challenged for 48 hours, all examined transcripts (albeit *gst-4*) were found to be more responsive and resulted in higher expression level changes (Fig. 5.8B).

5.3.5.2 The quantitative assessment of NIST 1648a responsive transcripts in wild-type *C. elegans*

A qRT-PCR was performed on a number of genes, which were selected based on their established involvement in oxidative stress and inflammatory pathways, or due to previously identified roles as possible biomarkers of metal and NPs induced toxicity (Stone et al., 2007; Roh et al., 2009; Oberdöster, 2000; Ghio et al., 2012). The following transcripts were examined for their response to NIST 1648a treatment: *ctl-2*, *ctl-3*, *sod-1*, *sod-2*, *sod-3*, *sod-4*, *sod-5*, *gst-4*, *gst-10*, *gsr-1*, *msra-1*, *hsp-16.1*, *hsp-70*, M162.5, FD0D6.11, *cuc-1*, *cnx-1*, *crt-1*, *ftn*-1, aco-*1*, *cep-1*, and *cct-1*. Exposure to NIST 1648a for 48 hours provided a snapshot of the physiological status of the nematode. The qRT-PCR results revealed that in wild-type nematodes the expression of seven transcripts (*ctl-2*, *ctl-3*, *sod-3*, *hsp-16.1*, *cep-1*, and *aco-1*) was significantly induced by NIST exposure (>1.5 - fold; $p<0.0001$), results that were biologically reproducible (for a replicated experiment see Appendix: NIST 1648a).

The *sod-4*, *gst-10*, and F20D6.11 transcripts expression levels were found to be all significantly down-regulated ($p<0.0001$). However, the expression of the *sod-5*, *cep-1*, and *aco-1* transcripts only significantly down-regulated at the highest (50 µg/mL NIST) concentration ($p<0.0001$) (for a replicated experiment see Appendix: NIST 1648a). All other transcripts tested were not significantly different upon NIST exposure (Fig. 5.9 and for a replicate experiment see Appendix: NIST 1648a). Overall, the mRNA

expression levels of many genes examined either failed to respond to NIST in a traditional concentration-dependent manner, or their expression level could not be biologically reproduced.

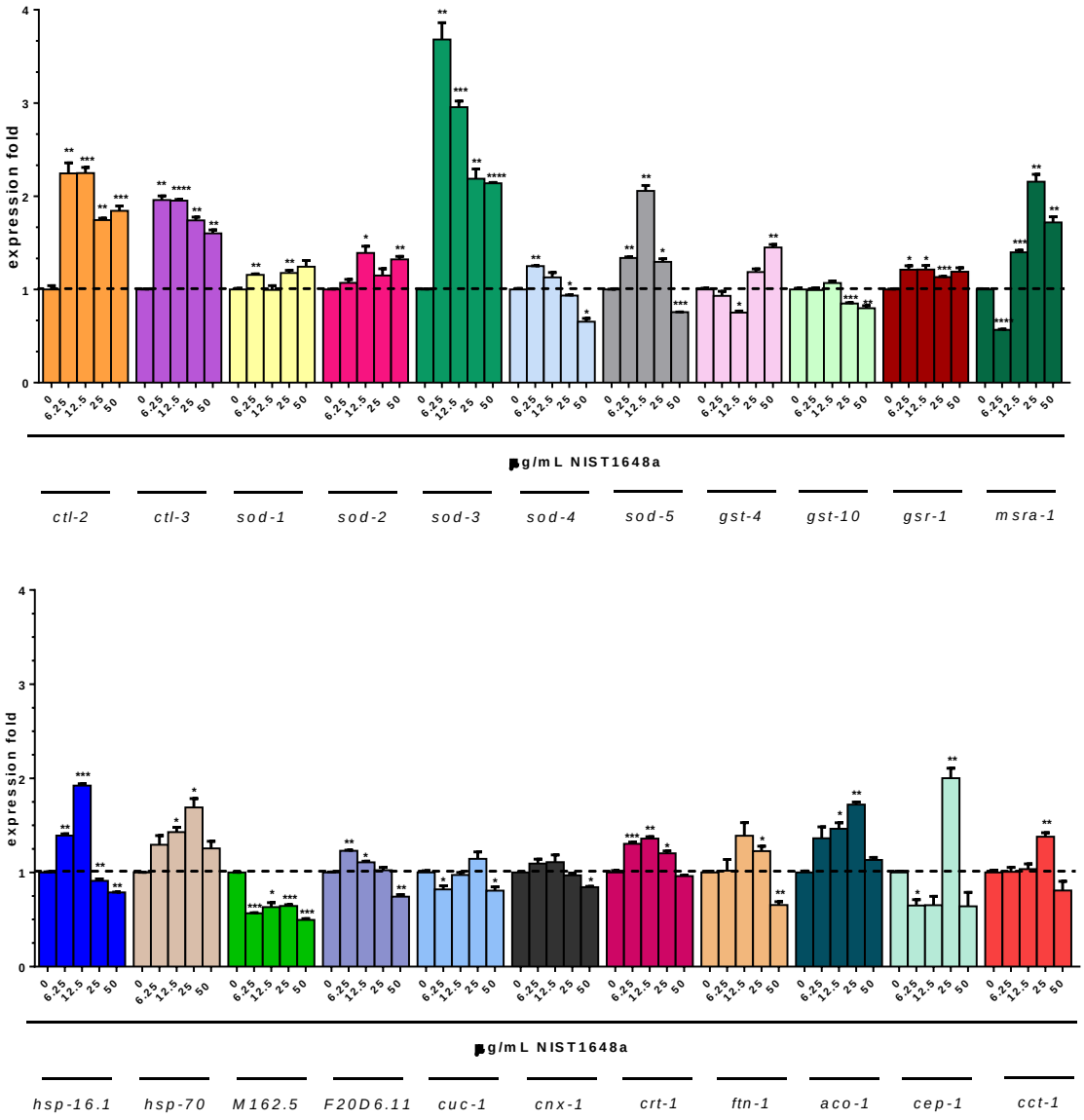

Fig. 5.9: Quantitative assessment of NIST 1648a -responsive gene expression in wild-type strain. Technical repeats n=3, biological repeats n=2. Error bars represent mean ± SEM. Statistical analysis utilized the two-tailed Student's t-test comparing untreated and NIST treated matched group sets of measurements, where * $p<0.05$, ** $p<0.01$, *** $p<0.001$, and ****$p<0.0001$.

5.3.5.3 Quantitative assessment of metallothionein (MT) transcripts following NIST 1648a exposure in wild-type *C. elegans*

The two *C. elegans* metallothioneins (MTs), *mtl-1* and *mtl-2*, are believed to be key players in binding heavy metals and providing protection against metal and ROS toxicosis (Margoshes et al., 1957; Sato et al., 1993; Hughes and Stürzenbaum, 2007). A quantitative approach was chosen to determine whether these metallochelators are transcriptionally activated by NIST 1648a, as their expression was previously reported to be increased in response to fine ambient PM in human alveolar macrophages (Huang et al., 2009).

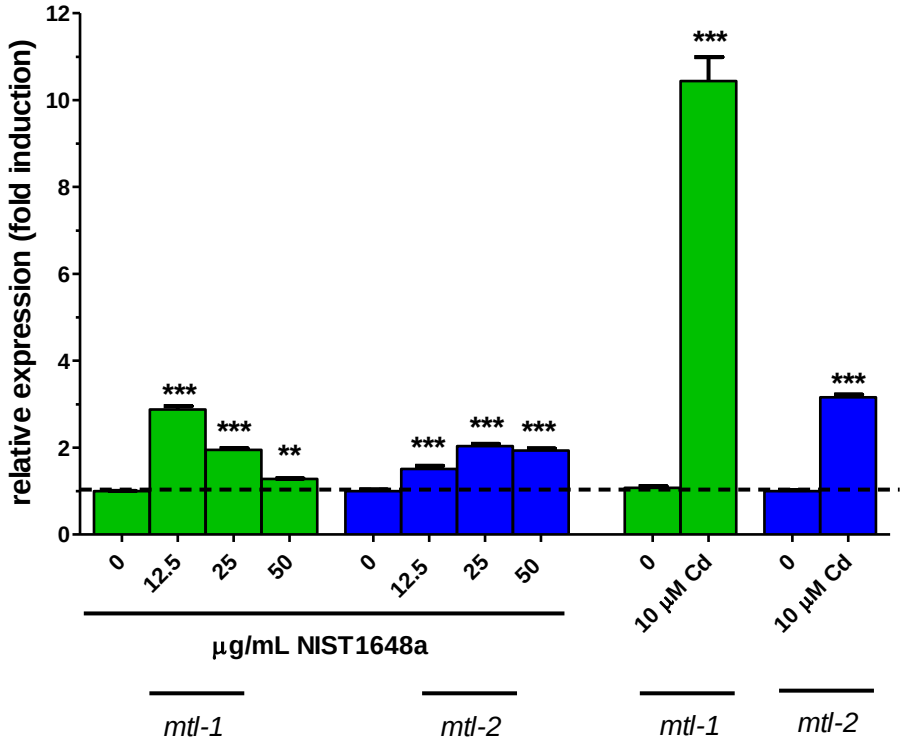

Fig. 5.10: Quantitative assessment of NIST 1648a-responsive MTs gene expression in wild-type strain. 10 µM $CdCl_2$ was utilized as a positive control. Technical repeats n=3, biological repeats n=2). Error bars represent mean ± SEM. Statistical analysis was performed using the one-way ANOVA comparing untreated and NIST treated group sets of measurements with significance, where **is $p<0.01$, and ***$p<0.001$.

Baseline levels of the two MT transcripts (*mtl-1* and *mtl-2*) were measured in the wild-type nematodes chronically exposed (48 hours) to different NIST concentrations. The qRT-PCR indicated that there was a significant up-regulation of *mtl-1* transcript ($p<0.05$) upon NIST treatment, however peaking at 12.5 µg/mL and then gradually reducing at higher doses. In contrast, the *mtl-2* transcript was significantly induced by NIST exposure in a dose dependent manner ($p<0.05$) (Fig. 5.10) (for a replicated experiment see Appendix: NIST 1648a). The 10 µM of $CdCl_2$ was utilized as a positive control for assessing the responsiveness of MT transcripts in the nematode.

5.3.5.4 Effects of metallothionein (*mtl-1*) expression following a joint exposure of wild-type *C. elegans* to Cd and NIST 1648a

Cadmium is a widespread heavy metal in the environment. It is well known that in nematodes excess dietary intake of Cd exposure can result in multiple-biological toxic effects, such as decrease in reproduction, life-span, development, as well as cause changes in transcript levels (Hughes and Stürzenbaum, 2007; Zeitoun-Ghandour et al., 2010). To investigate whether the metalochellator transcript (*mtl-1*) is transcriptionally modulated by a co-exposure to NIST 1648a and $CdCl_2$, two different experimental set-ups were prepared.

In the first, newly hatched (L1) worms were maintained on a large NGM agar tissue culture plate inoculated with 200 µL of OP50 supplemented with/without 12 µg/mL NIST and a concentration range of 0 - 20 µM $CdCl_2$. In parallel, newly hatched (L1) worms were exposed on a large tissue culture plate inoculated with 200 µL of OP50 supplemented with/without 10 µM $CdCl_2$ and a concentration range of 0 – 25 µg/mL NIST. To avoid starvation, a maximum of 500 worms were maintained on each plate. All plates were incubated at 20°C for 48 hours. Once worms reached L4 stage, RNA

was extracted for subsequent qRT-PCR analyses (for standard protocol see Chapter: Materials and methods).

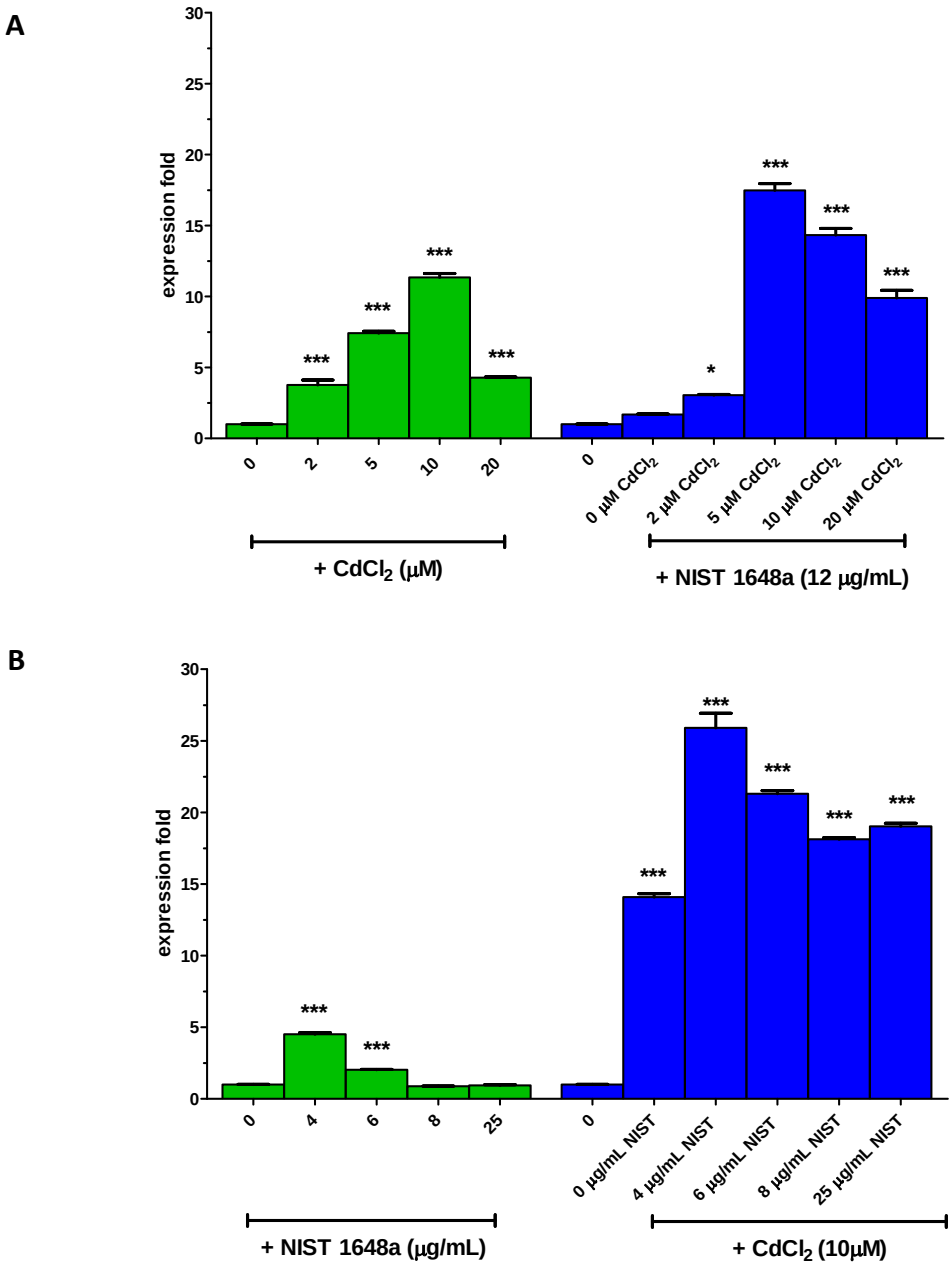

Fig. 5.11: Quantitative assessment of *mtl-1* gene expression in wild-type strain exposed to NIST and cadmium. Technical repeats n=3, biological repeats n=1. Error bars represent mean ± SEM. Statistical analysis was performed using the one-way ANOVA comparing untreated and NIST treated group sets of measurements with significance, *denotes $p<0.05$, **is $p<0.01$, and ***$p<0.001$.

The qRT-PCR results confirm that in wild-type nematodes *mtl-1* transcript expression level increases in a dose-responsive manner upon cadmium exposure, peaking at 10 µM $CdCl_2$ (Fig. 5.11A). Upon co-exposure to 12 µg/mL NIST and a range of 0 - 20 µM $CdCl_2$ doses, the *mtl-1* expression pattern resembles the cadmium response; however the induction level is increased.

As in the second experimental set-up, the *mtl-1* expression in wild-type nematodes results in a significant down-regulation upon NIST exposure (Fig. 5.11B). The co-exposure to a single 10 µM cadmium dose and a range of NIST (0 - 25 µg/mL), the *mtl-1* expression pattern resembles the NIST response; however the level of *mtl-1* response is significantly amplified. The preliminary results suggest that the co-exposure to NIST and Cd exerts an additive effect on the transcriptional level of *mtl-1*.

5.3.5.5 The effects of NIST 1648a exposure on *C. elegans* phytochelatin synthase *pcs-1*(tm1748) and superoxide dismutase *sod-3*(tm760) mutant alleles

The mRNA expression levels of the MT and SOD transcripts were quantified in the phytochelatin synthase knockout mutant *pcs-1*(tm1784) nematode. As in the wild-type, the *mtl-1* transcript was found to be induced by 12.5 µg/mL NIST 1648a, however its expression remained at basal level with the other NIST concentrations (Fig. 5.12A). Expression of the *mtl-2* transcript was in contrast, significantly down-regulated in NIST exposed worms. The *sod-2* transcript expression was significantly elevated at all NIST doses (Fig. 5.12A).

In order to examine how NIST effects the expression of antioxidant enzymes in worms lacking a key mitochondrial superoxide dismutase enzyme (MnSOD), transcription was evaluated in *sod-3*(tm760) mutants exposed for 48 hours to NIST. The major ROS scavenging enzymes, catalases (*ctl-2*, and *ctl-3*), and cytoplasmic superoxide dismutase

(*sod-1*) were measured. In addition, the transcriptional change of a second MnSOD isoform (*sod-2*) was examined.

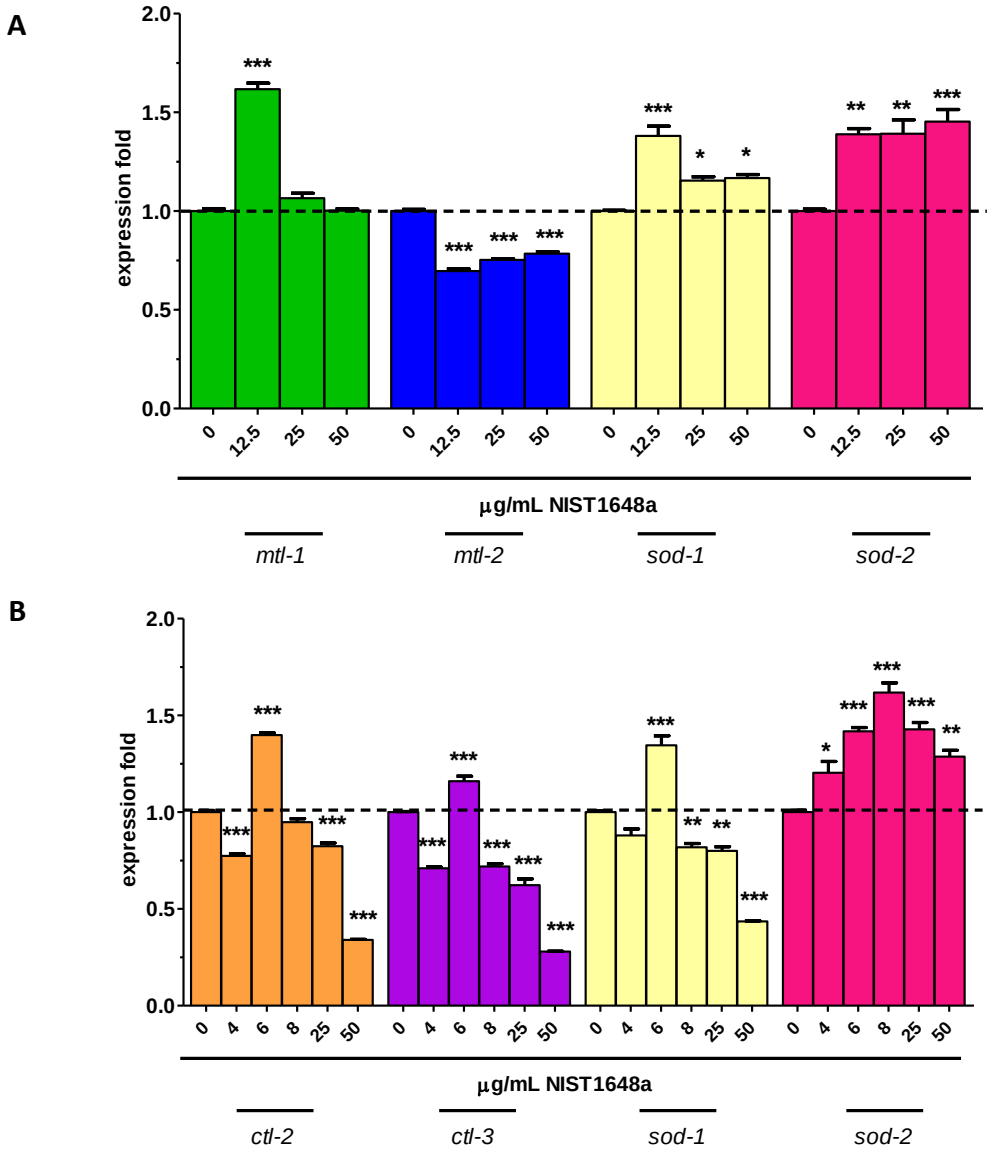

Fig. 5.12: (A) Quantitative assessment of MT and SOD gene expression in the *pcs-1*(tm1748) strain exposed to NIST 1648a. (B) Quantitative assessment of antioxidant enzymes gene expression in the *sod-3*(tm760) strain exposed to NIST 1648a. Technical repeats n=3, biological repeats n=1. Error bars represent mean ± SEM. Statistical analysis was performed using the one-way ANOVA comparing untreated and NIST treated group sets of measurements with significance, *denotes $p<0.05$, **is $p<0.01$, and ***$p<0.001$.

Whilst in wild-type NIST exposure-induced catalase expression, both *ctl-2* and *ctl-3* transcripts were found to be significantly down-regulated in the *sod-3*(tm760) mutant (Fig. 5.12B). The *sod-1* expression was also significantly decreased upon NIST treatment, whereas *sod-2* transcript resembled the wild-type response (Fig. 5.9).

5.3.5.6 Changes in gene expression in wild-type *C. elegans* exposed to modified NIST 1648a extracts

C. elagans were exposed to a concentration range of NIST 1648a extracts, modified by an additional filtration procedure to eliminate particulates/residuals greater than 20 nm in size.

The NIST extract was prepared according to the following procedure. The 500 µg/mL NIST 1648a stock suspension in 5 % methanol was first vortexed for 1 hour at room temperature, followed by a 1 hour centrifugation at 13,000 g. The supernatant was then filtered through a Whatman 0.02 µm nitrocellulose filer, using a 1 mL syringe, into a sterile cryogenic vial. Both, the NIST residual and filtered supernatant (or NIST extract) were frozen immediately at -20°C until further use or analysed by ICP-MS (Appendix: NIST 1648a).

The mRNA expression levels of the MT and SOD transcripts was quantified in the wild-type nematodes exposed to the NIST extract for 48 hours from L1 to L4 stage (for standard protocol see Chapter: Materials and methods). The expression of both MTs (*mtl-1*, and *mtl-2*), as well as *sod-1* transcripts, were found to be significantly down-regulated in nematodes exposed to the modified NIST extract (Fig. 5.13). The expression of *sod-3* remained unchanged.

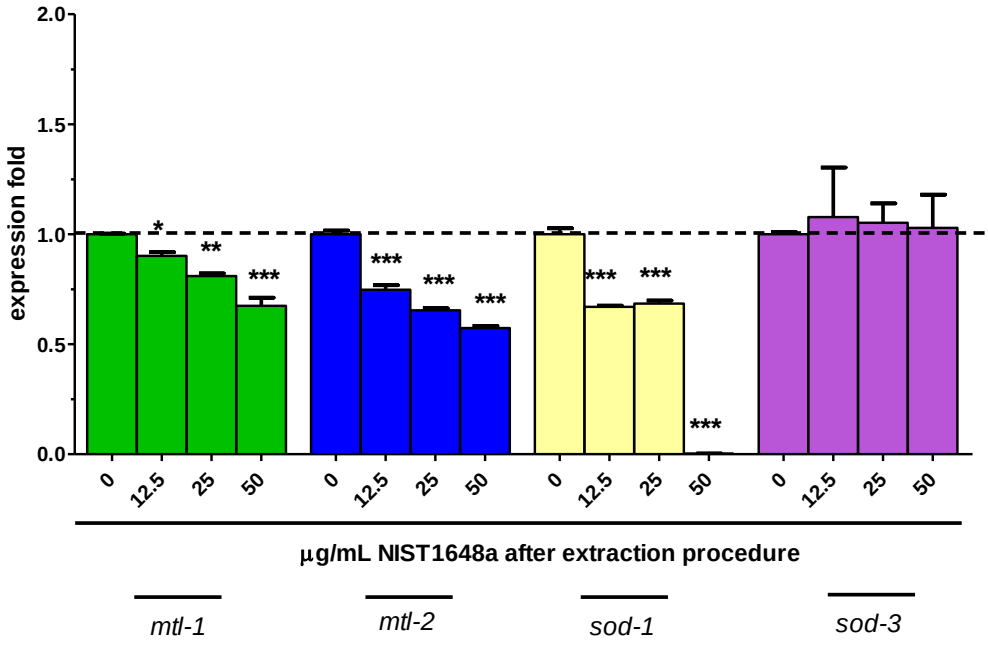

Fig. 5.13: Expression changes of *mtl-1*, *mtl-2*, *sod-1*, and *sod-3* transcripts in wild-type nematodes exposed to NIST 1648a extracts filtered to exclude particles >20nm in size. Technical repeats n=3, biological repeats n=1. Error bars represent mean ± SEM. Statistical analysis was performed using the one-way ANOVA comparing untreated and NIST treated group sets of measurements with significance, *denotes $p<0.05$, **is $p<0.01$, and ***$p<0.001$.

5.3.6 Wild-type *C. elegans* exposed to NIST 1648a: whole genome analysis

5.3.6.1 Biological pathways and gene ontology (GO) categories identified from microarray analysis

A whole genome-wide DNA microarray experiment was performed to pinpoint the key molecular genetic pathways involved in NIST 1648a toxicosis in a nematode. In total, five NIST concentrations (1, 5, 10, 20 and 50 µg/mL) were tested on wild-type *C. elegans* exposed for 48 hours.

Using the robust multivariate average (RMA) algorithm (Irizarry et al., 2003), the data intensities were log transformed and normalized within and between arrays with a quantile method (for details see Chapter: Materials and methods). Significantly up- and down- regulated differentially expressed genes (DEGs) were identified (Table 5.2). The principle component analysis (PCA) plot based on the top 32 genes whose expression was most significantly changed upon treatment with NIST was performed using Qlucore Omics Explorer (Qlucore AB, Lund, Sweden) to separate DEGs into the following three group types: a response at 1 and 5 µg/mL NIST; DEG's at 10 µg/mL NIST; and DEG's at 20 and 50 µg/mL NIST (Fig. 5.15A).

Of all 22627 *C. elegans* expression profiles, the maximum induction was identified as 3.2 - fold (*anc-1* / abnormal nuclear anchorage: in the 1 µg/mL NIST exposure sample) and the maximum repression was 0.018 - fold (*rrn-3.1* / large 26S subunit ribosomal RNA gene: in the 50 µg/mL NIST exposure sample). The majority of DEGs displayed a non-dose responsive change in their expression upon NIST exposure. Therefore, for further analysis, the expression data was divided into two categories: transcripts induced (>1.5 - fold) or repressed (<0.7 - fold) in all NIST doses (Table 5.2). Once the transcripts were sorted, Venn diagrams were utilized to identify common elements overlapping sets of data based on the selection criteria given (note: Venn diagrams are not shown) and gene ontology (GO) analysis. A total of 69 DEGs met the selection criteria, with the majority of genes (45) being down-regulated (<0.7 - fold) (Fig. 5.15B). Only 24 transcripts, were found to be up-regulated more than >1.5 - fold at all NIST concentrations.

Table 5.2: Number of transcripts characterized (after RMA analysis), as either up-or down- regulated at each NIST dose.

data set (µg/mL concentration)	no. of genes up- regulated (>1.5 fold)	no. of genes down-regulated (<0.7 fold)	no. of genes up-regulated (>2.0 fold)	no. of genes down-regulated (<0.5 fold)
1 NIST	630	880	74	51
5 NIST	556	1071	50	26
10 NIST	304	587	38	21
20 NIST	495	1342	20	212
50 NIST	443	1150	26	176

All transcripts up-regulated >1.5 - fold at every NIST concentration (1 - 50 µg/mL) were first searched for common elements. The analysis identified 24 common overlapping elements, which were entered to the Database for Annotation, Visualization and Integrated Discovery (DAVID) bioinformatics database for functional annotation.

Focusing on the 24 up-regulated genes, 14 significant biological processes (BP), and 3 cellular components (CC) gene ontology (GO) terms were identified. Many GO categories were represented by the same genes. To avoid redundancy, the Functional Annotation Clustering tool was used in DAVID, which groups similar annotations together (Huang et al., 2009). Therefore, the more common the gene annotation (according to kappa values; Kappa statistics), the higher the chance that those genes will be grouped together (based on heuristic clustering). Choosing the highest classification stringency and ″GOTERM_BP_ALL″, ″GOTERM_CC_ALL″, and ″GOTERM_MF_ALL″, the list was clustered into four BP GO, and one CC GOs functional clusters (Table 5.3).

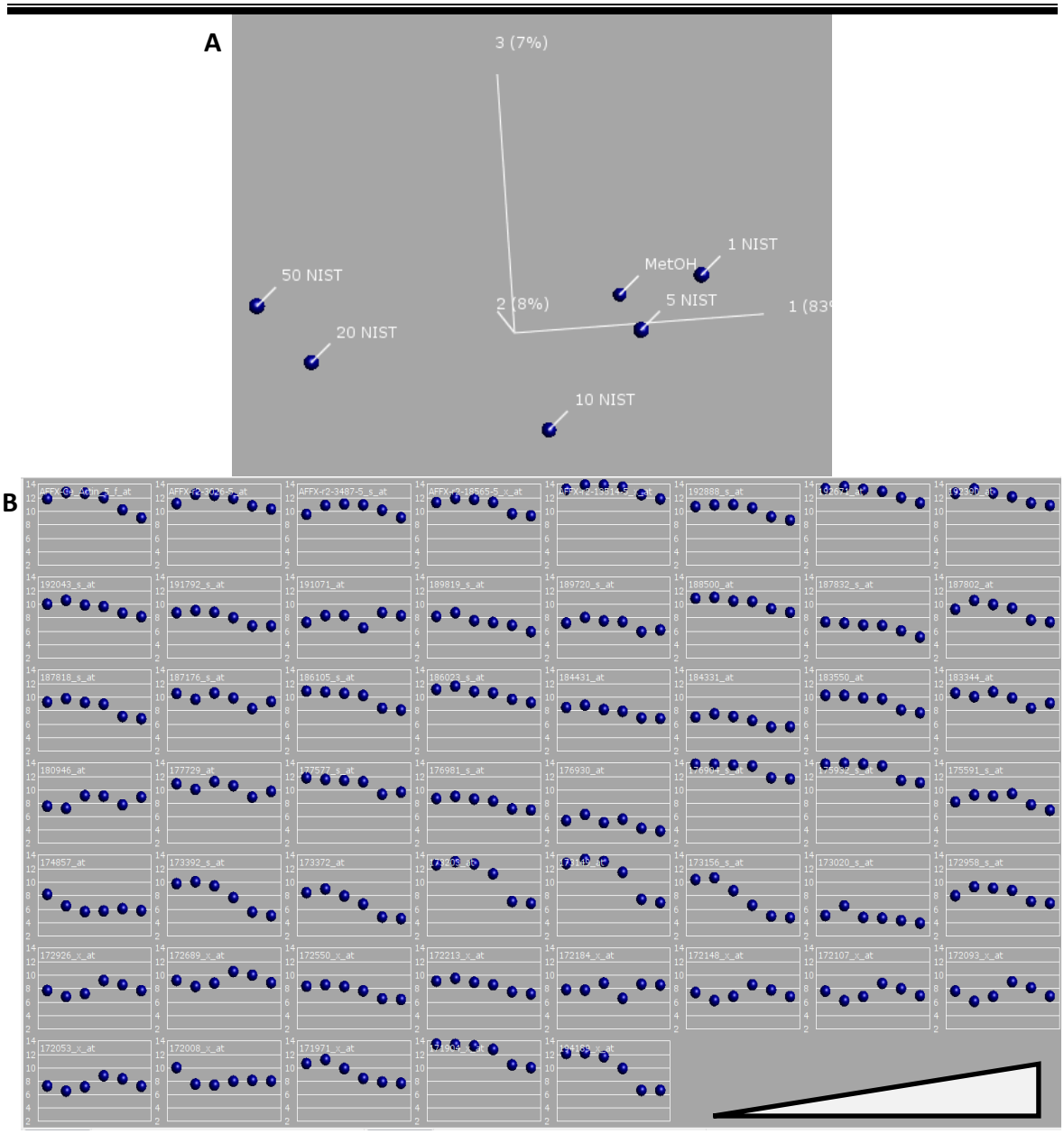

Fig. 5.15: Qlucore expression profiling – PCA plot capturing the expression profile of top 32 genes (A) and scatter plots (B) of the most responsive transcripts following NIST 1648a exposure. Majority of genes whose expression significantly changed were down-regulated following NIST exposure (0, 1, 5, 10, 20, and 50 µg/ml NIST). Data analyzed with Qlucore Omics Explorer (Qlucore AB, Lund, Sweden).

Table 5.3: Functional annotation clustering by DAVID of the top biological processes (BP) and cellular components (CC) terms for 24 up-regulated genes by minimum 1.5 - fold following RMA analysis (at every NIST 1648a concentration (1 - 50 µg/mL)). The Enrichment Score (EASE score on each term members) was used to predict whether representation of a gene group among selected genes was biologically significant. The Count represents number of genes that fall into each category. The P-values correspond to the probability that the members of the cluster are present together randomly in the gene list (Fisher Exact P-Value = 0, represents the perfect enrichment). Strongly enriched in the annotation categories, $p<0.05$.

Category	GO Term	Count	P_Value	Enrichment Score
Biological Process	multicellular organismal development	10	1.6E-1	0.68
	nematode larval development	6	2.1E-1	0.67
	positive regulation of growth rate	5	4.0E-1	0.33
	organ development	3	5.4E-1	0.22
Cellular components	integral to membrane	7	8.2E-1	0.08
	intrinsic to membrane	7	8.2E-1	0.08

The BP GO categories contained, multicellular organismal development (GO:0007275), nematode larval development (GO:0002119; GO:0002164), post-embryonic development (GO:0009791), positive regulation of growth rate (GO:0040010), and regulation of growth rate (GO:0040009), organ development (GO:0048513), anatomical structure development (GO:0048856). Within CC GO functional annotation cluster, categories of integral to membrane (GO:0016021), and intrinsic to membrane (GO:0031224) were identified (Table 5.3 and 5.4).The annotation summary of the results also identified five genes to be involved in functional Kyoto Encyclopaedia of Genes and Genomes (KEGG) and PANTHER pathways. Namely, pathways involved in oxidative phosphorylation (F59C6.5), and fatty acid biosynthesis (*fasn-1* / fatty acid synthase) identified by KEGG, and P00052:TGF-beta signalling pathway (*daf-14* / abnormal dauer formation), and P00036:Interleukin signalling pathway (*ets-4* / ETS

class transcription factor) within PANTHER pathways. One gene (Y54G2A.17) was ascribed an Enzyme Commission (EC) number 2.4.2.11, namely a Nicotinate phosphoribosyltransferase enzyme.

Table 5.4: Summary of ambiguous gene IDs. List of 24 genes that are significantly up-regulated by >1.5 - fold across all NIST 1648a concentrations (1 - 50 µg/mL) ($p<0.05$).

From	Gene symbol	David Gene Name	Chromoso-me location	Best BLASTP matches (%) to mamma-lian sequence	Human homologue/ortholog (ENSEMBL accession number)
182900_at	***acl-14***	ACyLtransferase-like	V	75.5%	Acyl-CoA:lysophosphatidylglycerol acyltransferase 1 **ENSP00000355963**
185885_at	***C15B12.6***	C15B12.6	X		
187500_at	***C53C9.2***	Uncharacterized protein C53C9.2	X	25.7%	Similar to Huntingtin-associated protein 1 isoform 4 **HIT000047870**
193666_at	***cap-2***	CAP-z protein	II	99.3%	Isoform 1 of F-actin-capping protein subunit beta **ENSP00000264202**
188360_at	***clu-1***	yeast CLU (mitochondrial clustering) related	III	89.7%	Protein KIAA0664 **ENSP00000388872**
187315_s_at	***cpna-2***	Temporarily Assigned Gene name	II	2.7%	Isoform 1 of Copine-4 **ENSP00000411904**
185375_at	***D1007.10***	D1007.10	I		
190867_s_at	***daf-14***	abnormal DAuer Formation	IV	81.9%	Isoform Short of Mothers against decapentaplegic homolog 2 **ENSP00000349282**
174744_s_at	***dnj-16***	DNaJ domain (prokaryotic heat shock protein)	III	21.5%	25 kDa protein **ENSP00000445536**
180919_s_at	***dnj-19***	DNaJ domain (prokaryotic heat shock protein)	V	97.7%	DnaJ homolog subfamily A member 2 **ENSP00000314030**
192249_at	***ets-4***	ETS class transcription factor	X	42.3%	cDNA FLJ59217, highly similar to SAM pointed domain-containing Ets transcription factor **ENSP00000442715**
191934_at	***F59C6.5***	F59C6.5	I	55.0%	NADH dehydrogenase [ubiquinone] 1 beta subcomplex subunit 10 **ENSP00000268668**
189768_at	***fasn-1***	Fatty Acid SyNthase	I	95.9%	Fatty acid synthase **ENSP00000304592**
177684_s_at	***icln-1***	ICLn ion channel homolog	IV	82.2%	Uncharacterized protein **ENSP00000433741**
182858_at	***lgc-54***	T15B7.1	V	84.4%	Gamma-aminobutyric acid receptor subunit rho-2 **ENSP00000386029**

177084_at	***M79.2***	M79.2	X	64.9%	Glycerol-3-phosphate acyltransferase 3 **ENSP00000264409**
185109_at	***nlp-16***	Neuropeptide-Like Protein	IV	51.8%	Sarcoplasmic reticulum histidine-rich calcium-binding protein **ENSP00000252825**
193008_at	***nrfl-1***	Temporarily Assigned Gene name	IV	28.5%	Na(+)/H(+) exchange regulatory cofactor NHE-RF2 isoform b **ENSP00000402857**
182610_at	***srh-171***	Serpentine Receptor, class H	V		
184913_s_at	***T22F3.11***	T22F3.11	V	83.7%	Solute carrier family 17 (Anion/sugar transporter), member 5, isoform CRA_a **ENSP00000348019**
176349_s_at	***T24E12.5***	T24E12.5	II		
188661_s_at	***tni-1***	TropoNin I	X	69.6%	Troponin I, fast skeletal muscle **ENSP00000252898**
177009_at	***Y54G2A.17***	Nicotinate phosphoribosyltransferase	IV	94.1%	Isoform 1 of Nicotinate phosphoribosyltransferase **ENSP00000401508**
172682_x_at	***ZC155.4***	ZC155.4	III	66.1%	Glycerophosphodiester phosphodiesterase 1 **ENSP00000261386**
>1.5		**>2**		**>3**	

Table 5.5: Functional annotation clustering by DAVID of the top gene ontology (GO) terms for 45 down-regulated genes identified in *C. elegans* exposed to 0 - 50 µg/mL of NIST 1648a. (Fisher Exact P-Value = 0, represents the perfect enrichment). Strongly enriched in the annotation categories, $p<0.05$.

Category	GO Term	Count	P_Value	Enrichment Score
Molecular Function	nucleoside-triphosphatase activity	3	2.6E-1	0.56
	purine ribonucleotide binding	5	3.1E-1	0.49
	ATP binding	4	4.3E-1	0.34
Cellular Compartment	integral to membrane	14	4.7E-1	0.29
Molecular Function	metal ion binding	6	5.4E-1	0.25
Biological Process	organ development	3	7.6E-1	0.08
	nematode larval development	4	8.9E-1	0.05
	transport	3	8.8E-1	0.04
	positive regulation of growth rate	3	9.7E-1	0.01

Venn diagrams were also compiled to identify transcripts that fell into the category of <0.7 - fold down-regulation in all NIST exposures. A total of 45 transcripts were submitted to DAVID for functional annotation; and 41 were successfully identified (genes see listed in Appendix: NIST 1648a). The functional annotation clustering tool, at highest classification constringency, classified them into 9 clusters: 14 significant biological processes (BP), 3 cellular component (CC), and 15 molecular function (MF) gene ontology (GO) terms. The GO categories for biological processes were anatomical structure development (GO:0048856), nematode larval development (GO:0002119), transport (GO:0006810), localization (GO:0051179), regulation of growth rate (GO:0040009). Among molecular function pathways, GO terms of nucleoside-triphosphatase- (GO:0017111), hydrolase- (GO:0016818), and pyrophosphatase- (GO:0016462) activity; purine ribonucleotide binding (GO:0032555); ATP binding (GO:0005524); nucleoside binding (GO:0001882); and metal ion binding (GO:0046872), were identified. Finally, the cellular component GO terms of integral to membrane (GO:0016021) and intrinsic to membrane (GO:0031224) were also present (Table 5.5).

The annotation summary of the results identified five genes to be involved in functional KEGG and PANTHER pathways. Namely, glyoxylate and dicarboxylate metabolism (F41E6.5); histidine, tyrosine, phenylalanine, and tryptophan metabolism (*tdc-1*/ tyrosine decarboxylase); and endocytosis (*vps-20* / related to yeast vacuolar protein sorting factor), were linked to KEGG pathways. The P00049: Parkinson disease, P00057: Wnt signalling pathway (C09B9.4); and P05914: Nicotine degradation (*ugt-28* / UDP-glucuronosyl transferase), were identified within PANTHER pathways. Two genes were ascribed an Enzyme Commission (EC) number. The cyclophylin (*cyn-7*) transcripts were assigned an EC number 5.2.1.8, a peptidylprolyl isomerase enzyme

(*cyn-7*); and an EC number 3.4.24, for peptide hydrolases; metalloendopeptidases was appointed to C02G6.1.

At least 15 DEGs were significantly up-regulated by more than 2.0 - fold at NIST concentration (1 and 5 µg/mL). Grouping by GO terms revealed that genes were linked to 5 significant biological processes (BP), 2 molecular function (MF), and one cellular component gene ontology (GO) terms (Table 5.6). The most enriched were genes involved in nematode biological processes of development. Among molecular function pathways, GO terms of nucleoside-triphosphatase- (GO:0017111), and nucleoside binding (GO:0001882).

Table 5.6: Functional annotation clustering by DAVID of the 15 genes up-regulated in the 1 and 5 µg/mL NIST 1648a dose by more than (>2.0 - fold). (Fisher Exact P-Value = 0, represents the perfect enrichment). Strongly enriched in the annotation categories, $p<0.05$.

Category	GO Term	Count	P_Value	Enrichment Score
15 common genes up-regulated with 1 and 5 µg/mL NIST dose more than >2.0 fold				
Biological Process	nematode larval development	7	1.3E-3	2.48
	regulation of growth rate	6	1.0E-2	1.84
	multicellular organismal development	8	9.9E-3	1.84
	hermaphrodite genitalia development	4	2.1E-2	1.48
	protein transport	3	2.0E-2	1.28
Molecular Function	nucleoside-triphosphatase activity	3	8.5E-2	0.73
	nucleotide-binding	3	1.0E-1	0.73
Cellular Compartment	nucleus	3	2.2E-1	0.43
	intrinsic to membrane	6	6.1E-1	0.19

Finally, the cellular component GO terms of intrinsic to membrane (GO:0031224) and nucleus (GO:0005634) were also identified (Table 5.6). Five genes were found to be associated with KEGG pathways: MAPK signalling pathway and Natural killer cell mediated cytotoxicity (*cdc-42* / cell division cycle related, and *let-60* / lethal); glycolysis /glucogenesis (*enol-1* / enolase), spliceosome (*hel-1* / helicase), and lysosome (F13D12.6 / uncharacterized serine carboxypeptidase). Only 4 DEGs were significantly

up-regulated more than 2.0 - fold by 20 and 50 µg/mL NIST, namely a nicotinate phosphoribosyltransferase (Y54G2A.17), and 3 non-annotated (*cpna-2* / CoPiNe domain protein, ZK353.9, ZC155.4) transcripts.

Table 5.7: Functional annotation clustering by DAVID of the 104 genes down-regulated (<0.5 - fold) at the highest two concentrations (20 and 50 µg/mL) of NIST 1648a. The Enrichment Score (EASE score on each term members) was used to predict whether representation of a gene group among selected genes was biologically significant. The Count represents number of genes that fall into category. The P-values correspond to the probability that the members of the cluster are present together randomly in the gene list (Fisher Exact P-Value = 0, represents the perfect enrichment). Strongly enriched in the annotation categories, $p<0.05$.

Category	GO Term	Count	P_Value	Enrichment Score
104 common genes down-regulated with 20 and 50 µg/mL NIST dose <0.5-fold				
Biological Process	nematode larval development	21	2.0E-3	2.68
	multicellular organismal development	34	8.5E-4	2.61
	hermaphrodite genitalia development	12	2.2E-3	2.11
	regulation of apoptosis	3	1.3E-2	1.64
	positive regulation of growth rate	17	4.1E-2	1.27
	oogenesis	4	2.4E-2	1.25
	intracellular protein transport	4	6.0E-2	1.13
	protein transport	5	6.0E-2	1.01
	negative regulation of multicellular organismal process	3	1.1E-1	0.97
	morphogenesis of an epithelium	5	1.4E-1	0.79
	aging	4	1.8E-1	0.75
	regulation of nucleobase, nucleoside, nucleotide and nucleic acid metabolic process	7	3.9E-1	0.36
	molting cycle, collagen and cuticulin-based cuticle	3	4.4E-1	035
	reproductive behavior	3	5.3E-1	0.28
	transport	9	4.9E-1	0.24
	regulation of transcription	6	5.5E-1	0.22
Molecular Function	nucleoside-triphosphatase activity	3	5.9E-1	0.21
	adenyl nucleotide binding	6	5.8E-1	0.21
	nucleotide-binding	5	4.9E-1	0.15
	ATP binding	5	7.1E-1	0.15
	ribonucleotide binding	5	8.3E-1	0.15
	metal ion binding	9	7.7E-1	0.1
Cellular Compartment	ribosome	3	1.8E-1	0.85

There were 4 common DEGs in the data derived from the 1 and 5 µg/mL NIST exposures to be down-regulated by < 0.5 - fold (namely, *tag-234* / temporarily assigned gene name, and T04G9.7), and 104 DEGs down-regulated by 20 and 50 µg/mL NIST. Grouping by GO terms revealed that these genes were involved in 16 significant biological processes (BP), and 6 molecular function (MF) and one cellular component (CC) namely, ribosome, gene ontology (GO) terms (Table 5.7). Interestingly, the genes with the highest enrichment score were involved in the biological processes of development, apoptosis, reproduction, and regulation of transcription. Molecular functions that were down-regulated were also involved in nucleotide, ATP and metal ion binding. Seventeen genes were found to be involved in KEGG pathways, such as: fatty acid metabolism (*acdh-7* / acyl CoA dehydrogenase), calcium signalling pathway (*cmd-1* / calmodulin), RNA degradation (*cgh-1* / conserved germline helicase), oxidative phosphorylation (*nuo-5* / NADH ubiquinone oxidoreductase), inositol phosphate metabolism (*pisy-1* / phosphatidyl inositol synthase), proteasome (*pbs-1* / proteasome beta subunit), spliceosome (C43H8.1, *sap-49* / spliceosome associated protein), ribosomes (*rpa-0*, *rpl-18*, Y73B3A.18; *rpl-7A*), and endocytosis (*vps-20* / related to yeast vacuolar protein sorting factor).

5.3.6.2 Changes in expression of large 26S subunit ribosomal RNA transcript in wild-type *C. elegans* exposed to NIST 1648a

In *C. elegans* there are approximately 1300 genes that produce noncoding RNA (ncRNA) genes that function at the RNA level. The ncRNA transcripts include: 275 ribosomal RNA (rRNA) genes, 590 transfer RNA (tRNA) genes, 120 microRNA (miRNA) genes, 140 trans-spliced leader RNA genes, 70 spliceosomal RNA genes, and

30 small nucleoar RNA (snoRNA) genes (Wormatlas). The function of most ncRNAs largely remains unknown, however the 18S, 5.8S, and 26S subunits of rRNA are known to be transcribed in worms by RNA polymerase I, which is located at the end of chromosome I.

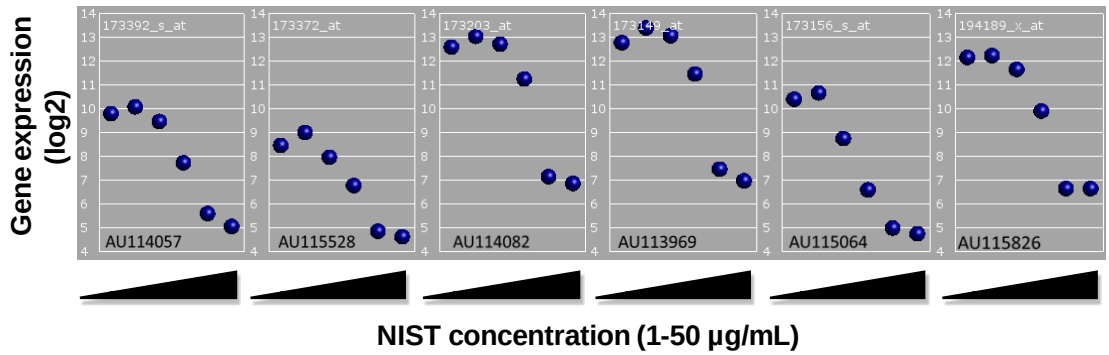

Fig. 5.16: Gene expression (log 2 scale) changes of the top 6 transcripts out of 22625 genes from the microarray, whose expression was significantly down-regulated upon NIST 1648a exposure. Each scatter plot represents the transcript expression of the target from nematodes exposed to a range of NIST doses (0, 1, 5, 10, 20, and 50 µg/mL). Data analysed with Qlucore Omics Explorer (Qlucore AB, Lund, Sweden).

	Representative Public ID	blastn sequence alignment (NCBI)	WormBase ID
173149_at	AU113969	*C. elegans* tandem repeat with genes for 18S, 5.8S and 26S rRNA	F31C3.9 WBGene00004622
173203_at	AU114082	*C. elegans* tandem repeat with genes for 18S, 5.8S and 26S rRNA	F31C3.9 WBGene00004622
194189_x_at	AU115826	*C. elegans* tandem repeat with genes for 18S, 5.8S and 26S rRNA	F31C3.9 WBGene00004622
173156_s_at	AU115064	*C. elegans* tandem repeat with genes for 18S, 5.8S and 26S rRNA	F31C3.9 WBGene00004622
173392_s_at	AU114057	*C. elegans* tandem repeat with genes for 18S, 5.8S and 26S rRNA	F31C3.9 WBGene00004622
173372_at	AU115528	*C. elegans* tandem repeat with genes for 18S, 5.8S and 26S rRNA	F31C3.9 WBGene00004622

Fig. 5.17: Annotation ID of the top 6 genes of 22625 genes whose expression significantly changed due to NIST 1648a exposure, by NCBI (blastn) and WormBase.

Six un-assigned probes out of 22625 were identified whose expression was most significantly changed by NIST exposure, following RMA analysis of microarray data. Interestingly, all six probes exhibited a similar dose-responsive down-regulation upon NIST 1648a exposure (Fig. 5.16). The probe set IDs were 173149_at; 173203_at; 194189_x_at; 173156_s_at; 173392_s_at; 173372_at, which were submitted to the NetAffx™ Analysis Center for transcript assignment and annotation. The probe set IDs were all identified to correspond to the *C. elegans* 26S ribosomal RNA (rRNA) gene *rrn-3.1*, or ensemble gene F31C3.9 (Fig. 5.17). In addition, all transcripts, bar probe 173372_at, were given an annotation grade A, which suggests that the probes match the transcript perfectly. The *rrn-3.1* gene sequence (3509 nucleotides in length) was derived from WormBase, and sequence alignments with the microarray probe sequences were performed (Fig. 5.18).

To validate the transcript expression in response to NIST, a set of primers was designed (for sequence details see table Primers and Probes in Appendix: Materials and methods) that covered the 173149_at target sequence (61 nt amplicon) and a qPCR was performed (Fig. 5.19). The quantitative assessment by qRT-PCR confirmed the significant dose-responsive down-regulation of the *rrn-3.1* gene on NIST exposure. The results were confirmed by cDNA generated from RNA that was utilized for microarrays, as well as by the RNA extracted from two biologically independent NIST exposure repeats (Fig. 5.19).

Fig. 5.18: The *rrn-3.1* transcript expression in wild-type strain, following NIST 1648a exposure. The *rrn-3.1* gene sequence (3509 nucleotides in length) derived from WormBase, and correspondent sequence alignments with all six microarray probe sequences. The primers were designed to span the transcript covered by probe 173149_at (red font colour and underline)**.**

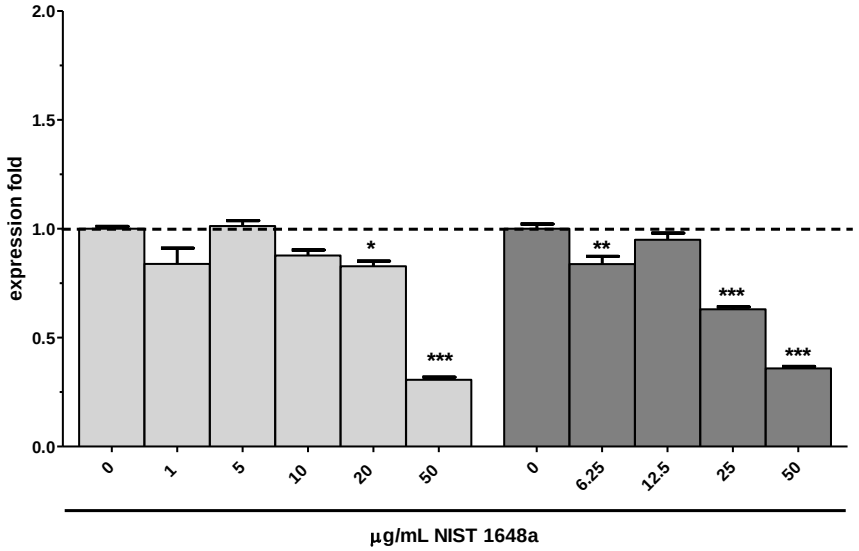

Fig. 5.19: Quantitative assessment of NIST 1648a-responsive *rrn-3.1* gene expression in wild-type strain. The qPCR performed on cDNA generated from RNA that was utilized for microarrays (light grey), and from RNA extracted from a biologically independent NIST exposure repeat (dark grey). Technical repeats n=3, biological repeats n=3. Error bars represent mean ± SEM. Statistical analysis was performed using the one-way ANOVA comparing untreated and NIST treated group sets of measurements with significance, *denotes $p<0.05$, **is $p<0.01$, and ***$p<0.001$.

5.3.6.3 Microarray validation by qRT-PCR

To validate the quality of the microarray data, a qRT-PCR was performed to compare the expression profiles of selected transcripts from microarray platform with RNA samples that were utilized for microarray processing, and RNA generated from two independently derived replicate samples.

24 genes, identified as differentially expressed were subjected for microarray validation by qRT-PCR (Table 5.8). The transcripts were selected to represent various deregulated pathways, such as being involved in stress response pathways (e.g. sod family; *cat-2*,

cat-3, *gsr-1*, GSTs, and *hsp-16.1*), transition metal binding (e.g. *mtl-1*, *mtl-2*, *ftn-1*, and *cuc-1*), calcium channel activity (e.g. *unc-68*), development (e.g. *cnx-1*, and *clec-13*), metabolic processes (e.g. *gei-7*, and *aco-1*), apoptosis (*cep-1*), and transcriptional regulation (e.g. *rrn-3.1*, *skn-1*, and *sdz-24*). The ones managed to be successfully analysed, were compared with their expression profile from microarray data.

Table 5.8: An overview of the transcript microarray validation by qRT-PCR. A successful conformation is indicated by tick; the tick is placed in brackets where the transcript profile was confirmed in at least 3 NIST 1648a doses; an un-successful validation is annotated as X.

Gene ID	qPCR performed utilizing microarray RNA samples (1)	qPCR performed utilizing independently derived RNA samples (2)	qPCR performed utilizing independently derived RNA samples (3)
ctl-2	X	X	X
ctl-3	X	X	X
sod-1	(√)	(√)	(√)
sod-2	not tested	√	√
sod-3	√	√	√
sod-4	not tested	(√)	(√)
sod-5	X	X	X
gst-4	√	(√)	(√)
gst-10	not tested	(√)	(√)
gsr-1	not tested	√	√
hsp-16.1	√	(√)	√
cuc-1	not tested	(√)	(√)
cnx-1	not tested	(√)	(√)
ftn-1	not tested	X	X
aco-1	not tested	√	√
cep-1	not tested	√	√
skn-1	X	X	not tested
sdz-24	X	X	not tested
gei-7	√	√	not tested
unc-68	√	√	not tested
clec-13	√	√	not tested
rrn-3.1	√	√	√
mtl-1	not tested	√	√
mtl-2	not tested	(√)	(√)

The qRT-PCR results confirmed that the expression from 11 transcripts (11/24) (*sod-2*, *sod-3*, *gsr-1*, *hsp-16.1*, *aco-1*, *cep-1*, *gei-7*, *unc-68*, *clec-13*, *rrn-3.1*, and *mtl-1*) was confirmed across all doses and the three validation steps/platforms utilized (from two independent RNA samples; or the cDNA synthesized from the RNA samples that were utilized in the microarray experiment) (Table 5.8). The transcript levels of a further seven genes (7/24), namely *sod-1*, *sod-4*, *gst-4*, *gst-10*, *cuc-1*, *cnx-1* and *mtl-2*, were verified to be close matches (matching in their expression at least 3 of the examined NIST doses) when compared to the microarray data. The qPCR expression profiles of *ctl-2*, *ctl-3*, *sod-5*, *ftn-1*, *skn-1*, and *sdz-24* did not replicate the results obtained by the microarray.

Taken together, the microarray validation by qPCR was deemed to be successful, and hence most of the observed transcriptional changes in wild-type worms are likely to be the consequences of NIST exposure.

5.3.7 The effects of NIST 1648a exposure on the life-history traits of *C. elegans*

5.3.7.1 Acute exposure of wild-type strain to NIST 1648a

As toxicity of the particles vary significantly between different exposure assays parameters (Sochova et al., 2007; Wang et al., 2009), the initial plan was to investigate the toxic effects of NIST 1648a on worms using M9 saline solution (in the absence of bacterial food). The pitfalls of this type of exposure are that it can only be conducted for acute exposure studies (maximum 24 hours). Under optimal conditions growth of *C. elegans* is exponential during the four molt stages (from L1 to L4) until it reaches a final

plateau phase post 120 hours (Jager et al., 2005). However, this trait can be negatively affected by some toxicants, such as cadmium (Hughes and Stürzenbaum, 2007), which is one of the metals also present in the polymorphic NIST sample.

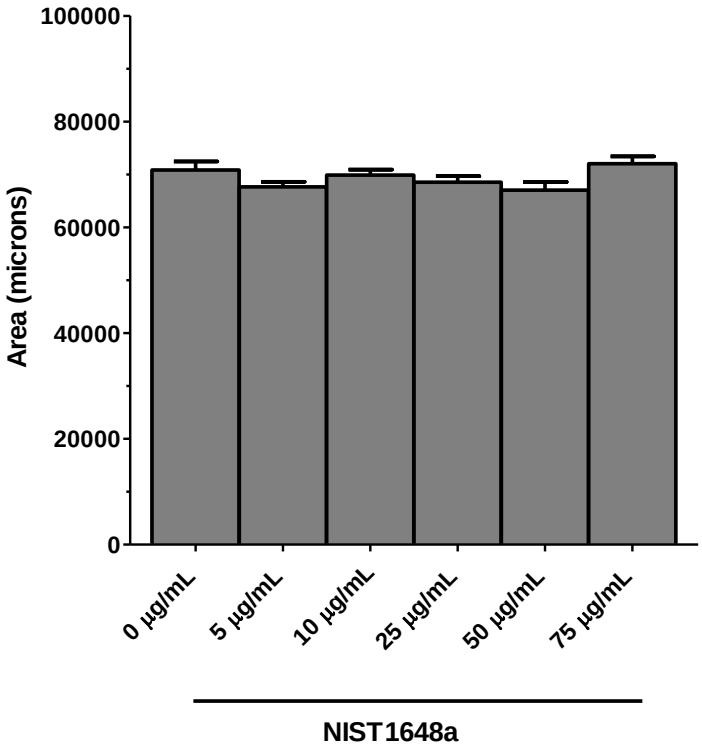

Fig. 5.20: Flat volumetric surface area of wild-type nematodes subjected to an acute exposure in M9 test medium to different NIST 1648a concentrations. The data plotted present the end point result of change in surface area of the nematode at 120 hours, expressed in microns. Data are represented as mean ± SEM (n = 20). Statistical analysis was performed using a one-way ANOVA comparing untreated and NIST treated matched group sets of measurements ($p<0.05$).

The flat volumetric surface area in wild-type *C. elegans* was examined in the presence and absence of NIST particles. Nematodes were exposed at L1 stage in M9 to 0, 5, 10, 25, 50, and 75 µg/mL NIST for 24 hours. Following this acute toxicant exposure, nematodes were placed onto fresh NGM agar plates with OP50 bacterial food in the absence of NIST. No statistically significant changes in the worms' flat volumetric

surface area were found at any of the tested NIST concentrations (Fig. 5.20). The experimental design was not tested and repeated in any of the worm mutants, as concerns were raised that once NIST is presented in M9 solution, media components (such as are phosphates, and sulphates) may partly quench the toxicity (see section part 5.3.1 Characterization of NIST 1648a for more details and evidence).

5.3.7.2 Chronic exposure of wild-type and metal sensitive triple knockout mutant (*mtl-1;mtl-2;pcs-1*(zs2)) strain to NIST 1648a

For chronic exposure, the newly hatched (L1) worms were maintained on a large NGM agar plate inoculated with 200 µL of OP50 supplemented with/without NIST 1648a. Every day animals were transferred to new NGM plates inoculated with a fresh food source (OP50) supplemented with/without NIST and examined for changes in their development, reproduction, and life-span.

The volumetric growth of chronically exposed wild-type nematodes and the metal sensitive triple knockout mutant was determined to observe whether NIST particles affect the physiological status of the animal. The initial growth rate was similar in both strains (wild-type and metal sensitive triple knockout mutant) and seemingly not affected by NIST exposure. All nematodes, irrespective of strain or exposure condition, reached adulthood within 4 days post-hatching (data not shown). In the control conditions the wild-type reached at 120 hours, a flat volumetric surface area of 70065 ± 1569 microns. The chronic exposure to 25 and 50 µg/mL NIST did not exert any effects on the wild-type body size (Fig. 5.21, Table 5.9) ($p<0.05$). Similar to the wild-type response, no statistically significant detectable changes were observed in the body size of the NIST exposed mutant *mtl-1;mtl-2;pcs-1*(zs2) strain (Fig. 5.21, Table 5.9)

($p<0.05$). The shape and the rate of the exponential curves in both nematode stains was also not affected by any of the NIST cocentrations tested.

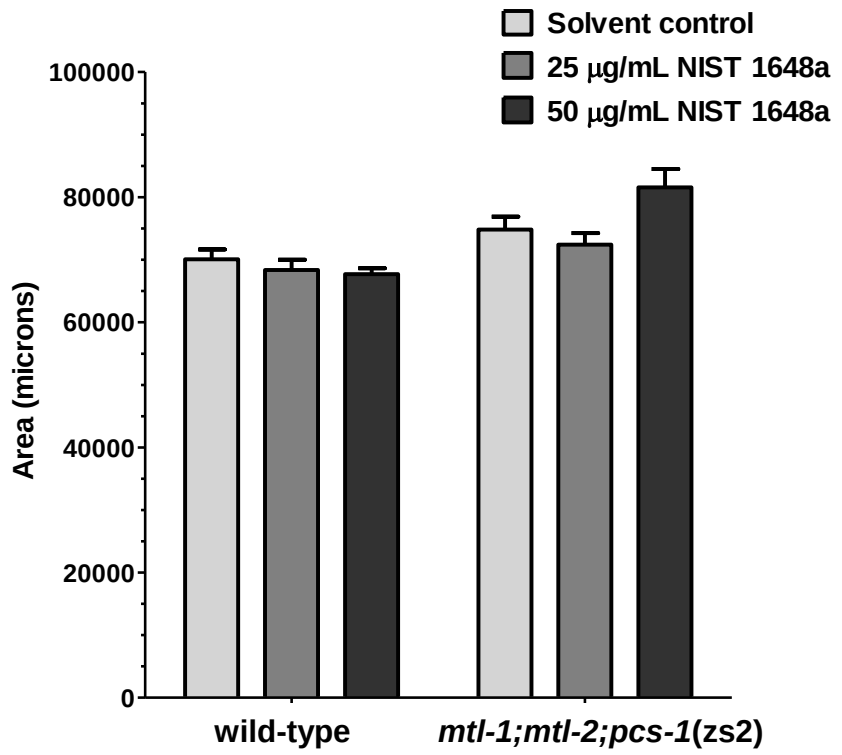

Fig. 5.21: Flat volumetric surface area of wild-type and *mtl-1;mtl-2;pcs-1*(zs2) nematode strains chronically exposed to different NIST 1648a concentrations. The data present the end point result of change in surface area of the nematode at 120 hours post L1 stage, expressed in microns. Data are represented as mean ± SEM (n=20). Statistical analysis was performed using the one-way ANOVA comparing untreated and NIST treated matched group sets of measurements ($p<0.05$).

The reproductive capacity of wild-type and the triple-knockout mutant following exposure to NIST 1648a was examined. In (solvent) control conditions, wild-type and *mtl-1;mtl-2;pcs-1*(zs2) produced 224.5 ± 7.2 and 94.1 ± 3.2 viable eggs, respectively (Table 5.9). In wild-type, only exposure to the 25 µg/mL of NIST concentration significantly reduced the number of viable offspring to 185.5 ± 8.8 ($p<0.05$) (Table 5.9).

No significant effects upon wild-type reproductive output were observed at higher 50 µg/mL NIST concentration. In the *mtl-1;mtl-2;pcs-1*(zs2) exposed mutant, exposure to NIST resulted in a non-dose responsive, bar significant, decrease in the number of viable eggs to 67.9 ± 3.3 at 25 µg/mL of NIST, and to 70.9 ± 3.7 when exposed to 50 µg/mL of NIST ($p<0.05$) (Table 5.9). The full data-set analysis using two-way ANOVA indicated a significant effect of both strain ($p<0.001$) and exposure concentration ($p<0.001$) on the total nematode brood size.

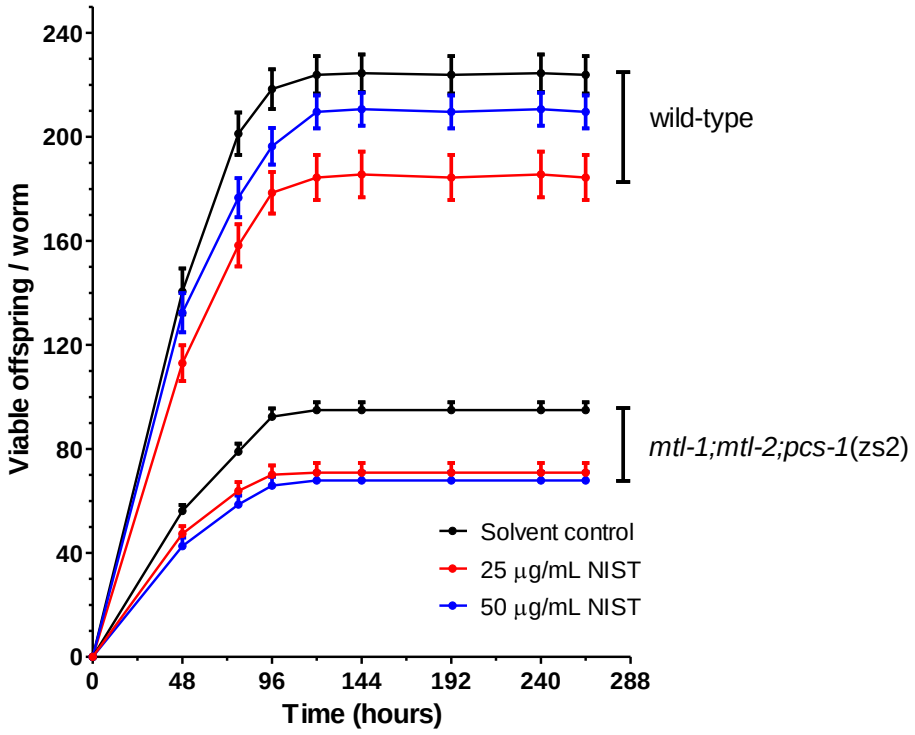

Fig. 5.22: Total cumulative brood size of wild-type and *mtl-1;mtl-2;pcs-1*(zs2) nematode strains exposed to different NIST 1648a concentrations. To compare statistical significance of data between groups, Tukey's Multiple Comparison Test was used at each NIST concentration. Error bars shown are standard error of the mean (n=24). Statistical analysis was performed using the one-way ANOVA comparing untreated and NIST treated unmatched group sets of measurements ($p<0.05$).

Table 5.9: Life-history traits of wild-type and *mtl-1;mtl-2;pcs-1*(zs2) mutants raised in the presence or absence of NIST 1648a. Growth was examined by analysing the total surface area of the worm; and the reproduction was assessed by counting the number of viable offspring per individual. (ns (non-significant), **p<0.01, and ***p<0.001).

			NIST 1648a (µg/mL)		
	Strain		0	25	50
Growth	wild-type	N	20	20	20
		Surface area (microns)	70065 ± 1569	68353 ± 1653	67682 ± 970
		Surface area (% of control)	100	97.56	96.6
		Statistical significance		ns	ns
	mtl-1;mtl-2;pcs-1(zs2)	N	20	20	20
		Surface area (microns)	74834 ± 2067	72427 ± 1842	81562 ± 2956
		Surface area (% of control)	100	96.78	109
		Statistical significance		ns	ns
Reproduction	wild-type	N	20	24	21
		Total brood size ± SEM	224.5 ± 7.2	185.5 ± 8.8	210.6 ± 6.3
		Brood size (% of control)	100	86	94
		Statistical significance		**	ns
	mtl-1;mtl-2;pcs-1(zs2)	N	21	23	23
		Total brood size ± SEM	94.1 ± 3.2	67.9 ± 3.3	70.9 ± 3.7
		Brood size (% of control)	100	75	79
		Statistical significance		***	***

Changes in life-span were investigated in wild-type exposed acutely (for 48 hours) or chronically to 6.25 or 25 µg/mL NIST, respectively.

For the acute exposures, staged nematodes were subjected to NIST from L1 larva stage until L4 larva stage, then maintaining them under control conditions (in absence NIST). For the chronic exposure, staged L1 nematodes were transferred every day to plates

with fresh OP50 supplemented with the corresponding NIST concentration (for life-span assay details see Chapter two: Materials and methods).

Following an acute exposure to increasing NIST concentrations, there was no significant effect on median life-span in wild-type worms ($p>0.05$) (Fig. 5.23A; Table 5.10), however life-span was significantly affected following the chronic exposure to NIST (Fig. 5.23B; Table 5.10). The median life-span was significantly decreased by 1 day at 6.25 µg/mL NIST, and for 2 days by 25 µg/mL NIST concentrations, respectively ($p<0.0001$) (Fig. 5.23B; Table 5.10). The maximum nematode life-span was 21 days in control conditions, and 20 days on NIST exposure.

To investigate whether metallochelators are functionally involved in providing protection against wild-type nematode life-span reduction induced by chronic exposure to NIST, a decision was taken to examine for the NIST effects in a metal hypertensive triple-knockout *mtl-1;mtl-2;pcs-1*(zs2) mutant strain for comparison (to address this issue/and to test the hypothesis).

The medium life-span of the wild-type strain under (solvent) control conditions was 13 days, as for *mtl-1;mtl-2;pcs-1*(zs2) mutant it was 9 days (Fig. 5.23). The exposure to NIST was found to have no significant effect on the medium life-span of the *mtl-1;mtl-2;pcs-1*(zs2) strain. At all examined NIST concentrations the median survival of the worm was 9 days ($p>0.05$), bar the highest 50 µg/mL NIST, where the medium survival was 8 days ($p>0.05$) (Fig. 5.23C; Table 5.10).

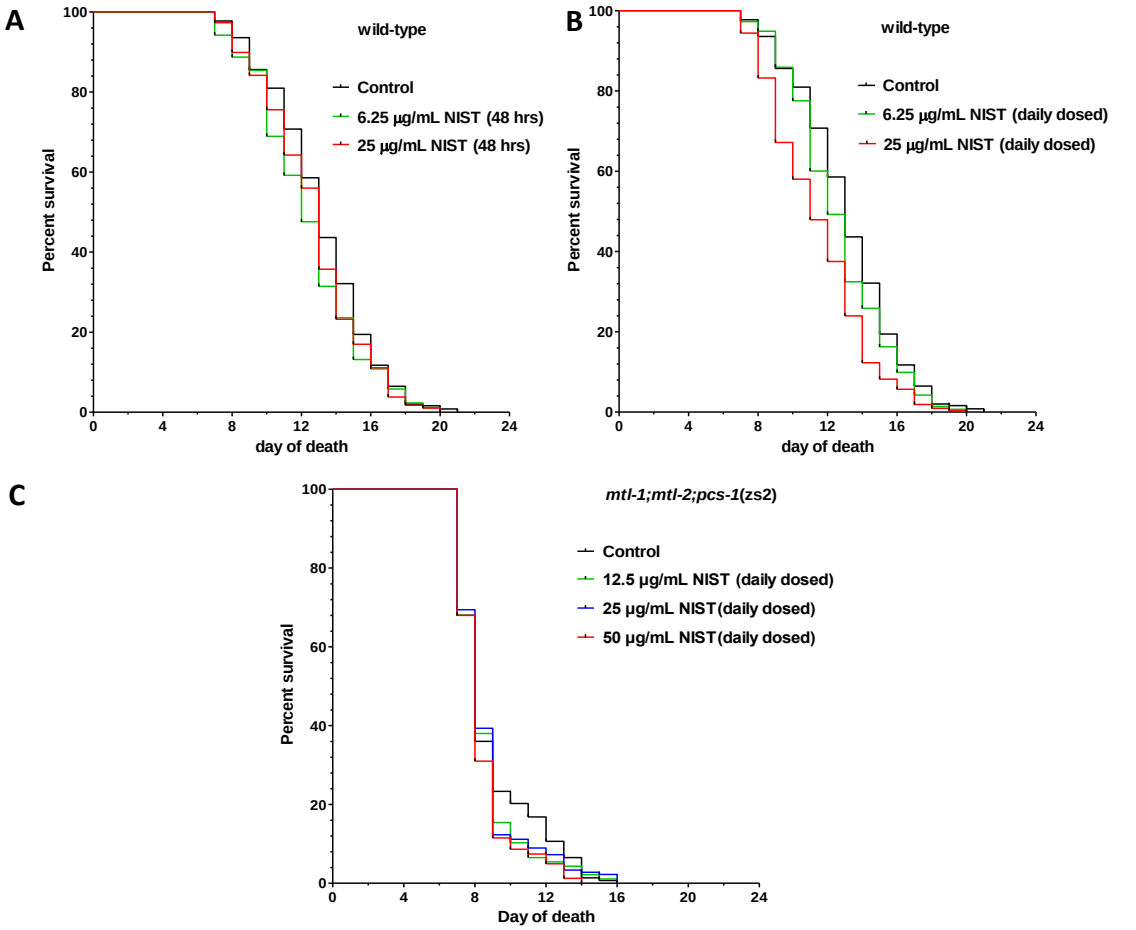

Fig. 5.23: Life-span of wild-type (A-B), and *mtl-1;mtl-2;pcs-1*(zs2) (C) nematode strains exposed to different NIST 1648a concentrations. Following treatment, the wild-type nematode had an average/median lifespan of 13 days, and the *mtl-1;mtl-2;pcs-1*(zs2) mutant an average life-span of 9 days. Lifespan of wild-type nematodes was not significantly affected by acute (48 hrs) NIST exposure **(A)**; however lifespan was significantly altered following chronic exposure to NIST **(B)**. In contrast, chronic exposure to NIST had no effect on the *mtl-1;mtl-2;pcs-1*(zs2) mutant lifespan **(C)**. Statistical analysis was performed using the Log-rank (Mantel-Cox) Test for comparison of survival curves comparing to control at each NIST concentration ($p < 0.0001$).

Although the medium life-span of the mutant nematode was not significantly affected, a Although the medium life-span of the mutant nematode was not significantly affected, a chronic exposure to NIST particles was found to cause, in some exposed nematodes (wild-type and in a mutant), an increased intestinal accumulation of NIST particles, which occurred in some, but not all, nematodes over time and may have affected the health of the nematodes (for image evidence see Appendix: NIST 1648a).

Table 5.10: Life-span trait investigated in NIST 1648a exposed wild-type and *mtl-1;mtl-2;pcs-1*(zs2) mutant strain. Nematodes were either dosed acutely (for 48 hours) or chronically (for entire life-span, and transferred to newly dosed plates every 24 hours). Life-span was investigated by counting the number of alive nematodes compared to total number of staring individuals (Kaplan-Meier survival method), where ns (non-significant), and ****is p< 0.0001.

LIFE-SPAN		NIST 1648a (µg/mL)				
Strain		**0**	**6.25**	**12.5**	**25**	**50**
wild-type (acute dosing)	**N**	254	266		291	
	Median survival (days)	13	12		13	
	Statistical significance		ns		ns	
wild-type (chronic dosing)	**N**	254	286		318	
	Median survival (days)	13	12		11	
	Statistical significance		****		****	
***mtl-1;mtl-2; pcs-1*(zs2) (chronic dosing)**	**N**	298		296	202	196
	Median survival (days)	9		9	9	8
	Statistical significance			ns	ns	ns

5.3.7.3 Chronic exposure of SOD (superoxide dismutase) mutant strains to NIST 1648a

Particle specific characteristics of NIST 1648a, such as composition, surface area, and size can induce oxidation of target molecules, such as proteins and DNA, and cause damage to the biological systems (Squadrito et al., 2001; Kelly, 2003). There is growing scientific evidence that metal oxide based urban particulate matter (SRM NIST 1648a) carry an oxidative capacity that causes (in *in vitro* assays) a depletion of the antioxidants glutathione and ascorbic acid. Related antioxidation pathways may also provide a protective role against ROS-mediated immune responses. Therefore measuring the generation of intracellular ROS (e.g. superoxide radical (O^{2-})) induced damage may potentially serve as a suitable biological marker of NIST toxicity (Landis and Tower, 2005; Doonan et al., 2008). Pools of cytoplasmic, extracellular and mitochondrial superoxide radicals are, in worms, detoxified by the assigned SOD isoforms (Doonan et al., 2008). In order to address the role of antioxidant enzymes in the protection against the oxidative potential of NIST particles, the organismal effects of *sod-1*, *sod-2*, and *sod-3* deletion was examined.

The Cu/Zn SOD (SOD-1) enzyme plays an important role in protecting cells against oxidative damage and aging in nematodes (Yanase et al., 2009). A loss of an allele, as in the mutant *sod-1*(tm776), may increase the sensitivity to free radicals, believed to be generated by NIST. In control conditions, the *sod-1*(tm776) mutant worms were approximately 10 % smaller in size compared to the wild-type strain (Fig. 5.24). The initial growth rates of NIST treated and untreated *sod-1*(tm776) nematodes were similar (data not shown). Changes upon nematode volumetric area became apparent at 120 hours, when the surface area of the nematodes exposed to 12.5 and 25 µg/mL NIST increased significantly by 16 % and 10 %, respectively ($p<0.05$) (Table 5.11).

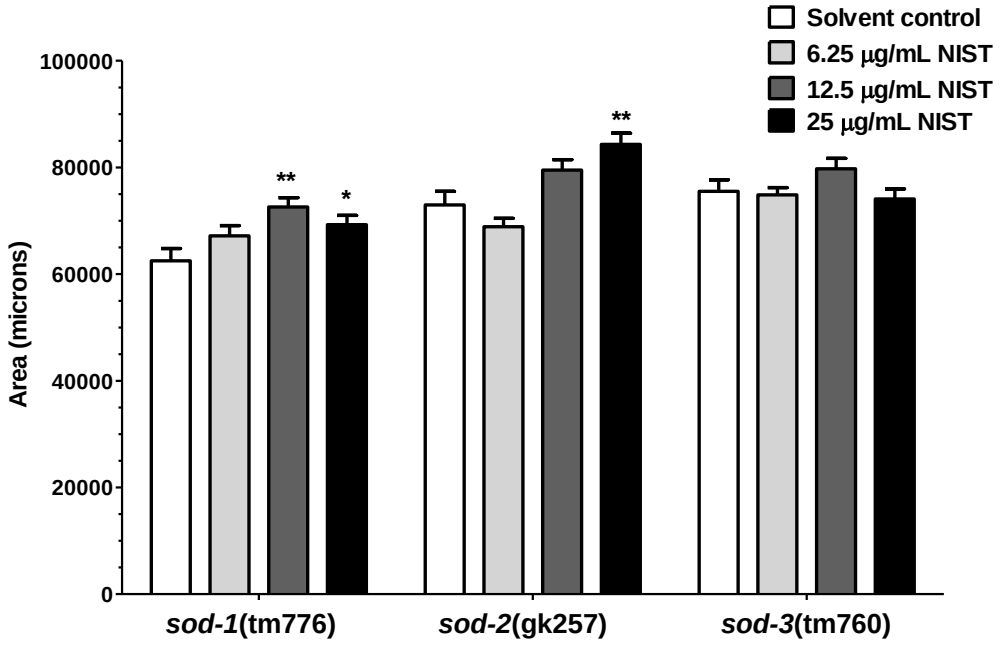

Fig. 5.24: Flat volumetric surface area of SOD mutants chronically exposed to different NIST 1648a concentrations. Shown is the surface area at 120 hours post L1 stage, expressed as the surface area of the nematode in microns. Data are represented as mean ± SEM (n=20). Statistical analysis was performed using the one-way ANOVA comparing untreated and NIST treated matched group sets of measurements, where *is $p<0.05$, and **$p<0.01$.

In nematodes, SOD-2 and SOD-3 are both Fe/Mn SOD enzymes, which are predicted to be mitochondrial and have a role in providing protection against oxidative stress (Van Raamsdonk and Hekimi, 2009). The *sod-2*(gk257) mutant nematode strain is characterized by an insertion of (TTATATTTGACTATTTGA) and a 159 bp deletion, and the *sod-3*(tm760) nematode strain by a 715 bp deletion. In control conditions, both *sod-2*(gk275) and s*od-3*(tm760) worms were similar in size compared to the wild-type strain (Fig. 5.24). The body size of the *sod-2*(gk275) nematode was only found to be significantly affected, at 120 hours, at the highest 25 µg/mL NIST concentrations ($p<0.05$) (Table 5.11). Notably, compared to the untreated controls, there were no

significant changes in either the growth rate or body size in the chronically exposed *sod-3*(tm760) (p>0.05).

Table 5.11: Volumetric area of SOD mutants raised in the presence or absence of NIST 1648a. Growth was examined by analysing the total surface area of the worm. (ns (non-significant), *p<0.05, and **p<0.01).

GROWTH		NIST 1648a (µg/mL)			
Strain		**Control**	**6.25**	**12.5**	**25**
***sod-1*(tm776)**	**N**	20	20	20	20
	Surface area (microns)	62502 ± 2283	67191 ± 1897	72606 ± 1713	69277 ± 1728
	Surface area (% of control)	100	107.5	116.2	110.8
	Statistical significance		ns	**	*
***sod-2*(gk257)**	**N**	20	20	20	20
	Surface area (microns)	72979 ± 2550	68878 ± 1573	79521 ± 1931	84323 ± 2094
	Surface area (% of control)	100	94.38	109	115.5
	Statistical significance		ns	ns	**
***sod-3*(tm760)**	**N**	20	20	20	20
	Surface area (microns)	75510 ± 2166	74871 ± 1368	79762 ± 1937	74106 ± 1863
	Surface area (% of control)	100	99.15	105.6	98.14
	Statistical significance		ns	ns	ns

5.3.7.4 Acute exposure of the *skn-1*(zu67) mutant to NIST 1648a

Short-term exposure experiments provide a snapshot of the physiological response of an animal, and provide insights into protection mechanisms that might be involved at the early stages when exposed to a toxicant. In nematodes, SKN-1 is a transcription factor involved in the primary defence against the cytotoxic effects of oxidative stress via the

activation of antioxidant enzymes, and contributes to longevity (An and Blackwell, 2003). Nevertheless, its exact role in the nematode immune defense is still unknown. In order to examine the biological and/or physiological consequences of NIST's 1648a ability to generate ROS, the nematode mutant *skn-1*(zu67) strain was utilized. Sensitivity of physiological and molecular level responses of the *C. elegans skn-1*(zu67) mutant strain exposed to NIST were explored and compared with those observed in the wild-type.

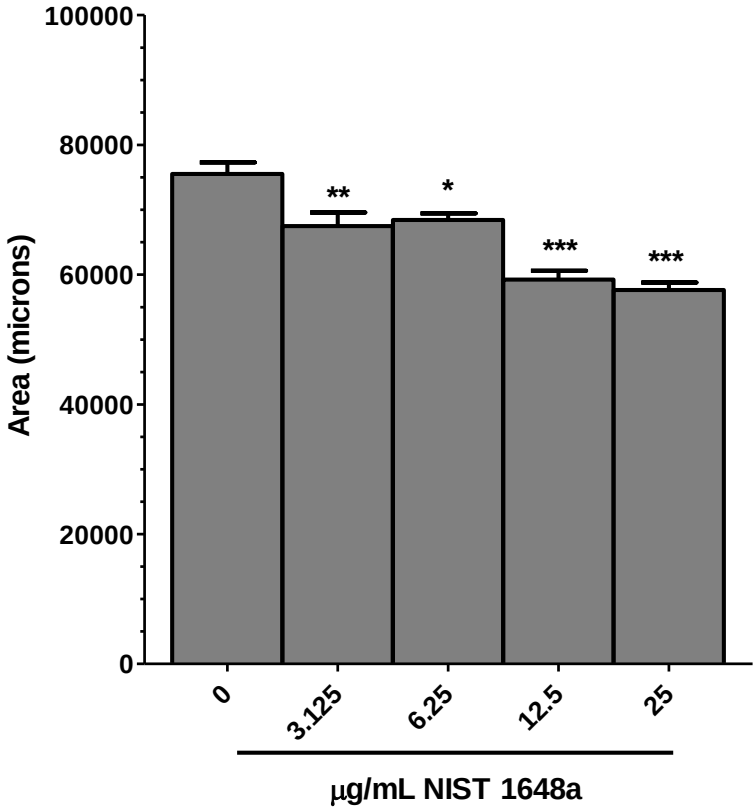

Fig. 5.25: Flat volumetric surface area of the *skn-1*(zu67) mutant subjected to an acute exposure of different NIST 1648a doses. The data plotted represents the end point size at 120 hours post L1 stage, expressed as the surface area of the nematode in microns. Data are presented as mean ± SEM (n=20). Statistical analysis was performed using the one-way ANOVA comparing untreated and NIST treated matched group sets of measurements, where *is $p<0.05$, **$p<0.01$, and ***$p< 0.001$.

The initial growth rate of the *skn-1*(zu67) mutant was similar to the wild-type strain, and was not affected by the NIST exposure until nematodes reached adulthood within 4 days post hatching (data not shown). Measured at 5 days post-hatching, a significant reduction in the *skn-1*(zu67) body size was observed in all NIST exposed nematodes (a statistical difference was observed at all concentrations tested, namely 3.125 - 25 µg/mL NIST). However, the phenotypic effect was found to be more pronounced at higher NIST concentrations (12.5 and 25 µg/mL), where reduction in the worm body size was found to be 22 % and 24 % respectively, compared to the untreated solvent control ($p<0.001$) (Fig. 5.25; Table 5.12).

The reproductive capacity of *skn-1*(zu67) mutant following an acute exposure to NIST 1684a was examined. In control conditions (i.e. in the absence of NIST), *skn-1*(zu67) produced 223.7 ± 3.7 viable eggs, an output similar to wild-type (Table 5.9). Following the NIST challenge, a significant (though concentration independent) reduction in reproductive output, was observed. The effect was moderately significant ($p<0.05$), when worms were exposed to 6.25 µg/mL NIST, and highly significant when nematodes were challenged to 3.125 and higher NIST concentrations ($p<0.001$) (Fig. 5.26; Table 5.12).

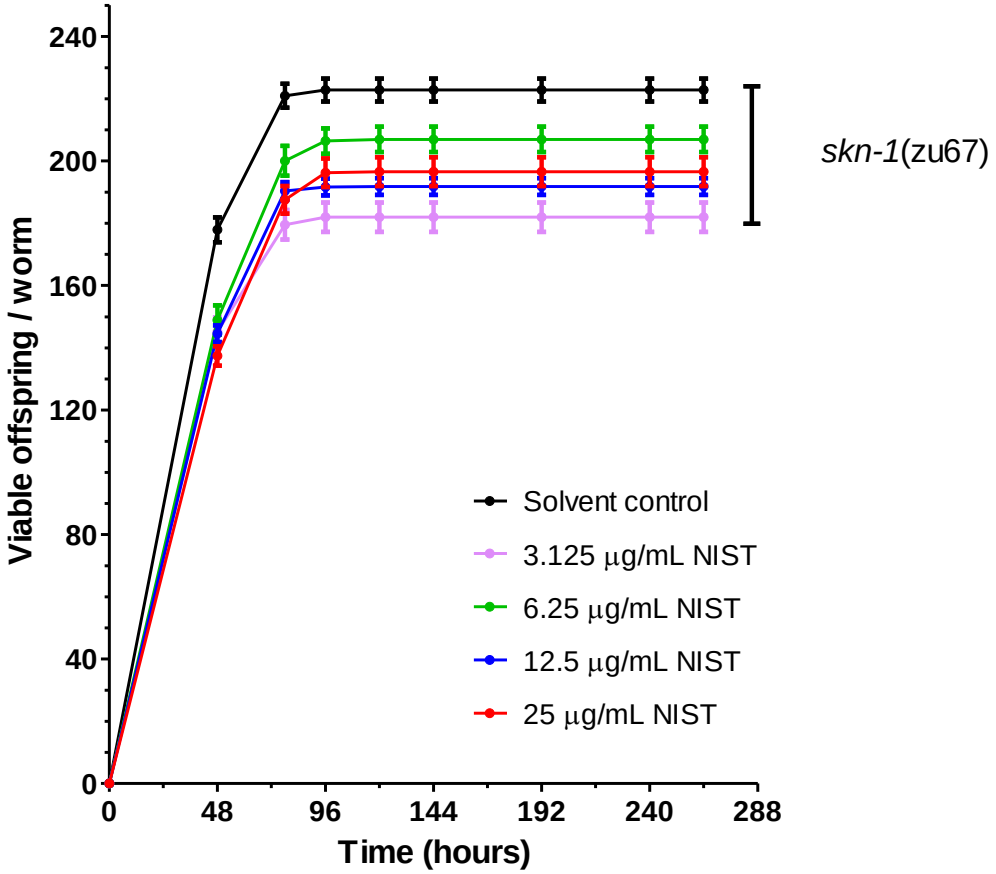

Fig. 5.26: Total cumulative brood size of the *skn-1*(zu67) mutant exposed to different NIST 1648a concentrations. To compare statistical significance of data between groups, Tukey's Multiple Comparison Test was used at each NIST concentration. Error bars shown are standard error of the mean (n=36). Statistical analysis was performed using the one-way ANOVA comparing untreated and NIST treated unmatched group sets of measurements ($p<0.05$).

For the lifespan assay, *skn-1*(zu67) mutant worms were acutely exposed for 48 hours (from L1 to L4 larva stage) to OP50 supplemented with/without NIST. The acute exposure was followed by maintaining worms in normal control conditions on NGM plates.

Under control conditions, the medium life-span of the *skn-1*(zu67) mutant was 12 days, two days shorter than the wild-type strain ($p<0.0001$) (Fig. 5.27). The medium life-span

of the *skn-1*(zu67) mutant was reduced by a 1 day at 3.125 µg/mL, and 2 days at 6.25 µg/mL NIST ($p<0.0001$). No significant effect on the mutants' life-span was observed at 12.5 or 25 µg/mL NIST exposures (Fig. 5.27; Table 5.12). The maximum life-span of the *skn-1*(zu67) mutant was 19 days when treated with 3.125 and 6.25 µg/mL NIST, and 21 days in control conditions or higher NIST concentrations exposures.

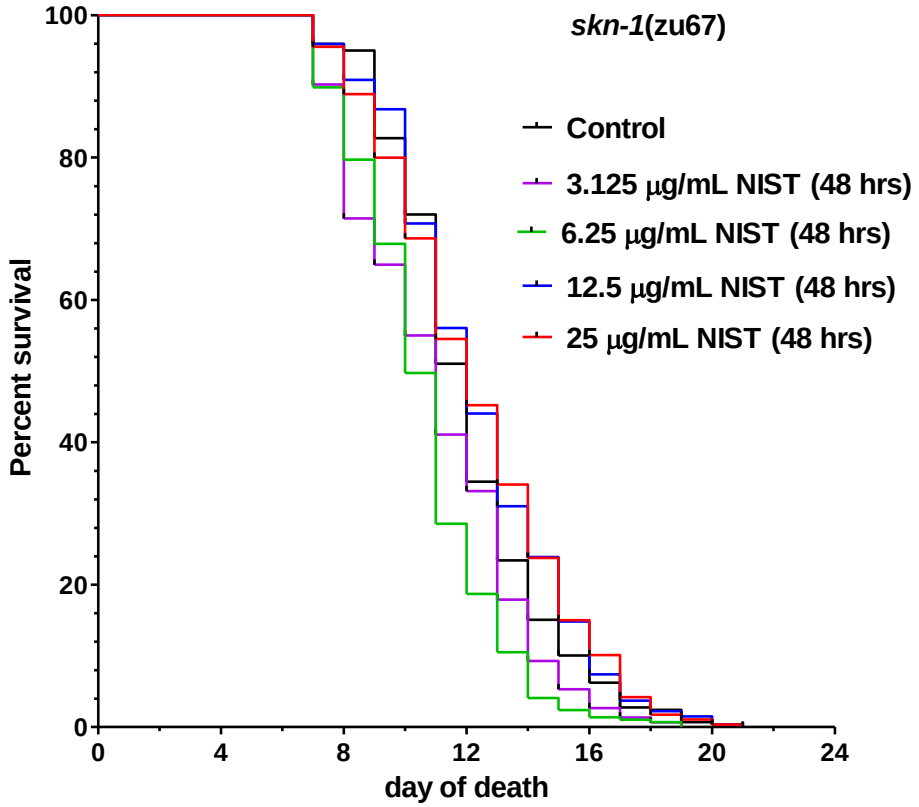

Fig. 5.27: Life-span of *skn-1*(zu67) mutants exposed to different NIST 1648a concentrations. Synchronised nematodes were acutely exposed (48 hours) from L1 stage to L4 stage to NIST and transferred to standard NGM plates. The *skn-1*(zu67) strain had a medium life-span of 12 days, but was significantly altered following an acute exposure to NIST. Statistical analysis was performed using the Log-rank (Mantel-Cox) Test for comparison of survival curves comparing to control at each NIST concentration ($p<0.0001$).

Table 5.12: Life-history traits of *skn-1*(zu67) mutants raised in the presence or absence of NIST 1648a. Growth was examined by analysing the total surface area of the worm; and the reproduction was assessed by counting the number of viable offspring per individual. (ns (non-significant), *p<0.05, **p<0.01, ***p<0.001, and ****p<0.0001.) Life-span was investigated by counting the number of alive nematodes compared to total number of staring individuals (Kaplan-Meier survival method), where ns (non-significant), and **** is p< 0.0001.

			NIST 1648a (µg/mL)				
Strain			**0**	**3.125**	**6.25**	**12.5**	**25**
Growth	***skn-1*(zu67)**	**N**	20	20	20	20	20
		Surface area (microns)	75516 ± 1794	67472 ± 2124	68440 ± 995	59245 ± 1365	57617 ± 1161
		Surface area (% of control)	100	89.35	90.63	78.45	76.30
		Statistical significance		**	*	***	***
Reproduction	***skn-1*(zu67)**	**N**	33	26	33	32	32
		Total brood size ± SEM	223.7 ± 3.7	178 ± 5.3	206.9 ± 4.1	191.8 ± 2.7	196.6 ± 4.6
		Brood size (% of control)	100	79.6	92.5	85.7	88
		Statistical significance		***	*	***	***
Life-span	***skn-1*(zu67)**	**N**	305	152	314	283	300
		Median survival (days)	12	11	10	12	12
		Statistical significance		****	****	ns	ns

5.4 Discussion

5.4.1 Particle characterization and effect of test medium on physicochemical properties of NIST 1648a

Physicochemical characteristics of the ambient particular matter (PM) can be determinants of biological activity (Seaton et al., 1995). In addition, PM is not a uniform material, but rather consists of a polymorphic mixture rich in toxic transition metals and organics (organic compounds and matter), as well as components that are lower in toxic potency (e.g. ammonium salts, chlorides, sulphates, nitrates) and endotoxins (Ayres et al., 2008). When developing a new bio-toxicity screening system, it is important to consider that, within the ambient particle mixture, each individual effect will contribute to the total combined cumulative toxic outcome of the tested PM itself. Therefore, it is essential to understand the biophysicochemical interactions that take place at the nano-bio interface (Nel et al., 2009; Love et al., 2012).

Physical characterization performed on NIST 1648a suggested that particles exist in the test media in individual and agglomerated states. TEM imaging provided information about shape and size of NIST in the stock solution; however it could not provide detailed information on the particle state once in a biological test medium. TEM analysis of NIST in the M9 test medium, which is primarily composed of sodium and potassium salts (Hitchcock et al., 1998), found the particle agglomerate surface to be modified by salt crystals. These crystal clusters contribute to the increase in the overall size of the aggregates in M9, and are likely to interfere with the bioavailability of NIST (Donkin and Williams, 1995). TEM imaging of NIST particles in the OP50 bacteria could not be performed as the contents of biological solutions (live bacteria) as well as the rapid aggregation of particles damaged the observation grid, and prevented imaging.

For this reason, the NanoSight NTA (NanoSight Ltd, UK) technique was used to characterize particles in the biological solutions (Carr and Warren, 2012). NanoSight characterisation suggested that in M9 solution NIST particles are more mobile, thus collisions are more likely. Smaller particles tend to be less stable, thus colloidal forces as well as dynamic biophysicochemical interactions cause the formation of aggregates, which are maintained via Van der Waals forces (Nel et al., 2009). NanoSight NTA reconfirmed the observations made with TEM imaging, namely that the addition of NIST to the M9 solution causes surface crystallinity of particle agglomerates via salt-particle interactions; an event, that occurs over time, and could be, in the future, exploited by employing X-rad and TEM-EDAX methodologies. Properties, such as size of aggregates can condition the deposition rate of the particles. Polymorphic particles, such as NIST, exhibit a range of particle sizes, which once agglomerated, can affect the stability of the chemical composition (Li et al., 2011; Mudunkotuwa et al., 2011; Kao et al., 2012). It is important to note that there is a question of reproducibility of each analysis performed, as particle samples were mixed in composition and of different diameters. Thorough and reproducible analysis may be achieved by expanding the experimental timeframe. There is also no supporting evidence as to NIST's ability to fully dissolve in the medium at the given concentration; hence an ICP-MS analysis would be required. Overall, the media interactions and modification taking place on NIST particle surfaces and their role in toxicity would need further clarification. Nevertheless, it is possible to conclude that the NanoSight can be used as the initial index when studying the toxicity of the natural nanoparticles.

Clearly, high concentrations of NIST may inflict changes on the metabolic system of *E. coli* (Zelikoff et al., 2003), a notion that cannot be assessed by TEM. Therefore, in order to investigate whether NIST exposures can induce an indirect effect via caloric

restriction, bacterial growth was monitored in the presence and absence of particles. No effects on OP50 bacterial growth or pH were found, even at the highest dose tested (>50 µg/mL NIST).

5.4.2 Reactive oxygen species (ROS) generation upon NIST 1648a exposure

A good indicator of oxidative damage is the presence of elevated intracellular ROS. In the nematode *C. elegans*, oxidative stress can significantly contribute to the organismal functional decline and increase mortality rate (Honda et al., 2002; Hughes and Stürzenbaum, 2007; Zeitoun-Ghandour et al., 2011). Evidence from previous studies has shown that exposure to redox-active metals present on the surface of NIST 1648a may result in increased oxidative stress and ROS production (Ball et al., 2000; Kelly, 2003). To evaluate the NIST's ability to induce the accumulation of intracellular ROS, a commonly used *in vitro* DCF test was applied (Catheart et al., 1983). In addition, a selection of *C. elegans* mutants with reduced resistance to environmental stressors (reduced antioxidant defences) were utilized in order to investigate/explore the correlation between aging and accumulation of oxidative damage, and the level of antioxidant defence (Hekimi et al., 2011).

DCFH-DA is a cell permeable dye, which has been reported to be a good tool for detecting ambient particulate-induced formation of free radical compounds, e.g. •OH (Goldsmith et al., 1998), however it has also been reported to lack specificity (Cohn et al., 2008; Karlsson et al., 2010). The amount of intracellular ROS present is indicated by the increased brightness in fluorescence of DCF.

Following incubation with NIST, a significant increase in endogenous cellular ROS was observed in the wild-type strain (Fig. 5.7). The effect was found to be even more pronounced in the NIST exposed antioxidant Nrf2-like transcription factor *skn-1*(zu67) mutant strain. In contrast, NIST was a poor inducer of ROS levels in in the metal hypersensitive *mtl-1;mtl-2;pcs-1*(zs2) nematode and in MnSOD strain mutants, as the intracellular levels of ROS were found to be significantly decreased compared to controls. In the CuZnSOD *sod-1*(tm776), ROS levels remained unchanged following NIST exposure. Irrespective of the mechanistic details, these results indicate that the initial biological response to NIST seems to be mediated in nematodes through pro-inflammatory oxidative stress reactions involving ROS.

To best explain the molecular mechanisms underlying the observed differences in ROS levels in the NIST exposed *C. elegans* strains, it is important to stress that there are differences in baseline levels of total endogenous superoxide in each nematode strain. Concurrently, there are differences in their respective threshold sensitivities to stress conditions. Furthermore, *C. elegans* has developed a very robust antioxidant defence mechanism to protect itself against undue oxidative challenges, including metal binding proteins (MTs, and PCS), and antioxidant enzymes, such as SOD, CAT, GSTs (Gems and Doonan, 2009; Back et al., 2012). It is conceivable that these antioxidant systems are differentially activated in the mutants. *C. elegans* has not just one, but two CuZnSODs, encoded by *sod-1* and *sod-5*, likewise it has two mitochondrial MnSODs, encoded by *sod-2* and *sod-3*, and an extracellular CuZnSOD (*sod-4*) (Landis and Tower, 2005). Primarily, the major contributors of total SOD activity are SOD-1 and SOD-2 enzymes, and in the absence of any one of them, results in other isoenzymes to functionally compensate the loss of activity (Back et al., 2012). Many studies have shown that the SOD mediated protection in nematodes is not simple (Doonan et al.,

2008; Van Raamsdonk and Hekime, 2011; Back et al., 2012), and suppression of any SOD enzyme might not necessarily lead to compromised organismal antioxidant defences and aging. In addition, numerous proteins can affect the level of ROS production, including metal-trafficking proteins (MTs and PCSs). Transition metals, such as Fe^{3+} (which is abundant in NIST) can also induce OH^- production, which can be counteracted by ferritins and metallothioneins in the SOD mutants. Similarly, the fully functional SODs can convert the production of O^{2-} into H_2O_2, and O_2 in the metal hypersensitive mutant. NIST is chemically complex and the forms of molecular damage induced will be diverse. Likewise, the particle surrogates, e.g. organic components carried on the particle surface, also play an important role in mediating the toxic outcome. For example, high levels of phosphates and sulphates can interfere and modulate the cellular metal uptake mechanisms (Nile et al., 2009) or/and enzyme activities (Hatzis et al., 2006). A particle bound endotoxin can also drive the toxicity associated with particle exposure (Alfaro-Moreno et al., 2007).

According to the oxidative damage theory, aging is characterized by the accumulation of molecular damage (Harman, 1956). Why this damage occurs in *C. elegans* is still unclear. Nevertheless, studies have shown that *C. elegans* carrying mutations that result in either suppression or loss of the transcription factor SKN-1, are marked by an increased accumulation of intracellular ROS and ageing (An and Blackwell, 2003; Sykiotis et al., 2011). In nematodes, SKN-1 functions as a regulator of baseline redox activity, as well as in situations of acute oxidative stress or chemical challenge (An and Blackwell, 2003; Sykiotis et al., 2011; Choe et al., 2012). Under stress conditions the SKN-1 signalling pathway involves SKN-1 protein translocation to the nuclei and activation of a broad range of phase II detoxification enzymes, such as glutathione synthesis (GS), glutathione S-transferases (GSTs), etc. to provide protection against

ROS and prolongation of its lifespan (Tullet et al., 2008). It is possible to hypothesize that the increase in endogenous ROS observed in this study is due to the reduced/or compromised function of SKN-1, hence resulting in a dysfunctional antioxidant organismal defence. However, which of the phase II enzymes or molecular mechanisms are responsible in *C. elegans* to provide protection against NIST mediated oxidative stress is still unclear. The results from the wild-type nematodes suggest that the presence of metallochelators and SODs do not provide sufficient antioxidant protection to the organism, findings that underline the complex mechanism of NIST induced oxidative damage.

Overall, it is possible to conclude that NIST seems to trigger redox sensitive pathways in the nematode and induce an oxidative stress response. Moreover, individual's genotype defines the efficiency of the antioxidant defence mechanisms.

5.4.3 The transcriptional response of *C. elegans* exposed to NIST 1648a

KNUDRA transgenic nematodes were chosen to quantitatively assess the transcriptional response of selected target genes to NIST 1648a. These transgenic nematodes allowed a rapid diagnostic profiling of transcriptional responses and molecular pathways (Boulin and Bessereau, 2007; Frøkjaer-Jensen et al., 2008). As NIST might exert its toxicity on the nematode through pro-inflammatory mechanisms, reporter genes believed to act as key players in the protection against oxidative stress and inflammation were examined. The panel consisted of: *mtl-2*, *ugt-1*, *gcs-1*, *cyp-35A2*, *gst-4*, *gst-38*, *hsp-16.2*, *hsp-16.41*, and *dnj-13*.

All transcriptional responses were examined at the maximum concentration of 50 µg/mL NIST over a 48 hour exposure time, which provided a snapshot of the nematode transcriptional status. The analysis showed that the expression pattern of the majority of genes tested did not deviate significantly from the basal control level (Fig. 5.6). Nevertheless, significant increase in the mCherry fluorescence signal was observed in *cyp35A2* and *gcs-1* transcripts, indicating that NIST modulates the transcriptome.

In a nematode, the *cyp-35A2* is expressed in the intestines, where it functions as an NADPH-dependent monooxygenase that metabolizes endogenous and exogenous compounds. Previous studies have demonstrated that cytochrome P450 (CYP) genes are attenuated in response to xenobiotic substances, such as PCBs and PAHs (Menzel et al., 2001; 2005); or in the presence of CeO_2 and TiO_2 nanoparticles (Roh et al., 2010).

In urban areas, ambient particles can carry a large amount of organic compounds, including PAHs. The major source of these compounds is thought to be diesel powered vehicles and the burning of fossil fuels. Studies on the role of DEP and PM organic extracts have shown their association in the induction of Phase I metabolic enzymes involving members of the CYP gene family. For example, an increased CYP1A1 mRNA expression was found in human bronchial epithelial cells (HBE) (Bauling et al., 2003), and in rats, and exposure to DEP induced the expression of CYP1A2 and CYP1B1 (Hatanaka et al., 2001). In the present study, the increase in *cy35A2* levels may be the result of the metabolic bioactivation by NIST. Transition metals are often transported into cells complexed to organic solutes, which could potentially undergo a biotransformation via CYP P450 to generate redox active intermediates that lead to ROS generation (Ghio et al., 2012).

Exposure to NIST also induced (but to a lesser extent) the antioxidant enzymes *gcs-1* and *ugt-1*, which suggested that exposure to NIST activates antioxidant protection

mechanisms in worms. In nematodes, *gcs-1* encodes for an ortholog of the gamma-glutamine cysteine synthetase (GCS), a phase II detoxification enzyme that is under the control of the SKN-1 transcription factor and is involved in the glutathione biosynthesis pathway (Choe et al., 2012). Transcriptional changes in this enzyme suggest that NIST might disturb the redox balance in the cells, which results in a possible increase in GSH generation. In addition, the glycosyltransferase enzyme (*ugt-1*), which is involved in glucorinidation process, also plays an important role in worm detoxification and the biotransformation of xenobiotic substances via phase II metabolism. Studies in nematodes have linked an increased *ugt-1* activation to substances, such as PCBs congomer 52 (Menzel et al., 2005), and was also found to be induced in response to herbicides (e.g. paraquat), thermal stress (An and Blackwell, 2003), and arsenic exposure (Liao and Yu, 1995). Previous studies demonstrated that exposure to DEP, ambient UFP, and organic DEP extracts can alter several antioxidant enzymes in lung target cells, including GSTs, catalase, SOD, GPx, and UGT enzymes (Li et al., 2002b; Li et al., 2004). For example, the increased expression of UGT enzymes (UGT1 family) has been linked to the metabolism and elimination of (pre)carcinogens, such as benzo(a)pyrene (B[a]P) and 4 (methylnitrosamino)-1-(3-pyridyl)-1-butanone nicotine-derived nitrosamine ketone (NNK), which are present in tobacco smoke (Lacko et al., 2009). Similarly, mRNA and protein expression levels of GCS were reported to be increased in lung epithelial cells and in mice exposed to asbestos (Shukla et al., 2004).

The quantitative assessment of the relative change in fluorescence in MosSCI nematodes revealed that the expression of small *hsp* transcripts (*hsp-16.2* and *hsp-16.41*), and glutatathione-S-transferases (*gst-4* and *gst-38*) was down-regulated on NIST exposure, however this was not statistically significant. The *hsp*s are known to be transcriptionally responsive to physical (e.g. heat) or chemical stresses (Lindquist, 1986;

Strayer et al., 2003) and function as passive ligands preventing unfolded proteins from aggregating in the cell. Whether the down-regulation of *hsp-16* found in this study is specific to a nematode response to NIST exposure remains to be established. Nevertheless, studies on other *hsp* family members, have reported reduced heat shock protein 70 expression levels in airway smooth muscle in COPD in patients chronically exposed to cigarette smoke (Xie et al., 2010). As in another occupational exposure study, a correlation between coal-mine dust exposure in the workplace and increased levels of HSP-27 expression in the plasma of coal-miners was reported (Wang et al., 2010).

In *C. elegans*, antioxidants, such as GSTs, are inducible via the activation of the SKN-1 pathway, which occurs as an adaptive response to stress (e.g. paraquat exposure). Similarly, in the human lung these enzymes are under transcriptional regulation of the Nrf2-ARE pathway, and consist of several subclasses, such as GSTM1 and GSTP1 (Gilliland et al., 2004; Wu et al., 2012). In the present study, NIST failed to induce GSTs enzymes, which aligns with the report by Schroer et al. (2011) stating that the glutathione S-transferase P1 subfamily (GST-Pi) was down-regulated following an allergen challenge in mouse models of asthma. It is been proposed that a decrease in cytosolic lung epithelium GSTPi expression might directly contribute to the asthma phenotype in children via the disruption of redox homeostasis, and an increase in oxidative stress (Tamar et al., 2004, Schroer et al., 2011).

The use of new transgenic technologies has allowed us to successfully utilize *C. elegans* to explore the link between toxicant exposure and gene expression. These results highlighted how NIST particles may be involved in the oxidation of macromolecules (proteins, lipids, DNA) via generation of ROS, and in turn cause oxidative stress that leads to the activation of antioxidant defences and adaptive responses.

5.4.4 Quantitative assessment of NIST 1648a-responsive transcripts in *C. elegans*

Timing is crucial, especially when it relates to nano- and ultrafine- particle toxicology. Therefore, for a predictive toxicological assessment of PM, it is essential to consider not only the physicochemical properties of the material, but also how the time/or length of exposure will affect transcriptional profiles.

To explore whether exposure time plays a critical role in modulating the transcriptional response, short- (15 hours) and long- (48 hours) term effects of NIST 1648a exposure was evaluated in wild-type nematodes. A 15 hour NIST exposure did not induce pronounced changes in transcriptional activation of antioxidant enzymes, including, SODs and CATs. Their expression resembled, at large, control levels. In contrast, the expression of *hsp-16.1* gene was found to be down-regulated, and the *gst-4* transcript significantly increased following the 15 hour NIST exposure.

The qRT-PCR results revealed that the chronic exposure to NIST for 48 hours triggered a more pronounced transcriptional response in six out of the seven genes examined. The exception was *gst-4* whose expression was decreased. From these results, it was possible to conclude that in *C. elegans* an exposure time of 48 hours is required to observe significant changes in transcription, at least for the genes investigated.

Understanding the effects of NIST toxicity on *C. elegans* requires insights into the mechanism of action and biomolecular pathways that might be implicated. To research further into this matter, the transcription of genes implicated in various cellular processes involved in oxidative stress and anti-apoptotic activity were quantified following a 48 hour exposure to NIST. Surprisingly, very few (of the examined) transcripts acted in a NIST dose-responsive manner or increased by more than 3 - fold.

Nevertheless, the qRT-PCR results revealed that NIST did cause an increase in some well-known antioxidants, such as catalases (*ctl-2* and *ctl-3*), MnSOD (*sod-3*) genes, and methionine sulfoxide reductase A (*msra-1*) in wild-type nematodes.

One of the mechanisms by which NIST may exert its toxicity and generate oxidative stress is via the presence of redox-cycling transition metals (Stohs and Bagchi, 1995; Kelly, 2003; Ghio et al., 2012). In *C. elegans*, MTs are up-regulated by glucocorticoids, oxidative stress and a variety of different heavy metals, such as cadmium, zinc, copper and mercury (Sato and Bremner, 1993; Andrews, 2000; Hughes et al., 2007; Hughes et al., 2009; Zeitoun-Ghandour et al., 2011). It has been suggested that apart from having a high affinity for binding heavy metals, MTs can also act as antioxidants (Zeitoun-Ghandour et al., 2011). To date, a large number of studies have focused into examining MTs responses on single metal toxicity, rather than complex metal mixtures. However, it has been shown that the expression of MTs can increase several fold during stress conditions, such as ambient PM exposure (Huang et al., 2009). In the present study, the role of nematode MTs in the protection against NIST induced oxidative stress was examined in more detail.

The qRT-PCR suggested that in wild-type nematodes the two MTs, *mtl-1* and *mtl-2*, are involved in conferring protection against NIST toxicosis, with the *mtl-1* transcript being slightly more responsive than *mtl-2*. It was anticipated that the examined transcripts would be more responsive in terms of their expression fold changes following exposure to NIST. It is possible that although NIST consists of a variety of different heavy metals, their overall toxic concentration may not be sufficiently high to exceed the threshold concentrations.

Co-exposure to an adjuvant, such as cadmium can enhance the response. This feature has been previously observed in PM co-exposure studies in both cultured epithelial cells

and rats to oil fly ash particles or carbon black (Kodovanti., 1998; Guo et al., 2009). To investigate whether this theory also holds true for nematodes exposed to NIST, a qRT-PCR assay was performed in worms co-exposed to NIST and cadmium and screened for changes in *mtl-1* expression level. Surprisingly, the transcription level of *mtl-1* was found to be greatly increased by the co-exposure of NIST and cadmium. Overall, this suggests that NIST toxicity may be increased by the presence of an adjuvant.

Oxidative stress generated by NIST can influence cells in a variety of ways, inducing protective as well as promoting injurious events (Stone et al., 2007; Ghio et al., 2012). The modest up-regulation of only a few phase II antioxidant genes did not allow the identification of major molecular mechanisms involved in the response to NIST exposure. In addition, any response could be expected to occur in a dose dependent manner, a feature which NIST particles failed to exhibit in a nematode model. One underlying reason might be subscribed to complex physicochemical characteristics of NIST particles (Oberdöster et al., 2005). The bioavailability of different chemicals and the cellular interaction of particles might differ between doses. Moreover, the majority of gene transcripts (involved in stress pathways) remain unchanged in NIST exposed wild-type, suggesting a tolerance towards the NIST insult, at least at the concentrations examined. However, if protection mechanisms are impaired or damaged, a greater sensitivity might be exhibited. Indeed, enhanced adverse health effects have been identified in susceptible parts of the population (such as asthmatics) (Pekkanen et al., 1997; Penttinen et al., 2001; WHO, 2004), as well as in susceptible models in rodents, involving instillation or inhalation to PM (Costa et al., 1997).

The concept of increased susceptibility to NIST exposure was investigated in hypersensitive nematode mutants bearing key mutations in PCS and MnSOD (*sod-3*) genes. Results suggest that both hypersensitive nematode mutants exhibited differential

transcript responses upon NIST exposure compared to the wild-type nematode, however the level of antioxidant gene expression (MTs and SODs) was not significantly increased. Interestingly, in the MnSOD mutant, catalases (*ctl-2* and *ctl-3*) and CuZnSOD (*sod-1*) were found to be decreased by NIST. As previously discussed, *C. elegans* has developed a very robust antioxidant defence mechanism to protect itself against oxidative, xenobiotic and environmental challenges (Back et al., 2012). Nevertheless, hypersensitive mutants are a powerful tool allowing the investigation and quantification of toxicogenomics of the chemical complex components of NIST.

Physicochemical characteristics can also be determinants of biological activity (Oberdöster et al., 2005; Schwarze et al., 2006; Valavanidis et al., 2008; Horie et al., 2012). Hence, to test how particle size can influence the NIST-driven activation of the antioxidant enzymes gene expression, worms were exposed to NIST supernatant (extract) that had undergone a filtration procedure, which removes all particles/residuals larger than 20 nm. Chemical analysis showed that the NIST extract exhibited a significantly lower concentration of metals compared to un-extracted NIST. Exposure to NIST extracts resulted in a significant down-regulation of both MTs, and *sod-1* expression, which is inverse to the trend observed in wild-type nematodes exposed to non-extracted NIST. Overall, these findings suggest that certain chemical constituents of NIST, other than metals or the particle size, are responsible for the down-regulation of the methallothionein genes.

5.4.5 Whole transcriptome response of *C. elegans* exposed to NIST 1648a

To date, numerous *C. elegans* studies have pint pointed the transcriptional responses following an exposure to chemical and physical stressors (Roh et al., 2009; Tyusko et al., 2012), however none have investigated the effect of NIST.

In this study, whole genome microarrays were utilized to identify transcriptional changes in NIST 1648a exposed *C. elegans*. The gene expression analysis provided an overview of the nematode molecular responses, and highlighted genes linked to NIST induced toxicosis.

Microarray analysis revealed that more genes were down-regulated, rather than up-regulated following a 48 hour NIST exposure. The gene ontology (GO) using DAVID, found that the most responsive genes in nematodes challenged to NIST were involved in organismal and organ development, and regulation of growth. Only 24 genes were significantly up-regulated > 1.5 - fold, in all NIST doses tested and were involved in oxidative phosphorylation (F59C6.5), and fatty acid biosynthesis (*fasn-1*) pathways; and TGF-beta (*daf-14*), and interleukin (*est-4*) signalling pathways. Persistent activation of these pathways suggests that NIST induces a mild proinflammatory response, which in turn may allow cells to cope with an oxidant insult. Some of the gene expression changes (e.g. TGF-beta signalling pathway, glycerolipid metabolism, and steroid hormone biosynthesis) have been previously reported to be deregulated in response to organic extracts from respirable air particles in human lung fibroblasts (Libalova et al., 2012).

NIST-concentration dependent (driven) variations in global transcriptional responses were identified by PCA (Fig. 5.15). Exposures to lower NIST concentrations (1 and 5

µg/mL NIST) may modulate responses that contribute to the wellbeing of the nematode, as significantly more genes were found to be up-regulated at lower NIST doses (> 2.0 - fold) (e.g. namely glutathione-S trasferase (*gst-21*), enolase (*enol-1*), helicase (*hel-1*), coenzyme Q (ubiquinone) biosynthesis (*coq-1*), cell division cycle (*cdc-42*), nuclear export receptor (*anc-1*), yeast Glc seven-like phosphatases (*gsp-1*)). The functional annotation, utilizing the DAVID clustering tool identified GO-biological pathways (BPs) involved in nematode development, positive regulation of growth, protein transport, and reproduction. Five out of 15 transcripts were linked to mitogen activated kinase (MAPK) signalling pathway, endocytosis, glycolysis/gluconeogenesis, RNA degradation, spliceosome, natural killer cell mediated cytotoxicity, progesterone-mediated oocyte maturation, and the lysosome.

The activation of some of these pathways suggested that the organic (soluble) fraction of NIST particles may be involved in these responses. It has been previously shown that exposure to DEP or PM triggers transduction pathways, including MAPK phosphorylation and NF-κβ (nuclear factor kappa-light-chain-enhancer of activated B cells) activation (Bonvallot et al., 2000). Increase in GST, and coenzyme Q (ubiquinone) biosynthesis also indicates an increased phase II antioxidant activity in the nematode that may provide protection against both the initiation and the propagation of lipid and protein oxidation.

Nevertheless, the overall effects of NIST on the nematode seemed to be characterized by transcriptional repression mechanisms, as indicated by the number of down-regulated genes (Table 5.2). The GO analysis of genes down-regulated by < 0.7 - fold identified molecular functions such as hydrolyse activity, pyrophosphotase activity, ATP binding, nucleoside binding, as well as metal ion binding. These 41 transcripts were all, regardless of the NIST dose, significantly down-regulated and involved in

glycosylate and dicarboxylate metabolism, endocytosis, and amino acid metabolism (e.g. histidine, tyrosine, etc.), nicotine degradation (*ugt-28*), Parkinson disease and Wnt signalling (C09B9.4) pathways.

Exposure to 20 and 50 µg/mL NIST had a significant impact on the global transcriptome (Table 5.2). Of the 104 transcripts identified to be differentially down-regulated in the 20 and 50 µg/mL NIST exposures, some were involved in molecular functions related to hydrolyse activity, pyrophosphotase activity, nucleoside binding, ATP binding, metal ion binding, cation and ion binding. Exposure to higher NIST concentrations also seemed to repress pathways involved in endocytosis, calcium and phosphatidylinositol (PI) signalling system, oxidative phosphorylation, and glycolysis / gluconeogenesis. In addition, pathways such as fatty acid and glycerophospholipid, amino-acid metabolism, glyoxylate and dicarboxylate metabolism, sugar (fructose and mannose) metabolism, pentose phosphate pathway were all significantly down-regulated. Striking was also the evidence of a transcriptional down-regulation of major cellular transcriptional processes, such as proteasome beta subunit (*pbs-1*), proteasome (helicase H20J04.4), ribosome (*rpl-18*, Y73B3A, *rpl-7A*), and spliceosome (*hrp-1*, and *sap-49*).

The mechanisms by which NIST seems to trigger nucleolar stress in nematodes is by inhibiting/or down-regulating the ribosomal RNA (rRNA). In general, overproduction of free radicals can damage the cellular compartments, thus resulting in progressive physiological dysfunction (e.g. decrease in reproductive output). Recent studies have shown that oxidative stress can induce mRNA and rRNA damage (Kong and Lin, 2010; Donatti et al., 2011; Suzuki et al., 2012). The oxidation of RNA is an early indicator of cellular pathogenesis that can interfere with translational processes and impair protein synthesis, which can result in cellular death. The non-coding rRNA is known to play a

critical role in pre-mRNA splicing, nonsplicing RNA modifications and translational regulation of mRNA (He et al., 2006; WormAtlas). Oxidized rRNA bound redox-active iron is increased in areas affected by Alzheimers disease (Honda et al., 2005), and those by mild cognitive impairment (Ding et al., 2006). Therefore RNA oxidation may be a common early event in the pathological cascade; impairment leads to decreased rRNA and hence, decreased protein synthesis capacity (Ding et al., 2005). In this study, the six most responsive targets were aligned to the 26S ribosomal RNA (*rrn-3.1*). In contrast to many other transcripts examined, the transcriptional response of *rrn-3.1* was found to be highly reproducible.

New biomarkers can help in predicting the effects of survival, reproduction, or growth, endpoints that control population sizes of organisms. In some cases, these bookmakers are unique to the chemical exposure, while other biomarkers were associated with impaired biological processes or molecular functions. In summary, the microarray data show that NIST affects the expression of some genes, however pro- and anti- oxidants, initially hypothesized to be highly inducible were not prominent in their response.

5.4.6 The key endpoints of the nematode life cycle following NIST 1648a exposure

To date, population based epidemiology studies have linked PM toxicity (such as pulmonary and cardiovascular effects), with either environmental (Miller et al., 1993; Dockery et al., 1993; Schwartz, 1994; Samet et al., 2000; Ma and Ma, 2002; Lodovici and Bigagli, 2011) or occupational (Harber et al., 2003; Inoue and Takano, 2011; Hailemariam et al., 2012) exposures. The mechanisms underlying the pulmonary and cardiovascular effects of PM have been studied in the laboratory setting, and the notion

of PM-induced acute/chronic cellular injury and inflammation has been established (Schwarze et al., 2006; Ghio et al., 2012). For example, human chamber studies have reported that short term exposure to PM can lead to an acute inflammatory effect on human airways (Kelly, 2003; Schwarze et al., 2006). This effect has been found to be exacerbated in susceptible parts of the population, e.g. asthmatics, where an acute exposure to PM may promote allergic sensitization and trigger an asthmatic attack (Pekkanen et al., 1997; Penttinen et al., 2001; WHO, 2004). In addition, repeated acute responses tend to lead to cumulative effects, which might result in a chronic disease status. Chronic PM exposures are believed to affect human health, however they are typically difficult to assess within a well-controlled environment (Valavanidis et al., 2008). Instillation studies in animals have shown that there is an increased risk and that chronic PM exposure could interfere with pulmonary clearance, hence lead to particle translocation and deposition to extrapulmonary tissues and cause, e.g. blood coagulation and systemic inflammation through the action of cytokines and other soluble mediators (Ferin et al., 1992; Donaldson et al., 2001).

In order to explore different pollution scenarios and the link to epidemiological evidence, there is an increased need for providing more toxicological information on both short- and chronic- effects of environmentally relevant PM exposures (Oberdöster et al., 2006; Wild et al., 2008). This information will allow a more targeted approach towards reducing emissions of compounds/particulates. Nevertheless, the utility of PM toxicity in the nematode model organism has yet to be convincingly demonstrated. In this study, wild-type nematode growth was used as one of a life-cycle trait to assess the toxic effect elicited by NIST. An acute, 24 hour liquid exposure of wild-type L1 larvae, to NIST did not induce any significant toxic effects on final nematode body size. The lack of nematode response to NIST within the exposure may have been due to the

physicochemical characteristics of NIST within the M9 exposure solution (Nel et al., 2009). It is possible that the presence of potassium and sodium salts within M9 quenches the toxicity of heavy metals (Cd, Pb, Cu, Hg, etc.), a notion previously described by Donkin and Williams, 1995. Thus, the low toxicity observed after a 24 hour exposure to NIST may not be surprising.

Increasing the exposure duration (rather than concentration), and changing the delivery method, resulted in more profound outcome effect. Repeat acute exposures can lead to cumulative effects, which manifest as a chronic disease, a feature that has been observed following long-term exposure to relatively low concentrations of PM in rats (Lippmann et al., 2005a/b; Fanning et al., 2009) and DEP (Mauderly et al., 1987). Toxicology and epidemiology rely on dose/response relationships, a concept that has been described in detail elsewhere (Oberdörster et al., 2005; Fanning et al., 2009, Russell and Brunekreef, 2009).

It is important to note that susceptible individuals can show completely different response slopes e.g. asthmatic human are more prone to PMs toxicity (Pekkanen et al., 1997; Penttinen et al., 2001; WHO, 2004). In this study, the nematode mutants with mutations in metallochelators have severely impaired life-history endpoints, such as reproduction, when exposed to heavy metals (Hughes, et al 2009). Given that NIST is composed of heavy metals, a metal hypersensitive nematode *mtl-1;mtl-2;pcs-1*(zs2) mutant strain was initially chosen to investigate a change in sensitivity towards NIST toxicosis.

Switching to a bacterial vehicle for particle delivery to the nematodes allowed chronic exposures to NIST and the subsequent assessment of life-cycle endpoints. Exposure to NIST conducted with wild-type and the *mtl-1;mtl-2;pcs-1*(zs2) strain provided evidence that NIST influences the reproductive output of both nematode strains, but has no

significant effect on their body size. Exposure to nanoparticles has previously been shown to reduce the brood size of nematodes (Roh et al., 2009; Pluskota et al., 2009; Hsu et al., 2012), possibly due to the particle-mediated generation of ROS. It is interesting to note that although brood size was reduced by NIST exposure, the effect was not NIST concentration dependent. This may be explained by the time-dependent release of different transition metals from NIST and the accumulation rate of particle agglomerates.

In this study, the effects on organismal life-span were examined following acute (48 hour) and chronic exposure to NIST. The wild-type nematode survival was not affected by acute NIST exposure; however, a significant reduction in median life-span was observed in chronically exposed nematodes. In contrast, survival of the metal hypersensitive triple knockout *mtl-1;mtl-2;pcs-1*(zs2) was not found to be exuberated by chronic exposure to NIST. The absence of effects may have been the result of the mutants' short life-span (even in control conditions), and due to a low number of worms examined. In addition, NIST particles seemed to accumulate in the nematode intestines in chronic exposures (Appendix: NIST 1648a). Particle accumulation represents a physical stress/constraint or internal pressure, which can contribute to a decrease in nematode survival (Pluskota et al., 2009; Hsu et al., 2012). Life-history studies utilizing wild-type and *mtl-1;mtl-2;pcs-1*(zs2) mutant strain provided proof that chronic exposure to NIST exerts a toxic effect, which manifests itself in reduced reproduction and survival. Whether the suggested toxicity can be attributed primarily to NIST metals, remains elusive.

In general, dysfunction in any of the antioxidant enzymes can disturb the balance of the endogenous ROS pool and thus result in oxidative stress and inflammation (Harman, 1956; Sies, 1991). Whether an increased susceptibility to NIST is observed in

individuals carrying key mutations in antioxidant superoxide radical scavengers, *sod-1*, *sod-2*, and *sod-3* mutants were examined. The chronic exposure of SOD mutants to NIST elicited a minor increase in *sod-1* and *sod-2* body size, which suggested that the overall toxicity was low. Although, SODs play an important protective role in scavenging free radicals, several studies have shown that they are not essential for life (Doonan et al., 2008; Van Raamsdonk and Hekimi, 2011). Given that nematodes poses additional antioxidant systems (Back et al., 2012), it is difficult to evaluate the direct contribution of each SOD isoenzyme in scavenging ROS upon NIST induced toxicosis.

Exposure to atmospheric pollutants can cause the activation of different signalling pathways that control cellular redox homeostasis, such as the nuclear factor erythroid 2-related factor 2 (Nrf2) (Li et al., 2004; Rubio et al., 2010). Although each pollutant has its own mechanism of toxicity, PM is known to act as a potent oxidant that can trigger and promote many redox-sensitive pathways to exert its toxic effects (Brunekreef and Holgate, 2002). In response to oxidative stress, the transcription factor Nrf2 binds to the ARE and regulates the expression of numerous cytoprotective genes that function in ROS detoxification, thus providing protection against damage (Kang et al., 2005). The activation of the Nrf2 pathway could therefore be crucial in providing protection against PM-induced oxidative DNA damage (Rubio et al., 2010, Li et al., 2000). Studies in animals have shown that mutations in the Nrf2 binding site can result in the loss of response to oxidative stress caused by DEP exposure (Pourazar et al., 2005; Bauling et al., 2003). Findings also reported that exposure to DEP activated nuclear localization of Nrf2 and increase in total Nrf2 protein concentration; however no changes were observed at the mRNA level, which may have been the result of the posttransductional modification of Nrf2 (Li et al., 2004; Pourazar et al., 2005; Bauling et al., 2003). In addition, exposure to PAHs has also been correlated to an increase in Nrf2 activation

and phase II enzyme induction (Ramos-Gómez et al., 2001 and 2003; Fahley et al., 2001). PM exposure can cause an activation of the Nrf2 pathway, hence it was deemed important to investigate and demonstrate whether the worm homolog of Nrf2, SKN-1, plays an equally important role in NIST induced responses.

In *C. elegans*, the SKN-1 pathway is linked to antioxidant genes and phase II genes involved in stress-tolerance and longevity (Tullet et al., 2008). Some of these genes include the activation of antioxidants, such as *gcs-1*, NQO1, GSTs, and SOD (An and Blackwell, 2003). Studies have shown that loss of function mutations in *skn-1* can result in a decrease in nematode life-span, when exposed to oxidative stressors, such as for example paraquat (An and Blackwell, 2003). To test whether SKN-1 is involved in early stages of ROS induced damage by NIST exposure, a null allele mutant strain was utilized. The *skn-1*(zu67) mutant strain exhibits, under control conditions, a similar phenotype as the wild-type strain (An and Blackwell, 2003). However, on acute exposure to NIST, the *skn-1*(zu67) nematode exhibited a decrease in body size, reproduction, and life-span. An acute exposure to low concentrations of NIST (3.123 and 6.25 µg/mL NIST) resulted in more severe effects on worm survival than higher NIST concentrations, which suggests that SKN-1 might be a marker for low-dose threshold sensitivity to NIST exposure. This is supported by the microarray analysis, which identified that the *skn-1* transcript was up-regulated (in wild-type nematodes) at lower NIST concentrations (2.6 - fold up at 1 µg/mL NIST). Given these findings, it is tempting to suggest that the function of SKN-1 in worms may be involved in early signalling and stress-response pathways providing protection against NIST induced oxidative cellular damage.

5.5 Conclusion

Taken together, it is currently not possible to precisely quantify the contributions from different sources and different NIST 1648a components to systemic nematode responses to NIST toxicity. Nevertheless, in this study it has become apparent that acute exposure to NIST does not affect wild-type nematode development or life-span, however it does have a significant effect on SKN-1 mutants. In addition, chronic exposure to NIST exerts a mild toxic response in wild-type, and the metal hypersensitive *mtl-1;mtl-2;pcs-1*(zs2), as well as the oxidative stress sensitive *sod-1*(tm766), *sod-2*(gk257), and *sod-3*(tm760) strains. The DCFH-DA assay provided *in vitro* evidence of the oxidative potential of NIST, as the intracellular total endogenous ROS levels were found to be increased in wild-type and the SKN-1 mutant. NIST-mediated activation of the cytochrome P450`s *cyp35A2* transcript, and the *gcs-1* transcript, highlighted key changes at the transcriptional level. Furthermore, the gene expression analyses provided evidence of the transcriptional up-regulation of metallochelator transcript (*mtl-1*), which is possibly driven by NIST metals and particle - organic complexes.

The whole genome and qPCR analyses suggested that the majority of transcripts involved in stress response pathways, development, and reproduction were down-regulated by elevated NIST concentrations. This may be due to NIST triggering a nucleolar stress on nematodes by inhibiting/or down-regulating the ribosomal RNA (rRNA). In addition, the low level of toxicity observed in nematode strains subjected to chronic NIST exposure can be explained by the time-dependent agglomeration of NIST particles, the rate of metal dissolution from the particle core and bioavailability, as well as the high threshold level to xenobiotic stressors. Results suggest that the use of hypersensitive nematode mutants in combination with toxicogenomic, and imaging

techniques, represent a powerful tool to assess the NIST induced metal toxicity and oxidative stress.

CHAPTER SIX

General discussion

6. 1 Introduction and significance of this work

We are daily exposed to billions of toxic particles surrounding us, and in the future this number will only increase. However, there are currently no comprehensive guidelines which encompass the relationship between NP exposure threshold levels and hazardous effects. It is of paramount importance to identify specific minimum/maximum exposure values. In order to provide toxicological evaluations on substances of public and environmental health concern, improved toxicology methods need to be developed, that are sensitive, specific, and rapid (Arora et al., 2012; Meng et al., 2009; Xia et al., 2009). The generated data has to be validated, interpreted, and stored (in an accessible format) to strengthen the science-base of risk assessments.

Toxicogenomics, or the application of gene expression analysis is a relatively new route/approach that is being embraced in the field of pharmaceutical science to investigate the safety of potentially toxic materials (Meng et al., 2009; Euling, 2013). By using genomics or other high- throughput molecular profiling technologies (e.g. transcriptomics, proteomics, or metabolomics) it is possible to elucidate which pathways and molecular networks are affected by chemical exposures and pint-point new predictive molecular biomarkers. Hence, employing toxicological tests to evaluate NPs are an indispensable tool to the field of nanotoxicology science (Thomas et al., 2011; Meng et al., 2009; Arora et al., 2012). Toxicological approaches can integrate both mitigating and harmful effects and thus provide understanding of the net influence of compounds in the given experimental condition. Therefore, toxicogenomic strategies

may help to develop new predictive models and exposure guidelines that will allow a fast approach in identifying human and environmental health hazards, and to identify rapid and precise molecular biomarkers of nanomaterials.

In order to address the multi-dimensional chemical and physical nature of NPs (such as their size, shape, solubility and aggregation), highly developed analyses are demanded (Nel et al., 2006; Nel et al., 2009). Therefore, a simple model organism that is amenable to comprehensive experimental analysis can serve as an excellent model tool to elucidate the molecular genetic architecture of complex traits (Thomas et al., 2011). The invertebrate *C. elegans* as a biological model organism has, to date, not been exploited as a screening tool for evaluating the toxicity of natural particulate matter (PMs), but was previously used to examine synthetic NPs (Kim et al., 2008; Wang et al., 2009; Pluskota et al., 2009) as well as metal oxide NPs (Wu et al., 2013; Khare et al., 2011; Ma et al., 2011; Ma et al., 2009; Wang et al., 2009). Advantage of utilizing worms is that they allow fast and efficient wide array of different genetic analysis to be performed in an automated, quantitative, and reproducible manner. In addition, they are less complex, thus having a lower level of redundancy in gene regulation, which can facilitate the identification of new regulatory pathways and pint-point biomarkers involved in detoxification processes (Kaletta and Hengartner, 2006; Lant and Storey, 2010; Shaye and Greenwald, 2011). Functional assays, such as changes in gene expression (either by single target approaches by qPCR and whole genome screening), DNA damage, immunogenicity, oxidative stress, or viability assays can be performed relatively easily. Overall, its simplicity and invariance make them a perfect whole model organism for obtaining information on potential safety of the nanomaterials (Leung et al., 2008).

The challenge of this present study was to investigate the applicability of the *C. elegans* model to study modes of toxic action of synthetic and natural ambient NPs. One of the central goals of this research was also trying to understand how different types of NPs can induce genotoxicity in nematode cells and to investigate similarity of these pathways. For this reason the same type of assays and analyses were frequently repeated for the different types of nanoparticles used in this study. Based on the preliminary results presented here, it was possible to draw up several conclusions regarding three contrasting particles, namely zinc oxide (ZnO) NPs, Carbon Black (CB) M120 particles and urban particulate matter (PM) NIST 1648a.

6.2 Major findings-summary of individual chapters

6.2.1 ZnONPs induce oxidative DNA damage and apoptosis in nematodes

Zinc oxide nanoparticles (ZnONPs) are widely used in consumer products, paints, food industry, and have been shown to induce both *in vitro* and *in vivo* cytotoxicity, genotoxicity and carcinogenic responses. The current understanding of the paradigm for ZnONP cytotoxicity is that ZnONPs undergo endocytosis into the cells, dissolve into bioavailable zinc and cause oxidative stress. Studies have also shown that the pathway of cytotoxic induction is cell-specific and can selectively induce apoptosis, which is likely to be mediated by reactive oxygen species via the p53 pathway (Wu et al., 2010; Sharma et al., 2009; Ahamed et al., 2011; Sharma et al., 2012).

Table 6.1: Summary of ZnONPs-responsive transcripts expression in wild-type nematodes. Arrows indicate a decrease (↓) in blue, or increase (↑) in red, in the transcript expression. The numbers of arrows rank the relative amount of transcript induction, in response to the particle exposure.

Genes	ZnONPs (5 mg/L)	ZnONPs (50 mg/L)
mtl-1	↑	↑↑
mtl-2	N/A	↑
pcs-1	N/A	↑
ctl-2	↓	NO change
ctl-3	↑	NO change
sod-1	NO change	↑
sod-3	↑	NO change
prdx-3	NO change	NO change
hsp-16.1	↓	↓↓
dct-1	↑↑	↑
cep-1	↑	↑↑

The present study revealed that ZnONPs induce a significant oxidative DNA damage using the qPCR method even at concentrations as low as 5 mg/L (Table 6.1). Corresponding increases in apoptotic markers *cep-1* and the *dct-1* were observed following a ZnONPs challenge (Fig. 3.7), which highlighted the carcinogenic potential of ZnONPs in worms. This could be attributed to the increased expression of metallothioneins (*mtl-1* and *mtl-2*) (Fig. 3.4 and 3.7A), and phytochelatins (*pcs-1*) (Fig. 3.4), thereby suggesting that ZnONP exposure and apoptosis may be interlinked, possibly through the generation of ROS (Fig. 6.1).

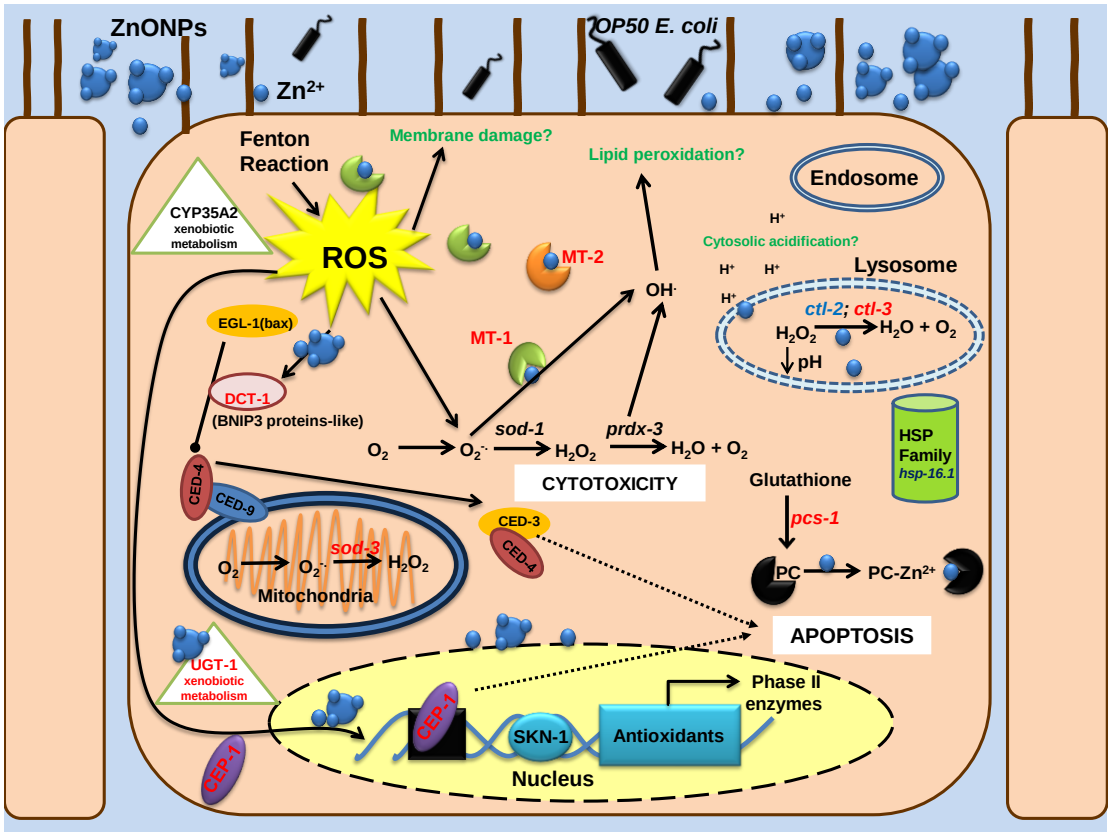

Fig. 6.1: Schematic illustration of molecular pathways affected in worms for ZnONPs stress in intestinal epithelial cell. Information about highlighted proteins and enzymes gathered from published articles on Zn and ZnONP toxicity, and were related to the molecular pathways identified in this study. Red colour indicates an increase, and blue a decrease of expression in response to ZnONP exposure. CED-3, initiator caspase; CED-4, caspase activator; CED-9, anti-apoptotic Bcl-2 family; CEP-1, *p53*-like protein; CTL, catalase; CYP, cytochrome P450 family; DCT-1, BNIP3 proteins-like; EGL-1, pro-apoptotic Bcl-2; HSP, heat shock proteins; MTs, metallothioneins; PC, phytochelatin; PRDX, peroxidoxin; ROS, reactive oxygen species; SKN, nuclear factor erythroid-derived 2-like; SOD, superoxide dismutase; UGT, UDP-glucuronosyl transferase.

ZnONPs exposure was shown to decrease growth and development, reproductive capacity, and lifespan (Table 3.2 and 3.3). Although, the exposure to ZnONPs was not lethal to nematodes, it suggested that the overall toxicity was relatively low. Indeed, this

may be explained by the time-dependent dissolution of ZnONPs to release ionic Zn (see Appendix: ZnONPs), thereby reducing the accumulation rate and toxicity (Franklin et al., 2007; Poynton et al., 2011).

The moderate, nevertheless toxic effects were amplified in the triple metallochelator knockout strain (*mtl-1;mtl-2;pcs-1*(zs2)) (Table 3.2 and 3.3), suggesting that metallochelators may indeed be important in conferring a protective role in ZnONP induced toxicosis. The DCFH-DA assay provided *in vitro* evidence of the increased oxidative potential of ZnONPs in the metal exposure sensitive triple mutant (Fig. 3.8). Subsequently, a nematode based biosensor platform system, which utilizes age synchronized MoSCI integrated transgenic nematode strains identified at elevated ZnONP concentrations a strong transcriptional responses in *ugt-1* transcript (Fig. 3.5). This finding suggested that ZnONPs are likely to be implicated in the process of glucuronidation, which presents a major part of phase II metabolism in cells.

Furthermore, the biomolecular phenotype was significantly altered in the metal sensitive knockout worm upon ZnONPs exposure, where changes in worm biomolecules such as proteins, amino acids (cytochrome c, amide I, phenylalanine) and nucleic acids were observed (Fig. 3.12 and 6.2). These highlighted both cytotoxic and apoptotic cellular damage to be present in worms exposed to ZnONPs, and that the metallochelators are instrumental in the protection against cytotoxic damage.

Overall, the toxicogenomic and spectroscopic strategies identified the importance of metallochelators in the protection from ZnONP induced toxicity. However, which of the three genes (in isolation or combination) drives the observed susceptibility towards ZnONP remains to be defined. Individuals (genotypes) housing mutations in key metallochelators, are more susceptible to ZnONP toxicosis.

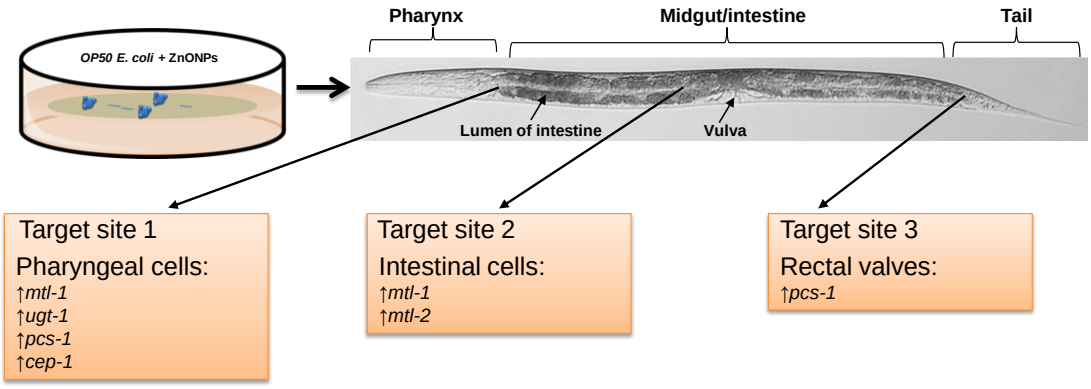

Fig. 6.2: Summary of worm target sites where changes in the worm biomolecular phenotype were identified in response to ZnONPs. Arrows indicate ZnONP-mediated increase (↑) or decrease (↓) in transcript expression, respectively.

6.2.2 Carbon Black (CB) M120 nanoparticles induce an oxidative response in nematodes via ROS and cytochrome P450 xenobiotic metabolism

Carbon Black (CB) M120 nanoparticles exerted a different type of cytotoxic damage on worms than metal-based ZnONPs and NIST. Consumed CB NPs were found to be distributed and accumulated throughout the entire worm body, rather than at a certain worm tissue target sites (see Appendix: Carbon Black M120). Some minor fluctuations were observed in transcripts expression of *hsp-16.41*, *hsp-16.2*, and *gst-38* in MoSCI transgenic strains on CB exposure, but there were not statistically significant (Fig. 4.6).

The major findings identified in this study were the increase in *cyp-35A2* expression (Fig. 4.5 and 6.3), and the reduction in worm fertility (Fig. 4.10), in response to CB NPs exposure. Cytochrome P450 is a well known phase I enzyme involved in xenobiotic biotransformation in vertebrates (Menzel et al., 2005; Roh et al., 2010), hence changes

in cyp35A2 transcript, highlights a novel/possible metabolic pathway in *C. elegans* CB NPs detoxification. Reduction in worm fertility could be explained as a part of defence system and/or compensatory mechanism to metabolize the toxicity induced by CB, and may be linked to an increased cyp35A2 gene expression.

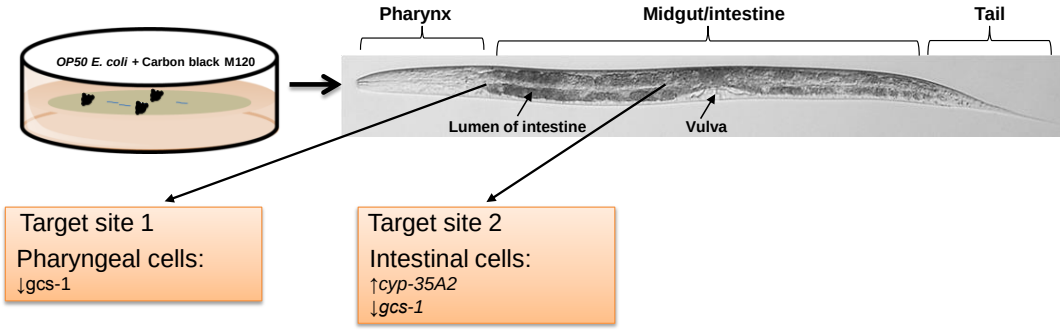

Fig. 6.3: Summary of worm target sites where changes in the worm biomolecular phenotype were identified in response to Carbon Black M120. Arrows indicate a CB NP- mediated increase (↑) or decrease (↓) in transcript expression, respectively.

There was no effect on nematode growth, when worms were subjected either to acute (Fig. 4.8), or chronic CB exposures (Fig. 4.9). Minor toxicity on worm development were observed in the triple metallochelator knockout strain (*mtl-1;mtl-2;pcs-1*(zs2)) (Table 4.2), and oxidative stress mutants (*sod-1*(tm776) and *sod-2*(gk257)) (Table 4.3), which most likely resulted due to failure of particle clearance, increased build up, inflammation, and ROS production (Fig. 6.4).

Indeed, DCFH-DA assay confirmed the increase in the endogenous ROS pool to be specific to wild-type and metal hypersensitive nematode strains, but not to any of the SOD mutants (Fig. 4.7). The resulting increase in ROS generation to higher CB concentrations could be contributed to nematodes suffering from a particle "overload"

phenomena, which gave rise to worm vulval damage and decreased reproduction (Fig. 4.10). Overall, results suggest that CB exposure had very little effect on either wild-type, or any of the mutant (metal hypersensitive, or the oxidative stress sensitive SOD) strains.

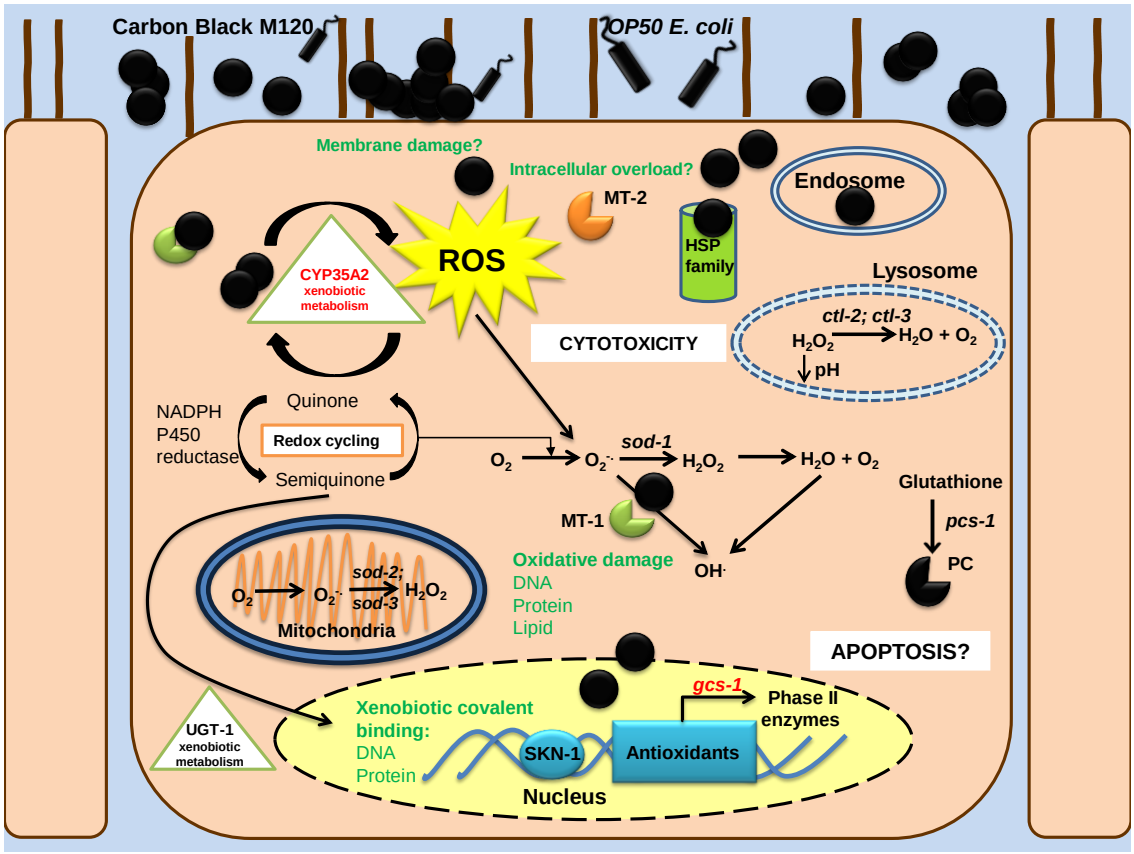

Fig. 6.4: Schematic illustration of molecular pathways affected in intestinal epithelial cells of worms challenged with CB M120 NP. Information about highlighted proteins and enzymes were gathered from published articles on CB toxicity, and were related to the molecular pathways identified in this study. Red colour indicates an increase, and blue a decrease of expression in response to CB NP exposure. CTL, catalase; CYP, cytochrome P450 family; DCT-1, BNIP3 proteins-like; GCS, gamma glutamylcysteine synthetase; HSP, heat shock proteins; MTs, metallothioneins; NADPH, nicotinamide adenine dinucleotide phosphate; PC, phytochelatin; PRDX, peroxidoxin; ROS, reactive oxygen species; SKN, nuclear factor erythroid-derived 2-like; SOD, superoxide dismutase; UGT, UDP-glucuronosyl transferase.

6.2.3 NIST 1648a induces an oxidative stress response via SKN-1 transcription factor, and triggers a nuclear stress via rRNA deregulation in nematodes

Exposure to natural and man-made combustion derived PMs (e.g. metals, PAHs, organic components and certain toxins) present an adverse risk factor to both the environment and human health. In this study, NIST 1648a (a representative PM) was examined for its toxicity on wild-type, metal hypersensitive and oxidative stress sensitive nematode mutants.

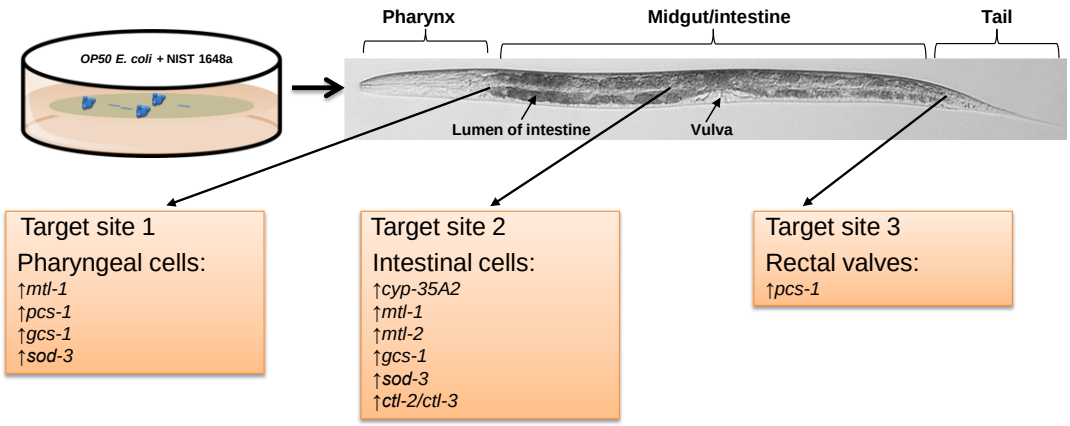

Fig. 6.4: Summary of worm target sites where changes in the worm biomolecular phenotype were identified in response to NIST 1648a. Arrows indicate NIST-mediated increase (↑) or decrease (↓) in transcript expression, respectively.

The DCFH-DA assay provided *in vitro* evidence of the oxidative potential of NIST, as the intracellular total ROS levels increased (Fig. 5.7). The toxic effects were amplified in the *skn-1*(zu67) mutant strain, suggesting that the Nrf transcription factor may indeed play an important role in the early antioxidant protection mechanism against NIST induced toxicosis (Fig. 6.6).

The results indicate that once NIST enters the worm, it exerts a minor toxic response that is primarily manifested by a decreased reproduction potential (Fig. 5.22), an effect

that was more significant in nematode mutant strains (particularly *skn-1*(zu67)) (Table 5.9 and 5.12). However, the toxic effects were not NIST concentration dependent. Chronic exposure to elevated NIST concentrations resulted in reduced worm survival (Fig. 5.23B), which could be attributed to stress induced by free metals and to particle overload. Indeed, an increased intestinal accumulation of NIST particles caused physical damage (see Appendix: NIST 1648a and Fig. 6.5), which manifested in a bag of worms phenotype and pre-mature death of the metal hypersensitive mutant strain (*mtl-1;mtl-2;pcs-1*(zs2)) (Fig. 5.23C).

The whole genome and qPCR analyses provided evidence that the majority of transcripts involved in stress response pathways, development and reproduction were down regulated with increasing NIST concentrations (Table 5.2). There was evidence of mild proinflammatory response triggered by NIST at all concentrations examined (Table 5.3). Furthermore, at elevated NIST concentrations there was also an increased expression in *cyp-35A2* and *gcs-1* transcripts identified to be involved in detoxification of NIST (Fig. 5.6). Nevertheless, the most profound effects identified were the down regulation of ribosomal RNA transcript (*rrn-3.1*) with increasing NIST concentrations (Fig. 5.19), suggesting that damage to be nucleus place.

These results suggest that hypersensitive nematode mutants can be used to assess the NIST induced metal toxicity and oxidative stress. Overall, the functional genomic tools are valuable to investigate and quantify (the contributions from metal oxides and organic components) to systemic responses to PMs toxicosis.

The gene expression analysis identified that certain transcripts play a role in the early stages of ROS induced damage by NIST exposures, namely: *mtl-1* and-*2*; *sod-1*,*-3*, and *-5*; *gsr-1*; *hsp-16.1*; *aco-1*; *clec-13*; and *sdz-24* (Table 6.2).

Table 6.2: Summary of NIST 1648a-responsive transcripts in wild-type nematodes validated by microarray and confirmed by qPCR. Arrows indicate a decrease (↓), or increase (↑), in the transcript expression. The numbers of arrows rank the relative amount of transcript induction, in response to the particle exposure.

Genes	NIST 1648a (5 mg/L)	NIST 1648a (50 mg/L)
mtl-1	↑↑	↑
mtl-2	↑	↑↑
ctl-2	↑↑	↑
ctl-3	↑↑	↑
sod-1	↑	↑
sod-2	NO change	NO change
sod-3	↑↑	↑
sod-5	↑	↓
gsr-1	↑	NO change
hsp-16.1	↑	↓
cep-1	↓	↓
ftn-1	NO change	↓
aco-1	↑	↑
rrn-3.1	↓	↓↓
gei-7	NO change	NO change
unc-68	NO change	NO change
clec-13	↑	↑
skn-1	NO change	NO change
sdz-24	↑	↑

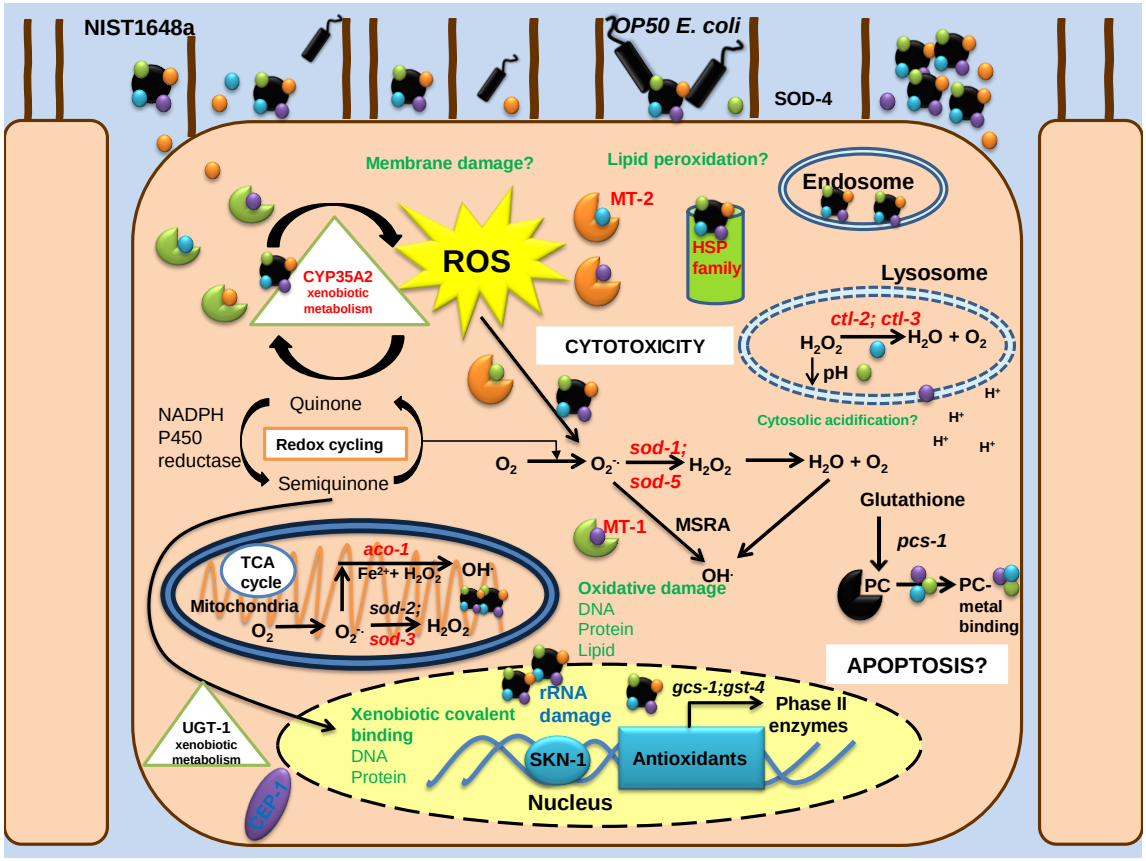

Fig. 6.5: Schematic illustration of molecular pathways affected in intestinal epithelial cells of worms challenged with NIST 1648a. Information about highlighted proteins and enzymes were gathered from published articles on PM toxicity, and were related to the molecular pathways identified in this study. Red colour indicates an increase, and blue a decrease of expression in response to NIST exposure. ACO-1, aconitase; CEP-1, *C. elegans p53*-like protein; CTL, catalase; CYP, cytochrome P450 family; GCS, gamma glutamylcysteine synthetase; GST, glutathione S-Transferase; HSP, heat shock proteins; MSRA, a methionine sulfoxide-S-reductase; MTs, metallothioneins; NADPH, nicotinamide adenine dinucleotide phosphate; NIST, National Institute of Standards and Technology; PC, phytochelatin; ROS, reactive oxygen species; rRNA, a 26s/28s ribosomal RNA; SKN, nuclear factor erythroid-derived 2-like; SOD, superoxide dismutase; TCA cycle, the tricarboxylic acid cycle; UGT, UDP-glucuronosyl transferase.

6.3 Comparison of nanomaterial toxicity in *C. elegans*

6.3.1 Particle behaviour in biological test media can play an important role when examining (for different type of) NPs toxicity in *C. elegans*

Before worm experimentation, NPs were characterized for their behaviour in different media. Detailed physicocharacteristics (particle primary size, hydrodynamic diameter when suspended in OP50 bacteria, and pH) of the NPs is provided in the Table 6.3. ZnONPs were of the smallest primary particle size, followed by the CB M120. Unfortunately, due to its complex mixture of elements, NIST primary particle sizes were not available for the powder form. However, the Standard Reference Material (SRM) particle size distributions once suspended in aqueous solution, were according to the NIST Certificate of Analysis, namely within the 100 nm-100 µm range.

The experimental data confirmed that particle size, surface area and composition are important features. Once particles are released into the environment, bioavailability (single or bound to other particles), charge, quantity, toxicity, and sedimentation speed can vary considerably (Auffan et al., 2009; Nel et al., 2009; Smita et al., 2012). For example, oxidisable metals such as ZnO can, once introduced into exposure media (e.g. water/or organic matter), release ionic Zn via a dissolution effect (Xia et al., 2008; Schilling et al., 2010) (see Appendix: ZnONPs).

Dosing, media pH, maintenance, and preparation of the NPs within the test medium are also deemed to be important factors when evaluating the toxicity effects of particle exposure in the screening system (Oberdörster et al., 2005; Krug and Wick, 2011; Aorora et al., 2012). Therefore, to ensure that the screening system resembles a realistic

and relevant environmental condition, only physical methods were applied to create homogenous synthetic/natural NP dispersions.

One of the major challenges is that NPs can change their aggregation status when they are transferred from the solvent stock solution to the exposure matrix (food or saline solution), which frequently contains a high percentage of organic matter (Nel et al., 2009; Auffan et al., 2009). For example, the addition of particles to the M9 test solution (Hitchcock et al., 1998), which is primarily composed of sodium and potassium salts, results in the formation of crystal aggregates on particle surfaces via salt-particle interactions. Salty crystals can play an important role in obscuring and/or inhibiting the metal-driven toxicity of NPs (Donkin and Williams, 1995).

In the test media, particles were found to exist in individual and agglomerated states (Fig. 3.1 and 4.1). Once in M9 test medium, the size range of NIST and CB particle aggregates were comparable (Table 6.3), regardless to their different primary sizes and chemical composition. However, after a 24 hrs incubation time in OP50 medium all three types of NPs displayed different agglomerate size ranges (Table 6.3). ZnONPs were found to agglomerate the most (500-1100 nm in size range), followed by CB NPs (50 - 900 nm), and finally NIST particles, whose agglomerates were in the range of 50 - 550 nm. These results are well aligned with the study by Wang et al., (2009), who reported considerable particle aggregation and wide particle size distributions of 478 - 980 nm for 20 nm ZnONPs.

Table 6.3: Physicochemical characteristics comparison of ZnONPs, Carbon Black M120, and NIST 1648a.

Comparative physicocharacteristics	Particle type		
	ZnONPs	**MONARCH® 120 (M120) Carbon Black (CB)**	**NIST (SRM) 1648a**
Primary particle size	30 nm	75 nm	N/A for dry powder
Malvern Mastersizer 2000 particle size analyzer	N/A	N/A	Particle size distributions in SRM 1648a: 100 nm-100 µm
Nanosight **NPs size range in M9 test medium**	N/A	50 - 350 nm	50 - 432 nm
Nanosight **NPs size range in OP50 medium**	N/A	50 - 900 nm	50 - 550 nm
Dynamic light scattering (DLS)	500 - 1100 nm	N/A	N/A
OP50 *E. coli* media pH changes with NPs	~pH7	~pH7.4	~pH7.4

Indeed, the dimension of aggregates can condition the uptake and deposition rate of the particles once presented to the nematode (Oberdörster et al., 2005; Pluskota et al., 2009; Mohan et al., 2010). Particle agglomerate stability over time and their role in toxicity are important features, which in future should be examined in greater detail. It is also important to note that there is a question of reproducibility of each analysis performed, as for example, low concentrations of polymorphic particles can exhibit a range of

particle sizes, which could only be thoroughly and reproducibly analysed if the analysis period was increased (Li et al., 2011; Mudunkotuwa et al., 2012; Kao et al., 2012).

6.3.2 Nanoparticles are able to affect the bacteria OP50 *E.coli*

Using bacteria as a vehicle to deliver NPs to nematode presents another challenge that needs to be carefully examined prior to any toxicology screen (Saier, 1998; Muñoz-Elías and McKinney, 2006; Li et al., 2011). Therefore, bacterial growth was monitored in the presence and absence of particles (Table 6.4). Whilst NIST 1648a did not cause an effect on bacterial growth (Fig. 5.4), the addition of CB M120 seemed to increase bacterial growth significantly (Fig. 4.4). In contrast, high levels of ZnONPs exhibited an inhibitory effect on bacteria growth (Fig. 3.3). It is conceivable that the carbon components in CB represent a source of energy to the bacteria, thereby promoting superior bacterial growth (see Appendix: Carbon Black M120); in contrast ZnO had an antibacterial effect and may ultimately induce caloric restriction in nematodes (Fig. 3.1E).

The antibacterial effect of low ZnONP concentration (60 mg/L) was reported before (Dutta et al., 2013). In their study it was suggested that the toxicity may have resulted due to higher ROS generation and lipid peroxidation, which subsequently damaged the *E.coli* cell membrane. Indeed, in this study ZnONPs adherence on *E. coli* cell wall and bacterial secretion of extracellular substance within 24 hrs timeframe was observed by TEM.

Table 6.4: The toxic dose range used in ZnONPs, CB M120, and NIST 1648a worm and *E.coli* studies, and comparison of different particle effects upon OP50 *E.coli* bacterium.

	Particle type		
	ZnONPs	**MONARCH® 120 (M120) Carbon Black (CB)**	**NIST (SRM) 1648a**
Dose ranges applied in the worm toxicity study	0-50 mg/L	0-50 mg/L	0-50 mg/L
Dose range applied in OP50 *E.coli* bacterium toxicity study	0-100 mg/L	0-100 mg/L	0-100 mg/L
Particle effects upon OP50 *E.coli* bacterium	Reduced bacteria growth at 100 mg/L ZnONP concentration	Increased bacteria growth at 50 mg/L CB concentration	No effect on bacteria growth

Besides bacteria, toxicity of ZnONPs to other microorganisms, such as yeast *Saccharomyces cerevisiae*, has also been reported and showed that 24 hrs ZnONPs (50–70 nm) exhibit a EC50s of 131 and 158 mg/L, respectively (Kasemets et al., 2009). In a recent review by Ma et al. (2013), ecotoxicity studies on ZnONPs were compared in different taxa: bacteria, algae and plants, aquatic and terrestrial invertebrates and vertebrates. It was concluded that particle dissolution to ionic zinc and particle-induced generation of ROS toxicity represent the primary toxic action for ZnONP across all species tested, and bacteria being most affected. Overall, these toxicity and exposure data suggested that a comprehensive pre-evaluation of exposure matrix/media conditions is essential and has to be taken into consideration when interpreting the toxic outcomes.

6.3.3 The DCFH-DA assay provided *in vitro* evidence of the oxidative potential of particles, (as the intracellular total ROS levels altered)

Oxidative stress is one of the most commonly assigned features of NP induced cytotoxicity (Stone et al., 2007; Meng et al., 2009; Wani et al., 2011; Ghio et al., 2012). An increase in ROS can result in cellular damage, disrupt key cellular processes, and even cause cellular death (reviewed by Ayres et al., 2008; Arora et al., 2012).

According to the free radical theory (Harman, 2003), accumulation of ROS and unrepaired oxidative damage can result in organismal ageing. Healthy individuals carry an endogenous ROS pool (Kelly, 2003; Hekimi et al., 2011), and their antioxidant defence mechanisms repair the potential oxidative damage caused by xenobiotic substances. However, mutants or individuals with a perturbed antioxidant system are more susceptible to excess of free radicals (An and Blackwell, 2003; Liao and Yu, 2005; Yanase et al., 2009; Zeitoun-Ghandour et al., 2011; Back et al., 2012). In consequence, free radicals will oxidise cell components to a greater extend, which in turn affects the organismal life-span. The ability to neutralize damage generated by free radicals will therefore, be directly proportional to the extent of functional antioxidant defences and corresponding level of oxidative damage induced by a toxicant (Gems and Doonan, 2009; van Raamsdonk and Hekime, 2012; Back et al., 2012).

The level of intracellular ROS can be assessed and quantified by means of spectrophotometric assays. Here, the DCFH-DA assay was used as a reporter to investigate the ability of NPs to induce endogenous ROS in nematodes (Catheart et al., 1983). The DCFH-DA method demonstrated the dissolution of metals from surfaces of NPs can contribute to an increase in endogenous ROS accumulation, at least in nematodes. The experiments presented here showed that ZnONPs or NIST 1648a were

able to affect the total intracellular ROS levels in nematodes (Table 6.5). However, whiles ZnONPs decreased the worm endogenous ROS pool (Fig. 3.8), the exposure to NIST resulted in increased amounts of cytosolic ROS (Fig. 5.7). The exposure to either Zn or Cd ions is known to cause oxidative stress in worms (Zeitoun-Ghandour et al., 2011), hence the observed changes in ROS can be attributed to the metal in ZnONPs and NIST. The fact that worm MT transcript expression remained elevated upon ZnONPs (Fig. 3.7) and NIST (Fig. 5.10) exposure (NP concentration of 20-25 mg/L), supports this theory. Interestingly, with increasing particle dose, MT expression remained elevated in worms fed with ZnONPs (Fig.3.7), but returned to basal levels upon NIST (Fig. 5.10) exposure. Since the NIST particles consist of a variety of metals, it is likely that at doses of 20-25 mg/L, the worm antioxidant defence mechanism is perturbed to the extent beyond cellular repair. The observed decrease in ROS levels in NIST challenged metal hypersensitive and mitochondrial iron/manganese SOD mutants may support this hypothesis (Fig. 5.10).

To understand the initial phase of oxidative stress induced in the case of NIST, Nrf transcription factor mutant nematode strain (*skn-1*(zu67)) was evaluated for endogenous cellular ROS levels. As expected, NIST particles were able to increase the intracellular state of ROS species in exposed mutant (Fig. 5.10). This proved that in worms SKN-1 may function to regulate the oxidative stress response and provide protection against NIST induced toxisosis.

Moreover, experiments presented here showed that nematodes exposed to high concentrations of NIST, suffered a particle “overload”, which contributed to an increase in ROS generation (see Appendix: NIST 1648a). Additional insights into the “overload” phenomena (Donaldson et al., 2001), were brought by experimental evidence that metal-free particles, such as CB, are also amenable once they enter the cellular environment

and thereby cause oxidative damage that leads to ROS generation in worms (Li et al., 1999; Renwick et al., 2004). This clearly points out that different mechanisms of cytotoxicity are triggered by different NPs.

Table 6.5: Comparison of ZnONPs, CB M120, and NIST 1648a free radical level production in *C. elegans* fed to maximum 25 mg/L particle concentrations for 48 hrs, collected, and analysed by in vitro DCFH-DA assay. Functional arrows indicate a decrease (↓), increase (↑), or non-available (N/A), in the total intracellular ROS production. The number of arrows rank the amount of oxidative stress generated in each individual strain, in response to the particle exposure.

DCFH-DA assay (ROS production)			
Nematode strain	**ZnONPs**	**Carbon Black M120**	**NIST 1648a**
wild-type	↓	↑	↑↑
***mtl-1;mtl-2;pcs-1*(zs2)**	↑	↑↑	↓
***sod-1*(tm776)**	**N/A**	↓	**NO change**
***sod-2*(gk257)**	**N/A**	↓	↓
***sod-3*(tm760)**	**N/A**	**NO change**	↓
***skn-1*(zu67)**	**N/A**	**N/A**	↑

The interrelationship between particle composition and oxidative effect can play a primary role in driving the underlying mechanisms by which cytotoxicity will be induced in nematodes. It is reasonable to expect that the chemical composition of the particles will be partially responsible for modulating the activity of certain enzymes, such as metalloenzymes and antioxidant enzymes. These enzymes will define the

differential sensitivities to bioavailable metal ions, and hence defence systems to combat ROS (Back et al., 2012).

6.3.4 Nanoparticle exposure impairs worm reproduction and development

In *C. elegans*, development, reproduction, and longevity have been shown to be affected by the level of ROS that accumulate over time. The fact that toxicology and epidemiology closely relies on dose/response relationships (Oberdörster et al., 2005; Fanning et al., 2009, Russell and Brunekreef, 2009), it was deemed important to assess organismal level endpoints. Once NPs are taken up, they will potentially affect vital organs (such as the reproductive system, the gonad, or eggs) of the exposed organism and cause damage. The extent of damage will depend on the physicochemical characteristics of the NPs examined, the surrounding exposure media, as well as the bioavailability of the NPs (Oberdörster et al., 2005). However to date, most studies have deployed high NP concentrations that are not environmental relevance.

This study focused on changes in life-history traits in worms exposed to NPs: ZnONPs, CB or NIST, and compared the effects in wild-type, metal and oxidative stress-sensitive nematode mutants. All tested particles exerted a shared toxic response that was manifested by a decreased nematodes reproduction potential (Table 6.6). The toxic effects were dose responsive to ZnONPs exposure (Fig. 3.15), but not to CB (Fig. 4.10) or NIST (Fig. 5.22). Indeed, prolonged exposure to NPs can result in particle accumulation in the nematode intestine, as well as in secondary organs such as the reproductive tract (Pluskota et al., 2009; Hsu et al., 2012). Eventually, this can induce physical stress/constraints or internal pressure upon the nematode, which may have

resulted in the observed decrease in reproductive output, which was most pronounced in nematodes challenged with CB (Table 6.6).

The extent to which an organism suffers and the level of damage invoked can be predisposed by an individual's susceptibility to the toxic material. In terms of risk assessments, it is important to note that susceptible individuals can show completely different dose-response slopes compared to healthy individuals (e.g. in human studies asthmatic individuals who are diagnosed as asthmatics are more prone to ambient PM challenges) (Pekkanen et al., 1997; Penttinen et al., 2001; WHO, 2004; Back et al., 2012). In fact, given that the toxic effects of ZnONPs and NIST were significantly amplified in the hyper metal sensitive nematode mutant (*mtl-1;mtl-2;pcs-1*(zs2)) strain (Table 6.6), highlights that the genotype can influence the toxicity of metal NPs, a fact that should be taken into account in safety risk assessments (Hughes et al., 2009; Zeitoun-Ghandour et al., 2011). Against expectation, chronic exposure to either NIST, or CB did not affect the development of mitochondrial SOD-3 mutant (*sod-3*(tm760)) (Table 6.6). This may be linked to the effects observed in the mitochondrial homologue SOD-2 mutant (*sod-2*(gk257), namely an increase in growth upon NIST exposure, and a reduction in worm size upon CB exposure (Table 6.6). Finally, NIST and CB exposure also exerted common toxic effects on the development of the intracellular Cu/Zn SOD mutant (*sod-1*(tm776)), where a significant increase in worm growth was reported (Table 6.6).

One of the regulators of the worm antioxidant response to NPs may be the Nrf2 transcription factor. In this study, the *skn-1*(zu67) nematode mutant strain was most sensitive to NP exposure, as all three life-history traits examined were significantly reduced by acute 48 hrs NIST dosing (Table 5.12 and 6.6).

To date, no thorough investigation has been undertaken to study the role of SKN-1 in response to NP exposure in nematodes. As the Nrf2 transcription factor is activated in early responses to increases in cellular ROS levels, it could serve as a possible future biomarker for nematode-NP toxicity. In contrast, several toxicogenomic studies of NP toxicity using *C. elegans* have reported noticeable changes in SOD induction with some NPs (e.g. TiO_2 (Li et al., 2012; Rui et al., 2013)), but not with others (e.g. AgNPs (Roh et al., 2009)). This suggests that the mechanistic pathways of worm antioxidant responses to repair the oxidative damage induced by different NPs in more complicated than originally thought. Further studies are needed to understand the signalling events that turn on the SOD and Nrf pathways in response to NP stress.

Taken together, reproductive damage was the major toxic effect of chronic exposure to CB particles (likely due to particle overload) (Fig. 4.10). These results are consistent with other NP studies (Kim et al., 2008; Roh et al., 2009; Pluskota et al., 2009; Hsu et al., 2012), where it was demonstrated that the prolonged exposure to NPs causes developmental and reproductive toxicity in *C. elegans*. Prior to this study, CB NPs were not tested in *C. elegans*, however their toxicity was examined in some invertebrates (e.g. *M. galloprovincialis* (Canesi et al., 2010)), and vertebrates (mice (Yoshida et al., 2008) and rats (Nikula et al., 2005)). Findings suggested that CB NPs adversely affect mouse spermatogenesis and the effect depends on particle mass rather than particle number.

In contrast, NIST mediated toxicity was primarily driven by its complex chemical composition and *in vivo* surface modifications (Schwarze et al., 2006; Ghio et al., 2012). These modifications also seemed to play an important role when studying the specific physiological responses in nematodes. Although, the overall toxicity of NIST was

relatively low, the results of this study highlight the mechanistic complexity of NIST toxicosis, which remains to be fully elucidated.

Table 6.6: Comparative effects of chronic exposure of ZnONPs, CB M120, and NIST 1648a on worm life-history traits exposed to 25 mg/L particles. Arrows indicate a decrease (↓), an increase (↑), or non-available (N/A) data, in worm life-cycle endpoint in response to the NP exposure. The number of arrows ranks the level of NP toxic effect imposed on each individual worm strain. NOTE: The key endpoints of the *skn-1*(zu67) nematode mutant strain are provided only for acute 48 hrs exposure to NIST.

Comparative effects on worm life-history traits									
Worm strain	**Growth**			**Reproduction**			**Life-span**		
	ZnONP	**CB M120**	**NIST 1648a**	**ZnONP**	**CB M120**	**NIST 1648a**	**ZnONP**	**CB M120**	**NIST 1648a**
wild-type	↓	**NO change**	**NO change**	↓	↓↓	↓	↓	**N/A**	↓
***mtl-1;mtl-2; pcs-1*(zs2)**	↓↓↓	↑↑	↑	↓↓	↓↓	↓↓	↓↓	**N/A**	↓
***sod-1* (tm776)**	**N/A**	↑	↑	**N/A**	**N/A**	**N/A**	**N/A**	**N/A**	**N/A**
***sod-2* (gk257)**	**N/A**	↓	↑	**N/A**	**N/A**	**N/A**	**N/A**	**N/A**	**N/A**
***sod-3* (tm760)**	**N/A**	**NO change**	**NO change**	**N/A**	**N/A**	**N/A**	**N/A**	**N/A**	**N/A**
***skn-1* (zu67)**	**N/A**	**N/A**	↓↓	**N/A**	**N/A**	↓	**N/A**	**N/A**	↓

The observed differential responses upon NP exposure reflect the disease processes, and the site of its contact (Krug and Wick, 2011; Mohan et al., 2010; Zanni et al., 2012; Hsu et al., 2012). Most NPs are believed to enter the worm via the mouth and cause harm with the anterior parts. Moreover, it was interesting to note that the sites of contact (intestine, mouth, and vulva), were harmed in worms chronically exposed to NIST (see Appendix: NIST 1648a). It is likely that regardless of the type of NPs presented to the worm, similar parts are affected. Indeed, Raman spectroscopy identified major metabolic changes in the anterior, but not the posterior, part of *C. elegans* exposed to ZnONPs (Fig. 3.12). To date no attempt has been made to investigate the metabolic changes in NIST exposed worms, and it would certainly be useful to follow this up in the future. Whether ZnONPs or NIST are taken up via cuticular penetration is still unknown (Schilling et al., 2010), but could be tested using cuticle collagen worm knock-out models.

In summary, this is the first attempt to explore the nematode toxicogenomic response to CB and natural nanoparticles.

6.3.5 Particles induce genotoxicity in exposed nematodes

Comparing and contrasting the findings that emerged using a single model organism species and controlled experimental setups, can bring new insights into the damaging mechanism and signalling pathways induced by nanomaterials. As NIST and ZnONPs are both metal based nanomaterials, there is a possibility that the biological activity of certain genes may be affected in a similar, but also contrasting response. The genotoxicity may in both cases be due to the metal ion release, as well as intracellular NP effects. In this study, the accrual of oxidative stress and damage was highlighted as

the dominant mechanistic driver of the underlying nanotoxicity on the nematode *C. elegans*.

In order to elucidate common molecular pathways, there is a need to provide sufficient contrast for dose-response effects suitable for mechanistic studies. Therefore, it was deemed important to check for common genotoxic damage impelled on worms when exposed to either low (~5 mg/L), or high (~50 mg/L) particle concentrations. As a result, eight common transcripts (*mtl-1*,*-2*; *ctl-2*,*-3*; *sod-1*,*-3*; *hsp-16.1*, and *cep-1*) were selected, whose expression were examined in worms challenged with either ZnONPs or NIST (Table 6.7). Expression analysis by qRT-PCR and transgenic nematodes revealed that the transcripts of some genes examined increased by more than 4 – fold (namely *cep-1* in ZnONP exposures). At lower NP doses, *mtl-1*, *ctl-2*, and *sod-3* transcripts expression were significantly induced by ZnONPs or NIST exposures (Table 6.7). Conversely, when nematodes were challenged with 50 mg/L of either NP, *mtl-1*, and *mtl-2* transcripts expression remained elevated, and *hsp-16.1* was found to be significantly decreased in NIST exposed animals (Table 6.7). In *C. elegans*, HSP-16.1 protects against heat-induced necrosis or other environmental stresses, where it functions as a passive ligand, temporarily preventing unfolded proteins from aggregating (Lindquist, 1986; Strayer et al., 2003). Decrease in expression of HSP-16.1 in this study suggested that no cytoprotection is taking place.

Expression analysis revealed that *cep-1* was significantly up-regulated in ZnONP exposed worms. The transcriptional up-regulation of a metallochelator (*mtl-1*) and an apoptotic marker (*cep-1*) following a ZnONP challenge, suggests that ZnONP exposure and apoptosis may be linked, possibly through the generation of ROS and the highlighted carcinogenic potential of ZnONPs (Wu et al., 2010; Sharma et al., 2009; Ahamed et al., 2011; Sharma et al., 2012). In contrast, *cep-1* expression was not

elevated upon exposure to NIST particles, and although metallothioneins (*mtl-1*, and *mtl-2*) were found to be implicated in the transcriptional response, their activity was less pronounced (compared to ZnONPs or cadmium challenges). It is also interesting to note that more genes were up-regulated by low NIST doses, than by low ZnONP doses (Table 6.7).

Table 6.7: Comparison of ZnONPs and NIST 1648a-responsive transcripts expression in wild-type nematodes. Arrows indicate the decrease (↓), the increase (↑), or non-available (N/A) data, in the transcript expression. The numbers of arrows indicate the relative amount of transcript induction, in response to the particle exposure.

Genes	ZnONPs (5 mg/L)	NIST 1648a (5 mg/L)	ZnONPs (50 mg/L)	NIST 1648a (50 mg/L)
mtl-1	↑	↑↑	↑↑	↑
mtl-2	N/A	N/A	↑↑	↑
ctl-2	↓	↑↑	NO change	↑
ctl-3	↑	↑↑	NO change	↑
sod-1	NO change	↑	NO change	↑
sod-3	↑	↑↑	↓↓	↓
hsp-16.1	↓	↑	↑↑	↓
cep-1	↑	↓	↑↑	↓

Some metals are essential to the organism, thus tight homeostatic regulation is needed. Any deregulation can result into a toxic outcome or even cause carcinogenicity (Rohrs, 1957; Blanc et al., 1993; Mocchegiani et al., 2011; Roh et al., 2012). NP solubility in general can be variable and dependent upon the source of material. Indeed, it was shown

in this study that the cytotoxic effects of ZnONPs are primarily related to the NP dissolution and release of Zn ions (more labile Zn is available at higher ZnONP doses).

It is likely that the damage in gene expression in response to low NIST exposures may have been caused by the release of metals, as well as co-factors, contributing to the generation of intracellular ROS. Eventually, at higher NIST concentrations the worm antioxidant system might become dysfunctional, leading to inflammation.

Furthermore, the transcriptional data indicated that many of the primary components that are involved in the antioxidant protection systems, such as superoxide dismutases (*sod-2*), glutathione disulfide reductases (*gsr-1*), glutathione transferases (GSTs), were not differentially expressed as a result of NIST exposure (Fig. 5.9). Nevertheless, DNA microarray analysis identified numerous targets which were indicative of developmental and reproductive impairment when worms were exposed to the chemical complex NIST. Also up-regulated were genes functionally involved in oxidative phosphorylation (F59C6.5), fatty acid biosynthesis (*fasn-1*), TGF-beta (*daf-14*), and interleukin (*ets-4*) signalling pathways.

DAF-14 encodes a SMAD-related protein in worms, and is predicted to function as a transducer of the DAF-7/TGF-beta-mediated signal that regulates multiple cellular processes, such as cell proliferation, apoptosis, and differentiation. In worms it promotes reproductive growth and negatively regulates dauer formation (Inoue and Thomas, 2000). A human homologue of *C. elegans daf-14*, is SMAD2 (also known as Mothers against decapentaplegic homolog 2 in vertebrates) (Witkowska and Smolewski, 2014). Studies have shown that mutations in SMAD2 protein contribute to the development of colorectal cancer (Takenoshita et al., 1998), and lung cancer in humans (Finger et al., 2008). Therefore, *daf-14* expression in response to NIST could prove to

be a valuable future prognostic factor or model for some neoplastic diseases and exposure to particulate matter.

ETS-4 is a transcription factor which functions in parallel to the insulin/IGF-1 signalling pathway, and requires the FOXO transcription factor, and *daf-16*, to modulate life span in *C. elegans* (Thyagarajan et al., 2010). Its persistent induction across all NIST concentrations implies that it plays an important role in the worm's response to NIST detoxification. A SAM pointed domain containing ETS transcription factor (SPDEF) (also known as PDEF/Prostate derived ETS factor) is a vertebrate ortholog of ETS-4 (Oettgen et al., 2000). SPDEF may have significant disease relevance, as tumour cell lines showed that SPDEF affects cell migration and invasion pathways (Gras et al., 2013). SPDEF was also found to act as a downstream molecule of the defective NOTCH pathway observed in asthma (Chen et al., 2009; Maeda et al., 2011). Hence, ETS-4/ SPDEF can potentially represent a candidate for future therapeutic targeting. Overall, these genes might play an important role in NIST detoxification and organismal protection mechanisms. Further investigation would be required to fully understand their biological meaning.

Moreover, toxigonomic worm studies have shown that the MAPK signalling pathway is involved in the response to AgNPs (Lim et al., 2012; Chatterjee et al., 2014) and AuNPs (Tsyusko et al., 2012). The ability of a given nanoparticle to evoke an immune response is an indicator for its toxicity on physiological systems. In nematodes, there are no mobile immunocytes present; hence intestinal epithelial cells take over the cell-mediated immune responses (Chitwood and Chitwood, 1950). Coelomocytes take over the role of phagocytic leukocytes to protect worms against bacteria and viruses through encapsulation, but not phagocytosis (Ewbank, 2002). These cells are fixed to the nematode body wall, and rely on the body movement of the worm and cavity fluid to

access the material. Whether these cells play an important role in providing worm immune protection against nanomaterial evoked toxicity has yet to be examined.

C. elegans is a soil organism, amenable to frequent encounters with pathogens and chemicals and thus has evolved a multifaceted response system, with higher threshold levels to certain xenobiotic challenges (Schulenburg et al., 2004; Irazoqui et al., 2010). It is therefore not surprising that the NP induced responses were overall relatively low, as reported by other toxicogenomic studies utilizing *C. elegans* as a model organism (Yang et al., 2014; Fajardo et al., 2014).

Surprisingly, a significantly large proportion of transcripts were found to be repressed by NIST treatment (Table 5.2). Given that many genes were found to be involved in regulating major cellular transcriptional processes, such as proteasome beta subunit (*pbs-1*), proteasome (helicase H20J04.4), ribosome (*rpl-18*, Y73B3A, *rpl-7A*), and spliceosome (*hrp-1*, and *sap-49*), suggested that NIST toxicity might be mediated via nucleolar stress. Similar changes in genes encoding proteasome transcripts were observed by transcriptome sequencing analysis conducted by Simon et al. (2013) in the eukaryotic green alga *C. reinhardtii*, after exposure to several metal-NPs. They suggested a possible mechanism of metal-NP induced proteasome inhibition, a phenomenon believed to underlie the development and progression of several diseases, such as Alzheimer's disease (Hegde and Upadhya, 2011), and multiple myeloma (Verani, 2012). Indeed, proteasome homeostasis in *S. cerevisiae* was also shown to be critical for cell viability under stressed conditions (Wang et al., 2010).

DNA damage is a fundamental example of cellular toxicity. Any disruption of the nucleolus, either by direct interference of ribosomal proteins, or by inhibiting ribosome biogenesis chemically was shown to cause the release of p53-stabilizing proteins, and resulted in elevated levels of active p53 in mice, and human cells, as well as nematodes

(Ljungman et al., 1999; Pestov et al., 2001; Rubbi and Milner, 2003; Yuan et al., 2005; Fuhrman et al., 2009). Therefore, these findings indicate that upon NP exposure, the nucleolus may act as a stress sensor responsible for maintaining low levels of active p53/*cep-1* and prevent damage. However, when nucleolar function becomes impaired, key cellular processes are disrupted and organismal damage takes place. Study by Hunt et al. (2013) showed that AgNPs can induce oxidative damage to the DNA of *C. elegans*, which exerted itself as an increase in the levels of 8-OH-Gua. 8-OH-Gua is an established biomarker of oxidative stress and a mutagenic lesion causing Guanine> Thymine transversion mutations (Cooke et al., 2003). This notion was supported by this study, where an impaired expression of ribosomal RNA (rRNA) was confirmed in NIST exposed animals.

Indeed, the worm CEP-1 appears to be able to sense specific damage and induce distinct responses associated with gamma, and UV irradiation, and mitochondrial electron transport chain (mETC) inhibition (Baruah et al., 2014). Therefore, increases in *cep-1* in response to ZnONP exposure may induce a core group of signal transduction molecules that initiate a downstream signalling cascade to mount a general stress response. Worm CEP-1 can act also as a potential model for human ADULT syndrome (DOID:0050601), esophagus squamous cell carcinoma (DOID:3748), Li-Fraumeni syndrome (DOID:3012), adrenocortical carcinoma (DOID:3948), lung cancer (DOID:1324), and choroid plexus papilloma (DOID:2626) (according to WormBase release version: WS241).

Table 6.8: Identification of key nematode genes and homologues/orthologs to their human counterparts.

Gene name	*C. elegans* description	Best BLASTP matches (%) to mammalian sequence	Human homologue/ortholog (ENSEMBL accession number)
ctl-2;-3	Catalase		Orthologous to catalase ENSEMBL:ENSP00000241052
cyp-35A2	Cytochrome P450 family	93.5%	Orthologous to cytochrome P4502C8 ENSEMBL:ENSP00000360317
dct-1	DAF-16/FOXO Controlled, germline tumor affecting	33.9%	Highly similar to BCL2/adenovirus E1B 19 kDa protein-interacting protein 3 ENSEMBL:ENSP00000446145
gsr-1	Glutathione disulfide reductase	95.1%	Isoform mitochondrial of glutathione reductase, mitochondrial ENSEMBL:ENSP00000221130
hsp-16.1	A 16-kD heat shock protein	64.8%	Alpha-crystallin B chain ENSEMBL:ENSP00000227251
mtl-1	Metallothionein	68.0%	Metallothionein-3 ENSEMBL:ENSP00000200691
mtl-2	Metallothionein	92.1%	Keratin-associated protein 5-9 ENSEMBL:ENSP00000431443
skn-1	Skinhead	45.7%	Nuclear factor erythroid-derived 2-like 2 transcript variant 1 ENSEMBL:ENSP00000380252
sod-1	Copper/zinc superoxide dismustase	86.1%	Superoxide dismutase [Cu-Zn] ENSEMBL:ENSP00000270142
sod -2	Iron/manganese superoxide dismutase	97.7%	Superoxide dismutase [Mn], mitochondrial isoform A precursor ENSEMBL:ENSP00000356022
sod-3	Iron/manganese superoxide dismutase	97.7%	Superoxide dismutase [Mn], mitochondrial isoform A precursor ENSEMBL:ENSP00000356022
sod -5	Predicted to be one of two cytoplasmic Cu/Zn SODs in *C. elegans*	85.4%	Superoxide dismutase [Cu-Zn] ENSEMBL:ENSP00000270142
ugt-1	UDP-glucuronosyl transferase	96.0%	UDP-glucuronosyltransferase 1-6 ENSEMBL:ENSP00000303174

As with NIST toxicity, mutations in the human orthologue SOD-1 have been linked to familial amyotrophic lateral sclerosis (Al-Chalabi and Leigh, 2000; Li et al., 2013). Human SOD1 has also shown to be able to interact with another metalloprotein, namely the copper chaperone for superoxide dismutase (CCS) (Casareno et al., 1998), as well as with B-cell lymphoma (Bcl-2) (Pasinelli et al., 2004).

Extrapolated to higher organisms, results of this study also highlight that the toxicity of ZnONPs and NIST may be exacerbated in individuals with mutations in key metalloproteins, akin to the impaired copper transport in Menkes and Wilson's disease (Mercer, 2001; Daniel et al., 2004). The increase of *C. elegans* CAT on NIST exposure, suggests that changes in peroxisomal function, including increased production of ROS, underlie the NIST exposure, and could serve as a convenient model for the study of the human disease acatalasemia (Petriv and Rachubinski, 2004).

Finally, to understand better the relationship between human and *C. elegans* genomes, the orthology between genes was sought. The list of genes that were investigated in the current study will hopefully help to identify *C. elegans* orthologs of human disease genes for potential functional analysis. A compelling list of candidates is provided in the Table 6.8 (a complete list of ortholog of human genes is provided in Appendix: Materials and Methods).

6.3.6 Assessing the ability of nanomaterials to induce cytotoxicity in *C. elegans* by high-throughput screening

As a proof of a concept, transgenic worms containing extrachromosomal copies of the metallothionein or phytochelatin promoter tagged to a green fluorescent protein (GFP)

were initially examined for evidence of ZnONP mediated metal toxicosis. At elevated concentrations strong transcriptional responses were identified, a finding which was supported by qRT-PCR (Fig. 3.4 and 3.7). Subsequently, a nematode based biosensor platform system, which utilizes age synchronized MoSCI integrated transgenic nematode strains (generated and provided by Knudra Transgenics, USA) was evaluated (Boulin and Bessereau, 2007; Frøkjaer-Jensen et al., 2008). The quantitative, *in vivo*, amplification of eight stress-responsive genes in nematodes exposed to ZnONPs, CB M120, or NIST 1648a was examined. *C. elegans* were fed with up to 50 mg/L of ZnONPs, CB, or NIST particles for 48 hrs, collected, and analyzed (Table 6.9).

Exposure to ZnONPs (but not CB and NIST) was found to modulate the expression of *hsp-16.41* and *ugt-1*. Interestingly, *cyp35A2* and *gcs-1* transcripts were both found to be responsive to a CB (Fig. 4.6) or NIST (Fig. 5.6) challenge. Roh et al. (2010) investigated the toxicity of CeO_2 and TiO_2 nanoparticles using gene expression, growth, fertility, and survival as endpoints in *C. elegans*. In their study, they suggest that cyp35A2 gene expression is related with reduced fertility and survival in worms exposed to NPs.

In nematodes, cyp35A2 belongs to the P450 family, and is 93.5% orthologous to human cytochrome (CYP) P450 2C8. CYP2C8 is responsible for the oxidative metabolism of many xenobiotics, such as drugs, carcinogens, and steroids. In humans, CYP2C8 genetic variations were associated with adverse effects of the statin cerivastatin, including acute rhabdomyolysis (Ishikawa et al., 2004). A nanoparticle albumin bound drug used in chemotherapy (Paclitaxel) is also used as a (moderate) CYP2C8 inhibitor, and may decrease the metabolism of CYP2C8 substrates (Dai et al., 2001).

Table 6.9: Screening of different nanomaterials for their ability to induce cytotoxicity in *C. elegans* by utilizing MoSCI integrated transgenic nematode strains. Functional arrows indicate a decrease (↓), an increase (↑) in the transcript expression.

MoSCI transcripts	ZnONPs	Carbon Black M120	NIST 1648a
hsp-16.2	NO change	NO change	NO change
hsp-16.41	↑	NO change	NO change
cyp-35A2	NO change	↑	↑
gcs-1	NO change	↓	↑
gst-4	NO change	NO change	NO change
gst-38	NO change	NO change	NO change
ugt-1	↑	NO change	NO change
dnj-13	NO change	NO change	NO change

GCS-1 is predicted to function, in the worms' response to ROS, as a phase II detoxification enzyme that is under transcriptional control of SKN-1 (An and Blackwell, 2003). Indeed, polymorphisms in the glutathione synthetase (GSS) enzyme were also found to be associated with a decreased lung function in children, and involved in the response to $PM_{2.5}$ (Breton et al., 2011; Minelli et al., 2011).

To maximize discovery rates, a system that is streamlined, rapid, convenient, high-throughput and fully quantitative is needed. Hence, utilizing a soil nematode screen, such as the MosSCI transgenic lines, can prove to be a useful approach when screening for the toxicogenomic effects of NPs with varying physicochemical properties. Novel

transcripts (even common transcripts) that can act as future biomarkers or drug targets for different types of NPs can easily be identified and compared. If expanded, this technology may serve as a simple, rapid and informative bioassay of NP stress.

6.4 Data gaps and research needs

6.4.1 Routes to exposure

Microorganisms can come in direct contact with NPs via numerous products, which are distributed by air, water, and the ground. The ecotoxicity for the organisms and the mechanisms of potential transfer in the food chain will differ. Taking into consideration the routes of exposure to NPs, more studies on gastrointestinal uptake, their transport, and direct toxicological effects on the gastrointestinal tract are required. More attention is also required to define the NPs ability to damage the worm vulva, and modify the worm egg-laying behaviour. Indeed, in this study, worms were exposed to NP suspensions via food. Therefore, future experiments could compare and contrast the toxic outcomes using the same NPs, but different delivery systems, such as e.g. via inhalation, or within a liquid environment in the absence/presence of food. The physicochemical characteristics of NPs prior to their interaction with the worm will certainly affect the toxicological effects (including genotoxicity, teratogenicity).

The complexity of toxicity and behaviour of natural NPs, such as is NIST, is still a "black box". Due to the complex physicochemical characteristics of the NPs, different exposure settings might reveal different cytotoxic pathways than were elicited in this study (e.g. different genes might become activated).

6.4.2 Detection of nanoparticles within the nematode – Raman microscopy and Electron microscopy (EM) imaging

In this study a method was introduced to monitor particle localization throughout the nematode body and the effects on its metabolome, namely Raman microspectroscopy.

Given the microscopic size of *C. elegans* it was not possible to apply Inductively Coupled Plasma Mass Spectrometry (ICP-MS) to quantify the changes in internal metal load within an individual nematode, however Raman microscopy identified an intense signal, characteristic of the ZnONP shift only in nematodes exposed to 50 mg/L ZnONP (see Appendix: ZnONPs). This provided a strong, albeit circumstantial, evidence that ZnONPs are readily taken up by worms with bacteria (*E. coli*) via pharyngeal pumping, which results in their localization inside their digestive tract. Ingested ZnONPs were primarily large agglomerates, and were detected in the head, middle, and tail regions. It is unknown whether singlet particles are also retained within the nematode's body or whether they are excreted. Future work should examine the particle interactions with the corresponding subcellular structures in *C. elegans* in greater detail, rather than just focusing upon specific regions. Eventually this could be achieved by employing electron microscopy (EM) (Hall et al., 2012), or by using a CytoViva Nano-scale microscope system (©CytoViva®, AL, USA). Although EM is technically demanding, due to the laborious worm fixation procedure (Hall, 1995), it offers high resolution images of small objects, such as NPs. In contrast, the CytoViva microscope system was designed to enable researchers to spectrally characterize and map nanoscale samples in a wide range of environments (von der Kammer et al., 2012). Others have observed the interactions between fluorescently labelled NPs (Moussa et al., 2011) or bacteria (Vishnupriya et al., 2013) and unlabelled cells (Grabinski et al., 2011), and in worms (Meyer et al., 2010; Arnold et al., 2013). These techniques would allow us to obtain

visual information about cellular components NPs and their agglomerates come to interact with. Studying NPs uptake behaviour via EM or CytoViva, would not only remove much of the variation experienced in the case of Raman microspectroscopy, but also allowed us to obtain comprehensive information upon the cellular permeation ability and the uptake behaviour of NPs in worms.

Although in this study Raman microspectroscopy was only used to examine the role of ZnONPs toxicity in worms, it would be interesting to use the same approach to examine and compare the results with nematodes exposed to CB or NIST nanoparticles. To date, this technology does allow us to analyse carbon materials (Wang et al., 1990). The normalized visible Raman spectrum corresponding to the carbon nanoparticles is known to be represented by two significant bands, near 1350 cm^{-1} (disordered graphite) and near 1580 cm^{-1} (nanocrystalline graphite), respectively (Chen et al., 2004). Note that, these peaks might not be exactly the same once CB NPs are ingested by the nematode, however they should retain the same signature motif characteristics of carbon materials. Whilst technically feasible with CB NPs, it is questionable whether Raman would be suitable to analyse NIST exposures. Current concerns are that NIST data would be characterized by worm to worm variability; hence it would be impossible to perform statistics and identify common trends. In addition, it would take a very long time to characterize individual Raman spectra corresponding to the NIST metals.

In this study it was revealed that metal oxide nanoparticle toxicity induced in worms was also partially due to dissolution of ionic Zn, hence it would be prudent to investigate this further. To fully understand the dissolution effect, inductively coupled plasma mass-spectrometry (ICP-MS) would be an appropriate choice of analysis, however due to detection limits worms would have to be exposed to relatively high ZnONPs concentration (in excess of 50 mg/L). Alternatively, the number of worms

could be increased to over 20,000 animals per treatment, which is both, time and labour intensive.

6.4.3 Changes in *E.coli* metabolism after ZnONPs, CB M120, and NIST 1648a exposure

In this study, TEM imaging indicated that once NPs come in contact with bacteria, they are able to induce morphological changes on the membrane surface of *E.coli* (Fig. 3.1E and Appendix: Carbon Black M120). Thus, in future, it would be interesting to examine how bacterial metabolism is affected by NPs exposure. This could potentially be determined by employing Raman microspectroscopy. EDX analyses and chemical mapping were employed in the ZnONP study, which indicated that Zn dissolves from the ZnO agglomerates and diffuses into the media within 24 hrs. It is also deemed important to measure metal ion release from the nanoparticles using ICP-MS (for results on ZnONPs see Appendix: ZnONPs). At this stage it is not possible to exclude the notion that Zn ion release within the cellular and sub-cellular environment may contribute, to some extent, to the toxicity of the nanoparticles tested.

6.4.4 Doses to check the levels of antioxidants

Paracelsus, the "father" of toxicology, stated "All things are poison, and nothing is without poison; only the dose permits something not to be poisonous." In other words, the amount of the substance a person is exposed to bears equal importance as the nature of the substance. An example is the analgesic drug "*aspirin*". Small doses of aspirin can be beneficial to a person, but when an ordinarily harmless substance is given at very

high doses or over-consumed; it can be deadly (Kreplick, 2001). Aspirin may even be deadly at very low doses, in some susceptible individuals, e.g. Reye's syndrome (Belay et al., 1999). Therefore, as with any other man-made and natural materials, we ask ourselves "Are nanoparticles toxic and at what dose?" (SCENIHR, 2006). This question has been a major concern in the field of nanotoxicology research for almost two decades, and has yet to be fully answered. Researchers have confirmed that materials at nanoscale level can display unusual and unexpected toxicity (Meng et al., 2009). Unlike the soluble chemicals tested in traditional toxicology studies, NPs diffuse, aggregate/agglomerate and sediment, according to their density, size, and physicochemical properties in solution (Nel et al., 2009). Therefore, the NPs data obtained from traditional *in vitro* assays may turn out to be less comparable for soluble drugs (Oberdörster et al., 2005). Many studies have tested these materials at much higher doses that would be presented in real-life emission and occupational exposures scenarios. In addition, once nanomaterials are released into the environment they are typically coated with organic matter, which modifies their bioavailability and influences their reactivity (Fajardo et al., 2014; Yang et al., 2014). It can therefore be expensive and time consuming to study the dose, time and exposure route of these NPs.

The small roundworm organism *C. elegans* might not be the perfect model, but at least it can provide ecotoxicological perspectives of NP toxicity. Throughout this study, the NP concentration range tested was carefully chosen to align with the published literature (e.g. for ZnONPs, Ma et al., 2009, though significantly higher than the concentrations tested in Wu et al., 2013 and by Sahu et al., 2014 for CB), and was considered to be environmentally relevant. For example the predicted soil concentration of engineered ZnONPs arising from use in consumer products has been estimated to be 3.2 mg/kg soil (Tiede et al., 2009). Likewise, the Environment Agency UK Soil and Herbage Pollutant

Survey (DEFRA, 2007) states that (in the UK) the mean and median Zn concentrations are 81 and 65 mg/kg dry weight respectively, and can be significantly higher in soil surrounding industrial sites.

Approximately 21.5% of the tires (30% of the tire dust) are made up of carbon black (OECD, 2006). To date, experimental ecological effect data are mainly available for aquatic pelagic organisms (CEPA, 1999). These data indicate that at exposure concentrations of up to 58 000 mg of tire dust/L of water for zebrafish, 68 000 mg of tire dust/L of water for Daphnia, and 13 000 mg of tire dust/L of water for algae, is not hazardous to these organisms (Basel Convention, 1999). Nevertheless, concerns were raised that nano-CB particles can alter the phagocytic capacity of monocytes, and induce an inflammatory response (at much lower concentrations 50 - 800 mg/L) (Ferrin et al., 1992; Li et al., 1999; Sahu et al., 2014).

In this study, neither of the three particles tested reached the LC50 or EC50 levels in wild-type nematodes. For this reason it was decided to use particle concentrations in the range of 0 - 50 mg/L. The initial aim was to examine the antioxidant responses and DNA damage following the worm treatment with particles. Surprisingly, in CB and NIST exposed animals the expression of genes involved in antioxidant protection were found to be primarily at the basal level (Fig. 3.7 and 5.9), with little evidence of oxidative DNA damage and apoptosis (Fig. 3.7). These results were in contrast to the initial hypothesis, but aligned with other studies which concluded that low cytotoxicity might be due to an increased antioxidant activity at lower NP concentrations (Drobne et al., 2009; reviewed by Iavicoli et al., 2010; Guo et al., 2011).

Whether NPs can induce hormesis in worms, namely a low dose stimulation, and high dose inhibition (Ristow and Zarse, 2010; Zhao and Wang, 2012) is yet unknown. However, some NIST results of this present study (e.g. Fig. 5.8) displayed changes in

gene expression resembling the common β- or U- shaped hormetic dose-response curves (Cox, 2006; Nascarella and Calabrese, 2012). Although, the exact biochemical mechanisms involved in this type of response are still unclear, it would be worth investigating them further. It is conceivable that low doses of NPs might activate repair mechanisms in the nematode body, including the metallochelator molecules. It would be interesting to examine how worms are affected at lower NP doses (less than 5 mg/L), in order to define the antioxidant worm threshold level.

6.4.5 Oxidative stress and ROS generation

When worms are exposed to chemical or/and physical insult it can result in the production of ROS. Cells combat the different ROS species with an extensive antioxidant defence system, which can be divided into primary (GPX, SOD, CTL, and TRDX) and secondary defence (reduced GSH) mechanisms (Bremner, 1998). Once NPs interact with biological tissue, their surface coatings, composition, electronic structure, and solubility can change, leading to either a decreased or amplified formation of pro-oxidants. Nematode specific biological and mechanistic pathways can be investigated (under controlled *in vitro* and *in vivo* conditions) using different antioxidant assays to measure ROS species (Back et al., 2012). Recent methodologies and technologies of ROS measurement in biological systems have allowed the study of the ROS mechanism at a previously unachievable level of precision (Uusitalo and Hempel, 2012; Woolley et al., 2013).

The DCFH-DA (H_2DCFDA; Molecular Probes) dye was used to evaluate cellular oxidative stress in *C. elegans* exposed to NPs. It is important to emphasize that one assay is not enough to provide a fully quantitative intracellular ROS measurement

facilitated by NPs. Although to date, DCF remains to be most widely used and reviewed dye, it lacks specificity for defined ROS species. DCF also does not provide information on reaction rates or cellular location (Cohn et al., 2008; Karlsson et al., 2010).

In this study, worms were first exposed to NPs, then washed and homogenated, and finally analysed for ROS production using H_2DCFDA. It would be interesting to compare and contrast the results using a similar compound, namely, CM-H($_2$)DCFDA (Molecular Probes®), which is a chloromethyl derivative of H_2DCFDA, and can be used as an indicator for ROS and worm staining (Sakaue et al., 2010; Li et al., 2012). Subsequent oxidation of this dye yields a fluorescent adduct that is trapped inside the worm cells, and can be semiquantified using fluorescence microscopy.

Additional comparative studies could be performed using different assays. In *C. elegans* the major site of zinc storage are lysosome-related organelles, the gut granules (Roh et al., 2012), which can accumulate labile Zn. To address the role of Zn^{2+} dissolution inside intestinal cells upon ZnONPs exposure, a cell permeable molecular probe FluoZin™-3 (Molecular Probes®) could be utilized. The biosynthesis and pathogenesis of lysosomes following NP exposure could also be investigated by applying acridine orange staining (AO) (ImmunoChemistry Technologies, LLC., USA) of worms, or usage of LysoTracker® (Molecular Probes®) probes, which are highly selective for acidic organelles (Klapper et al., 2011).

To date, it has been shown that some NPs are able to stimulate a widespread, physiologically relevant and selective signalling molecule H_2O_2. This molecule is also considered to be the most abundant and stable compared to other free radicals (Hancock et al., 2001). Therefore, in this study it could serve as a good biomarker of NP toxicity. In worms we could monitor H_2O_2 production using an intracellular H_2O_2-specific, reversible biosensor – HyPer (Belousov et al., 2006).

In vitro studies have shown that exposure to NIST can reduce the GSH level and hence destabilize the cellular redox state present in respiratory tract lining fluid (RTLF) (Mudway et al., 2004). Changes of the intracellular GSSG/GSH ratio following worm NP exposure, could be measured via a redox-sensitive sensor such as Grx-roGFP2 (Albrecht et al., 2013). Throughout this study one focus was to examine the role of SODs and catalase (CAT) enzymes in providing protection against NP toxicity. It would be interesting to examine the mitochondrial superoxide production in live cells of wild-type and SOD mutant worms, using the mitochondrial superoxide indicator MitoSOX™ Red (Mukhopadhyay et al., 2007; Sakaue et al., 2010). As, in worms catalase activity could easily be measured by following its ability to split H_2O_2 within 1 minute of incubation time (Aebi, 1984), the outcome could be used to validate the experimental qRT-PCR evidence.

In addition, the production of ROS and the accumulation of cellular damage is directly related to ATP production by the mitochondria (Murphy, 2009). The levels of ATP are thought to be associated with the subsequent induction of protective pathways, as well as nematode dietary restriction (Gruber et al., 2011). Whether the three types of NPs tested here are also able to disturb the balance in ATP production remains to be established. Indeed, previous studies have shown that metal oxide and carbon black NPs are able to cause a loss in mitochonidrial membrane potential in bronchial epithelial cells (Hussain et al., 2010). It would be interesting to examine whether a similar molecular cytotoxic pathway is induced in nematodes.

Finally, to determine whether exposure to NPs can irreversibly alter worm protein structure and function, the amount of damage could be determined using an Oxyblot™ assay kit (Van Raamsdonk et al., 2010) or Biotin–Avidin-Capture methodology (Stankowski et al., 2011), that detects the carbonyl group formation on protein side

chains. Studies have reported that exposure to engineered NPs can induce membrane damage by lactate dehydrogenase (LDH) leakage (Kroll et al., 2011; Yu et al., 2011). Hence, to examine the extent of membrane lipid peroxidation damage induced by NP exposure in worms Bodipy fluorophore probe (Klapper et al., 2011) fluorescence, or malondialdehyde (MDA) formation (Zhang et al., 2011), could be measured.

6.4.6 Genotoxicity assays

Almost all kinds of metallic, metal oxide, and carbon based nanomaterials were reported to be able to induce cytotoxic effects (Singh et al., 2009; Donaldson et al., 2010; Klien and Godnić-Cvar, 2012; Vandebriel and De Jong, 2012). This study established the genotoxic nature of ingested ZnONPs, as *cep-1* worm transcript (p53 human orthologous) was found to be elevated (Fig 3.7). Several further genotoxic assays should be carried out to define the safety of these 3 types of materials in question. One of the fundamental *in vitro* assays used in research for DNA damage and repair is the comet assay (Collins, 2014). This assay has also been the most extensively reviewed methodology in nanotoxicology research (Karlsson, 2010).

Indeed, activation of caspases and subsequent DNA fragmentation are known to be biochemical hallmarks of apoptosis in the case of AgNPs (Arora et al., 2008), CB and TiO_2 (Hussain et al., 2010). The activity of caspase-3 and caspase-9 enzymes could also be measured in worms treated with different types of NPs using a standard caspase kit (Lee and Xue, 2014). Cell death induced by NPs could also be characterized by double staining of worms with fluorescein diacetate/ethidium bromide (FDA/EtBr) (Lemaire et al., 1998), which can differentiate between apoptotic and necrotic cells.

6.4.7 Linking the toxicant doses with apoptosis/necrosis/pro-inflammatory responses

The precise innate immune responses of *C. elegans* challenged with NPs are still not known, and would need to be characterized for each type of NP. However, the primary site of infection in *C. elegans* is the intestine. The nematodes do not have a cell-mediated immunity, but their systemic immunity depends primarily upon secretion and action of antimicrobial molecules, such as lectins, lysozymes, (Mallo et al., 2002), and antimicrobial factors (Kato et al., 2002). The defence systems are regulated by a number of different signalling pathways (see Appendix: NIST 1648a) e.g. the insulin signalling/DAF-2, the p38 and extracellular signal-regulated kinase (ERK) mitogen-activated protein kinases (MAPKs), and transforming growth factor β (TGF-β) /DBL-1 pathways (Marsh and May, 2012).

Indeed, the GO analysis of differentially expressed genes in wild-type *C. elegans* exposed to NIST identified immune system signalling pathways (TGF-beta and interleukin signalling pathways) to be activated regardless of NIST dose. In addition, some of the major transcripts involved in the ERK/MAPK, and RTK/Ras/MAPK signalling pathways were also found to be increased at lower NIST doses (0-10 mg/L), but not at higher (10-50 mg/L). Other, findings suggested that worms exposed to elevated concentrations of ZnONPs had increased p53 transcript levels (Fig 3.7). In the antioxidant transcription factor SKN-1 knock-out worm model, the sensitivity to NPs toxicity was found to be enhanced, and resulted in premature death.

To date only a limited number of studies have focused on immunological responses of nanoparticles (Moghini et al., 2005; Curtis et al., 2006; reviewed by Shvedova et al., 2010; Syed et al., 2013), and few have investigated antigenicity of NPs in worms (Roh

et al., 2012). This highlights the need for further research in this area. In addition, worm innate immune responses should be investigated in more detail not only at the transcriptional level, but also by means of immune assays.

6.4.8 Epigenetic study

Exposure to all three types of NPs was shown to decrease growth and development, reproductive capacity, and life-span, effects which were amplified in the 5 knockout models used in this study. Although the effects were not of the same magnitude, there were at least some common effects which indicated that repeated administrations of NPs can cause more damage than acute exposures to worm life-cycle traits such as body size.

To date, animal studies have found over 90% orally administrated engineered NPs are excreted through faeces (Lozano et al., 2012; Hughes et al., 2013). Nevertheless, due to their small size and ability to attract bio-molecules on their surface, they are able to translocate and be retained in tissues, such as kidneys and liver (Oberdörster et al., 2005). Indeed, in nematodes, NPs were shown to be able to translocate though the intestinal epithelial cells, and cause damage to the reproductive system. The decrease in reproduction seems to be the most common and pronounced NPs-specific toxic effect described so far (Pluskota et al., 2009; Hsu et al., 2012; Wu et al., 2012; Contreras et al., 2013; Kim et al., 2013). Reduced worm reproduction capacity may be explained as a part of the defence and/or compensatory mechanism to metabolite and/or detoxify the toxicity induced by ingested NPs.

In recent years "nano-epigenetic" research has attracted interest (Pacchierotti and Eichenlaub-Ritter, 2011; Stoccoro et al., 2013). Epigenetic changes have been observed to occur in response to environmental exposure, and involve alterations in DNA methylation patterns, chromatin remodelling, posttranslational modification of histones tails, and in non-coding RNA (ncRNA) (Liebers et al., 2014; Peschansky and Wahlestedt, 2014; Guérin et al., 2014). Throughout cell division these gene expression patterns modifications can be either reversible, or become heritable. NPs can contribute to a cellular increase in ROS production, cause oxidative DNA damage and modify the chromatin (Jennifer and Maciej, 2013).

Indeed, whole genome transcriptomics of wild-type *C. elegans* exposed to NIST, identified that the histone deacetylase family (*hda-1*, *hda-3*, and *hda-6*) was significantly affected. Maternal and zygotic expression of *hda-1* (a histone deacetylase 1 gene) for example, is essential for embryonic viability, and zygotic expression is required for gonadogenesis and vulval development (Dufourcq et al., 2002). The microarray analysis found these 4 transcripts expressions to be down-regulated with increasing NIST concentrations (see Appendix: NIST 1648a). Whether this can be considered to be evidence of a "nano-epigenetic" effect in worms remains to be elucidated.

Studies in cells have shown that NPs can affect the ability of methyltransferases to interact with DNA, leading to DNA hypomethylation (Choi et al., 2008, Gong et al., 2010). Furthermore, exposure to metal ions, such as cadmium, can also alter the expression of DNA-methylation pattern and result in DNA hypermethylation in cells (Takiguchi et al., 2003).

In *C. elegans*, the H3K36 methyltransferase MES-4 (maternal effect sterile) and the H3K4 demethylase SPR-5 (suppressor of presenilin defect) are implicated in mechanisms of epigenetic programming between generations (Wenzel et al., 2011; Katz et al., 2009; Rechtsteiner et al., 2010). MES-4 functions in epigenetic memory of germ cells, and its expression was elevated in NIST exposed worms across all examined doses (see Appendix: NIST 1648a). In addition, *spr-1* and *spr-5*, which function as repressors of the presenilin gene and mediate transcriptional repression in *C. elegans*, were transcriptionally activated by lower NIST concentrations, but not at higher doses (see Appendix: NIST 1648a). Whether these play an important role in germline stability in NP exposed worms remains inconclusive, and further investigations are needed.

One of the most studied and best understood environmental factors in epigenetic change is diet (DelCurto et al., 2013; Williams et al., 2013). A well balanced diet will allow the organism to live a healthy and normal life. In contrast, a methyl deficient diet of mothers can affect the infant development and cause certain regions of the genome to be under-methylated for life (Hino et al., 2013). It is likely that once NPs enter the food chain, they can modify the nutrient balance, hence affect the metabolic pathways and ultimately the DNA molecule (Stoccoro et al., 2013; Kim et al., 2013). Since, ZnONPs were able to affect the worm metabolome (Fig. 3.12), it would be interesting to examine whether NPs are also able to induce epigenetic changes affecting expression of genes in *C. elegans*.

6.5 Concluding remarks

The results and discussion presented in this thesis emphasise the need for more research on both natural and synthetic NPs, mainly to fully understand the mechanisms driving the toxicity of these materials. The development of new platforms will allow the detailed elucidation of molecular-mechanisms and biochemical interactions that take place at the nano/bio interface.

The use of *C. elegans* as an alternative animal model enables the impact assessment of long- or short- term exposures to different sizes and concentrations of synthetic and natural NPs. However, there are also potential disadvantages of this model organism, as not all critical exposure routes and aspects of human physiology can be modelled, including inhalation studies or effects on the cardiovascular system.

Nevertheless, by combining molecular and organismal / phenotypic assays, it was possible to start dissecting the multi-factorial responses, as well as health and environmental risks of NPs toxicity - all with the help of a microscopic worm.

REFERENCES

Aebi. H. Catalase *in vitro*. *Methods in Enzymology*. **1984**, *105*:121-126.

Ahamed, M.; Akhtar, M.J.; Raja, M.; Ahmad, I.; Siddiqui, M.K.; AlSalhi, M.S.; Alrokayan, S.A. ZnO nanorod-induced apoptosis in human alveolar adenocarcinoma cells via p53, surviving and *bax*/*bcl-2* pathways: role of oxidative stress. *Nanomedicine.* **2011**, *7*(6):904-13.

Akhtar, M.J.; Ahamed, M.; Kumar, S.; Khan, M.M.; Ahmad, J.; Alrokayan, S.A. Zinc oxide nanoparticles selectively induce apoptosis in human cancer cells through reactive oxygen species. *Int J Nanomedicine.* **2012**, *7*:845-57.

Albrecht, S.C.; Sobotta, M.C.; Bausewein, D.; Aller, I.; Hell, R.; Dick, T.P.; Meyer, A.J. Redesign of genetically encoded biosensors for monitoring mitochondrial redox status in a broad range of model eukaryotes. *J Biomol Screen*. **2014**, *19*(3):379-86.

Al-Chalabi, A.; Leigh, P.N. Recent advances in amyotrophic lateral sclerosis. *Curr Opin Neurol*. **2000**, *13*(4):397-405.

Alessandrini, F.; Shulz, H.; Takenaka, S.; Lentner, B.; Karg, E.; Behrendt, H.; Jakob, T. Effects of ultrafine carbon particle inhalation on allergic inflammation of the lung. *J Allergy Clin Immunol.* **2006**, *117*:824-30.

Alfaro-Moreno, E.; Ponce-de-León, S.; Osornio-Vargas, A.R.; García-Cuellar, C.; Martínez, L.; Rosas, I. Potential toxic effects associated to metals and endotoxin present in PM10: an ancillary study using multivariate analysis. *Inhal Toxicol.* **2007**, *19*(1):49-53.

An, J. H.; Blackwell, T. K. SKN-1 links *C. elegans* mesendodermal specification to a conserved oxidative stress response. *Genes Dev.* **2003**, *17*:1882-93.

Anderson, P.J.; Wilson, J.D.; Hiller, F.C. Respiratory tract deposition of ultrafine particles in subjects with obstructive or restrictive lung disease. *Chest.* **1990**, *97*(5):1115-20.

André, E.; Stoeger, T.; Takenaka, S.; Bahnweg, M.; Ritter, B.; Karg, E.; Lentner, B.; Reinhard, C.; Schulz, H.; Wjst, M. Inhalation of ultrafine carbon particles triggers biphasic pro-inflammatory response in the mouse lung. *Eur Respir J.* **2006**, *28*(2):275-85.

Andrews, G.K. Regulation of metallothionein gene expression by oxidative stress and metal ions. *Biochem Pharmacol.* **2000**, *59*:95-104.

Arnold, M.C.; Badireddy, A.R.; Wiesner, M.R.; Di Giulio, R.T.; Meyer, J.N. Cerium oxide nanoparticles are more toxic than equimolar bulk cerium oxide in *Caenorhabditis elegans*. *Arch Environ Contam Toxicol*. **2013**, *65*(2):224-33.

Arora, S.; Jain, J.; Rajwade, J.M.; Paknikar, K.M. Cellular responses induced by silver nanoparticles: *In vitro* studies. *Toxicol Lett*. **2008**, *179*(2):93-100.

Arora, S.; Rajwade, J.M.; Paknikar, K.M. Nanotoxicology and *in vitro* studies: the need of the hour. *Toxicol Appl Pharmacol*. **2012**, *258*(2):151-65.

ASTM E2834 - 12 (**2012**) Standard Guide for Measurement of Particle Size Distribution of Nanomaterials in Suspension by Nanoparticle Tracking Analysis (NTA), Active Standard ASTM E2834 Developed by Subcommittee: E56.02|Book of Standards Volume: 14.02, DOI: 10.1520/E2834-12.

Auffan, M.; Rose, J.; Bottero, J.Y.; Lowry, G.V.; Jolivet, J.P.; Wiesner, M.R. Towards a definition of inorganic nanoparticles from an environmental, health and safety perspective. *Nat Nanotechnol.* **2009**, *4*(10):634-41.

Ayres, J.G.; Borm, P.; Cassee, F.R.; Castranova, V.; Donaldson, K.; Ghio, A.; Harrison, R.M.; Hider, R.; Kelly, F.; Kooter, I.M.; Marano, F.; Maynard, R.L.; Mudway, I.; Nel, A.; Sioutas, C.; Smith, S.; Baeza-Squiban, A.; Cho, A.; Duggan, S.; Froines, J. Evaluating the toxicity of airborne particulate matter and nanoparticles by measuring oxidative stress potential--a workshop report and consensus statement. *Inhal Toxicol.* **2008**, *20*(1):75-99.

Baan, R.; Straif, K.; Grosse, Y.; Secretan, B.; El Ghissassi, F.; Cogliano, V. Carcinogenicity of carbon black, titanium dioxide, and talc. *The lancet oncology*. **2006**, *7*:295-296.

Back, P.; Braeckman, B.P.; Matthijssens, F. ROS in aging *Caenorhabditis elegans*: damage or signaling*? Oxid Med Cell Longev.* **2012**:608478.

Baggs, R.B.; Ferin, J.; Oberdörster, G Regression of pulmonary lesions produced by inhaled titanium dioxide in rats. *Veterinary Pathology*. **1997**, *34*:592-597.

Bai, W.; Zgang, Z.; Tian, W.; He, X.; Ma, Y., Zhao, Y.; Chai, Z. Toxicity of zinc nanoparticles to zebrafish embryo: a physicochemical study of toxicity mechanism. *J Nanopart. Res.* **2010**, *12*:1645-1654.

Ball, J. C.; Straccia, A. M.; Young, W. C.; Aust, A. E. The formation of reactive oxygen species catalyzed by neutral, aqueous extracts of NIST ambient particulate matter, and diesel engine particles. *J. Air Waste Manage. Assoc.* **2000**, *50*:1897-1903.

Baruah, A.; Chang, H.; Hall, M.; Yuan, J.; Gordon, S.; Johnson, E.; Shtessel, L.L.; Yee, C.; Hekimi, S.; Derry, W.B.; Lee, S.S. CEP-1, the *Caenorhabditis elegans* p53 Homolog, Mediates Opposing Longevity Outcomes in Mitochondrial Electron Transport Chain Mutants. *PLoS Genet*. **2014**, *10*(2):e1004097.

Basel Convention, editor. **1999**. Technical guidelines on the identification and management of used tyres. Prepared by the Technical Working Group of the Basel Convention with support from industry and adopted by the fifth meeting of the Conference of the Parties; 12 Jan 99.

Baulig, A.; Garlatti, M.; Bonvallot, V.; Marchand, A.; Barouki, R.; Marano, F.; Baeza-Squiban, A. Involvement of reactive oxygen species in the metabolic pathways triggered by diesel exhaust particles in human airway epithelial cells. *Am J Physiol Lung Cell Mol Physiol*. **2003**, *285*(3):L671-9.

Beck-Speier, I.; Dayal, N.; Karg, E.; Maier, K.L.; Schumann, G.; Schulz, H.; Semmler, M.; Takenaka, S.; Stettmaier, K.; Bors, W.; Ghio, A.; Samet, J.M.; Heyder, J. Oxidative stress and lipid mediators induced in alveolar macrophages by ultrafine particles. *Free Radic Biol Med.* **2005**, *38*(8):1080-92.

Belay, E.D.; Bresee, J.S.; Holman, R.C.; Khan, A.S.; Shahriari, A.; Schonberger, L.B. Reye's syndrome in the United States from 1981 through 1997. *N. Engl. J. Med.* **1999**, *340*(18):1377-82.

Belousov, V.V.; Fradkov, A.F.; Lukyanov, K.A.; Staroverov, D.B.; Shakhbazov, K.S.; Terskikh, A.V.; Lukyanov, S. Genetically encoded fluorescent indicator for intracellular hydrogen peroxide. *Nat Methods*. **2006**, *3*(4):281-6.

Bhatnagar, A. Environmental cardiology: studying mechanistic links between pollution heart disease. *Circ Res*. **2006**, *99*:692-705.

Blackwell, T.K.; Bowerman, B.; Priess, J.; Weintraub, H. Formation of a monomeric DNA binding domain by Skn-1 bZIP and homeodomain elements. *Science*. **1994**, *266*:621-628.

Blanc, P.D.; Boushey, H.A.; Wong, H.; Wintermeyer, S.F.; Bernstein, M.S. Cytokines in metal fume fever. *Am Rev Respir Dis*. **1993**, *147*(1):134-8.

Bodian, D.; Howe, H.A. Experimental studies on intraneural spread of poliomyelitis virus. *Bull Johns Hopkins Hosp*. **1941a**, *69*:248-267.

Bodian, D.; Howe, H.A. The rate of progression of poliomyelitis virus in nerves. *Bull Johns Hopkins Hosp.* **1941b**, *69*:79-85.

Bonvallot, V.; BaezaSquiban, A.; Baulig, A.; Brulant, S.; Boland, S.; Muzeau, F.; Barouki, R.; Marano, F. Organic compounds from diesel exhaust particles elicit a proinflammatory response in human airway epithelial cells and induce cytochrome p450 1A1 expression. *Am J Respir Cell Mol Biol.* **2001**, *25*:515-21.

Boulin, T.; Bessereau, J.L. Mos1-mediated insertional mutagenesis in *Caenorhabditis elegans*. *Nat Protoc.* **2007**, *2*(5):1276-87.

Boulin, T.; Hobert, O. (**2012**) From genes to function: the *C. elegans* genetic toolbox. *WIREs Dev. Biol.* Volume 1, Issue 1, 114–137.

Bourdon, J.A.; Saber, A.T.; Jacobsen, N.R.; Jensen, K.A.; Madsen, A.M.; Lamson, J.S.; Wallin, H.; Møller, P.; Loft, S.; Yauk, C.L.; Vogel, U.B. Carbon black nanoparticle instillation induces sustained inflammation and genotoxicity in mouse lung and liver. *Part Fibre Toxicol.* **2012**, *2*(9):5.

Bowden, D.H. The alveolar macrophage. *Environ. Health Perspect.* **1984**, *55*:327-41.

Bowerman, B.; Eaton, B.A.; Priess, J.R. skn-1, a maternally expressed gene required to specify the fate of ventral blastomeres in the early C. elegans embryo. *Cell.* **1992**, *68*:1061–1075.

Boyd, R.D.; Pichaimuthu, S.K.; Cuenat, A. New approach to inter-technique comparisons for nanoparticle size measurements; using atomic force microscopy, nanoparticle tracking analysis and dynamic light scattering. *Colloid. Surf. A.* **2011**, *387*(1-3):35-42.

Bremner, I. Manifestations of copper excess. *Am. J. Clin. Nutr.* **1998**, *67*:1069S-1073S.

Brenner, S. The genetics of *Caenorhabditis elegans*. *Genetics* **1974**, *77*:71-94.

Breton, C.V.; Salam, M.T.; Vora, H.; Gauderman, W.J.; Gilliland, F.D. Genetic variation in the glutathione synthesis pathway, air pollution, and children's lung function growth. *Am J Respir Crit Care Med*. **2011**, *183*:243-248.

Brignull, H.R.; Morley, J.F.; Morimoto, R.I. The stress of misfolded proteins: *C. elegans* models for neurodegenerative disease and aging. *Landes Bioscience*. **2007**, *594*:167-189.

Brook, R.D.; Franklin, B.; Cascio, W.; Hong, Y.; Howard, G.; Lipsett, M.; Luepker, R.; Mittleman, M.; Samet, J., Smith, S.C.Jr.; Tager, I.; Expert Panel on Population and Prevention Science of the American Heart Association. Air pollution and cardiovascular disease: a statement for healthcare professionals from the Expert Panel on Population and Prevention Science of the American Heart Association. *Circulation.* **2004**, *109*:2655-2671.

Brown, D.M.; Stone, V.; Findlay, P.; MacNee, W.; Donaldson, K. Increased inflammation and intracellular calcium caused by ultrafine carbon black is independent of transition metals or other soluble components. *Occup. Environ. Med.* **2000**, *57*:685-691.

Brown, J.S.; Zeman, K.L.; Bennett, W.D. Ultrafine particle deposition and clearance in the healthy and obstructed lung. *Am J Respir Crit Care Med*. **2002**, *166*:1240-1247.

Brown, J.S; Zeman, K.L.; Bennett, W.D. Regional deposition of coarse particles and ventilation distribution in patients with cystic fibrosis. *J. Aerosol Med.* **2001**, *14*:443-454.

Brown, R. "A brief account of microscopical observations made in the months of June, July and August, 1827, on the particles contained in the pollen of plants; and on the general existence of active molecules in organic and inorganic bodies." *Phil. Mag.* **1828**, *4*:161-173.

Brunekreef, B.; Holgate, S.T. Air pollution health. *Lancet*. **2002**, *360*:1233-1242.

Buchanan, B.B. (Editor); Gruissem, W. (Editor); Jones, R.L. (Editor) (**2000**) Biochemistry & molecular biology of plants, 1st edition, *American Society of Plant Physiology*. Published by: John Wiley & Sons Inc.

Cabreiro, F.; Ackerman, D.; Doonan, R.; Araiz, C.; Back, P.; Papp, D.; Braeckman, B.P.; Gems, D. Increased life span from overexpression of superoxide dismutase in *Caenorhabditis elegans* is not caused by decreased oxidative damage. *Free Radic. Biol. Med.* **2011**, *51*(8):1575-82.

Cadenas, E.; Boveris, A.; Ragan, C.I.; Stoppani, A.O.M. Production of superoxide radicals and hydrogen peroxide by NADH-ubiquinone reductase and ubiquinolcytochrome c reductase from beef-heart mitochondria. *Arch Biochem Biophys*. **1977**, *180*:248-257.

Calderon-Garcidueñas, L.; Azzarelli, B.; Acuna, H.; Garcia, R.; Gambling, T.M.; Osnaya, N.; Monroy, S.; DEL Tizapantzi, M.R.; Carson, J.L.; Villarreal-Calderon, A.; Rewcastle, B. Air pollution and brain damage. *Toxicol Pathol.* **2002**, *30*:373-389.

Canadian Environmental Protection Act (CEPA) (**1999**). S.C., 1999, c. 33, Canada Gazette. Part III. vol. *22*, no. 3.

Canesi, L.; Fabbri, R.; Gallo, G.; Vallotto, D.; Marcomini, A.;, Pojana, G. Biomarkers in *Mytilus galloprovincialis* exposed to suspensions of selected nanoparticles (Nano carbon black, C60 fullerene, Nano-TiO2, Nano-SiO2). *Aquat Toxicol.* **2010**, *100*(2):168-77.

Carr, B.; Hole, P.; Malloy, A.; Nelson, P.; Smith, J. Applications of Nanoparticle Tracking analysis (NTA) in Nanoparticle Research – a Mini-Review. www.nanosight.com

Carr, B.; Malloy, A. NanoParticle Tracking Analysis–The NANOSIGHT system. www.nanosight.co.uk

Carr, B.; Warren, J. Company profile: NanoSight: delivering practical solutions for biological nanotechnology. *Nanomedicine (Lond).* **2012**, *7*(8):1129-32.

Casareno, R.L.; Waggoner, D.; Gitlin, J.D. The copper chaperone CCS directly interacts with copper/zinc superoxide dismutase. J. Biol. Chem. **1998**, *273*(37):23625-8.

Cathcart, R.; Schwiers, E.; Ames, B.N. Detection of picomole levels of hydroperoxides using a fluorescent dichlorofluorescein assay. *Anal Biochem.* **1983**, *134*(1):111-6.

Chatterjee, N.; Eom, H.J.; Choi, J. Effects of silver nanoparticles on oxidative DNA damage-repair as a function of p38 MAPK status: a comparative approach using human Jurkat T cells and the nematode *Caenorhabditis elegans*. *Environ Mol Mutagen*. **2014**, *55*(2):122-33.

Chen, G. X.; Hong, M. H.; Chong, T. C. Preparation of carbon nanoparticles with strong optical limiting properties by laser ablation in water. *Journal of Applied Physics*. **2004**, *95*:3.

Chen, G.; Korfhagen, T.R.; Xu, Y.; Kitzmiller, J.; Wert, S.E.; Maeda, Y.; Gregorieff, A.; Clevers, H.; Whitsett, J.A. SPDEF is required for mouse pulmonary goblet cell differentiation

and regulates a network of genes associated with mucus production. *J Clin Invest*. **2009**, *119*:2914-2924.

Chen, P. C.; Mwakwari, S.C.; Oyelere; A. K. Gold nanoparticles: From nanomedicine to nanosensing. *Nanotechnology, Science and Applications.* **2008**, *1*:45-66.

Chitwood, B.G.; Chitwood, M.B. (Authors) (**1950**)**.** Somatic musculature, connective tissue, body cavity, and organs of body cavity. *In An introduction to nematology.*, Chapter *4*:48-56. Published by: Baltimore, University Park Press.

Choe, K.P.; Leung, C.K.; Miyamoto, M.M. Unique structure and regulation of the nematode detoxification gene regulator, SKN-1: implications to understanding and controlling drug resistance. *Drug Metab Rev.* **2012**, *44*(3):209-23.

Choi, A.O.; Brown, S.E.; Szyf, M.; Maysinger, D. Quantum dot-induced epigenetic and genotoxic changes in human breast cancer cells. *J Mol Med (Berl)*. **2008**, *86*(3):291-302.

Cobbett, C.; Goldsbrough, P. Phytochelatins and metallothioneins: roles in heavy metal detoxification and homeostasis. *Annu Rev Plant Biol.* **2002**, *53*:159-182.

Cobbett, C.S. Phytochelatins and their roles in heavy metal detoxification. *Plant Physiol*. **2000**, *123*(3):825-32.

Cohn, C. A.; Simon, S. R.; Schoonen, M. A. A. Comparison of fluorescence-based techniques for the quantification of particle-induced hydroxyl radicals. *Part. Fibre Toxicol.* **2008**, *5*:2.

Collins, A.R. Measuring oxidative damage to DNA and its repair with the comet assay. *Biochim Biophys Acta*. **2014**, *1840*(2):794-800.

Colvin, V.L. The potential environmental impact of engineered nanomaterials. *Nature Biotechnology.* **2003**, *21*:1166-1170.

Contreras, E.Q.; Cho, M.; Zhu, H.; Puppala, H.L.; Escalera, G.; Zhong, W.; Colvin, V.L. Toxicity of quantum dots and cadmium salt to *Caenorhabditis elegans* after multigenerational exposure. *Environ Sci Technol*. **2013**, *47*(2):1148-54.

Cooke, M.S.; Evans, M.D.; Dizdaroglu, M.; Lunec, J. Oxidative DNA damage: mechanisms, mutation, and disease. *FASEB J.* **2003**, *17*:1195-1214.

Costa, D.L.; Dreher, K.L. Bioavailable transition metals in particulate matter mediate cardiopulmonary injury in health and compromised animal models. *Environ Health Perspect.* **1997**, *105*:1053-60.

Coulson, A. R.; Kozono, Y.; Lutterbach, B.; Shownkeen, R.; Sulston, J.; Waterston, R. YACs and the *C. elegans* genome. *BioEssays.* **1991**, *13*:413-417.

Cox, L.A.Jr. Universality of J-shaped and U-shaped dose-response relations as emergent properties of stochastic transition systems. *Dose Response*. **2006**, *3*(3):353-68.

Crosera M.; Bovenzi, M.; Maina, G.; Adami, G.; Zanette, C.; Florio, C.; Larese, F. F. Nanoparticle dermal absorption and toxicity: a review of the literature. *Int Arch Occup Environ Health.* **2009**, *82*(9):1043-55.

Curtis, J.; Greenberg, M.; Kester, J.; Phillips, S.; Krieger, G. Nanotechnology and nanotoxicology: a primer for clinicians. *Toxicol. Sci*. **2006**, *25*:245-260.

Curtis, L.; Rea, W.; Smith-Willis, P.; Fenyves, E.; Pan, Y. Adverse health effects of outdoor air pollutants. *Environ Int.* **2006**, *32*:815-830.

Dai, D.; Zeldin, D.C.; Blaisdell, J.A.; Chanas, B.; Coulter, S.J.; Ghanayem, B.I.; Goldstein, J.A. Polymorphisms in human CYP2C8 decrease metabolism of the anticancer drug paclitaxel and arachidonic acid. *Pharmacogenetics.* **2001**, *11*(7):597-607.

Daniel, K.G.; Harbach, R.H.; Guida, W.C.; Dou Q.P. Copper storage diseases: Menkes, Wilsons, and cancer. *Front. Biosci*. **2004**, *9*:2652-2662.

Dasenbrock, C.; Peters, L.; Creutzenberg, O.; Heinrich, U. The carcinogenic potency of carbon particles with and without PAH after repeated intratracheal administration in the rat. *Toxicology Letters*. **1996**, *88*:15-21.

De Bono, M.; Tobin, D.M.; Davis, M.W.; Avery, L.; Bargmann, C.I. Social feeding in *Caenorhabditis elegans* is induced by neurons that detect aversive stimuli. *Nature*. **2002**, *419*:899-903.

DEFRA, The Environment Agency UK Soil and Herbage Pollutant Survey (**2007**) 978-1-84432-692-1published by Environment Agency, Rio House, Waterside Drive, Aztec West, Almondsbury, Bristol (BS32 4UD).

DelCurto, H.; Wu, G.; Satterfield, M.C. Nutrition and reproduction: links to epigenetics and metabolic syndrome in offspring. *Curr Opin Clin Nutr Metab Care*. **2013**, *16*(4):385-91.

Delfino, R.; Sioutas, C.; Malik, S. Potential role of ultrafine particles in associations between airborne particle mass and cardiovascular health. *Environ Health Perspect.* **2005**, *113*:934-946.

Dennis, G. Jr.; Sherman, B. T.; Hosack, D. A.; Yang, J.; Gao, W.; Lane, H. C.; Lempicki, R. A. DAVID: Database for Annotation, Visualization, and Integrated Discovery. *Genome Biology*. **2003**, *4*:R60.

Derry, W.B.; Putzke, A.P.; Rothman, J.H. *Caenorhabditis elegans* p53: role in apoptosis, meiosis, and stress resistance. *Science.* **2001**, *294*(5542):591-5.

Ding, Q.; Markesbery, W.R.; Cecarini, V.; Keller, J.N. Decreased RNA, and increased RNA oxidation, in ribosomes from early Alzheimer's disease. *Neurochem Res.* **2006**, *31*:705–710.

Ding, Q.; Markesbery, W.R.; Chen, Q.; Li, F.; Keller, J.N. Ribosome dysfunction is an early event in Alzheimer's disease. *J Neurosci*. **2005,** *25*:9171-9175.

Dockery, D.W.; Pope III, A.C.; Xu, X.; Spengler, J.D.; Ware, J.H.; Fay, M.E.; Ferris, B.G.; Jr, Speizer, F.E. An association between air pollution and mortality in six U.S. cities. *N Engl J Med.* **1993**, *329*(24):1753-9.

Domingos, R.F.; Baalousha, M.A.; Ju-Nam, Y.; Reid, M.M.; Tufenkji, N.; Lead, J.R.; Leppard, G.G.; Wilkinson, K.J. Characterizing manufactured nanoparticles in the environment: multimethod determination of particle sizes. *Environ. Sci. Technol.* **2009**, *43*(19):7277-84.

Donaldson, K.; Poland, C.A.; Schins, R.P. Possible genotoxic mechanisms of nanoparticles: criteria for improved test strategies. *Nanotoxicology.* **2010**, *4*:414-20.

Donaldson, K.; Stone, V. Current hypotheses on the mechanisms of toxicity of ultrafine particles. *Ann. Ist Super. Sanita.* **2003**, *39*:405-410.

Donaldson, K.; Stone, V.; Clouter, A.; Renwick, L.; MacNee, W. Ultrafine particles. *Occup. Environ. MED.* **2001**, *58*:211-216.

Donaldson, K.; Stone, V.; Gilmour, P. S.; Brown, D. M.; MacNee, W. Ultrafine particles: Mechanisms of lung injury. *Phil. Trans. R. Soc. Lond. A.* **2000**, *358*:2741-2749.

Donaldson, K.; Tran, L.; Jimenez, L.A.; Duffin, R.; Newby, D.E.; Mills, N.; MacNee, W.; Stone, V. Combustion-derived nanoparticles: a review of their toxicology following inhalation exposure. *Part. Fibre Toxicol.* **2005**, *21*(2):10.

Donati, G.; Brighenti, E.; Vici, M.; Mazzini, G.; Treré, D.; Montanaro, L.; Derenzini, M. Selective inhibition of rRNA transcription downregulates E2F-1: a new p53-independent mechanism linking cell growth to cell proliferation. *J Cell Sci.* **2011**, *124*(Pt 17):3017-28.

Donkin, S.G.; Williams, P.L. Influence of developmental stage, salts and food presence on various end points using *Caenorhabditis elegans* for aquatic toxicity testing. *Environmental Toxicology and Chemistry*. **1995**, *14*:2139-2147.

Doonan, R.; McElwee, J.J.; Matthijssens, F.; Walker, G.A.; Houthoofd, K.; Back, P.; Matscheski, A.; Vanfleteren, J.R.; Gems, D. Against the oxidative damage theory of aging: superoxide dismutases protect against oxidative stress but have little or no effect on life span in *Caenorhabditis elegans. Genes & Developmen*, **2008**, *22*(23):3236-3241.

Drobne, D.; Jemec, A.; Pipan Tkalec, P. In vivo screening to determine hazards of nanoparticles: Nanosized TiO_2. *Environmental Pollution*. **2009**, *157*:1157-1164.

Dufour, E.K.; Kumaravel, T.; Nohynek, G.J.; Kirkland. D.; Toutain, H. Clastogenicity, photo-clastogenicity or pseudo-photo-clastogenicity: Genotoxic effects of zinc oxide in the dark, in pre-irradiated or simultaneously irradiated Chinese hamster ovary cells. *Mutat. Res.* **2006**, *607*(2):215-224.

Dufourcq, P.; Victor, M.; Gay, F.; Calvo, D.; Hodgkin, J.; Shi, Y. Functional requirement for histone deacetylase 1 in *Caenorhabditis elegans* gonadogenesis. *Mol Cell Biol.* **2002**, *22*: 3024-34.

Dutta, R.K.; Nenavathu, B.P.; Gangishetty, M.K. Reddy, A.V. Antibacterial effect of chronic exposure of low concentration ZnO nanoparticles on *E. coli*. *J Environ Sci Health A Tox Hazard Subst Environ Eng.* **2013**, *48*(8):871-8.

Eder, C.; Frankenberger, M.; Stanzel, F.; Seidel, A., Schramm, K.W.; Ziegler-Heitbrock, L.; Hofer, T.P. Ultrafine carbon particles down-regulate CYP1B1 expression in human monocytes. *Part. Fibre Toxicol*. **2009**, *6*:27.

Elchuri, S.; Oberley, T.D.; Qi, W.; Eisenstein, R.S.; Jackson Roberts, L.; Van Remmen, H.; Epstein, C.J.; Huang, T.T. CuZnSOD deficiency leads to persistent and widespread oxidative damage and hepatocarcinogenesis later in life. *Oncogene.* **2005**, *24*(3):367-80.

Elder, A.C.P.; Gelein, R.; Finkelstein, J.N.; Cox, C.; Oberdörster, G. Pulmonary inflammatory response to inhaled ultrafine particles is modified by age, ozone exposure, and bacterial toxin. *Inhalation Toxicology.* **2000**, *12*:227-246.

Environmental Protection Agency (U.S. EPA). Air Quality Criteria for Ozone and Related Photochemical Oxidants. Research Triangle Park, NC: Office of Research and Development; 2006. Report no. EPA/600/R-05/004aF. U.S. EPA, Research Triangle Park, NC.

Environmental Protection Agency (U.S. EPA). Air Quality Index Reporting and Significant Harm Level for Fine Particulate Matter. 2009. 40 CFR Parts 51 and 58 [EPA-HQ -OAR-2007-0195; FRL-] RIN 2060-AO11

Environmental Protection Agency (U.S. EPA). PM Centers. Washington, DC: U.S. Environmental Protection Agency; 2008. [[accessed 12 July 2012]].

Environmental Protection Agency (U.S. EPA). Report to Congress on Black Carbon. 2012. Report no. EPA-450/R-12-001

Euling, SY. Toxicogenomics in risk assessment. *Toxicol Appl Pharmacol*. **2013**, pii:S0041-008X(13)00260-3.

Ewbank, J.J. Tackling both sides of the host-pathogen equation with *Caenorhabditis elegans*. *Microbes Infect*. **2002**, *4*:247-256.

Fahey, J.W.; Haristoy, X.; Dolan, P.M.; Kensler, T.W.; Schotus, I.; Stephenson, K.K.; Talay, P.; Lorzniewki, A. Sulforaphane inhibits extracellular, intracellular antibiotic-resistant strains of Helicobacter pylori prevents benzo[a]pyrene-induced stomach tumors. *Proc Natl Acad Sci*. **2001**, *99*:7610-7615.

Fajardo, C.; Saccà, M.L.; Costa, G.; Nande, M.; Martin, M. Impact of Ag and Al_2O_3 nanoparticles on soil organisms: in vitro and soil experiments. *Sci Total Environ*. **2014**, *473-474*:254-61.

Fanning, E.W.; Froines, J. R.; Utell, M. J.; Lippmann, M.; Oberdörster, G.; Frampton, M.; Godleski, J.; Larson, T. V. Particulate Matter (PM) Research Centers (1999–2005) and the Role of Interdisciplinary Center-Based Research. *Environ Health Perspect*. **2009**, *117*:167-174.

Faux, S. P. (Author); Tran, C. L.; Miller, B. G.; Jones, A. D.; Montellier, C., Donaldson, K. (**2003**) *In vitro* determinants of particulate toxicity: The dose metric for poorly soluble dusts. *Research Report Series. 154*, HSE Books.

Ferin, J.; Oberdorster, G.; Penney, D.P. Pulmonary retention of ultrafine and fine particles in rats. *Am. J. Respir. Cell Mol. Biol.* **1992**, *6*:535-42.

Ferin, J.; Oberdörster, G.; Penney, D.P.; Soderholm, S.C.; Gelein, R.; Piper, H.C. Increased pulmonary toxicity of ultrafine particles? I. Particle clearance, translocation, morphology. *J Aerosol Sci.* **1990**, *21*:381-384.

Feynman, R. There is plenty room at the bottom. **1959,** www.its.caltech.edu/~feynman/plenty.html

Filipe, V.; Hawe, A.; Jiskoot, W. Critical evaluation of Nanoparticle Tracking Analysis (NTA) by NanoSight for the measurement of nanoparticles and protein aggregates. *Pharm Res*. **2010**, *27*(5):796-810.

Finger, E.C.; Turley, R.S.; Dong, M.; How, T.; Fields, T.A.; Blobe, G.C. TbetaRIII suppresses non-small cell lung cancer invasiveness and tumorigenicity. *Carcinogenesis*. **2008**, *29*(3):528-35.

Franklin, N.M.; Rogers, N.J.; Apte, S.C.; Batley, G.E.; Gadd, G.E.; Casey, P.S. Comparative toxicity of nanoparticulate ZnO, bulk ZnO, and $ZnCl_2$ to a freshwater microalga (*Pseudokirchneriella subcapitata*): the importance of particle solubility. *Environ Sci Technol*. **2007**, *41*(24):8484-90.

Freedman, J.H.; Slice, L.W.; Dixon, D.; Fire, A.; Rubin, C.S. The novel metallothionein genes of *Caenorhabditis elegans*. Structural organization and inducible, cell-specific expression. *J Biol Chem*. **1993**, *268*(4):2554-64.

Frøkjær-Jensen, C.; Davis, M.W.; Hopkins, C.E.; Newman, B.J.; Thummel, J.M.; Olesen, S.P.; Grunnet, M.; Jorgensen, E.M. Single-copy insertion of transgenes in *Caenorhabditis elegans*. *Nat. Genet.* **2008**, *40*:1375-1383.

Fuhrman, L.E.; Goel, A.K.; Smith, J.; Shianna, K.V.; Aballay, A. Nucleolar proteins suppress *Caenorhabditis elegans* innate immunity by inhibiting p53/CEP-1. *PLoS Genet.* **2009**, *5*(9):e1000657.

Gaetke, L.M.; Chow, C. K. Copper toxicity, oxidative stress, and antioxidant nutrients. *Toxicology*. **2003**, *189*:147-163.

Galloway, T.; Lewis, C.; Dolciotti, I.; Johnston, B.D.; Moger, J.; Regoli, F. Sublethal toxicity of nano-titanium dioxide and carbon nanotubes in a sediment dwelling marine polychaete. *Environ. Pollut*. **2010**, *158*(5):1748-1755.

Gardiner, K.; van Tongeren, M.; Harrington, M. Respiratory health effects from exposure to carbon black: results of the phase 2 and 3 cross sectional studies in the European carbon black manufacturing industry. *Occup Environ Med*. **2001**, *58*(8):496-503.

Garza, K.M.; Soto, K.F.; Murr, L.E. Cytotoxicity and reactive oxygen species generation from aggregated carbon and carbonaceous nanoparticulate materials. *Int. J. Nanomedicine*. **2008**, *3*(1):83-94.

Gems, D.; Doonan, R. Antioxidant defense and aging in *C. elegans*: is the oxidative damage theory of aging wrong? *Cell Cycle*. **2009**, *8*(11):1681-7.

George, S., Pokhrel, S.; Xia, T.; Gilbert, B.; Ji, Z., Schowalter, M.; Rosenauer, A.; Damoiseaux, R.; Bradley, K.A.; Mädler, L.; Nel, A.E. Use of a rapid cytotoxicity screening approach to engineer a safer zinc oxide nanoparticle through iron doping. *ACS Nano*. **2010**, *4*(1):15-29.

Gercel-Taylor, C.; Atay, S.; Tullis, R.H.; Kesimer, M.; Taylor, D.D. Nanoparticle analysis of circulating cell-derived vesicles in ovarian cancer patients. *Anal. Biochem*. **2012**, *428*(1):44-53.

Ghelfi, E.; Rhoden, C.; Wellenius, G.A.; Lawrence, J.; González-Flecha, B. Cardiac oxidative stress and electrophysiological changes in rats exposed to concentrated air particles are mediated by TRP-dependent pulmonary reflexes. *Toxicol Sci*. **2008**, *102*:328-336.

Ghio, A.J.; Carraway, M.S.; Madden, M.C. Composition of air pollution particles and oxidative stress in cells, tissues, and living systems. *J Toxicol Environ Health B Crit Rev*. **2012**, *15*(1):1-21.

Giacomotto, J.; Ségalat, L. High-throughput screening and small animal models, where are we? *Br. J. Pharmacol*. **2010**, *160*(2):204-16.

Gilliland, F.D.; Li, Y.F.; Saxon, A.; Diaz-Sanchez, D. Effect of glutathione-S-transferase M1 and P1 genotypes on xenobiotic enhancement of allergic responses: randomised, placebo-controlled crossover study. *Lancet*. **2004**, *363*(9403):119-25.

Gilmour, P.S.; Ziesenis, A.; Morrison, E.R.; Vickers, M.A.; Drost, E.M.; Ford, I.; Karg, E.; Mossa, C.; Schroeppel, A.; Ferron, G.A.; Heyder, J.; Greaves, M.; MacNee, W.; Donaldson, K. Pulmonary and systemic effects of short-term inhalation exposure to ultrafine carbon black particles. *Toxicol. Appl. Pharmacol*. **2004**, *195*(1):35-44.

Godleski, J.J. Responses of the heart to ambient particle inhalation. *Clin Occup Environ Med*. **2006**, *5*:849-864.

Goldsmith, C.A.; Imrich, A.; Danaee, H.; Ning, Y.Y.; Kobzik, L Analysis of air pollution particulate-mediated oxidant stress in alveolar macrophages. *J Toxicol Environ Health A*. **1998**, *54*:529-545.

Gong, C.; Tao, G.; Yang, L.; Liu, J.; Liu, Q.; Li, W.; Zhuang, Z. Methylation of PARP-1 promoter involved in the regulation of nano-SiO2-induced decrease of PARP-1 mRNA expression. Toxicol Lett. **2012**, *209*: 264-269.

Gong, C.; Tao, G.;, Yang, L.; Liu, J.; Liu, Q.; Zhuang, Z. SiO(2) nanoparticles induce global genomic hypomethylation in HaCaT cells. *Biochem Biophys Res Commun*. **2010**, *397*(3):397-400.

Gordon, S.B.; Reid, R.C. Macrophage defences against respiratory tract infections. *Br. Med. Bull.* **2002**, *61*:45-61.

Grabinski, C.; Schaeublin, N.; Wijaya, A.; D'Couto, H.; Baxamusa, S.H.; Schifferli, K.H.; Hussain, S.M. Effect of Gold Nanorod Surface Chemistry on Cellular Response. *ACS Nano*. **2011**, *5*(4):2870-2879.

Gras, D.; Chanez, P.; Vachier, I.; Petit, A.; Bourdin, A. Bronchial epithelium as a target for innovative treatments in asthma. *Pharmacol Ther.* **2013**, *140*(3):290-305.

Gratton, S. E.; Ropp, P.A.; Pohlhaus, P.D.; Luft, J. C.; Madden, J. V.; Napier, M. E.; DeSimone, J. M. The effect of particle design on cellular internalization pathways. *PNAS.* **2008**, *33*:11613-11618.

Grill, E.; Loffler, S.; Winnacklet, E. L.; Zenk, M.H. Phytochelatins, the heavy-metal-binding peptides of plants, are synthesized from glutathione by a specific y-glutamylcysteine dipeptidyl transpeptidase (phytochelatin synthase). *Proc. Nati. Acad. Sci. USA.* **1989**, *86*:6838-6842.

Gruber, J.; Ng, L.F.; Fong, S.; Wong, Y.T.; Koh, S.A.; Chen, C.B.; Shui, G., Cheong, W.F.; Schaffer, S.; Wenk, M.R.; Halliwell, B. Mitochondrial changes in ageing *Caenorhabditis elegans*--what do we learn from superoxide dismutase knockouts? *PLoS One.* **2011**, *6*(5):e19444.

Guarieiro, L.L.N.; Guarieiro, A.L.N. (**2013**). Vehicle Emissions: What Will Change with Use of Biofuel?, Biofuels - Economy, Environment and Sustainability, Prof. Zhen Fang (Editor), ISBN: 978-953-51-0950-1, InTech, DOI: 10.5772/52513.

Guérin, T.M.; Palladino, F.; Robert, V.J. Transgenerational functions of small RNA pathways in controlling gene expression in *C. elegans*. *Epigenetics*. **2014**, *9*(1):37-44.

Gunaratna, M.; Ogden, L.; Brock, T.; Hopkins, C. (**2012**) Detection and discrimination of oxidative stress response using a transgenic *C. elegans* system of transcription-activated fluorescent reporters. BioTechniques.

Guo, R.; Zebda, R.; Drake, S.J.; Sayes, C.M. Synergistic effect of co-exposure to carbon black and Fe_2O_3 nanoparticles on oxidative stress in cultured lung epithelial cells. *Part. Fibre Toxicol.* **2009**, *6*:4.

Guo, Y.Y.; Zhang, J.; Zheng, Y.F.; Yang, J.; Zhu, X.Q. Cytotoxic and genotoxic effects of multi-wall carbon nanotubes on human umbilical vein endothelial cells *in vitro*. *Mutat Res*. **2011**, *721*(2):184-91.

Hailemariam, Y.; Amiri, H.M.; Nugent, K. Acute respiratory symptoms following massive carbon black exposure. *Occup. Med. (Lond).* **2012**, *62*(7):578-80.

Hall, D.H. Electron microscopy and three-dimensional image reconstruction. *Methods Cell Biol*. **1995**, *48*:395-436.

Hall, D.H.; Hartwieg, E.; Nguyen, K.C. Modern electron microscopy methods for *C. elegans*. *Methods Cell Biol*. **2012**, *107*:93-149.

Halliwell, B.; Whiteman, M. Measuring reactive species and oxidative damage *in vivo* and in cell culture: how should you do it and what do the results mean? *Br. J. Pharmacol*. **2004**, *142*:231-255.

Hancock, J.T.; Desikan, R.; Neill, S.J. Role of Reactive Oxygen Species in Cell Signaling Pathways. *Biochemical and Biomedical Aspects of Oxidative Modification*. **2001**, *29*(2):345-350.

Hanley, C.; Thurber, A.; Hanna, C.; Punnoose, A.; Zhang, J.; Wingett, D.G. The Influences of Cell Type and ZnO Nanoparticle Size on Immune Cell Cytotoxicity and Cytokine Induction. *Nanoscale Res Lett.* **2009**, *4*(12):1409-20.

Harber, P.; Muranko, H.; Solis, S.; Torossian, A.; Merz, B. Effect of carbon black exposure on respiratory function and symptoms. *J. Occup. Environ. Med.* **2003**, *45*(2):144-55.

Harman D. Aging: a theory based on free radical and radiation chemistry. *J Gerontol.* **1956**, *11*(3):298-300.

Harman, D. The free radical theory of aging. *Antioxid Redox Signal.* **2003**, *5*(5):557-61.

Hatanaka, N.; Yamazaki, H.; Kizu, R.; Hayakawa, K.; Aoki, Y.; Iwanari, M.; Nakajima, M.; Yokoi, T. Induction of Cytochrome P450 1B1 in Lung, Liver and Kidney of Rats Exposed to Diesel Exhaust. *Carcinogenesis* **2001**, *22*:2033-2038.

Hatzis, C.; Godleski, J.J.; González-Flecha, B.; Wolfson, J.M.; Koutrakis, P. Ambient particulate matter exhibits direct inhibitory effects on oxidative stress enzymes. *Environ Sci Technol.* **2006**, *40*(8):2805-11.

Hayes, J.D.; McMahon, M. Molecular basis for the contribution of the antioxidant responsive element to cancer chemoprevention. *Cancer Lett.* **2001**, *174*:103-113.

He, H.; Cai, L.; Skogerbø, G.; Deng, W.; Liu, T.; Zhu, X.; Wang, Y.; Jia, D.; Zhang, Z.; Tao, Y.; Zeng, H.; Aftab, M.N.; Cui, Y.; Liu, G.; Chen, R. Profiling *Caenorhabditis elegans* non-coding RNA expression with a combined microarray. *Nucleic Acids Res.* **2006**, *34*(10):2976-83.

Hegde, A.N.; Upadhya, S.C. Role of ubiquitin-proteasome-mediated proteolysis in nervous system disease. *Biochim. Biophys. Acta.* **2011**, *1809*:128-140.

Heggelund, L.R.; Diez-Ortiz, M.; Lofts, S.; Lahive, E.; Jurkschat, K.; Wojnarowicz, J.; Cedergreen, N.; Spurgeon, D.; Svendsen, C. Soil pH effects on the comparative toxicity of dissolved zinc, non-nano and nano ZnO to the earthworm Eisenia fetida. *Nanotoxicology.* **2014**, *8*(5):559-72.

Heinrich, U.; Fuhst, R.; Rittinghausen, S.; Creutzenberg, O.; Bellmann, B.; Koch, W.; Levsen, K. Chronic inhalation exposure of wistar rats and two different strains of mice to diesel engine exhaust, carbon black and titanium dixoide. *Inhal. Toxicol.* **1995**, *7*:533-556.

Hekimi, S.; Lapointe, J.; Wen, Y. Taking a "good" look at free radicals in the aging process. *Trends Cell Biol.* **2011**, *21*(10):569-76.

Hillier, L.W.; Coulson, A.; Murray, J. I.; Bao, Z.; Sulston, J. E.; Waterston, R. H. Genomics in *C. elegans*: So many genes, such a little worm. *Genome Res.* **2005**, *15*:1651-1660.

Hillyer, J. F.; Albrecht, R.M. Gastrointestinal persorption and tissue distribution of differently sized colloidal gold nanoparticles. *J. Pharm. Sci.* **2001**, *90*:1927-36.

Hino, S.; Nagaoka, K.; Nakao, M. Metabolism-epigenome crosstalk in physiology and diseases. *J Hum Genet.* **2013**, *58*(7):410-5.

Hitchcock, D.R.; Law, S.E.; Wu, J.; Williams, P.L. Determining toxicity trends in the ozonation of synthetic dye wastewaters using the nematode *Caenorhabditis elegans*. *Arch. Environ. Contam. Toxicol.* **1998**, *34*:259-264.

Holgate, S. (**2008)** Exposure, uptake, distribution and toxicity of nanomaterials (review).

Holgate, S. Exposure, uptake, distribution and toxicity of nanomaterials. *J Biomed Nanotechnol.* **2010**, *6*(1):1-19.

Honda, K.; Smith, M.A., Zhu, X.; Baus, D.; Merrick, W.C.; Tartakoff, A.M.; Hattier, T.; Harris, P.L., Siedlak, S.L.; Fujioka, H.; Liu, Q., Moreira, P.I.; Miller, F.P., Nunomura, A.; Shimohama, S.; Perry, G. Ribosomal RNA in Alzheimer disease is oxidized by bound redox-active iron. *J Biol Chem*. **2005**, *280*:20978-20986.

Honda, S., Ishii, N.; Suzuki, K.; Matsuo, M. Oxygen-dependent perturbation of life span and aging rate in the nematode. *J Gerontol.* **1993**, *48*(2):B57-61.

Honda, S., Matsuo, M. Lifespan shortening of the nematode *Caenorhabditis elegans* under higher concentrations of oxygen. *Mech Ageing Dev*. **1992**, *63*(3):235-46.

Honda, Y.; Honda, S. Oxidative stress and life span determination in the nematode *Caenorhabditis elegans*. *Ann N Y Acad Sci.* **2002**, *959*:466-74.

Honda, Y.; Honda, S. The *daf-2* gene network for longevity regulates oxidative stress resistance and Mn-superoxide dismutase gene expression in *Caenorhabditis elegans*. *The FASEB Journal*. **1999**, *13*(11):1385-1393.

Honda, Y.; Tanaka, M.; Honda, S. Modulation of longevity and diapause by redox regulation mechanisms under the insulin-like signaling control in *Caenorhabditis elegans*. *Experimental Gerontology.* **2008**, *43*(6):520-529.

Hong, Y.C.; Lee, J.T.; Kim, H.; Kwon, H.J. Air pollution: a new risk factor in ischemic stroke mortality. *Stroke.* **2002**, *33*:2165-2169.

Hooper, H.L.; Jurkschat, K.; Morgan, A.J., Bailey, J.; Lawlor, A.J.; Spurgeon, D.J.; Svendsen, C. Comparative chronic toxicity of nanoparticulate and ionic zinc to the earthworm *Eisenia veneta* in a soil matrix. *Environ. Int.* **2011**, *37*:1111-1117.

Horie, M.; Kato, H.; Fujita, K.; Endoh, S.; Iwahashi, H. In vitro evaluation of cellular response induced by manufactured nanoparticles. *Chem. Res. Toxicol.* **2012**, *25*(3):605-19.

Hsu, P.C., O'Callaghan, M.; Al-Salim, N.; Hurst, M.R. Quantum dot nanoparticles affect the reproductive system of *Caenorhabditis elegans*. *Environ Toxicol Chem.* **2012**, *31*(10):2366-74.

Huang, C.C.; Aronstam, R.S.; Chen, D.R.; Huang, Y.W. Oxidative stress, calcium homeostasis, and altered gene expression in human lung epithelial cells exposed to ZnO nanoparticles. *Toxicol In Vitro.* **2010**, *24*(1):45-55.

Huang, D.W.; Sherman, B.T.; Lempicki, R.A. Bioinformatics enrichment tools: paths toward the comprehensive functional analysis of large gene lists. *Nucleic Acids Res*. **2009**, *37*(1):1-13.

Huang, D.W.; Sherman, B.T.; Lempicki, R.A. Systematic and integrative analysis of large gene lists using DAVID Bioinformatics Resources. *Nature Protoc*. **2009**, *4*(1):44-57.

Huang, Y.C.; Li, Z.; Carter, J.D.; Soukup, J.M.; Schwartz, D.A.; Yang, I.V. Fine ambient particles induce oxidative stress and metal binding genes in human alveolar macrophages. *Am J Respir Cell Mol Biol*. **2009**, *41*(5):544-52.

Huggins, F.E.; Huffman, G.P.; Robertson, J.D. Speciation of elements in NIST particulate matter SRMs 1648 and 1650. *J Hazard Mater*. **2000**, *74*(1-2):1-23.

Hughes, M.F.; Long, T.C.; Boyes, W.K.; Ramabhadran, R. Whole-body retention and distribution of orally administered radiolabelled zerovalent iron nanoparticles in mice. *Nanotoxicology*. **2013**, *7*:1064-1069.

Hughes, S.; Stürzenbaum, S. R. Single and double metallothionein knockout in the nematode *C. elegans* reveals cadmium dependent and independent toxic effects on life history traits. *Environmental Pollution*. **2007**, *145*:395-400.

Hughes, S.L.; Bundy, J.G.; Want, E.J.; Kille, P.; Stürzenbaum, S.R. The metabolomic responses of *Caenorhabditis elegans* to cadmium are largely independent of metallothionein status, but dominated by changes in cystathionine and phytochelatins. *J Proteome Res.* **2009**, *8*(7):3512-9.

Hunt, P.R.; Marquis, B.J.; Tyner, K.M.; Conklin, S.; Olejnik, N.; Nelson, B.C.; Sprando, R.L. Nanosilver suppresses growth and induces oxidative damage to DNA in *Caenorhabditis elegans*. *J Appl Toxicol*. **2013**, doi: 10.1002/jat.2872.

Hussain, S.; Boland, S.; Baeza-Squiban, A.; Hamel, R.; Thomassen, L.C.; Martens, J.A.; Billon-Galland, M.A.; Fleury-Feith, J.; Moisan, F.; Pairon, J.C.; Marano, F. Oxidative stress and proinflammatory effects of carbon black and titanium dioxide nanoparticles: role of particle surface area and internalized amount. *Toxicology*. **2009**, *260*(1-3):142-9.

Hussain, S.; Thomassen, L.C.; Ferecatu, I.; Borot, M.C.; Andreau, K.; Martens, J.A.; Fleury, J.; Baeza-Squiban, A., Marano, F.; Boland, S. Carbon black and titanium dioxide nanoparticles elicit distinct apoptotic pathways in bronchial epithelial cells. *Part. Fibre Toxicol.* **2010**, *7*:10.

IARC Working Group on the Evaluation of Carcinogenic Risks to Humans Carbon black, titanium dioxide, and talc. *IARC Monogr. Eval. Carcinog. Risks Hum.* **2010**, *93*:1-413.

Iavicoli, I.; Calabrese, E.J.; Nascarella, M.A. Exposure to Nanoparticles and Hormesis. *Dose Response*. **2010**, *8*(4):501-17.

Inoue, H.; Hisamoto, N.; An, J.H.; Oliveira, R.P.; Nishida, E.; Blackwell, T.K.; Matsumoto, K. The *C. elegans* p38 MAPK pathway regulates nuclear localization of the transcription factor SKN-1 in oxidative stress response. *Genes Dev.* **2005**, *19*:2278-2283.

Inoue, K.; Takano, H. Biology of diesel exhaust effects on allergic pulmonary inflammation. *Yakugaku Zasshi.* **2011**, *131*(3):367-71.

Inoue, T.; Thomas, J. H. Targets of TGF-beta signaling in *Caenorhabditis elegans* dauer formation. *Dev Biol*. **2000**, *217*:192-204.

Irazoqui, J.E.; Urbach, J.M., Ausubel, F.M. Evolution of host innate defence: insights from *Caenorhabditis elegans* and primitive invertebrates. *Nat Rev Immunol*. **2010**, *10*(1):47-58.

Irizarry, R.A.; Hobbs, B.; Collin, F.; Beazer-Barclay, Y.D.; Antonellis, K.J.; Scherf, U.; Speed, T.P. Exploration, normalization, and summaries of high density oligonucelotide array probe level data. *Biostatistics.* **2003**, *4*(2):249-264.

Ishikawa, C.; Ozaki, H.; Nakajima, T.; Ishii, T.; Kanai, S.; Anjo, S.; Shirai, K.; Inoue, I. A frameshift variant of CYP2C8 was identified in a patient who suffered from rhabdomyolysis after administration of cerivastatin. *J. Hum. Genet.* **2004**, *49*:582-585.

Jager, T.; Alda álvarez, O.; Kammenga, J.E.; Kooijman, S. Modelling nematode life cycles using dynamic energy budgets. *Functional Ecology.* **2005**, *19*:136-144.

Jennifer, M.; Maciej, W. Nanoparticle Technology as a Double-Edged Sword: Cytotoxic, Genotoxic and Epigenetic Effects on Living Cells. *JBNB.* **2013**, *l.4*:53-63.

Jensen, L.T.; Culotta, V.C. Activation of CuZn superoxide dismutases from *Caenorhabditis elegans* does not require the copper chaperone CCS. *J. Biol. Chem*. **2005**, *280*:41373-41379.

Jia, G.; Wang, H.; Yan, L.; Wang, X.; Pei, R.; Yan, T.; Zhao, Y.; Guo, X. Cytotoxicity of carbon nanomaterials: single-wall nanotube, multi-wall nanotube, and fullerene. *Environ. Sci. Technol.* **2005**, *39*(5):1378-83.

Jiang, G.C.; Hughes, S.; Stürzenbaum, S.R.; Evje, L.; Syversen, T.; Aschner, M. *Caenorhabditis elegans* Metallothioneins Protect against Toxicity Induced by Depleted Uranium. *Toxicol Sci.* **2009**, *111*(2):345-54.

Jiang, W.; Mashayekhi, H.; Xing, B. Bacterial toxicity comparison between nano- and micro-scaled oxide particles. *Environ Pollut.* **2009**, *157*(5):1619-25.

Johnston, B.D.; Scown, T.M.; Moger, J.; Cumberland, S.A.; Baalousha, M.; Linge, K.; van Aerle, R.; Jarvis, K.; Lead, J.R.; Tyler, C.R. Bioavailability of nanoscale metal oxides TiO_2, CeO_2, and ZnO to fish. *Environ. Sci. Technol*. **2010**, *44*(3):1144-1151.

Kadiiska, M.B.; Mason, R.P.; Dreher, K.L.; Costa, D.L.; Ghio, A.J. *In vivo* evidence of free radical formation in the rat lung after exposure to an emission source air pollution particle. *Chem Res Toxicol.* **1997**, *10*:1104-8.

Kaletta, T.; Hengartner, M. O. Finding function in novel targets: *C. elegans* as a model organism. *Nature Reviews Drug Discovery*. **2006**, *5*:387-399.

Kang, K.W.; Lee, S.J.; Kim, S.G. Molecular mechanism of Nrf2 activation by oxidative stress. *Antioxid Redox Signal*. **2005**, *7*:1664-1673

Kao, Y.Y.; Chen, Y.C.; Cheng, T.J.; Chiung, Y.M.; Liu, P.S. Zinc oxide nanoparticles interfere with zinc ion homeostasis to cause cytotoxicity. *Toxicol. Sci.* **2012**, *125*(2):462-472.

Kaplan, E.L.; Meier P. Nonparametric estimation from incomplete observations. *J Am Stat Assoc.* **1958**, *53*:457-81.

Karlsson, H.L. The comet assay in nanotoxicology research. *Anal Bioanal Chem.* **2010**, *398*(2):651-66.

Karlsson, M.; Kurz, T.; Brunk, U.T.; Nilsson, S.E.; Frennesson, C.I. What does the commonly used DCF test for oxidative stress really show? *Biochem J.* **2010**, *428*(2):183-90.

Kasemets, K.; Ivask, A.; Dubourguier, H.C.; Kahru, A. Toxicity of nanoparticles of ZnO, CuO and TiO_2 to yeast *Saccharomyces cerevisiae*. *Toxicology in Vitro.* **2009**, *23* (6):1116-1122.

Kato, Y.; Aizawa, T.; Hoshino, H.; Kawano, K.; Nitta, K.; Zhang, H. *abf-1* and *abf-2*, ASABF-type antimicrobial peptide genes in *Caenorhabditis elegans*. *Biochem. J*. **2002**, *361*:221-230.

Katz, D.J.; Edwards, T.M.; Reinke, V.; Kelly, W.G. A *C. elegans* LSD1 demethylase contributes to germline immortality by reprogramming epigenetic memory. *Cell*. **2009**, *137*:308-320.

Kelly, F. J. Oxidative stress: Its role in air pollution and adverse health effects. *Occup. Enviorn. Med.* **2003**, *60*:612-616.

Kenyon, C.; Chang, J.; Gensch, E.; Rudner, A.; Tabtiang, A.A. A *C. elegans* mutant that lives twice as long as wild type. *Nature (Lond.)*. **1993**, *366*:461-464.

Khare, P.; Sonane, M.; Pandey, R.; Ali, S.; Gupta, K.C.; Satish, A. Adverse effects of TiO_2 and ZnO nanoparticles in soil nematode, *Caenorhabditis elegans. J Biomed Nanotechnol*. **2011**, *7*(1):116-7.

Kim, J.; Takahashi, M.; Shimizu, T.; Shirasawa, T.; Kajita, M.; Kanayama, A.; Miyamoto, Y. Effects of the potent antioxidant, on the lifespan of the *Caenorhabditis elegans*. *Mechanisms of Ageing and Development.* **2008**, *129*:322-331.

Kim, S.W.; Kwak, J.I.; An, Y.J. Multigenerational study of gold nanoparticles in *Caenorhabditis elegans*: transgenerational effect of maternal exposure. *Environ Sci Technol.* **2013**, *47*(10):5393-9.

King, C. D.; Rios, G. R.; Green, M. D.; Tephly, T. R. UDP-Glucuronosyltransferases *Current Drug Metabolism*. **2000**, *1*:143-161.

Klapper, M.; Ehmke, M.; Palgunow, D.; Böhme, M.; Matthäus, C.; Bergner, G.; Dietzek, B.; Popp, J.; Döring, F. Fluorescence-based fixative and vital staining of lipid droplets in *Caenorhabditis elegans* reveal fat stores using microscopy and flow cytometry approaches. *J Lipid Res*. **2011**, *52*(6):1281-93.

Klien, K.; Godnić-Cvar, J. Genotoxicity of metal nanoparticles: focus on *in vivo* studies. *Arh Hig Rada Toksikol*. **2012**, *63*(2):133-45.

Kodavanti, U.P.; Hauser, R.; Christiani, D.C.; Meng, Z.H.; McGee, J.; Ledbetter, A.; Richards, J.; Costa, D.L. Pulmonary responses to oil fly ash particles in the rat differ by virtue of their specific soluble metals. *Toxicological Sciences.* **1998**, *43*:204-212.

Koike, E.; Kobayashi, T. Chemical and biological oxidative effects of carbon black nanoparticles. *Chemosphere*. **2006**, *65*(6):946-51.

Kong, Q.; Lin, C.L. Oxidative damage to RNA: mechanisms, consequences, and diseases. *Cell Mol Life Sci*. **2010**, *67*(11):1817-29.

Kreplick, L.W. Salicylate Toxicity in Emergency Medicine. **2001**.

Kreyling, W.G.; Scheuch, G. Clearance of particles deposited in the lungs. In: Particle-Lung Interactions (Gehr P, Heyder J, eds). *New York:Marcel Dekker Inc*. **2000**, 323-376.

Kroll, A.; Dierker, C.; Rommel, C.; Hahn, D.; Wohlleben, W.; Schulze-Isfort, C.; Göbbert, C.; Voetz, M.; Hardinghaus, F.; Schnekenburger, J. Cytotoxicity screening of 23 engineered nanomaterials using a test matrix of ten cell lines and three different assays. *Part Fibre Toxicol*. **2011**, *8*:9.

Krug, H.F.; Wick, P. Nanotoxicology: an interdisciplinary challenge. *Angew Chem Int Ed Engl.* **2011**, *50*(6):1260-78.

Kulmala, M.; Vehkamäkia, H.; Petäjää, T.; Dal Masoa, M.; Lauria, A.; Kerminenb, V.-M.; Birmilic, W.; McMurryd, P.H. Formation and growth rates of ultrafine atmospheric particles: a review of observations. *J Aerosol Sci.* **2004**, *35*:143-176.

Lacko, M.; Roelofs, H.M.; te Morsche, R.H.; Voogd, A.C.; Ophuis, M.B.; Peters, W.H.; Manni, J.J. Genetic polymorphisms in the tobacco smoke carcinogens detoxifying enzyme UGT1A7 and the risk of head and neck cancer. *Head Neck.* **2009**, *31*(10):1274-81.

Lademann, J., Weigmann, H.; Rickmeyer, C.; Barthelmes, H.; Schaefer, H., Mueller, G.; Wolfram, S. Penetration of titanium dioxide microparticles in a sunscreen formulation into the horny layer and the follicular orifice. *Skin Pharmacol Appl Skin Physiol*. **1999**, *12*:247-256.

Landis, G.N.; Tower, J. Superoxide dismutase evolution and life span regulation. *Mech. Ageing Dev.* **2005**, *126*(3):365-79.

Lant, B.; Storey, K.B. An overview of stress response and hypometabolic strategies in *Caenorhabditis elegans*: conserved and contrasting signals with the mammalian system. *Int J Biol Sci.* **2010**, *6*(1):9–50.

Lawther, P. J.; Ellison, J. M. K.; Waller, R. E. Some medical aspects of aerosol research. *Proc. R. Soc. Lond. A.* **1968**, *307*:223-234.

Lebowitz, M.D. Epidemiological studies of the Respiratory effects of sir pollution. *Eur Respir J.* **1996**, *9*:1029-1054.

Lee, E.S.; Xue, D. Caspase protocols in *Caenorhabditis elegans*. *Methods Mol Biol*. **2014**, *1133*:101-8.

Lee, J.; Nam, S., Hwang, S.B., Hong, M., Kwon, J.Y.; Joeng, K.S., Im, S.H., Shim, J., Park, M.C. Functional genomic approaches using the nematode *Caenorhabditis elegans* as a model system. *J Biochem Mol Biol.* **2004**, *37*(1):107-13.

Lemaire, C.; Andréau, K.; Souvannavong, V.; Adam, A. Inhibition of caspase activity induces a switch from apoptosis to necrosis. FEBS Lett. 1998, 425(2):266-70.

Levy, L.; Chaudhuri, I.S.; Krueger, N.; McCunney, R.J. Does carbon black disaggregate in lung fluid? A critical assessment. *Chem. Res. Toxicol.* **2012**, *25*(10):2001-6.

Li, C.H.; Shen, C.C.; Cheng, Y.W.; Huang, S.H.; Wu, C.C.; Kao, C.C.; Liao, J.W.; Kang, J.J. Organ biodistribution, clearance, and genotoxicity of orally administered zinc oxide nanoparticles in mice. *Nanotoxicology.* **2011**, 1-11.

Li, J.; Huang, K.X.; Le, W.D. Establishing a novel *C. elegans* model to investigate the role of autophagy in amyotrophic lateral sclerosis. *Acta Pharmacol Sin.* **2013**, *34*(5):644-50.

Li, M.; Zhu, L.; Lin, D. Toxicity of ZnO nanoparticles to *Escherichia coli*: mechanism and the influence of medium components. *Environ Sci Technol.* **2011**, *45*(5):1977-83.

Li, N.; Alam, J.; Venkatesan, M.I.; Eiguren-Fernandez, A., Schmitz, D.; Di Stefano, E.M.; Slaughter, N.; Killeen, E.; Wang, X.; Huang, A.; Wang, M.; Miguel, A.H.; Cho, A., Sioutas C.; Nel, A.E. Nrf2 is a key transcription factor that regulates antioxidant defense in macrophages and epithelial cells: protecting against the pro-inflammatory and oxidizing effects of diesel exhaust chemicals. *J. Immunol.* **2004**, *173*:3467-3481.

Li, N.; Sioutas, C.; Cho, A.; Schmitz, D.; Misra, C.; Sempf, J., Wang, M.Y.; Oberley, T., Froines, J.; Nel, A. Ultrafine particulate pollutants induce oxidative stress and mitochondrial damage. *Environ Health Perspect.* **2003**, *111*:455-460.

Li, N.; Venkatesan, M.I.; Miguel, A.; Kaplan, R.; Gujuluva, C.; Alam, J.; Nel, A.E. Induction of the heme oxygenase-1 expression in macrophages by diesel exhaust particles quinones via antioxidant response element. *J Immunol*. **2000**, *165*:3393-3401.

Li, N.; Wang, M.; Sempf, J. M.; Oberley, T. D.; Nel, A. E. Comparison of the oxidative stress effects of organic DEP chemicals in bronchial epithelial cells and macrophages. *J. Immunol.* **2002b**, *169*:4531-4541.

Li, N.; Xia, T.; Nel, A.E. The role of oxidative stress in ambient particulate matter-induced lung diseases and its implications in the toxicity of engineered nanoparticles. *Free Radic Biol Med*. **2008**, *44*(9):1689-99.

Li, X.Y.; Brown, D.; Smith, S.; MacNee, W.; Donaldson, K. Short-term inflammatory responses following intratracheal instillation of fine and ultrafine carbon black in rats. *Inhal. Toxicol.* **1999**, *11*(8):709-31.

Li, X.Y.; Gilmour, P.S., Donaldson, K.; MacNee, W. Free radical and pro-inflammatory activity pf particulate air pollution (PM10) in vivo and *in vitro.Thorax*. **1996**, *51*:1216-22.

Li, Y.; Wang, W.; Wu, Q.; Li, Y.; Tang, M.; Ye, B.; Wang, D. Molecular control of TiO_2-NPs toxicity formation at predicted environmental relevant concentrations by Mn-SODs proteins. *PLoS One.* **2012**, *7*(9):e44688.

Li, Y.; Yu, S.; Wu, Q.; Tang, M.; Pu, Y.; Wang, D. Chronic Al_2O_3-nanoparticle exposure causes neurotoxic effects on locomotion behaviors by inducing severe ROS production and disruption of ROS defense mechanisms in nematode *Caenorhabditis elegans*. *J Hazard Mater*. **2012**, *219-220*:221-30.

Liao, V.H.; Yu, C.W. *Caenorhabditis elegans gcs-1* confers resistance to arsenic-induced oxidative stress. *Biometals.* **2005**, *18*(5):519-28.

Líbalová, H.; Uhlířová, K.; Kléma, J.; Machala, M.; Šrám, R.J.; Ciganek, M.; Topinka, J. Global gene expression changes in human embryonic lung fibroblasts induced by organic extracts from respirable air particles. *Part. Fibre Toxicol*. **2012**, *9*:1.

Liebers, R.; Rassoulzadegan, M.; Lyko, F. Epigenetic Regulation by Heritable RNA. *PLoS Genet*. **2014**, *10*(4):e1004296.

Lim, D.; Roh, J.Y.; Eom, H.J.; Choi, J.Y.; Hyun, J.; Choi, J. Oxidative stress-related PMK-1 P38 MAPK activation as a mechanism for toxicity of silver nanoparticles to reproduction in the nematode *Caenorhabditis elegans*. *Environ Toxicol Chem.* **2012**, *31*(3):585-92.

Lin, D.; Xing, B. Phytotoxicity of nanoparticles: inhibition of seed germination and root growth. *Environ Pollut.* **2007**, *150*(2):243-50.

Lindquist, S. The heat-shock response. *Annu. Rev. Biochem.* **1986**, *55*:1151-91.

Lippmann, M.; Gordon, T.; Chen, L.C. Effects of subchronic exposures to concentrated ambient particles (CAPs) in mice. I. Introduction, objectives, and experimental plan. *Inhal Toxicol.* **2005a**, *17*:177-187.

Lippmann, M.; Gordon, T.; Chen, L.C. Effects of subchronic exposures to concentrated ambient particles in mice. IX. Integral assessment and human health implications of subchronic exposures of mice to CAPs. *Inhal Toxicol.* **2005b**, *17*:255-261.

Liu, Y.; He, L.; Mustapha, A.; Li, H.; Hu, Z.Q.; Lin, M. Antibacterial activities of zinc oxide nanoparticles against Escherichia coli O157:H7. *J Appl. Microbiol*. **2009**, *107*(4):1193-1201.

Ljungman, M.; Zhang, F.; Chen, F.; Rainbow, A.J.; McKay, B.C. Inhibition of RNA polymerase II as a trigger for the p53 response. *Oncogene*. **1999**, *18*: 583-592.

Lodovici, M.; Bigagli, E. Oxidative Stress and Air Pollution Exposure. *Journal of Toxicology*. **2011**, Article ID 487074, 9 pages.

Longo, V. D.; Gralla, E. B.; Valentine, J. S. Superoxide dismutase activity is essential for stationary phase survival in *Saccharomyces cerevisiae*: mitochondrial production of toxic oxygen species *in vivo*. *The Journal of Biological Chemistry*. **1996**, *271*(21):12275-12280.

Love, S.A., Maurer-Jones, M.A.; Thompson, J.W.; Lin, Y.S., Haynes, C.L. Assessing nanoparticle toxicity. *Annu. Rev. Anal. Chem.* **2012**, *5*:181-205.

Lozano, O.; Laloy, J.; Alpan, L.; Mejia, J.; Rolin, S.; Toussaint, O.; Dogné, J.M.; Lucas, S.; Masereel, B. Effects of SiC nanoparticles orally administered in a rat model: Biodistribution, toxicity and elemental composition changes in feces and organs. *Toxicology and Applied Pharmacology*. **2012**, *264*:232-245.

Lundborg, M.; Bouhafs, R.; Gerde, P.; Ewing, P.; Camner, P.; Dahlén, S.E.; Jarstrand, C. Aggregates of ultrafine particles modulate lipid peroxidation and bacterial killing by alveolar macrophages. *Environ. Res.* **2007**, *104*(2):250-7.

Lundborg, M.; Dahlén, S.E.; Johard, U.; Gerde, P.; Jarstrand, C.; Camner, P.; Låstbom, L. Aggregates of ultrafine particles impair phagocytosis of microorganisms by human alveolar macrophages. *Environ. Res.* **2006**, *100*(2):197-204.

Lundborg, M.; Johard, U.; Låstbom, L.; Gerde, P.; Camner, P. Human alveolar macrophage phagocytic function is impaired by aggregates of ultrafine carbon particles. *Environ Res.* **2001**, *86*(3):244-53.

Ma, H.; Bertsch, P.M.; Glenn, T.C.; Kabengi, N.J.; Williams, P.L. Toxicity of manufactured zinc oxide nanoparticles in the nematode *Caenorhabditis elegans*. *Environ Toxicol Chem.* **2009a**, *28*(6):1324-30.

Ma, H.; Glenn, T.C.; Jagoe, C.H.; Jones, K.L.; Williams, P.L. A transgenic strain of the nematode *Caenorhabditis elegans* as a biomonitor for heavy metal contamination. *Environ. Toxicol. Chem*. **2009b**, *28*(6):1311-1318.

Ma, H.; Kabengi, N.J.; Bertsch, P.M.; Unrine, J.M.; Glenn, T.C.; Williams, P.L. Comparative phototoxicity of nanoparticulate and bulk ZnO to a free-living nematode *Caenorhabditis elegans*: the importance of illumination mode and primary particle size. *Environ Pollut.* **2011**,*159*(6):1473-80.

Ma, H.; Williams, P.L.; Diamond, S.A. Ecotoxicity of manufactured ZnO nanoparticles--a review. *Environ Pollut*. **2013**, *172*:76-85.

Ma, J.Y.; Ma, J.K. The dual effect of the particulate and organic components of diesel exhaust particles on the alteration of pulmonary immune/inflammatory responses and metabolic enzymes. *J. Environ. Sci. Health C. Environ. Carcinog. Ecotoxicol. Rev.* **2002**, *20*(2):117-47.

Maeda, Y.; Chen, G.; Xu, Y.; Haitchi, H.M.; Du, L.; Keiser, A.R.; Howarth, P.H.; Davies, D.E.; Holgate, S.T.; Whitsett, J.A. Airway epithelial transcription factor nk2 homeobox 1 inhibits mucous cell metaplasia and th2 inflammation. *Am J Respir Crit Care Med*. **2011**, *184*:421-429.

Magas, O.K.; Gunter, J.T.; Regans, J.L. Ambient air pollution and daily pediatric hospitalizations for asthma. *Environ Sci Pollut Res.* **2007**, *14*(1):19-23.

Maisonet, M.; Correa, A.; Misra, D.; Jaakkola, J. A review of the literature on the effects of ambient air pollution on fetal growth. *Environ. Res*. **2004**, *95*:106-115.

Mallo, G.V.; Kurz, C.L.; Couillault, C.; Pujol, N.; Granjeaud, S.; Kohara, Y.; Ewbank, JJ. Inducible antibacterial defense system in *C. elegans*. *Curr. Biol.* **2002**, *12*:1209-1214.

Margoshes, M.; Vallee, B. L. A cadmium protein from equine kidney cortex. *J. Am. Chem. Soc.* **1957**, *79*(17):4813-4814.

Marsh, E.K.; May, R.C. *Caenorhabditis elegans*, a model organism for investigating immunity. *Appl Environ Microbiol.* **2012**, *78*(7):2075-81.

Martinez, G.R.; Loureiro, A.P.; Marques, S.A.; Miyamoto, S.; Yamaguchi, L.F.; Onuki, J.; Almeida, E.A.; Garcia, C.C.; Barbosa, L.F.; Medeiros, M.H.; Di Mascio, P. Oxidative and alkylating damage in DNA. *Mutat Res.* **2003**, *544*:115-27.

Mauderly, J.L.; Jones, R.K.; Griffith, W.C.; Henderson, R.F.; McClellan, R.O. Diesel Exhaust is a Pulmonary Carcinogen in Rats Exposed Chronically by Inhalation. *Fund. Appl. Toxicol.* **1987**, *9*:208-221.

Maupas, E. Modes et formes de reproduction des nématodes. *Arch. Zool. Exp. Gen.* **1900**, *8*: 463-624.

McCord, J.M.; Fridovich, I. Superoxide dismutase. An enzymic function for erythrocuprein (hemocuprein). *J Biol Chem*. **1969**, *244*(22):6049-55.

Meng, H.; Xia, T.; George, S.; Nel, A.E. A predictive toxicological paradigm for the safety assessment of nanomaterials. *ACS Nano.* **2009**, *3*(7):1620-7.

Menzel, R.; Bogaert, T.; Achazi, R. A systematic gene expression screen of *Caenorhabditis elegans* cytochrome P450 genes reveals CYP35 as strongly xenobiotic inducible. *Arch. Biochem. Biophys.* **2001**, *395*:158-68.

Menzel, R.; Rodel, M.; Kulas, J.; Steinberg, C. E. CYP35: xenobiotically induced gene expression in the nematode *Caenorhabditis elegans. Arch. Biochem. Biophys.* **2005**, *438*:93-102.

Mercer, J.F.The molecular basis of copper-transport diseases. *Trends Mol. Med*. **2001**, *7* (2):64–69.

Meyer, J.N.; Lord, C.A.; Yang, X.Y.; Turner, E.A. Badireddy, A.R.; Marinakos, S.M.; Chilkoti, A.; Wiesner, M.R.; Auffan, M. Intracellular uptake and associated toxicity of silver nanoparticles in *Caenorhabditis elegans*. *Aquat Toxicol.* **2010**, *100*(2):140-50.

Miller, F.W. (Author); Miller, R.M. (Author) (**1993**) Environmental Hazards: Air Pollution-A Reference Handbook. Santa Barbara, CA. Published by: ABC-CLIO.

Miller, M. R.; Shaw, C. A.; Langrish, J.P. From particles to patients: oxidative stress and the cardiovascular effects of air pollution. *Future Cardiol.* **2012**, *8*(*4*):577-602.

Mills, N.L.; Amin, N.; Robinson, S.D.; Anand, A.; Davies, J.; Patel, D.; de la Fuente, J.M.; Cassee, F.R.; Boon, N.A.; Macnee, W.; Millar, A.M.; Donaldson, K.; Newby, D.E. Do inhaled carbon nanoparticles translocate directly into the circulation in humans? *Am. J. Respir. Crit. Care Med.* **2006**, *173*(4):426-31.

Minelli, C.; Wei, I.; Sagoo, G.; Jarvis, D.; Shaheen, S.; Burney, P. Interactive effects of antioxidant genes and air pollution on respiratory function and airway disease: a HuGE review. *Am J Epidemiol.* **2011**, *173*:603-620.

Mocchegiani, E.; Costarelli, L.; Giacconi, R.; Piacenza, F.; Basso, A.; Malavolta, M. Zinc, metallothioneins and immunosenescence: effect of zinc supply as nutrigenomic approach. *Biogerontology.* **2011**, *12*(5):455-65.

Moger, J.; Johnston, B.D.; Tyler, C.R. Imaging metal oxide nanoparticles in biological structures with CARS microscopy. *Opt. Express*. **2008**, *16*(5):3408-3419.

Moghimi, S.M.; Hunter, A.C.; Murray, J.C. Nanomedicine: current status and future prospects. *FASEB J*. **2005**, *19*:311-330.

Mohan, N.; Chen, C.S.; Hsieh, H.H.; Wu, Y.C.; Chang, H.C. In vivo imaging and toxicity assessments of fluorescent nanodiamonds in *Caenorhabditis elegans. Nano Lett*. **2010**, *10*(9):3692-3699.

Montes–Burgos, I.; Walczyk, D.; Hole, P.; Smith, J.; Lynch, I.; Dawson, K. Characterisation of Nanoparticle Size and State Prior to Nanotoxicological Studies. *Journal of Nanoparticle Research.* **2010**, *12*:47-53.

Mossman, B. T.; Bignon, J.; Corn, M.; Seaton, A.; Gee, J. B. L. Asbestos: scientific development and implications for public policy. *Science*. **1990**, *247*:294-301.

Moussa, R.; Kuznetsov, A.; Neiser E.; Zakhidov, A.A. Search for Negative Refraction in the Visible Region of Light by Fluorescent Microscopy of Quantum Dots Infiltrated into Regular

and Inverse Synthetic Opals. *Nanoscale Photonics*. *Lecture Notes in Nanoscale Science and Technology*. **2010**, *9*:65-76.

Mudunkotuwa, I.A.; Rupasinghe, T.; Wu, C.M.; Grassian, V.H. Dissolution of ZnO nanoparticles at circumneutral pH: a study of size effects in the presence and absence of citric acid. *Langmuir*. **2012**, *28*(1):396-403.

Mudway, I. S.; Stenfors, N.; Duggan, S. T.; Roxborough, H.; Zielinski, H.; Marklund, S. L.; Blomberg, A.; Frew, A. J.; Sandstrom, T.; Kelly, F. J. An in vitro and in vivo investigation of the effects of diesel exhaust on human airway lining fluid antioxidants. *Arch. Biochem. Biophys.* **2004**, *423*:200-12.

Mukhopadhyay, P.; Rajesh, M.; Yoshihiro, K.; Haskó, G.; Pacher, P. Simple quantitative detection of mitochondrial superoxide production in live cells. *Biochem Biophys Res Commun.* **2007**, *358*(1):203-8.

Muñoz-Elías, E.J.; McKinney, J.D. Carbon metabolism of intracellular bacteria. *Cellular Microbiology* **2006**, *8*(1):10-22.

Murphy, M.P. How mitochondria produce reactive oxygen species. *Biochem J.* **2009**, *417*(1):1-13.

Nascarella, M.A.; Calabrese, E.J. A method to evaluate hormesis in nanoparticle dose-responses. *Dose Response*. **2012**, *10*(3):344-54.

National Institute of Standards and Technology, Certificate of Analysis, Standard Reference Material 1648, Urban particulate Matter, January 5, **2012**, 7 pp.

Nel, A.; Xia, T.; Madler, L.; Li, N. Toxic potential of materials at the nanolevel. *Science*. **2006**, *311*:622-627.

Nel, A.E.; Mädler, L.; Velegol, D.; Xia, T.; Hoek, E.M.; Somasundaran, P.; Klaessig, F.; Castranova, V.; Thompson, M. Understanding biophysicochemical interactions at the nano-bio interface. *Nat Mater.* **2009**, *8*(7):543-57.

Nemmar, A.; Hoylaerts, M.F.; Hoet, P.H.; Vermylen, J.; Nemery, B. Size effect of intraytracheally instilled particles on pulmonary inflammation and vascular thrombosis. *Toxicol Appl Pharmacol*. **2003**, *186*:38-45.

Nicholas, W. L.; Dougherty, E.C.; Hansen, E.L. Axenic cultivation of *C. briggsae* (Nematoda: Rhabditidae) with chemically undefined supplements; comparative studies with related nematodes. *Ann. N.Y. Acad. Sci.* **1959**, *77*:218-236.

Nikula, K.J.; Snipes, M.B.; Barr, E.B.; Griffith, W.C.; Henderson, R.F.; Mauderly, J.L. Comparative pulmonary toxicities and carcinogenicities of chronically inhaled diesel exhaust and carbon black in F344 rats. *Fundam. Appl. Toxicol.* **1995**, *25*(1):80-94.

Nohyek, G.J.; Dufour, E.K; Roberts, M.S. Nanotechnology, cosmetics and the skin: Is there a health risk? *Skin Pharmacology and Physiology*. **2008**, *21*:136-149.

Nohynek, G.J.; Antignac, E.; Re, T., Toutain, H. Safety assessment of personal care products/cosmetics and their ingredients. *Toxicol Appl Pharmacol.* **2010**, *243*(2):239-59.

Nordberg, G.F. (Editor); Fowler, B.A. (Editor); Nordberg, M. (Editor); Friberg, L. (Editor) (**2007**) Handbook on the Toxicology of Metals, 3rd edition. Published by: Academic Press.

Nowack, B.; Brouwer, C.; Geertsma, R.E.; Heugens, E.H.; Ross, B.L.; Toufektsian, M.C.; Wijnhoven, S.W.; Aitken, R.J. Analysis of the occupational, consumer and environmental

exposure to engineered nanomaterials used in 10 technology sectors. *Nanotoxicology*. **2012**, Early Online, 1-5.

Nriagu, J. O.; Pacyna, J. M. Quantative assessment of worldwide contamination of air, water and soils by traced metals. *Nature*. **1998**, *333*:134-139.

Oberdörster, E.; Zhu, S.; Blickley, T.; McClellan-Green, P.; Haasch, M. Ecotoxicology of carbon-based engineered nanoparticles: Effects of fullerene (C60) on aquatic organisms. *Carbon*. **2006**, *44*(6):1112-1120.

Oberdörster, G.; Ferin, J; Lehnert, B.E. Correlation between particle size, *in vivo* particle persistence, and lung injury. *Environ Health Perspect*. **1994**, *102*:173-179.

Oberdörster, G.; Finkelstein, J.N.; Johnston, C.; Gelein, R.; Cox, C.; Baggs, R.; Elder, A.C. Acute pulmonary effects of ultrafine particles in rats and mice. *Res Rep Health Eff Inst.* **2000**, *96*:5-74.

Oberdörster, G.; Maynard, A.; Donaldson, K.; Castranova, V.; Fitzpatrick, J.; Ausman, K.; Carter, J.; Karn, B.; Kreyling, W.; Lai, D.; Olin, S.; Monteiro-Riviere, N.; Warheit, D.; Yang, H. Principles for characterizing the potential human health effects from exposure to nanomaterials: elements of a screening strategy. *Part. Fibre Toxicol.* **2005**, *2*:8.

Oberdörster, G.; Oberdörster, E.; Oberdörster, J. Nanotoxicology: An emerging discipline evolving from studies of ultrafine particles. *Environmental Health Perspectives.* **2005**, *113*:823-839.

Oettgen, P.; Finger, E.; Sun, Z.; Akbarali, Y.; Thamrongsak, U.; Boltax, J.; Grall, F.; Dube, A.; Weiss, A.; Brown, L.; Quinn, G.; Kas, K.; Endress, G.; Kunsch, C.; Libermann, T.A. PDEF, a novel prostate epithelium-specific ets transcription factor, interacts with the androgen receptor and activates prostate-specific antigen gene expression. *J Biol Chem.* **2000**, *275*:1216-1225.

Oksanen, J.; Blanchet, G.F.; Kindt, R.; Legendre, P.; Minchin, P.R.; O'Hara, R.B.; Simpson, G.L.; Solymos, P.; Henry, M.; Stevens, H.; Wagner, H. Vegan: Community Ecology Package R package version 20-5. **2012**, http://CRANR-projectorg/package=vegan.

Organisation for Economic Co-operation and Development (OECD) (**2006**). Carbon black, CAS 1333-86-4; SIDS initial assessment report for carbon black; CAS No. 1333-86-4.

Osburn, W.O.; Kensler, T.W. Nrf2 signaling: an adaptive response pathway for protection against environmental toxic insults. *Mutat Res*. **2008**, *659*(1–2):31-39.

Osmond, M.J., McCall, M.J. Zinc oxide nanoparticles in modern sunscreens: an analysis of potential exposure and hazard. *Nanotoxicology*. **2010**, *4*(1):15-41.

Pacchierotti, F.; Eichenlaub-Ritter, U. Environmental hazard in the aetiology of somatic and germ cell aneuploidy. *Cytogenet Genome Res*. **2011**, *133*(2-4):254-68.

Pasinelli, P.; Belford, M.E.; Lennon, N.; Bacskai, B.J.; Hyman, B.T.; Trotti, D.; Brown, R.H. Amyotrophic lateral sclerosis-associated SOD1 mutant proteins bind and aggregate with Bcl-2 in spinal cord mitochondria. *Neuron.* **2004**, *43*(1):19-30.

Pekkanen, J., Timonen, K.L.; Ruuskanen, J.; Reponen, A.; Mirme, A. Effects of ultrafine and fine particles in urban air on peak expiratory flow among children with asthmatic symptoms. *Environ Res.* **1997**, *74*:24-33.

Penttinen, P., Timonen, K.L.; Tiittanen, P.; Mirme, A.; Ruuskanen, J.; Pekkanen, J. Ultrafine particles in urban air and respiratory health among adult asthmatics. *Eur Resp J*. **2001**, *17*:428-435.

Peschansky, V.J.; Wahlestedt, C. Non-coding RNAs as direct and indirect modulators of epigenetic regulation. *Epigenetics*. **2014**, *9*(1):3-12.

Pestov, D.G.; Strezoska, Z.; Lau, L.F. Evidence of p53-dependent cross-talk between ribosome biogenesis and the cell cycle: effects of nucleolar protein Bop1 on G(1)/S transition. *Mol Cell Biol*. **2001**, *21*:4246-4255.

Petriv, O.I.; Rachubinski, R.A. Lack of peroxisomal catalase causes a progeric phenotype in *Caenorhabditis elegans*. *J Biol Chem*. **2004**, *279*(19):19996-20001.

Pfaffl, M.W.; Horgan, G.W.; Dempfle, L. Relative expression software tool (REST) for group-wise comparison and statistical analysis of relative expression results in real-time PCR. *Nucleic Acids Research.* **2002**, *30*:e36.

Phillips, J. P.; Campbell, S. D.; Michaud, D.; Charbonneau, M.; Hilliker, A. J. Null mutation of copper/zinc superoxide dismutase in *Drosophila* confers hypersensitivity to paraquat and reduced longevity. *Proceedings of the National Academy of Sciences of the United States of America*. **1989**, *86*(8):2761-2765.

Pinkston-Gosse, J.; Kenyon, C. DAF-16/FOXO targets genes that regulate tumor growth in *Caenorhabditis elegans*. *Nat Genet*. **2007**, *39*(11):1403-1409.

Pluskota, A.; Horzowski, E.; Bossinger, O.; von Mikecz, A. In *Caenorhabditis elegans* nanoparticle-bio-interactions become transparent: Silica-nanoparticles induce reproductive senescence. *PLoS ONE*. **2009**, *4*(8):e6622.

Pope, C. A., III; Burnett, R. T.; Thun, M. J.; Calle, E. E.; Krewski, D.; Ito, K.; Thurston, G. D. Lung cancer, cardiopulmonary mortality, and long-term exposure to fine particulate air pollution. *J. Am. Med. Assoc.* **2002**, *287*:1132-1141.

Pope, C.A. III; Dockery, D.W. Epidemiology of particle effects. In: Air Pollution and Health (Holgate ST, Samet JM, Koren HS,Maynard RL, eds). *Academic Press, San Diego CA*. **1999**, 673-705.

Pourazar, J.; Mudway, I.S.; Samet, J.M., Helleday, R.; Blomberg, A.; Wilson, S.J.; Frew, A.J.; Kelly, F.J.; Sstrom, T. Diesel exhaust particles activates redox-sensitive factors kinases in human airways. *Am J Physiol Lung Cell Mol Physiol*. **2005**, *289*:L724-L730.

Poynton, H.C.; Lazorchak, J.M.; Impellitteri, C.A.; Smith, M.E.; Rogers, K.; Patra, M.; Hammer, K.A.; Allen, H.J.; Vulpe, C.D. Differential gene expression in *Daphnia magna* suggests distinct modes of action and bioavailability for ZnO nanoparticles and Zn ions. *Environ Sci Technol*. **2011**, *45*(2):762-8.

Rahman, I.; MacNee, W. Regulation of redox glutathione levels and gene transcription in lung inflammation: therapeutic approaches. *Free Radic Biol Med.* **2000**, *28*:1405-1420.

Ramage, L.; Proudfoot, L.; Guy, K. Expression of C-reactive protein in human lung epithelial cells and upregulation by cytokines and carbon particles. *Inhal. Toxicol.* **2004**, *16*(9):607-13.

Ramos-Gomez, M., Kwak, M.K.; Dolan, P.M.; Itoh, K.; Yamamoto, M.; Talalay, P.; Kensler, T.W. Sensitivity to carcinogenesis is increased chemoprotective efficacy of enzyme inducers is lost in Nrf2 transcription factor-deficient mice. *Proc Natl Acad Sci U S A.* **2001**, *98*:3410-3415.

Ramos-Gomez, M.; McDolan, P.; Itoh, K.; Yamamoto, M.; Kensler, T.W. Interactive effects of Nrf2 genotype olipraz on benzo[a]oyrene-DNA adducts tumor yield in mice. *Carcinogenesis*. **2003**, *24*:461-467.

Rankin, C.H. From gene to identified neuron to behaviour in *Caenorhabditis elegans*. *Nat. Rev. Genet*. **2002**, *3*:622-630.

RCore Team, R. A language and environment for statistical computing. **2012**, *R Foundation for Statistical Computing Vienna, Austria* ISBN 3-900051-07-0, URL, wwwR-projectorg/

Rechtsteiner, A.; Ercan, S.; Takasaki, T.; Phippen, T.M.; Egelhofer, T.A.; Wang W.; Kimura, H.; Lieb, J.D.; Strome, S. The histone H3K36 methyltransferase MES-4 acts epigenetically to transmit the memory of germline gene expression to progeny. *PLoS Genet.* **2010**, *6*:e1001091.

Reddy, K.M.; Feris, K.; Bell, J.; Wingett, D.G.; Hanley, C.; Punnoose, A. Selective toxicity of zinc oxide nanoparticles to prokaryotic and eukaryotic systems. *Appl Phys Lett.* **2007**, *90*(213902):2139021-2139023.

Rengasamy, A.; Barger, M.W.; Kane, E.; Ma, J.K.H.; Castranova, V.; Ma,J.Y.C. Diesel Exhaust Particles-Induced Alterations of Pulmonary Phase I and Phase II Enzymes of Rats. *J. Toxicol. Environ. Health A.* **2003**, *66*(2):153-67.

Renwick, L.C.; Brown, D.; Clouter, A.; Donaldson, K. Increased inflammation and altered macrophage chemotactic responses caused by two ultrafine particle types. *Occup. Environ. Med.* **2004**, *61*(5):442-7.

Renwick, L.C.; Donaldson, K.; Clouter, A. Impairment of alveolar macrophage phagocytosis by ultrafine particles. *Toxicol Appl Pharmacol*. **2001**, *172*:119-127.

Rich, J.T.; Neely, J.G.; Paniello, R.C.; Voelker, C.C.; Nussenbaum, B.; Wang. E.W. A practical guide to understanding Kaplan-Meier curves. *Otolaryngol Head Neck Surg*. **2010**, *143*(3):331-6.

Ristow, M.; Zarse, K. How increased oxidative stress promotes longevity and metabolic health: The concept of mitochondrial hormesis (mitohormesis). *Exp Gerontol*. **2010**, *45*(6):410-8.

Roh, H.C.; Collier, S.; Guthrie, J.; Robertson, J.D.; Kornfeld, K. Lysosome-related organelles in intestinal cells are a zinc storage site in *C. elegans*. *Cell Metab.* **2012**, *15*(1):88-99.

Roh, J.Y.; Lee, J.; Choi, J. Assessment of stress-related gene expression in the heavy metal-exposed nematode *Caenorhabditis elegans*: a potential biomarker for metal-induced toxicity monitoring and environmental risk assessment. *Environ Toxicol Chem.* **2006**, *25*(11):2946-56.

Roh, J.Y.; Park, K.; Choi, J. A cadmium toxicity assay using stress responsive *Caenorhabditis elegans* mutant strains. *Environ Toxicol Pharmacol.* **2009**, *28*(3):409-13.

Roh, J.Y.; Park, Y.K.; Park, K.; Choi, J. Ecotoxicological investigation of CeO_2 and TiO_2 nanoparticles on the soil nematode *Caenorhabditis elegans* using gene expression, growth, fertility, and survival as endpoints. *Environ. Toxicol. Pharmacol.* **2010**, *29*:167-172.

Roh, J.Y.; Sim, S.J.; Yi, J.; Park, K.; Chung, K.H.; Ryu, D.Y.; Choi, J. Ecotoxicity of silver nanoparticles on the soil nematode *Caenorhabditis elegans* using functional ecotoxicogenomics. *Environ Sci Technol.* **2009**, *43*(10):3933-40.

Rohrs L.C. Metal-fume fever from inhaling zinc oxide. *AMA Arch Ind Health.* **1957**, *16*(1):42-7.

Roselli, M.; Finamore, A.; Garaguso, I.; Britti, M.S.; Mengheri, E. Zinc oxide protects cultured enterocytes from the damage induced by *Escherichia coli*. *J Nutr*. **2003**, *133*:4077-4082.

Rubbi, C.P.; Milner, J. Disruption of the nucleolus mediates stabilization of p53 in response to DNA damage and other stresses. *Embo J.* **2003**, *22*:6068-6077.

Rubio, V., Valverde, M.; Rojas, E. Effects of atmospheric pollutants on the Nrf2 survival pathway. *Environ Sci Pollut Res Int.* **2010**, *17*(2):369-82.

Rui, Q.; Zhao, Y.; Wu, Q.; Tang, M.; Wang, D. Biosafety assessment of titanium dioxide nanoparticles in acutely exposed nematode *Caenorhabditis elegans* with mutations of genes required for oxidative stress or stress response. *Chemosphere*. **2013**, *93*(10):2289-96.

Runge-Morris, M.; Kocarek, T.A. Regulation of Sulfotransferase and UDP-Glucuronosyltransferase Gene Expression by the PPARs. *PPAR Research*. **2009**, Article ID 728941, 14 pages.

Russell, A.G.; Brunekreef, B. A focus on particulate matter and health. *Envior. Sci. Technolol.* **2009**, *43*:4620-4625.

Saier, M.H. Jr. Multiple mechanisms controlling carbon metabolism in bacteria. *Biotechnol. Bioeng.* **1998**, *58*(2-3):170-4.

Sakaue, Y.; Kim, J.; Miyamoto, Y. Effects of TAT-conjugated platinum nanoparticles on lifespan of mitochondrial electron transport complex I-deficient *Caenorhabditis elegans, nuo-1*. *Int J Nanomedicine*. **2010**, *5*:687-95.

Samet, J.M.; Dominici, F.; Curriero, F.C.; Coursac, I.; Zeger, S.L. Fine particulate air pollution and mortality in 20 U.S. cities. *N Engl J Med.* **2000**, *343*(24):1742-9.

Sarkar, S.; Sharma, C.; Yog, R; Periakaruppan, A.; Jejelowo, O.; Thomas, R.; Barrera, E.V.; Rice-Ficht, A.C.; Wilson, B.L.; Ramesh, G.T. Analysis of stress responsive genes induced by single-walled carbon nanotubes in BJ Foreskin cells. *J Nanosci Nanotechnol.* **2007**, *7*(2):584-92.

Sato, M., Bremner, I. Oxygen free radicals and metallothionein. *Free Radic Biol Med.* **1993**, *14*(3):325-37.

Sayes, C.M.; Gobin, A.M., Ausman, K.D., Mendez, J.; West, J.L.; Colvin, V.L. Nano-C60 cytotoxicity is due to lipid peroxidation. *Biomaterials.* **2005**, *26*(36):7587-95.

Schafer, F.Q.; Buettner, G.R. Redox environment of the cell as viewed through the redox state of the glutathione disulfide/glutathione couple. *Free Radic Biol Med*. **2001**, *30*:1191-1212.

Schilling, K.; Bradford, B.; Castelli, D.; Dufour, E.; Nash, J.F.; Pape, W.; Schulte, S.; Tooley, I.; van den Bosch, J.; Schellauf, F. Human safety review of "nano" titanium dioxide and zinc oxide. *Photochem Photobiol Sci*. **2010**, *9*(4):495-509.

Schroer, K.T.; Gibson, A.M., Sivaprasad, U.; Bass, S.A.; Ericksen, M.B.; Wills-Karp, M., Lecras, T., Fitzpatrick, A.M., Brown, L.A.; Stringer, K.F.; Hershey, G.K. Downregulation of glutathione S-transferase pi in asthma contributes to enhanced oxidative stress. *J Allergy Clin Immunol*. **2011**, *128*(3):539-48.

Schulenburg, H.; Kurz, C.L.; Ewbank, J.J. Evolution of the innate immune system: the worm perspective. *Immunol Rev.* **2004**, *198*:36-58.

Schulz, J.; Hohenberg, H.; Pflücker, F.; Gärtner, E.; Will, T.; Pfeiffer, S.; Wepf, R.; Wendel, V., Gers-Barlag, H.; Wittern, K.P. Distribution of sunscreens on skin. *Adv Drug Deliv Rev.* **2002**, *54* Suppl 1:S157-63.

Schwartz, J. Air pollution and daily mortality: a review and meta analysis. *Environmental Research.* **1994**, *64*(1):36-52.

Schwartz, M.S.; Benci, J.L.; Selote, D.S., Sharma, A.K.; Chen, A.G.; Dang, H.; Fares, H., Vatamaniuk, O.K. Detoxification of multiple heavy metals by a half-molecule ABC transporter, HMT-1, and coelomocytes of *Caenorhabditis elegans. PLoS One*. **2010**, *5*(3): e9564.

Schwarze, P.E.; Ovrevik, J.; Låg, M.; Refsnes, M.; Nafstad, P.; Hetland, R.B.; Dybing, E. Particulate matter properties and health effects: consistency of epidemiological and toxicological studies. *Hum Exp Toxicol.* **2006**, *25*(10):559-79.

Sciau, P. (**2012**). Nanoparticles in Ancient Materials: The Metallic Lustre Decorations of Medieval Ceramics, The Delivery of Nanoparticles, Dr. Abbass A. Hashim (Editor), ISBN: 978-953-51-0615-9, InTech, DOI: 10.5772/34080. www.intechopen.com/books/the-delivery-of-nanoparticles/nanoparticles-in-ancient-materials-the-metallic-lustre-decorations-of-medieval-ceramics

Scientific Committee on Emerging and Newly Identified Health Risks (**2006**)"modified Opinion (after public consultation) on the appropriateness of existing methodologies to assess the potential risks associated with engineered and adventitious products of nanotechnologies", (SCENIHR/002/05).

Seaton, A.; Donaldson, K. Nanoscience, nanotoxicology, and the need to think small. *Lancet.* **2005**, *365*(9463):923-4.

Seaton, A.; MacNee, W.; Donaldson, K.; Godden, D. Particulate air pollution and acute health effects. *The Lancet.* **1995**, *345*:176-178.

Sharma, V.; Anderson, D.; Dhawan, A. Zinc oxide nanoparticles induce oxidative DNA damage and ROS-triggered mitochondria mediated apoptosis in human liver cells (HepG2). *Apoptosis.* **2012**, *17*(8):852-70.

Sharma, V.; Shukla, R.K.; Saxena, N.; Parmar, D.; Das, M.; Dhawan, A. DNA damaging potential of zinc oxide nanoparticles in human epidermal cells. *Toxicol Lett.* **2009**, *185*(3):211-8.

Sharma, V.; Singh, P.; Pandey, A.K.; Dhawan, A. Induction of oxidative stress, DNA damage and apoptosis in mouse liver after sub-acute oral exposure to zinc oxide nanoparticles. *Mutat Res.* **2012**, *745*(1-2):84-91.

Shaye, D.D.; Greenwald, I. OrthoList: a compendium of *C. elegans* genes with human orthologs. *PLoS One*. **2011**, *6*(5):e20085.

Shukla, A., Flanders, T.; Lounsbury, K.M., Mossman, B.T. The gamma-glutamylcysteine synthetase and glutathione regulate asbestos-induced expression of activator protein-1 family members and activity. *Cancer Res.* **2004**, *64*(21):7780-6.

Shukla, A.; Timblin, C., BeruBe, K.; Gordon, T.; McKinney, W.; Driscoll, K.; Vacek, P.; Mossman, B.T. Inhaled particulate matter causes expression of nuclear factor (NF)-kappaB-related genes and oxidant-dependent NF-kappaB activation *in vitro*. *Am. J. Respir. Cell Mol. Biol.* **2000**, *23*(2):182-7.

Shvedova, A.A.; Kisin, E.R.; Mercer, R.; Murray, A.R.; Johnson, V.J.; Potapovich, A.I.; Tyurina, Y.Y.; Gorelik, O.; Arepalli, S.; Schwegler-Berry, D.; Hubbs, A.F.; Antonini, J.; Evans, D.E.; Ku, B.K.; Ramsey, D.; Maynard, A.; Kagan, V.E.; Castranova, V.; Baron, P. Unusual inflammatory and fibrogenic pulmonary responses to single walled carbon nanotubes in mice. *Am. J. Physiol. Lung Cell. Mol. Physiol*. **2005**, *289*:698-708.

Sies, H. (1991) Oxidative stress II. In: Oxidants and antioxidants. London: Academic Press.

Simon, D.F.; Domingos, R.F.; Hauser, C.; Hutchins, C.M.; Zerges, W.; Wilkinson, K.J. Transcriptome sequencing (RNA-seq) analysis of the effects of metal nanoparticle exposure on the transcriptome of *Chlamydomonas reinhardtii*. *Appl Environ Microbiol*. **2013**, *79*(16):4774-85.

Singh, N.; Manshian, B.; Jenkins, G.J.; Griffiths, S.M.; Williams, P.M.; Maffeis, T.G.; Wright, C.J.; Doak, S.H. NanoGenotoxicology: the DNA damaging potential of engineered nanomaterials. *Biomaterials.* **2009**, *30*(23-24):3891-914.

Smita, S.; Gupta, S.K.; Bartonova, A.; Dusinska, M.; Gutleb, A.C.; Rahman, Q. Nanoparticles in the environment: assessment using the causal diagram approach. *Environ Health.* **2012**, *28*:11.

Sochova, I.; Hofman, J.; Holoubek, I. Effects of seven organic pollutants on soil nematode *Caenorhabditis elegans*. *Environment International* **2007**, *33*:798-804.

Song, Y.; Li, X.; Du, X. Exposure to nanoparticles is related to pleural effusion, pulmonary fibrosis and granuloma. *European Respiratory Journal*. **2009**, *34*:559-567.

Sorahan, T., Hamilton, L.; van Tongeren, M.; Gardiner, K.; Harrington, J.M. A cohort mortality study of UK carbon black workers, 1951-1996. *Am J Ind Med.* **2001**, *39*:158-170.

Squadrito, G.L.; Cueto, R., Dellinger, B.; Pryor, W.A. Quinoid redoxcycling as a mechanism for sustained free radical generation by inhaled airborne particulate matter. *Free Radical Biology and Medicine*. **2001**, *31*:1132-1138.

Stankowski, N. J.; Codreanu, S.G.; Liebler, D.C.; McLaughlin, B. Analysis of Protein Targets by Oxidative Stress Using the OxyBlot and Biotin–Avidin-Capture Methodology. *Cell Culture Techniques Neuromethods.* **2011**, *56*:365-381.

Stegeman, J. J.; Solow, A. R. A Look Back at the London Smog of 1952 and the Half Century Since; A Half Century Later: Recollections of the London Fog. *Environmental Health Perspectives*. **2002**, *110*:A734-735.

Stoccoro, A.; Karlsson, H.L.; Coppedè, F.; Migliore, L. Epigenetic effects of nano-sized materials. *Toxicology*. **2013**, *313*(1):3-14.

Stohs, S.J.; Bagchi, D. Oxidative mechanisms in the toxicity of metal ions. *Free Radic Biol Med.* **1995**, *18*(2):321-36.

Stoimenov, P.K.; Klinger, R.L.; Marchin, G.L., Klabunde, K.J. Metal oxide nanoparticles as bactericidal agents. *Langmuir.* **2002**, *18*:6679-6686.

Stone, V.; Johnston, H.; Clift, M.J. Air pollution, ultrafine and nanoparticle toxicology: cellular and molecular interactions. *IEEE Trans Nanobioscience*. **2007**, *6*(4):331-40.

Stone, V.; Shaw, J.; Brown, D.M.; MacNee, W.; Faux, S.P.; Donaldson, K. The role of oxidative stress in the prolonged inhibitory effect of ultrafine carbon black on epithelial cell function. *Toxicol. In Vitro.* **1998**, *12*:649-659.

Strayer, A.; Wu, Z.; Christen, Y.; Link, C.D.; Luo, Y. Expression of the small heat-shock protein Hsp16-2 in *Caenorhabditis elegans* is suppressed by Ginkgo biloba extract EGb 761. *FASEB J.* **2003**, *17*(15):2305-7.

Sulston, J.E.; Horvitz, H.R. Post-embryonic cell lineages of the nematode *Caenorhabditis elegans*. *Develop. Biol.* **1977**, *56*:110-156.

Suzuki, A.; Kogo, R.; Kawahara, K.; Sasaki, M.; Nishio, M.; Maehama, T.; Sasaki, T.; Mimori, K.; Mori, M. A new PICTure of nucleolar stress. *Cancer Sci*. **2012**, *103*(4):632-7.

Swain, S.C.; Keusekotten, K.; Baumeister, R.; Stürzenbaum, S.R. *C. elegans* Metallothioneins: New Insights into the Phenotypic Effects of Cadmium Toxicosis. *Journal of Molecular Biology*. **2004**, *341*:951–959.

Swain, S.C.; Wren, J.F.; Stürzenbaum, S.R.; Kille, P.; Morgan, A.J.; Jager, T.; Jonker, M.J.; Hankard, P.K.; Svendsen, C.; Owen, J.; Hedley, B.A.; Blaxter, M.L.; Spurgeon, D.J. Linking toxicant molecular and physiological mode of action in *Caenorhabditis elegans*. *BMC Systems Biology*. **2010**, *4*:32.

Syed, S.; Zubair, A.; Frieri, M. Immune response to nanomaterials: implications for medicine and literature review. *Curr Allergy Asthma Rep*. **2013**, *13*(1):50-7.

Sykiotis, G.P., Habeos, I.G.; Samuelson, A.V., Bohmann, D. The role of the antioxidant and longevity-promoting Nrf2 pathway in metabolic regulation. *Curr Opin Clin Nutr Metab Care.* **2011**, *14*(1):41-8.

Takano, H.; Yanagisawa, R.; Ichinose, T.; Sadakane, K.; Inoue Ki, K.; Yoshida, S.; Takeda, K.; Yoshino Si, S.; Yoshkawa, T.; Morita, M. Lung Expression of Cytochrome P450 1A1 as a Possible Biomarker of Exposure to Diesel Exhaust *Particles. Arch. Toxicol.* **2002**, *76*:146-151.

Takenoshita, S.; Tani, M.; Mogi, A.; Nagashima, M.; Nagamachi, Y.; Bennett, W.P.; Hagiwara, K.; Harris, C.C.; Yokota, J. Mutation analysis of the Smad2 gene in human colon cancers using genomic DNA and intron primers. *Carcinogenesis*. **1998**, *19*(5):803-7.

Takiguchi, M.; Achanzar, W. E.; Qu, W.; Li, G.; Waalkes, M. P. Effects of Cadmium on DNA-(Cytosine-5) Methyltransferase Activity and DNA Methylation Status during Cadmium-Induced Cellular Transformation. *Ex- perimental Cell Research*. **2003**, *286*: 355-365.

Tamer, L., Calikoglu, M., Ates, N.A., Yildirim, H., Ercan, B.; Saritas, E.; Unlü, A.; Atik, U. Glutathione-S-transferase gene polymorphisms (GSTT1, GSTM1, GSTP1) as increased risk factors for asthma. *Respirology*. **2004**, *9*:493-8.

Taniguchi, N. On the basic concenpt of nanotechnology. *In Proceedings of the International Congress on Prod Eng.* **1974**, Tokyo, Japan: JSPE.

Tapiero, H.; Townsend, D.M.; Tew, K.D. Trace elements in human physiology and pathology. Copper. *Biomedicine and Pharmacotherapy*. **2003**, *57*:386-398.

Tayel, A.A.; El-Tras, W. F.; Moussa, S.; el-Baz, A.F.; Mahrous, H.; Salem, M. F.; Brimer, L. Antibacterial activity and mechanism of action of zinc oxide nanoparticles against foodborne pathogens. *Journal of Food Safety.* **2011**, *31*:211-218.

The Royal Society & The Royal Academy of Engineering (**2004**) Nanoscience and nanotechnologies: opportunities and uncertainties. Published by: Latimer Trend Ltd, Plymouth, UK.

Thomas, C.R.; George, S.; Horst, A.M., Ji, Z.; Miller, R.J.; Peralta-Videa, J.R.; Xia, T.; Pokhrel, S.; Mädler, L.; Gardea-Torresdey, J.L.; Holden, P.A.; Keller, A.A., Lenihan, H.S.; Nel, A.E.; Zink, J.I. Nanomaterials in the environment: from materials to high-throughput screening to organisms. *ACS Nano.* **2011**, *5*(1):13-20.

Thyagarajan, B.; Blaszczak, A.G.; Chandler, K.J.; Watts, J.L.; Johnson, W.E.; Graves, B.J. ETS-4 is a transcriptional regulator of life span in *Caenorhabditis elegans*. *PLoS Genet.* **2010**, *6*.

Tiede, K.; Hassellöv, M.; Breitbarth, E.; Chaudhry, Q.; Boxall, A.B.A. Considerations for environmental fate and ecotoxicity testing to support environmental risk assessments for engineered nanoparticles. *J. Chromatogr. A.* **2009**, *1216*:503-509.

Tiittanen, P.; Timonen, K.L.; Ruuskanen, J.; Mirme, A.; Pekkanen, J. Fine particulate air pollution, resuspended road dust and respiratory health among symptomatic children. *Eur Resp J.* **1999**, *13*(2):266-273.

Tsyusko, O.V., Unrine, J.M.; Spurgeon, D.; Blalock, E.; Starnes, D., Tseng, M.; Joice, G.; Bertsch, P.M. Toxicogenomic responses of the model organism *Caenorhabditis elegans* to gold nanoparticles. *Environ Sci Technol.* **2012**, *46*(7):4115-24.

Tullet, J.M.; Hertweck, M.; An, J.H.; Baker, J.; Hwang, J.Y.; Liu, S.; Oliveira, R.P.; Baumeister, R., Blackwell, T.K. Direct inhibition of the longevity-promoting factor SKN-1 by insulin-like signalling in *C. elegans*. *Cell.* **2008**, *132*(6):1025-38.

Uusitalo, L.M.; Hempel, N. Recent Advances in Intracellular and *In Vivo* ROS Sensing: Focus on Nanoparticle and Nanotube Applications. *Int. J. Mol. Sci*. **2012**, *13*:10660-10679.

Valavanidis, A.; Fiotakis, K.; Vlachogianni, T. Airborne particulate matter and human health: toxicological assessment and importance of size and composition of particles for oxidative damage and carcinogenic mechanisms. *J Environ Sci Health C Environ Carcinog Ecotoxicol Rev.* **2008**, *26*(4):339-62.

Valberg, P.A.; Watson, A.Y. Lung cancer rates in carbon-black workers are discordant with predictions from rat bioassay data. *Regul. Toxicol. Pharmacol.* **1996**, *24*(2 Pt 1):155-70.

Van Beurden, W.J.; Wielders, P.L.; Scheepers, P.J.; van Herwaarden, C.L.; Dekhuijzen, P.N. Superoxide production by peripheral polymorphonuclear leukocytes in patients with COPD. *Respir. Med.* **2003**, *97*(4):401-6.

Van Gelder, R.N.; von Zastrow, M.E.; Yool, A.; Dement, W.C.; Barchas, J.D., Eberwine, J.H. Amplified RNA synthesized from limited quantities of heterogeneous cDNA. *Proc Natl Acad Sci U S A.* **1990**, *87*(5):1663-7.

Van Raamsdonk, J. M.; Hekimi, S. Reactive oxygen species and aging in *Caenorhabditis elegans*: causal or casual relationship? *Antioxidants & Redox Signaling*. **2010**, *13*(12):1911-1953.

Van Raamsdonk, J.M.; Hekimi, S. Deletion of the mitochondrial superoxide dismutase *sod-2* extends lifespan in *Caenorhabditis elegans*. *PLoS Genet.* **2009**, *5*(2):e1000361.

Van Raamsdonk, J.M.; Hekimi, S. Superoxide dismutase is dispensable for normal animal lifespan. *Proc. Natl. Acad. Sci. U S A.* **2012**, *109*(15):5785-90.

Van Tongeren, M.J.; Gardiner, K.; Rossiter, C.E.; Beach, J.; Harber, P.; Harrington, M.J. Longitudinal analyses of chest radiographs from the European Carbon Black Respiratory Morbidity Study. *Eur. Respir. J.* **2002**, *20*(2):417-25.

Vandebriel, R.J.; De Jong, W.H. A review of mammalian toxicity of ZnO nanoparticles. *Nanotechnol Sci Appl.* **2012**, *5*:61-71.

Vatamaniuk, O.K.; Bucher, E.A.; Sundaram, M.V.; Rea, P.A. CeHMT-1, a putative phytochelatin transporter, is required for cadmium tolerance in *Caenorhabditis elegans*. *J Biol Chem.* **2005**, *280*(25):23684-90.

Vatamaniuk, O.K.; Bucher, E.A.; Ward, J.T.; Rea, P.A. A new pathway for heavy metal detoxification in animals. Phytochelatin synthase is required for cadmium tolerance in *Caenorhabditis elegans*. *J Biol Chem.* **2001**, *276*(24):20817-20.

Verani, C.N. Metal complexes as inhibitors of the 26S proteasome in tumor cells. *J. Inorg. Biochem.* **2012**, *106*:59-67.

Vishnupriya, S.; Chaudhari, K.; Jagannathan, R.; Pradeep, T. Single-Cell Investigations of Silver Nanoparticle–Bacteria Interactions. *Particle & Particle Systems Characterization*. **2013**, *30*:1056-1062.

Von der Kammer, F.; Ferguson, P.L.; Holden, P.A.; Masion, A.; Rogers, K.R.; Klaine, S.J.; Koelmans, A.A.; Horne, N.; Unrine, J.M. Analysis of engineered nanomaterials in complex matrices (environment and biota): general considerations and conceptual case studies. *Environ Toxicol Chem*. **2012**, *31*(1):32-49.

Walker, G.; Houthoofd, K.; Vanfleteren, J.R.; Gems, D. Dietary restriction in *C. elegans*: from rate-of-living effects to nutrient sensing pathways. *Mech. Ageing Dev*. **2005**, *126*:929-937.

Wang, H., Xing, J., Wang, F.; Han, W.; Ren, H.; Wu, T.; Chen, W. Expression of Hsp27 and Hsp70 in lymphocytes and plasma in healthy workers and coal miners with lung cancer. *J Huazhong Univ Sci Technolog Med Sci.* **2010**, *30*(4):415-20.

Wang, H.; Wick, R. L.; Xing, B. Toxicity of nanoparticulate and bulk ZnO, Al_2O_3 and TiO_2 to the nematode *Caenorhabditis elegans. Enviornmental Pollution*. **2009**, *157*:1171-1177.

Wang, L.; Pinkerton, K.E. Air pollution effects on fetal early postnatal development. *Birth Defects Res Part C*. **2007**, *81*:144-157.

Wang, X.; Xu. H.; Ha, S.W.; Ju, D.; Xie, Y. Proteasomal degradation of Rpn4 in Saccharomyces cerevisiae is critical for cell viability under stressed conditions. *Genetics*. **2010**, *184*:335-342.

Wang, Y.; Alsmeyer, D.C.; McCreery, R.L. Raman Spectroscopy of Carbon Materials: Structural Basis of Observed Spectra. *Chem. Mater*. **1990**, *2*:557-563.

Wang, Z.L. Zinc oxide nanostructures: Growth, properties, and applications. *Journal of Physics: Condensed Matter*.**2004**, *16*:R829-R858.

Wani, M.Y.; Hashim, M.A.; Nabi, F.; Firdosa Nabi, Malik, M.A. Nanotoxicity: Dimensional and Morphological Concerns. *Advances in Physical Chemistry*. **2011**, Article ID 450912, 15 pages.

Weissenberg, A.; Sydlik, U.; Peuschel, H.; Schroeder, P.; Schneider, M.; Schins, R.P.; Abel, J.; Unfried, K. Reactive oxygen species as mediators of membrane-dependent signaling induced by ultrafine particles. *Free Radic. Biol. Med.* **2010**, *49*(4):597-605.

Wenzel, D.; Palladino, F.; Jedrusik-Bode, M. Epigenetics in *C. elegans*: facts and challenges. Genesis. **2011**, *49*(8):647-61.

Wild, C. (Author); Vineis, P. (Author); Garte, S. (Author) (**2008**) Molecular Epidemiology of Chronic Diseases, 1st edition, Copyright © John Wiley & Sons, Ltd.

Williams, L.; Seki, Y.; Vuguin, P.M.; Charron, M.J. Animal models of in utero exposure to a high fat diet: a review. *Biochim Biophys Acta*. **2014**, *1842*(3):507-19.

Wilson, M.R.; Lightbody, J.H.; Donaldson, K.; Sales, J.; Stone, V. Interactions between ultrafine particles and transition metals *in vivo* and *in vitro*. *Toxicol. Appl. Pharmacol.* **2002**, *184*(3):172-9.

Witkowska, M.; Smolewski, P. SMAD family proteins: the current knowledge on their expression and potential role in neoplastic diseases. *Postepy Hig Med Dosw (Online)*. **2014**, *68*:301-9.

Wood, W. B. (Author) (**1988**). The nematode *Caenorhabditis elegans,* 1st edition, Published by: Cold Spring Harbor Laboratory Press.

Woolley, J.F.; Stanicka, J.; Cotter, T.G. Recent advances in reactive oxygen species measurement in biological systems. *Trends Biochem Sci*. **2013**, *38*(11):556-65.

World Health Organization (WHO) (**2003**) "Health Aspects of Air Pollution with Particulate Matter, Ozone and Nitrogen Dioxide."

World Health Organization (WHO) (**2004**) "Answer to follow-up questions from CAFÉ."

World Health Organization (WHO) (**2005**) "Health risk of particulate matter from longrange transboundary air pollution."

WormAtlas, Altun, Z.F.; Herndon, L.A.; Crocker, C.; Lints, R.; Hall, D.H. (ed.s) (**2002-2012**), www.wormatlas.org

WormBook, ed. The *C. elegans* Research Community, WormBook, www.wormbook.org.

Wu, Q.; Li, Y.; Tang, M.; Wang, D. Evaluation of Environmental Safety Concentrations of DMSA Coated Fe_2O_3-NPs Using Different Assay Systems in Nematode *Caenorhabditis elegans*. *PLoS One*. **2012**, *7*(8):e43729.

Wu, Q.; Nouara, A.; Li, Y.; Zhang, M.; Wang, W.; Tang, M.; Ye, B.; Ding, J.; Wang, D. Comparison of toxicities from three metal oxide nanoparticles at environmental relevant concentrations in nematode *Caenorhabditis elegans. Chemosphere*. **2013**, *90*(3):1123-31.

Wu, W.; Peden, D.B.; McConnell, R.; Fruin, S.; Diaz-Sanchez, D. Glutathione-S-transferase M1 regulation of diesel exhaust particle-induced pro-inflammatory mediator expression in normal human bronchial epithelial cells. *Part. Fibre Toxicol.* **2012**, *6*(9):31.

Wu, W.; Samet, J.M.; Peden, D.B.; Bromberg, P.A. Phosphorylation of p65 is required for zinc oxide nanoparticle-induced interleukin 8 expression in human bronchial epithelial cells. *Environ Health Perspect.* **2010**, *118*(7):982-7.

Xia, T.; Kovochich, M.; Brant, J.; Hotze, M.; Sempf, J.; Oberley, T.; Sioutas, C.; Yeh, J.I.; Wiesner, M.R.; Nel, A.E. Comparison of the abilities of ambient and manufactured nanoparticles to induce cellular toxicity according to an oxidative stress paradigm. *Nano Lett.* **2006**, *6*(8):1794-807.

Xia, T.; Kovochich, M.; Liong, M.; Mädler, L.; Gilbert. B.; Shi, H.; Yeh, J.I.; Zink, J.I.; Nel, A.E. Comparison of the mechanism of toxicity of zinc oxide and cerium oxide nanoparticles based on dissolution and oxidative stress properties. *ACS Nano*. **2008**, *2*(10):2121-34.

Xia, T.; Li, N.; Nel, A. E. Potential Health Impact of Nanoparticles. *Annu. Rev. Public Health*. **2009**, *30*:137-150.

Xie, J.; Zhao, J.; Xiao, C.; Xu, Y.; Yang, S.; Ni, W. Reduced heat shock protein 70 in airway smooth muscle in patients with chronic obstructive pulmonary disease. *Exp Lung Res*. **2010**, *36*(4):219-26.

Xie, Y.; He, Y.; Irwin, P.L.; Jin, T.; Shi, X. Antibacterial activity and mechanism of action of zinc oxide nanoparticles against *Campylobacter jejuni*. *Appl Environ Microbiol*. **2011**, *77*(7):2325-31.

Yanase, S.; Onodera, A.; Tedesco, P.; Johnson, T.E.; Ishii, N. SOD-1 deletions in *Caenorhabditis elegans* alter the localization of intracellular reactive oxygen species and show molecular compensation. *J. Gerontol. A. Biol. Sci. Med. Sci.* **2009**, *64*(5):530-9.

Yang, W.; Li, J. J.; Hekimi, S. A measurable increase in oxidative damage due to reduction in superoxide detoxification fails to shorten the life span of long-lived mitochondrial mutants of *Caenorhabditis elegans*. *Genetics*. **2007**, 177(4):2063-2074.

Yang, X.; Jiang, C.; Hsu-Kim, H.; Badireddy, A.R.; Dykstra, M.; Wiesner, M.; Hinton, D.E.; Meyer, J.N. Silver Nanoparticle Behavior, Uptake, and Toxicity in *Caenorhabditis elegans*: Effects of Natural Organic Matter. *Environ Sci Technol*. **2014**, *48*(6):3486-95.

Yasuda, M.; D'Sa-Eipper, C.; Gong, X.L.; Chinnadurai, G. Regulation of apoptosis by a *Caenorhabditis elegans* BNIP3 homolog. *Oncogene.* **1998**, *17*(19):2525-30.

Yoshida, S.; Hiyoshi, K.; Ichinose, T.; Takano, H.; Oshio, S.; Sugawara, I.; Takeda, K.; Shibamoto, T. Effect of nanoparticles on the male reproductive system of mice. *Int J Andol.* **2008**, *3*:337-342.

Yu, T.; Malugin, A.; Ghandehari, H. Impact of silica nanoparticle design on cellular toxicity and hemolytic activity. *ACS Nano*. **2011**, *5*(7):5717-28.

Yuan, X.; Zhou, Y.; Casanova, E.; Chai, M.; Kiss, E.; Gröne, H.J.; Schütz, G.; Grummt, I. Genetic inactivation of the transcription factor TIF-IA leads to nucleolar disruption, cell cycle arrest, and p53-mediated apoptosis. *Mol Cell.* **2005**, *19*:77-87.

Zanni, E.; De Bellis, G.; Bracciale, M.P.; Broggi, A., Santarelli, M.L.; Sarto, M.S.; Palleschi, C.; Uccelletti, D. Graphite nanoplatelets and *Caenorhabditis elegans*: insights from an *in vivo* model. *Nano Lett.* **2012**, *12*(6):2740-4.

Zeitoun-Ghandour, S.; Charnock, J.M.; Hodson, M.E.; Leszczyszyn, O.I.; Blindauer, C.A.; Stürzenbaum, S.R. The two *Caenorhabditis elegans* metallothioneins (CeMT-1 and CeMT-2) discriminate between essential zinc and toxic cadmium. *FEBS J.* **2010**, *277*(11):2531-42.

Zeitoun-Ghandour, S.; Leszczyszyn, O.I.; Blindauer, C.A.; Geier, F.M.; Bundy, J.G.; Stürzenbaum, S.R. *C. elegans* metallothioneins: response to and defence against ROS toxicity. *Mol. Biosyst.* **2011**, *7*(8):2397-406.

Zelikoff, J.T.; Chen, L.C.; Cohen, M.D.; Fang, K.; Gordon, T.; Li, Y.; Nadziejko, C.; Schlesinger, R.B. Effects of inhaled ambient particulate matter on pulmonary antimicrobial immune deffense. *Inhal. Toxicol.* **2003**, *15*:131-150.

Zhang, H.; He, X.; Zhang, Z.; Zhang, P.; Li, Y.; Ma, Y.; Kuang, Y.; Zhao, Y.; Chai, Z. Nano-CeO_2 exhibits adverse effects at environmental relevant concentrations. *Environ Sci Technol.* **2011**, *45*(8):3725-30.

Zhang, L.;, Jiang, Y.; Ding, Y.; Daskalakis, N.; Jeuken, L.; Povey, M.; O'Neill, A. J.; York, D.W. Mechanistic investigation into antibacterial behaviour of suspensions of ZnO nanoparticles against *E. coli*. *Journal of Nanoparticle Research*. **2010**, *12*:1625-1636.

Zhao, Y.; Nalwa, H.S. (Author and editor) (**2007**) Nanotoxicology: Interactions of nanomaterials with biological systems. Published by *American Scientific Publishers*.

Zhao, Y.L.; Wang, D.Y. Formation and regulation of adaptive response in nematode *Caenorhabditis elegans*. *Oxid Med Cell Longev.* **2012**, *2012*:564093.

Zielinski, H.; Mudway, I.S.; Berube, K.A.; Murphy, S.; Richards, R.; Kelly, F.J. Modeling the interactions of particulates with epithelial lining fluid antioxidants. *Am J Physiol.* **1999**, *277*(4 pt 1):L719–L726.